BROADLY NEUTRALIZING ANTIBODY THERAPY AS POST-EXPOSURE PROPHYLAXIS IN A NONHUMAN PRIMATE MODEL OF PERINATAL HIV INFECTION

By

Mariya B. Shapiro

A DISSERTATION

Presented to the Department of Molecular Microbiology and Immunology

and the Oregon Health & Science University School of Medicine

in partial fulfillment of

the requirements for the degree of

Doctor of Philosophy

August 2020

TABLE OF CONTENTS

Acknowledgements……v

List of figures and tables……vii

Abstract……xi

CHAPTER 1: Introduction

I. Human and simian immunodeficiency viruses

A. History of the HIV/AIDS pandemic……1

B. Classification of HIV and SIV viruses……4

C. Nonhuman primate models of HIV infection and AIDS……..5

D. Virology of HIV and SIV

i. Viral replication: cell entry, reverse transcription, integration……..……9

ii. Viral replication: gene expression, virion assembly, egress……...…13

iii. Viral proteins and their functions……16

iv. Timeline of infection and pathogenesis……21

v. The persistent reservoir as an obstacle to HIV cure……24

E. Immune responses to HIV

i. Intrinsic and innate immunity……..25

ii. Adaptive immunity……28

II. Perinatal HIV infection

A. The scale of the problem……...32

B. HIV infection in infants and children

i. Transmission……32

ii. Viral loads, disease progression, and prognosis……....34

C. Clinical care for HIV-exposed and -infected children

i. Diagnosis and treatment……..35

ii. Disadvantages of existing strategies……37

D. Notable cases of HIV remission in children……...38

E. Nonhuman primate models of perinatal HIV infection……..39

III. Antibodies as passive therapy for HIV

A. Antibody structure and function……40

B. Broadly neutralizing antibodies

i. Discovery and characterization……...…44

ii. Evidence of antiviral efficacy in human trials and animal studies……..47

C. Rationale for using broadly neutralizing antibodies in infants……..49

D. Recent key findings……50

CHAPTER 2: Single-dose bNAb cocktail or abbreviated ART post-exposure regimens achieve tight SHIV control without adaptive immunity

I. Abstract……52

II. Authors, Affiliations, Contributions, and Acknowledgements……..52

III. Introduction……..54

IV. Materials and Methods……..57

V. Results

A. Study design……...…74

B. Durable control of plasma viremia after bNAbs or ART……...75

C. bNAb pharmacokinetics and anti-drug antibody responses……79

D. Quantitation of viral reservoir seeding in tissues……...82

E. Detection of adaptive immune responses to SHIV……84

F. SHIV pathogenesis and clinical outcomes……..86

VI. Discussion……....87

VII. Supplementary Data……...91

CHAPTER 3: Immune Perturbation is More Profound in Newborn than in Infant Macaques during Acute SHIV Infection

I. Abstract……..106

II. Authors, Affiliations, Contributions, and Acknowledgements……106

III. Introduction……108

IV. Materials and Methods……112

V. Results

A. Study design……124

B. SHIV infection dynamics and reservoir seeding……129

C. Adaptive immune responses……..132

D. Leukocyte dynamics in peripheral blood……..135

E. Transcriptome analysis……143

VI. Discussion…… 148

VII. Supplementary Data……153

CHAPTER 4: Implications and Future Directions

I. Implications

A. "Hit early, hit hard": the importance of early intervention to limit reservoir seeding……..158

B. Considerations for optimizing antibody treatment regimens……160

C. Antibody therapy as a strategy to reduce the "effective" viral dose……165

D. Validity and utility of the macaque/SHIV model for understanding HIV transmission and treatment in human newborns……168

II. Future directions

A. Designing combination therapies to deploy different mechanisms of action……170

B. Examining the impact of dose- and age-dependent immunologic differences on viral infection and treatment outcomes in newborns……173

III. Concluding Thoughts……..174

References……175

Acknowledgements

First and foremost, I want to thank Cory for being an exceptional partner, for celebrating my successes, listening to my rants, “sure dear”-ing my impostor syndrome and associated crises of self-confidence, and reminding me to take care of myself. I also thank our daughter Brielle for being her silly, mischievous, inquisitive, and sweet self and always challenging and inspiring me. I love you both deeply.

I next want to acknowledge my thesis advisor, Dr. Nancy Haigwood, for her superb mentorship and fostering my growth as a scientist. Even as she set high expectations for my independence, Nancy has always been willing to discuss the science with me and offer guidance and support. I am likewise grateful to Dr. Ann Hessell for helping to mold my scientific thinking during our many conversations about Fc receptors and effector functions, and of course for maintaining the lab’s supply of peanut M&Ms to fuel our hard work. A special shout-out goes to Tracy Cheever’s tireless efforts on the infant projects; I’m pretty sure my Ph.D. would have taken 10 years without her help. I thoroughly enjoyed working with everyone, and want to thank all the members of the Haigwood/Hessell Lab for their camaraderie.

Third, I acknowledge my dissertation advisory committee (DAC) members Drs. Daniel Streblow, Tania Vu, Tim Nice, and Jonah Sacha for their constructive feedback. Dr. Sacha not only Chaired my DAC, but also acted as an informal scientific advisor and helped me mature as a scientist. As I pursued research in Nancy’s lab, members of the Sacha lab next door were unfailingly generous with their time, reagents, and expertise. In particular, Drs. Shaheed Abdulhaqq, Gabby Webb, and Helen Wu were invaluable role models for me as I navigated the ups and downs of grad school. I would also like to thank my Portland friends for all the fun adventures along the way, and my non-Portland friends for staying in touch all these years.

Finally, I wish to thank my parents, Tanya and Boris Shapiro. After completing STEM doctoral degrees in the Soviet Union, they came to the US as refugees, worked their way up from jobs as a grocery cashier and a gas station attendant, and paved the way for me to accomplish my own educational and career goals. When I was struggling with self-doubt, or rewriting my manuscript while caring for three-month-old Ellie, my mom listened, understood, encouraged me, and shared her experience of writing her dissertation while on bed rest at 8 months pregnant. My parents worked tirelessly so that I would never need to choose between pursuing a fulfilling career and being a committed and involved parent, and I have endless gratitude for their sacrifices and the example they set.

List of Figures and Tables

CHAPTER 1: Introduction

Figure 1.1. Structures and key properties of HIV, SIV, and SHIV…….....……8

Figure 1.2. Illustration of the HIV-1 replication cycle and steps targeted by inhibitors……..…..……..10

Figure 1.3. HIV-1 Envelope trimer structure and key sites of vulnerability targeted by broadly neutralizing antibodies……..……46

Table 1.1. NHP studies of bNAbs as post-exposure prophylaxis after SHIV infection…51

CHAPTER 2: Single-dose bNAb cocktail or abbreviated ART post-exposure regimens achieve tight SHIV control without adaptive immunity

Figure 2.1. Study design……75

Figure 2.2. Viremia is attenuated by bNAbs or ART post-exposure……..……78

Figure 2.3. Pharmacokinetics of bNAb treatments……..…..81

Figure 2.4. bNAb and ART treatments reduce virus in tissues……..83

Figure 2.5. bNAbs and ART modulate adaptive immunity……..85

Supplementary Figure 2.1. Emergent virus is not resistant to bNAbs…….91

Supplementary Figure 2.2. CD8α depletion in four Group 2B animals (bNAbs at 48 hours)……..…..92

Supplementary Figure 2.3. Post-exposure bNAbs or ART prevent persistent viremia……..…….92

Supplementary Figure 2.4. Effects of bNAb and treatment regimen on concentration and half-life…….93

Supplementary Figure 2.5. Viral DNA in inguinal lymph nodes is stable over time……94

Supplementary Figure 2.6. Inducible replication-competent virus in spleen and lymph nodes……94

Supplementary Figure 2.7. Longitudinal $CD4^+$ T cell counts……..95

Supplementary Figure 2.8. Gating strategy for $CD4^+$ and $CD8^+$ T cell counts by flow cytometry……...95

Supplementary Table 2.1. Titration of $SHIV_{SF162P3}$ stocks *in vivo* by single dose oral challenge in infant rhesus macaques……..…….96

Supplementary Table 2.2. Viral DNA in tissues at time of death in Group 1 (untreated controls)……97

Supplementary Table 2.3. Viral DNA in tissues at time of death in Group 2A (bNAbs at 48 hours)……...98

Supplementary Table 2.4. Viral DNA in tissues at time of death in Group 2B (bNAbs at 48 hours)……...99

Supplementary Table 2.5. Viral DNA in tissues at time of death in Group 3 (bNAbs at 30 hours)…….……...100

Supplementary Table 2.6. Viral DNA in tissues at time of death in Group 4 (ART at 48 hours)……..101

Supplementary Table 2.7. Spearman correlations between tissue viral DNA copies and plasma viremia for Groups 1, 2B, 3, and 4……102

Supplementary Table 2.8. Clinical histories and pathologic findings for Group 1 (untreated controls)……..……..103

Supplementary Table 2.9. Clinical histories and pathologic findings for Group 2A (bNAbs at 48 hours)……103

Supplementary Table 2.10. Clinical histories and pathologic findings for Group 2B (bNAbs at 48 hours)……..104

Supplementary Table 2.11. Clinical histories and pathologic findings for Group 3 (bNAbs at 30 hours)……104

Supplementary Table 2.12. Clinical histories and pathologic findings for Group 4 (ART at 48 hours)……105

Supplementary Table 2.13. List of primers used in this study……105

CHAPTER 3: Immune Perturbation is More Profound in Newborn than in Infant Macaques during Acute SHIV Infection

Figure 3.1. Moderate dose oral SHIV infection in infant rhesus macaques shows differences in viremia by age at time of challenge……125

Figure 3.2. Study design……126

Table 3.1. Study demographics and pathology summary……128

Figure 3.3. Viral loads during the acute phase following high dose challenge with SHIV do not vary by age at time of exposure in infant macaques……129

Figure 3.4. Viral DNA in tissues of Newborns and Infants……131

Figure 3.5. Acute SHIV infection impairs humoral responses to Hepatitis B vaccine in Newborns……133

Figure 3.6. T cell responses to Gag and Env peptide pools……135

Figure 3.7. Newborn CD8+ T cells and monocytes are strongly skewed toward differentiated phenotypes during acute SHIV infection……138

Figure 3.8. Between-group differences in leukocyte counts and phenotypes during SHIV infection in early life……142

Figure 3.9. RNA-seq reveals distinct transcriptomic signatures in Newborns and Infants on day 42 of SHIV infection……145

Supplementary Figure 3.1. Flow cytometry gating strategy for Panel 1 (B cells, NK cells, NKT cells, monocytes)……153

Supplementary Figure 3.2. Flow cytometry gating strategy for Panel 2 (T cells)……154

Supplementary Figure 3.3. Major leukocyte populations in newborns and infants before and during SHIV infection……155

Supplementary Figure 3.4. T cell counts, CD4+ subsets, and activation phenotypes in newborns and infants before and during SHIV infection……..156

Supplementary Figure 3.5. Transcriptional signatures in background and between-group contrasts……157

CHAPTER 4: Implications and Future Directions

Figure 4.1. Monoclonal antibodies produced in *N. benthamiana* cross the placenta less efficiently than antibodies produced in mammalian cells……162

Figure 4.2. Antibodies produced in *N. benthamiana* bind poorly to human FcγRI-expressing cells compared with mammalian-produced antibodies……...163

Figure 4.3. Plant-produced bNAbs do not mediate ADCC against SHIV-infected target cells……..164

Figure 4.4. Oral SHIV infection in infants is dose-dependent……...166

Figure 4.5. Replication-competent inducible virus correlates with total viral DNA copies in spleens and mesenteric LNs of SHIV-infected infants……..……..167

Abstract

There is an urgent unmet need for short-term interventions to prevent infection in infants exposed to HIV-1 at birth, who have higher mortality rates than infants infected at an older age. Although passively administered antibodies disperse into tissues more slowly than antiretroviral drugs (ART), potent broadly neutralizing monoclonal antibodies (bNAbs) are an attractive approach for post-exposure prophylaxis because of their longer half-life, good safety profile, and the potential for opsonization and Fc-mediated killing of infected cells. Like human infants exposed to HIV-1, newborn rhesus macaques exposed orally to the simian-human immunodeficiency virus $SHIV_{SF162P3}$ experience high viral loads, weak antiviral adaptive immunity, and rapid pathogenesis. In this nonhuman primate model of perinatal HIV-1 infection, we showed previously that 4-dose course of bNAbs beginning 24 hours after $SHIV_{SF162P3}$ exposure halted reservoir establishment and blocked disease progression. However, key unanswered questions remain about the window of opportunity for post-exposure prophylaxis using bNAbs, as well as the mechanisms of increased pathogenesis in newborns compared with older children and their implications for HIV-1 prevention and treatment. In this dissertation, we test the hypotheses that 1) SHIV clearance with bNAbs is achievable when treatment is delayed to 48 hours after exposure, 2) bNAbs are more effective than ART for post-exposure prophylaxis, and 3) the infant macaque/SHIV model recapitulates age-dependent differences in HIV-1 pathogenesis. In Chapter 2, we evaluate the outcomes of delayed short-term treatments using bNAbs and ART. We demonstrate that clearance is achievable with either a single large dose of bNAbs given at 30 hours or a 3-week ART regimen beginning 48 hours after SHIV exposure, while a 4-dose bNAb treatment beginning at 48 hours is only partially effective. This surprising finding suggests that, when early timing is critical, the rapid biodistribution to sites of active viral replication gives ART an advantage over bNAbs in terms of clearance efficacy. However, the

finding that a single treatment with bNAbs was fully effective is also encouraging, as it demonstrates the potential of passive antibodies to overcome the formidable challenges associated with ART adherence in newborns. In Chapter 3, we compare the virologic and immunologic outcomes of SHIV infection in newborn and older infant macaques in order to determine whether this model can recapitulate age-dependent differences in the pathogenesis of HIV-1. We show that, while viral loads are similar between groups, subtle differences emerge in the frequencies of leukocyte subsets, as well as transcriptional signatures that indicate distinct innate immune responses to acute/early chronic SHIV infection. In addition to providing valuable information about the animal model, these observations lay a crucial foundation for future studies of interventions to limit pathogenesis in newborns and older infants exposed to HIV-1. In Chapter 4, we discuss the implications of these findings and propose future research directions.

CHAPTER 1: Introduction

I. Human and simian immunodeficiency viruses

A. History of the HIV/AIDS pandemic

The HIV/AIDS pandemic remains one of the greatest public health challenges of our time. Since its discovery in the early 1980s, the AIDS-causing virus HIV-1 (HIV) has infected 75 million people worldwide and claimed 32 million lives (UNAIDS 2019). In 2018, there were 38 million people living with HIV, of which 1.7 million were children under 15 years of age (UNAIDS 2019). The related human virus HIV-2 is much less prevalent and not nearly as pathogenic; hence, by convention, the shorthand term HIV is used interchangeably with HIV-1.

Sequence analysis of HIV subtypes in central Africa suggests that HIV began spreading in Kinshasa in the early 20th century[1]. Over the following decades, increasing human migration and urbanization drove the regional and global spread of HIV. The virus is thought to have reached the US around 1970[2] and spread largely undetected until 1981, when unusual cases of Kaposi's Sarcoma and opportunistic infections began to be reported in previously healthy young gay men[3,4], suggesting underlying defects in cellular immunity[5]. Officially termed acquired immunodeficiency syndrome (AIDS) by the Centers for Disease Control (CDC), the disease was also seen in people with hemophilia[6], people who inject drugs[7], infants[8], immigrants from Haiti[9], and female sex partners of male patients[10]. In 1983-1984, researchers at the Pasteur Institute, the National Cancer Institute, and University of California San Francisco separately identified the agent of this syndrome: a new retrovirus dubbed human T-cell lymphotropic virus type III (HTLV-III), lymphadenopathy-associated virus (LAV), and AIDS-associated retrovirus (ARV) by the various research groups[11-13]. The International

Committee on the Taxonomy of Viruses standardized the nomenclature to “human immunodeficiency virus” (HIV) in 1986[14].

The discovery that HIV caused AIDS was a major advance, igniting hopes for the rapid development of a protective vaccine. However, the task proved more challenging than expected. The first two large-scale Phase III vaccine trials, known as VAX003 (ClinicalTrials.gov NCT00006327) and VAX004 (ClinicalTrials.gov NCT00002441), immunized participants in Thailand (VAX003) or the US and Netherlands (VAX004) with the recombinant viral Env (gp120) proteins from HIV subtypes matched to the strains circulating in the geographic region where each study was conducted. Neither vaccine conferred protection. A different approach was tested in the STEP trial: an adenovirus (Ad5) vectored HIV vaccine was given to high-risk participants in hopes of eliciting T cell immunity which, at the time, was predicted to prevent infection. This trial was halted early due to lack of efficacy[15]. In 2009, the RV144 trial in Thailand tested a “prime/boost” regimen using a canarypox vector bearing HIV sequences in combination with recombinant gp120 proteins from HIV-1 subtypes B and E, which were most prevalent in Thailand. This vaccine was found to be modestly protective, with 31% efficacy[16], spurring substantial efforts to first understand and then to elicit the kinds of antibody responses that correlated with protection in RV144. However, optimism was dashed by the recent failure of the HVTN 702 trial (ClinicalTrials.gov NCT02968849), which was designed to replicate the RV144 vaccine regimen in South Africa using subtype C immunogens. To this day, a vaccine for HIV remains elusive.

Despite these obstacles, progress in treatment and prevention of HIV/AIDS has been substantial. HIV was found to be transmissible via sexual intercourse[17], receipt of blood and blood products[18], and from HIV-positive mothers to their children[19,20]; thus, specific interventions to mitigate these risks could be implemented. Blood banks began screening donated blood for the virus; public awareness campaigns advocated for safer

sex practices; and the CDC recommended exclusive formula feeding to prevent postnatal transmission through breastmilk[21]. Despite the controversy surrounding needle exchange programs in the United States, their implementation has effectively reduced transmission among people who inject drugs in Europe and elsewhere (WHO 2004). These policy-based prevention strategies were complemented by new pharmaceuticals to block viral replication and prolong life in AIDS patients. The first antiretroviral drug, zidovudine (AZT), targets the viral reverse transcriptase (RT) and was approved by the FDA in 1987 for adults[22] and in 1990 for children with AIDS[23]. Additional potent drugs and new drug classes were developed, including protease inhibitors, integrase inhibitors, RT inhibitors (nucleoside and non-nucleoside), and entry inhibitors (fusion inhibitors and co-receptor antagonists) (for a detailed discussion, see **Section I.D.v. The persistent reservoir as an obstacle to HIV cure**). The use of multiple drug classes in combination—a strategy termed "highly active antiretroviral therapy" (HAART)—was found to better limit viral replication and viral escape due to drug pressure, turning an HIV diagnosis from a death sentence into a manageable chronic disease for those that could access lifelong daily treatment. Clinical trials in the 1990s revealed that outcomes improved significantly when treatment was started before the onset of symptomatic AIDS, revolutionizing the clinical management of HIV infection[24].

Still, the prevalence of HIV/AIDS grew worldwide. By 1999, an estimated 33 million people were living with HIV; AIDS was the leading cause of death in Africa and the fourth leading cause of death globally (WHO World Health Report 1999). In the late 1990s and early 2000s, government initiatives and policies were put in place to increase access to low-cost antiretroviral treatment in developing countries and boost funding for community-based prevention programs. As a result of these efforts, infection and mortality rates gradually decreased. As of 2018, the infection rate has been reduced by

40% since peaking at 16,000 new infections per day in 1997. The number of AIDS-related deaths has likewise decreased by 56% since its peak in 2004 (UNAIDS 2019).

Over time, as new and better antiretrovirals were developed and multi-drug therapy became standard, the term “combination antiretroviral therapy” (cART) supplanted HAART. Today, the management of HIV with antiretroviral small-molecule drugs is simply called “antiretroviral therapy” (ART). Although monoclonal antibodies, gene therapies, and other innovative concepts are being explored in preclinical or clinical trials, small-molecule ART remains the only FDA-approved treatment modality for HIV/AIDS. In addition to treatment for people living with HIV, ART drugs may also be used preventatively by uninfected people at high risk of HIV infection in a strategy known as pre-exposure prophylaxis (PrEP). This approach is available in the US[25] and several other countries, but not yet worldwide. While PrEP can be highly effective, it requires strict daily adherence to an oral combination drug tablet. However, a recent clinical trial (HPTN 083) showed promising results for a new long-acting injectable PrEP drug, cabotegravir. Alternative PrEP strategies using monoclonal antibodies are also being pursued.

B. Classification of HIV and SIV viruses

The two major human immunodeficiency viruses, HIV-1 and HIV-2, are species in the genus *Lentivirus* within the family *Retroviridae*. Lentiviruses have been found in many mammals, including about 40 species of African monkeys and apes, and have species-specific tropism for their primate hosts[26]. Simian immunodeficiency viruses (SIVs) are lentiviruses that infect nonhuman primates, and are typically designated according to the host species. For example, SIV_{gor} is endemic in Western lowland

gorillas[27]. Specific SIV strains used in research are given a unique name, such as SIV_{smE660}[28].

Both HIV-1 and HIV-2 entered the human population via multiple zoonotic transmission events. HIV-1 is thought to have arisen from SIV_{cpz} in chimpanzees, and HIV-2 from SIV_{smm} in sooty mangabeys[29]. Of the two viruses, HIV-1 is more highly transmissible and virulent, and is the cause of most HIV infections worldwide, while HIV-2 is found mainly in western Africa. HIV-1 is further classified into groups M, N, O, and P[26]. Of these, Group M is responsible for the HIV pandemic, and is subdivided based on sequence similarity into subtypes (also called clades) designated with letters of the Latin alphabet, as well as a number of circulating recombinant forms (CRFs) harboring sequences from more than one subtype. The prevalence of different subtypes and CRFs varies by world region. Subtype C is most common in India and southern Africa; subtype B in the Western Hemisphere, Europe, and Oceania; subtype A in eastern Europe and parts of East Africa; CRF01_AE in Asia; and CRF02_AG in western Africa[30]. Less common subtypes include D, F, G, H, J, K and other CRFs. Worldwide, subtypes C and B are most prevalent.

HIV is unique among viruses in its exceptionally high genetic diversity, posing a formidable obstacle to eliciting broadly protective immune responses by immunization. Variation in HIV-1 Env sequences within a single chronically HIV-infected individual may be comparable to the total diversity of HA1 domain sequences in H3N2 influenza strains circulating worldwide in 1996[31].

C. Nonhuman primate models of HIV infection and AIDS

HIV-1 has a narrow species tropism, infecting only humans and chimpanzees and causing disease only in humans. To facilitate research on the mechanisms of HIV-1

infection and pathogenesis, and to test vaccines and therapies, various animal models have been developed, each with its own advantages and disadvantages[32]. Humanized mice—immunocompromised mice that are transplanted with human tissues to reconstitute the human immune system—are widely used to study HIV, and are able to mimic some aspects of HIV-1 infection. For example, the bone marrow-liver-thymus (BLT) mouse is created by engrafting fetal human thymus and liver into a mouse with a non-obese diabetic/severe combined immunodeficiency (NOD/*scid*) genetic background, followed by autologous hematopoietic stem cell transplant[33]. BLT mice infected with HIV-1 recapitulate the high viral loads and CD4+ T cell loss. Unlike some of the other mouse models, they support mucosal HIV transmission and T cell development in a human thymus. However, these mice are technically challenging to generate and maintain. Moreover, they lack a microbiome, have deficiencies in myeloid cell development, and do not recapitulate the effects of HIV-1 infection in non-hematopoietic tissues[32].

Given the shortcomings of mouse models, nonhuman primates (NHPs) have emerged as an indispensable tool for studying HIV-1 transmission, immunity, and pathogenesis. The most widely used NHP species is the rhesus macaque (*Macaca mulatta*), though other species including the pigtailed macaque (*M. nemestrina*) and cynomolgus macaque (*M. fascicularis*) have been used as well. In addition to living and reproducing well in captivity, rhesus macaques share 93% of their genome sequence with humans[34] and have similar physiology, neurobiology, and immune function, including responses to infectious pathogens. Rhesus macaques are classified into subspecies based on Indian or Chinese geographic origin, and most rhesus macaques in research colonies in the United States are descended from Indian-origin rhesus macaques.

Rhesus macaques are not natural hosts of SIV, but were infected with the virus from sooty mangabeys in captivity[35]. Extensive passage of SIV in rhesus macaques

ultimately gave rise to the viral swarms and clones used to model HIV infection. SIV_{mac239} is a commonly used molecularly cloned virus that causes AIDS in macaques in a time frame well suited to laboratory research[36]. Notably, it differs from HIV-1 due to its relatively weak macrophage tropism[37] and marked resistance to antibody neutralization[38], as well as its clonal nature. Because natural HIV-1 infection is characterized by high genetic diversity, viral swarms such as SIV_{smE660} and SIV_{mac251} have also been used to model HIV-1 transmission dynamics following mucosal exposure[39]. However, stochastic seeding of variants during transmission and adaptation during animal passage can change the swarm over time, necessitating characterization of the viral inoculum composition by deep sequencing[40]. Finally, it should be noted that not all SIVs cause disease in their natural host species; indeed, comparative studies of pathogenic and nonpathogenic lentiviral infections have helped to shed light on the determinants of virulence[41-43].

A major thrust of HIV research has been to develop a vaccine that elicits protective antibody responses against the HIV-1 Envelope glycoprotein (Env). A second, closely related goal has been to determine what properties of passively transferred monoclonal antibodies against HIV-1 Env are important for protective or therapeutic efficacy. However, SIV_{mac} Envs differ enough from their HIV-1 counterparts that antibodies to the latter do not usually recognize the former. To solve this problem, chimeric simian/human immunodeficiency viruses (SHIVs) have been constructed by inserting HIV-1 Env into the SIV (usually SIV_{mac239}) backbone. The result is a chimeric virus with most SIV proteins intact, but carrying Env from a particular HIV-1 isolate. Because sequences encoding the multiply-spliced HIV-1 accessory proteins Vpu, Tat, and Rev are located within the HIV-1 Env gene, and Vpr is adjacent to Env in the genome, these genes may be partially or fully incorporated in the SHIV genome as well (**Figure 1.1**)[44].

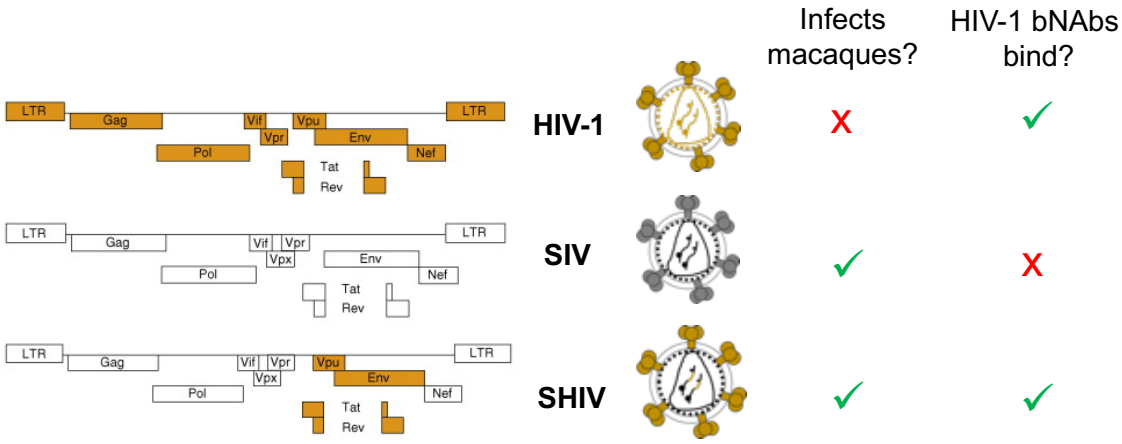

Figure 1.1. Structures and key properties of HIV, SIV, and SHIV. A map of the viral genome showing open reading frames (ORFs) and cartoons depicting the corresponding virion structures are shown for each virus. Genes and proteins of HIV-1 are in orange and those of SIV are in grayscale. The prototypical SHIV represented here incorporates HIV-1 Env, Vpu, Tat, and Rev into an SIV backbone. Figure adapted from Ambrose, et al., 2007 *Trends Biotechnol*.

It is important to note here that chimeric viruses with other combinations of HIV-1 and SIV genes exist, and are useful for studying other aspects of HIV-1 infection and treatment in macaques. For instance, SIV reverse transcriptase (RT) is insensitive to the non-nucleoside reverse transcriptase inhibitor (NNRTI) class of ART drugs; in order to test these drugs in macaques, RT-SHIVs have been developed in which the SIV RT is replaced with its HIV-1 counterpart[45]. In addition, simian-tropic (st)HIV-1 strains have been developed by replacing the HIV-1 *vif* gene with that from SIV_{mac239} or HIV-2, and Env with a macaque adapted SHIV Env. These viruses established productive acute infection in pigtailed macaques, though they were soon controlled by CD8+ T cells and did not cause CD4+ T cell loss[46], making them a poor model of HIV-1 pathogenesis.

Being artificially constructed viruses, SHIVs typically require adaptation by serial passaging in rhesus macaques to increase replicative capacity and pathogenicity[47-51]. Many different SHIVs exist and vary in their coreceptor usage, target cell tropism, CD4+ T cell depletion kinetics, pathogenesis *in vivo*, and sensitivity to antibody neutralization; these factors together determine how closely a SHIV models natural HIV-1 infection and predicts vaccine efficacy. HIV-1 infection is initiated by transmitted/founder variants that

exclusively use the CCR5 coreceptor for cell entry[52]. In some chronically infected individuals, however, emergence of CXCR4-tropic variants is a biomarker for disease progression[53]. Some SHIVs utilize both the CCR5 and CXCR4 co-receptors[47], while other SHIVs are exclusively CXCR4-tropic[54] or CCR5-tropic[49,51,55]. Coreceptor usage has been shown to dictate the SHIV target cell specificity and CD4+ depletion dynamics[56]. In general, CCR5-tropic SHIVs are similar to HIV-1 and SIV_{mac239} in that they cause a gradual decline in CD4+ T cell counts over months or years[51,55], while SHIVs that use CXCR4 cause rapid and profound CD4+ lymphopenia within the first few weeks[47,57]. Even closely related SHIVs can differ greatly in pathogenicity; for example, $SHIV_{DH12R}$, a highly pathogenic swarm, arose in a rhesus macaque infected with the nonpathogenic $SHIV_{DH12}$ molecular clone[48]. Finally, HIV-1 Envs have been classified into Tiers 1A, 1B, 2, and 3 based on the sensitivity of the Env-pseudovirus to antibody-mediated neutralization[58]. The same framework can be applied to SHIV Envs in order to evaluate the potency of vaccine-elicited antibody responses in NHP challenge and protection studies.

D. Virology of HIV and SIV

i. Viral replication: cell entry, reverse transcription, and integration

HIV-1 and SIV are enveloped positive-sense single-stranded RNA viruses with a genome approximately 10 kb in length. During viral replication, the process of reverse transcription generates a provirus, or DNA copy, which is integrated into the genomic DNA of the host cell and serves as a template for the production of new virions (**Figure 1.2**)[59]. The provirus has identical sequences known as long terminal repeats (LTRs) at the 5' and 3' ends. Each LTR can be subdivided into three regions called U3, R, and U5 that contain regulatory elements necessary for viral transcription and translation. The U3

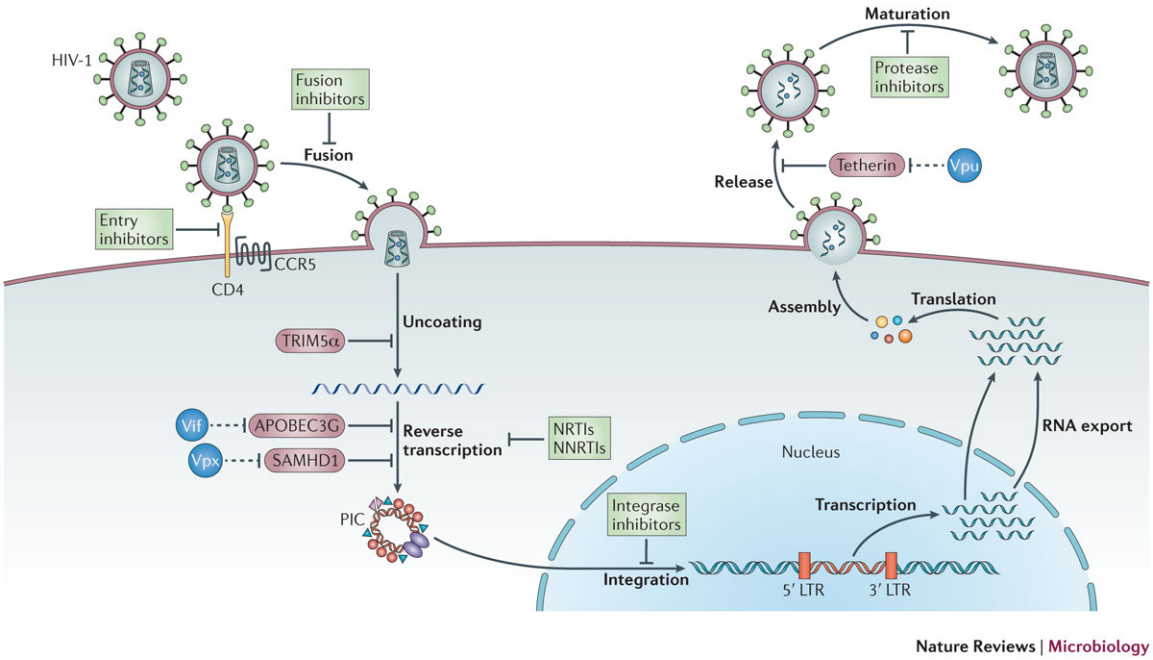

Figure 1.2. Illustration of the HIV-1 replication cycle and steps targeted by inhibitors. Binding of the HIV-1 virion to CD4 and CCR5 on the target cell surface triggers fusion of the viral and host membranes, leading to capsid internalization. The capsid then uncoats in the cytosol, and the viral RNA genome undergoes reverse transcription, generating cDNA. Next, the pre-integration complex (PIC) is formed and imported into the nucleus, where the viral cDNA is integrated into the host cell DNA. The integrated viral DNA (the provirus) serves as the template for the production of progeny virions. Viral RNAs are transcribed, exported, and translated, generating viral proteins that assemble at the cell membrane into immature virions. After budding and release from the cell membrane, the virion matures into an infectious particle. Host cell restriction factors (TRIM5α, APOBEC3G, SAMHD1, tetherin) that inhibit the viral replication cycle are shown in red. Viral accessory proteins (Vif, Vpx, Vpu) that counteract the restriction factors are shown in blue. Antiretroviral drug classes that inhibit the indicated steps of viral replication are shown in green. LTR, long terminal repeat. NRTIs, nucleoside reverse transcription inhibitors. NNRTIs, non-nucleoside reverse transcription inhibitors. Figure is from Barre-Sinoussi, et al., 2013 *Nat Rev Microbiol*.

region has numerous transcription factor binding sites and acts as an enhancer and promoter for the transcription of viral RNA from the integrated provirus, while the R and U5 regions contain signals for 5' capping, transcription termination, polyadenylation, packaging, as well as priming reverse transcription. Although the 5' and 3' LTRs are identical in sequence, the 5' LTR has much stronger promoter activity[60], while the 3' LTR mainly functions in transcript termination and polyadenylation.

Each viral particle is about 120 nm in diameter, and contains two copies of 5'-capped, polyadenylated, unspliced viral RNA packaged along with viral and host proteins inside a conical capsid. The capsid is surrounded by a lipid envelope derived from the host cell plasma membrane. The RNA genome contains all the sequences of

the DNA provirus except for the U3 of the 5' LTR and the U5 of the 3' LTR. The only viral protein on the virion surface is the Envelope glycoprotein (Env), a heterotrimer containing the membrane-spanning glycoprotein gp41 (TM) and a soluble glycoprotein gp120 (SU) that is noncovalently bound to gp41. Each Env trimer has three binding sites to the primary receptor, CD4, and three binding sites to the co-receptor, which is typically either CCR5 or CXCR4 for pathogenic lentiviruses including HIV-1 and SIV_{mac}. Notably, alternative coreceptors such as CXCR6 have been reported to mediate entry of non-pathogenic SIV into lymphocytes of their natural hosts[61,62], and loss of CXCR6 tropism is associated with emergence of lentiviral pathogenicity[63]. The major coreceptors CCR5 and CXCR4 are expressed mainly on CD4+ T cells and macrophages, restricting viral tropism to these cell types. The binding of Env to CD4 triggers a conformational change in Env that exposes a binding site for CCR5/CXCR4. Upon binding to the co-receptor, Env undergoes yet another rearrangement that results in the fusion of the viral and cell membranes, resulting in viral entry and release of the capsid into the cell cytoplasm[64].

Although HIV-1 typically infects target cells via CD4 and CCR5/CXCR4, it has also been reported to infect brain astrocytes, which do not express CD4, suggesting another mechanism for entry. This mechanism was later shown to depend on gp120 binding to the mannose receptor, followed by clathrin-mediated endocytosis[65,66].

As the viral capsid is partially disassembled, the viral reverse transcriptase (RT) enzyme makes a double-stranded DNA copy from the single-stranded RNA genome by a stepwise process. First, primed by a $tRNA^{Lys}$ bound to the PBS (primer binding site) located within the U5 region of the 5' LTR, the RT synthesizes a complimentary negative-sense DNA strand using the positive-sense RNA as template, forming an RNA-DNA duplex. As the RT moves along, it degrades the hybridized RNA template using its RNAse H endonuclease activity. Because the 5' and 3' LTR of the RNA genome overlap

in the R region, a template switch allows DNA synthesis to continue uninterrupted, picking up in the 3' LTR where it left off on the 5' LTR. An RNAse-H resistant section in the 3' LTR known as the polypurine tract (PPT) remains intact, enabling it to serve as a primer for the synthesis of the positive-sense DNA strand. The synthesis of this second strand proceeds through the PBS using the $tRNA^{Lys}$ as template, displacing the tRNA from its complementary RNA sequence. Meanwhile, the first DNA strand synthesis proceeds in the negative sense direction until it reaches the PBS, whereupon a second template switch results in the hybridization of the first and second DNA strands. All remaining RNA is degraded, and DNA synthesis proceeds to completion for both strands. The final product is a double-stranded linear provirus flanked by identical LTR sequences containing the U3, R, and U5 regions at both the 5' and 3' ends[67].

The provirus is bound by numerous viral and host proteins to form the pre-integration complex (PIC) which is imported into the nucleus. Key components of the PIC include the viral integrase (IN), which catalyzes proviral DNA processing and integration, and Vpr, a viral accessory protein that interacts with nuclear import machinery to ferry the provirus across the nuclear pore. Inside the nucleus, the PIC is targeted to the chromosomal DNA by the chromatin-associated host factor LEDGF/p75. The provirus is then inserted into the DNA of the host cell by the viral integrase (IN) enzyme. In the cytoplasm prior to nuclear import, IN cleaves a dinucleotide from each 3' end of the viral cDNA, leaving hydroxyl groups that attack the phosphate backbone of the chromosomal DNA in the nucleus. Termed DNA strand transfer, this reaction creates an intermediate in which the proviral and cellular DNA are covalently linked. The two 5' overhanging nucleotides are then cleaved from the proviral DNA, and the gap is filled in and ligated by cellular DNA repair machinery, completing proviral integration[68].

Importantly, not all viral cDNA is destined for integration into the host cell genome. The cDNA, digested at the 3' ends, can attack its own phosphate backbone to

generate truncated or internally rearranged circular viral DNA by auto-integration. The presence of double-stranded DNA in the cytosol can also trigger a protective host response whereby the linear DNA is circularized by DNA repair mechanisms into 1-LTR or 2-LTR products, which cannot integrate into the cellular DNA and are subsequently degraded[69]. Most PCR-based methods for quantifying total viral DNA in cells do not distinguish between integrated proviral DNA, unintegrated linear or circular proviral DNA, and 1- and 2-LTR circles.

ii. Viral replication: gene expression, virion assembly, and egress

The integrated proviruses of HIV-1, HIV-2, and SIV all contain 9 genes that encode the structural and nonstructural proteins required for immune evasion and virion assembly, albeit with some virus-specific differences in genes and functions. The conserved genes are *gag*, *pol*, *env*, *nef*, *vif*, *vpr*, *tat*, and *rev*. SIV and HIV-2 also have *vpx*, while HIV-1 lacks *vpx* but has *vpu*. Transcription is driven by the 5' LTR, which has binding sites for RNA polymerase II (RNAP II) and associated machinery, as well as numerous constitutive and inducible transcription factors including NFκB, NFAT, and AP-1. Transcription is strongly influenced by the activation state of the cell; NFκB becomes active in response to stimulation via the T cell receptor (TCR), so viral transcription is greater in activated T cells than in resting T cells. Histone acetyltransferases (HATs) and deacetylases (HDACs), as well as chromatin remodeling complexes, also modulate the accessibility of the LTR promoter and enhancer regions for initiating viral transcription. Under certain physiological conditions, the provirus is not actively transcribed and instead exists in a quiescent state known as latency. Cells that are latently infected harbor an integrated provirus but do not have active viral

expression. The mechanisms of induction and maintenance of latency are not fully elucidated, but may include cell quiescence, silencing of the LTR promoter by chromatin modifications, and transcriptional interference[70].

Transcription of the provirus can yield a single long primary transcript that begins with the first base of the R region in the 5' LTR and ends with the last base of the R region in the 3' LTR. However, initially, transcription tends to be prematurely terminated just downstream of the transcription start site and only rarely generates a full-length transcript. Once the complete transcript is produced and processed, the spliced mRNA is exported from the nucleus and translated in the cytoplasm. One of the first viral proteins generated is a protein called transactivator (Tat). Tat then enters the nucleus, where it binds to the transactivation response (TAR) element near the 5' end of the nascent RNA transcript to recruit an elongation complex, P-TEFb, that increases RNAP II processivity. This process in turn results in the production of much greater levels of full-length primary transcripts and therefore more Tat. This positive-feedback loop ramps up viral production exponentially. Viral production is greater in activated cells in part because of higher levels of the P-TEFb component Cyclin T1[71].

In addition to serving as the unspliced full-length RNA genome, the primary transcript can be processed into >30 partially or fully spliced mRNA species of various lengths. Because intron sequences present in unspliced and partially spliced mRNAs prevent their nuclear export, these transcripts stay in the nucleus. In contrast, the fully-spliced mRNAs are the first to be exported and the proteins they encode—Tat, Nef, and Rev—are the earliest to be translated. Once made, Rev returns to the nucleus, where it binds to the Rev response element (RRE) in partially spliced and unspliced mRNAs. Rev then interacts with nuclear export machinery, allowing these incompletely spliced mRNAs to be exported from the nucleus despite containing introns[72].

Most of the non-structural accessory proteins, including Tat, Rev, Nef, Vif, Vpr, Vpx (SIV and HIV-2 only), and Vpu (HIV-1 only), as well as the spike glycoprotein Env, are encoded by genes on multiply-spliced or singly-spliced transcripts. In contrast, the *gag* and *pol* genes are translated from the unspliced full-length transcript, and post-translationally cleaved to generate the mature structural proteins and enzymes from their polyprotein precursors. The Pol polyprotein cannot be translated alone. However, because *gag* is directly upstream of *pol* but in a different reading frame, a ribosomal -1 frameshift mechanism in 5-10% of *gag* translation events results in the Gag-Pol polyprotein[73]. More commonly, translation terminates at the end of *gag*, resulting in the Gag polyprotein. The ratio of Gag to Gag-Pol is tightly regulated for efficient virion assembly and maturation[74]. During virion maturation, which occurs after viral egress, the Gag polyprotein ($Pr55^{Gag}$) is cleaved by the viral protease into matrix (MA, p17), capsid (CA, p24 or p27 in HIV-1 and HIV-2/SIV respectively), nucleocapsid (NC, p7), p6, and spacer peptides SP1 and SP2. The Gag-Pol polyprotein ($Pr160^{GagPol}$) is likewise cleaved into MA, CA, protease (PR, p10), reverse transcriptase (RT, p66/p51), and integrase (IN, p32)[75].

Except for *env* and *vpu*, all viral genes are translated in the cytoplasm. The Gag and Gag-Pol polyprotein precursors orchestrate virion assembly and are packaged into immature viral particles at the plasma membrane[75]. Env is encoded by the *env* gene, and is synthesized as a polyprotein (gp160) by ER-associated ribosomes. The gp160 precursor is glycosylated, assembled into trimers, cleaved by the host cell protease furin into the soluble SU (gp120) and transmembrane TM (gp41) subunits, and delivered to the plasma membrane, where its gp41 cytoplasmic domain associates with Gag MA at the virion assembly site[76]. The full-length unspliced RNA genome is recruited to the virion by Gag NC, which recognizes an RNA packaging sequence (Ψ) located in the 5' region of unspliced RNA yet absent from spliced transcripts. Two copies of the RNA

genome are incorporated into each virion, recruited together as a dimer. Each copy is hybridized to a $tRNA^{Lys}$ in the 5' LTR to prime reverse transcription in the target cell[75]. Other viral proteins incorporated into the virion include Vif, Vpr, Nef, Tat, and (in the cases of HIV-2 and SIV) Vpx. As assembly of the spherical immature virion is completed, viral budding is triggered by the recruitment of the cellular ESCRT (endosomal sorting complexes required for transport) pathway by Gag. This mechanism, highly conserved across eukaryotes and hijacked by many enveloped viruses, involves a signaling cascade that leads to the polymerization of ESCRT-III filaments into a "dome" structure that constricts the membrane, resulting in membrane fission[77]. After viral release, the non-infectious immature virion undergoes a maturation process in which the Gag and Pol polyproteins are cleaved by viral protease, leading to structural rearrangement and assembly of the characteristic conical capsid enclosing the RNA genome copies and associated proteins. This maturation process is required for viral particle infectivity[75].

iii. Viral proteins and their functions

The genomes of HIV-1, HIV-2, and SIV share most of their proteins, with a few differences. All of these viruses have a set of structural proteins encoded by the *gag* gene, enzymes encoded by *pol*, and glycoproteins that mediate entry encoded by *env*. In addition, there are several regulatory and accessory proteins that play key roles in viral replication and evasion of the host immune response.

The *env* gene codes for a polyprotein, gp160, that is post-translationally cleaved into two subunits, TM (gp41) and SU (gp120). The TM subunit has a transmembrane domain, a trimerization domain, an intracellular C-terminus that interacts with Gag MA during viral assembly, and an extracellular N-terminus that binds noncovalently to the

soluble SU. Env normally exists as a trimer of TM/SU heterodimers on the surface of virions and infected cells, and is the spike that mediates cell entry by binding to CD4 and either CCR5 or CXCR4. However, the conformation of Env varies on a spectrum from closed, with the three SU monomers are in contact at the trimer apex, to open, in which they shift outward to expose the top of the TM stump. In addition, the non-covalently-linked SU may be shed entirely, revealing a naked TM stump. Only the closed Env trimer is able to mediate cell entry. Each of these conformations exposes a different set of potential antibody epitopes, many of which are decoys that distract the antibody response from targeting the closed trimer on the infectious virus. Env is also heavily glycosylated on its surface, shielding its protein core from host antibodies. However, numerous sites of vulnerability have been identified that, when bound by neutralizing antibodies, prevent viral entry. Due to their roles in receptor binding and membrane fusion, many of these neutralizing epitopes tend to be more conserved in sequence and structure than other, more variable parts of Env.

The *gag* gene codes for the structural proteins, which are translated as a polyprotein and cleaved inside the virion after budding to generate matrix (MA, p17), capsid (CA, p24 in HIV-1 or p27 in HIV-2 and SIV), nucleocapsid (NC, p7), and p6, as well as the two spacer peptides SP1 and SP2. Each of the Gag polyprotein domains plays a key role in virion assembly and maturation. The N-terminus MA domain contains a binding site for phosphatidylinositol-4,5-bisphospate ($PI[4,5]P_2$) which targets it to the plasma membrane, and a myristoyl moiety that stably anchors it in the membrane[75]. MA also recruits the cytoplasmic tail of Env into the Gag polyprotein lattice during virion assembly, although the mechanism of how Env is incorporated into virions is incompletely understood[78]. In addition, MA is a component of the PIC, and contains two nuclear targeting signals that allow it to act as a chaperone for the nuclear import of viral DNA in the target cell[79]. The Gag NC domain contains two zinc finger motifs that

recognize the packaging signal Ψ in the unspliced RNA genome, promoting its recruitment into the virion[75]. After the polyprotein is cleaved during maturation, CA becomes the subunit that self-assembles into the conical capsid, enclosing the viral RNA and other proteins inside[75]. The p6 polypeptide domain facilitates incorporation of Vpr into virions[80] and promotes efficient budding from the plasma membrane[81]. SP1 promotes the organization of Gag polyproteins into a stable lattice and is required for viral particle assembly[82]. The role of SP2 itself is less well defined, but proteolytic cleavage at the SP2-p6 junction appears to be important for virion infectivity and proviral integration[83,84].

The *pol* gene is translated from unspliced viral RNA as a result of a ribosomal frameshift during Gag translation, yielding a Gag-Pol polyprotein that includes the protease (PR), reverse transcriptase (RT) and integrase (IN) domains[73]. The PR domain acts *in cis* and *in trans* during virion maturation to cleave Gag and Gag-Pol into their monomeric components, and is required for making an infectious viral particle[75]. RT and IN both act inside the target cell after viral entry. RT synthesizes a DNA copy of the viral RNA genome, and IN catalyzes its 3' processing and integration into the genome of the host cell.

In addition to the main structural genes, HIV-1, HIV-2, and SIV contain a set of accessory proteins that enhance viral replication and promote evasion of the host immune response. In HIV-1, these proteins include Vif, Vpr, Vpu, Nef, Tat, and Rev. SIV and HIV-2 lack Vpu, but have a protein called Vpx that is not present in HIV-1.

Viral infectivity factor (Vif) promotes reverse transcription in the target cell by interfering with a host antiviral defense mechanism involving the cytidine deaminase APOBEC3G[85]. In the absence of Vif, APOBEC3G is incorporated into progeny virions during viral assembly in the infected cell. During reverse transcription in the target cell, APOBEC3G introduces mutations into the viral genome by catalyzing the deamination of

cytidine to uracil in the nascent viral cDNA, resulting in G-to-A hypermutation that renders the proviral genome replication-defective. However, Vif depletes APOBEC3G concentrations by inhibiting its translation and increasing its proteasomal degradation in the infected cell, thereby preventing its incorporation into progeny virions[86].

Viral protein R (Vpr) facilitates the nuclear import of the PIC, enables the infection of non-dividing cells such as macrophages, and activates transcription from the LTR[87]. One of the most well-studied functions of Vpr is its induction of a DNA damage response that leads to cell cycle arrest in G_2, a stage conducive to increased LTR-driven transcription[88,89].

Viral protein U (Vpu), which is present in HIV-1 and SHIV but not HIV-2 and SIV, is encoded on the same mRNA transcript as Env. It is likewise translated by ER ribosomes and enters the secretory pathway, ending up in the plasma membrane. However, it is not incorporated into virions, but assists with virion release by directing the degradation of the host protein tetherin[90]. Tetherin is upregulated by the host cell as an antiviral defense mechanism, and is a cell surface protein that binds the viral particle and prevents its release from the plasma membrane after budding. Vpu has an additional role in promoting the degradation of CD4 in the ER, so as to prevent Env-CD4 interactions that would interfere with Env incorporation into virions and downstream viral entry into target cells[91,92].

Negative infectivity factor (Nef) is an accessory protein that is encoded by a single unspliced ORF in the 3' end of the provirus, although it is translated from a multiply spliced transcript. Nef plays myriad and complex roles in viral infectivity and pathogenesis that are incompletely elucidated. It downregulates CD4 expression in infected cells[93] and contributes to evasion of the immune response by promoting the internalization of MHC-I molecules on the cell surface[94]. Nef also triggers the downregulation of the T cell receptor (TCR), CD3, and CD28; interferes with signaling

pathways involved in lymphocyte activation; and enhances the intrinsic infectivity of viral particles[95]. The *nef* gene is under strong selective pressure *in vivo*, as demonstrated in macaques by the evolution of a live attenuated *nef*-deficient SIV to a pathogenic form resulting in progression to AIDS[96]. Key insights into the role of *nef* in human HIV-1 infection were gained from the Sydney Blood Bank Cohort (SBBC), which consists of a donor and eight transfusion recipients infected with an attenuated strain of HIV-1 with deletions in the *nef*-LTR region. Longitudinal analysis of a subset of this cohort revealed variable outcomes, with some individuals showing high viremia and CD4 decline, and others remaining aviremic and asymptomatic for 14-18 years after infection[97]. Over time, SBBC *nef*-LTR sequences converged toward a minimal form containing only LTR elements absolutely required for viral replication, suggesting that while partial *nef* deletions are detrimental to viral fitness, Nef itself is not strictly required for HIV-1 replication and pathogenesis[98].

Like Nef, Transactivator (Tat) is expressed from a multiply-spliced mRNA transcript. Tat binds to the transactivator response (TAR) element on nascent RNAs near the viral transcription start site, and has motifs to recruit elongation factors that modify RNAP II, increasing the production of full-length viral RNA transcripts. In the absence of Tat, transcription is arrested just downstream of the start site and full-length transcripts are generated only rarely[71].

Regulator of expression of virion proteins (Rev) is involved in the export of viral mRNA containing introns, which would normally be retained in the nucleus. Expressed from a multiply spliced mRNA transcript, it is one of the first viral proteins to be translated in the cytoplasm. Rev has a nuclear import signal that allows it to return to the nucleus, where it binds to the Rev response element (RRE) motif located in an intron downstream of the *env* gene on nascent mRNAs. It also contains a nuclear export signal

that allows it to interact with nuclear pore factors to mediate the export of unspliced or partially spliced mRNA transcripts from the nucleus[99].

Viral protein X (Vpx) is conserved in SIV and HIV-2, and is absent in HIV-1. It is packaged into virions and functions in the newly-infected target cell to counteract SAMHD1, a host cell factor that inhibits reverse transcription by depleting cytosolic pools of deoxynucleoside triphosphates (dNTPs). Macrophages, dendritic cells, monocytes, and resting CD4+ T cells normally have high levels of SAMHD1 and low levels of cytosolic dNTPs. By targeting SAMHD1 for proteasomal degradation, Vpx allows SIV and HIV-2 to infect these cell types. In contrast, HIV-1 lacks Vpx and is therefore restricted in these cell types by SAMHD1[100]. In addition, Vpx was recently shown to antagonize the cGAS-STING pathway and interfere with NFκB nuclear translocation and induction of type I interferons[101]. Because cGAS-STING and NFκB induce type I interferons in response to SAMHD1 depletion[102,103], Vpx-mediated suppression of this pathway is effectively a counterattack to the cell-intrinsic response to SAMHD1 depletion by Vpx.

iv. Timeline of infection and pathogenesis

Although the kinetics of typical time to disease differs for HIV-1, SIV, and SHIV, they all share the same general course of infection and mechanisms of pathogenesis. HIV-1 infection is most commonly initiated at mucosal sites (oral, vaginal, rectal) but may also occur through direct blood exposure (intravenous inoculation, needle stick), and SIV and SHIV are transmissible by these routes as well. At the portal of entry, viral particles may directly infect CD4+ CCR5+ target cells, initiating viral reservoir seeding. Virions may also encounter patrolling myeloid cells that can take up the virus and transport it to

lymphoid tissues, which are rich in target cells and can support robust viral replication[104]. We and others have shown in the rhesus model that SIV and SHIV are present in distal tissues within one day of oral exposure and increase rapidly over the first 1-2 weeks[105,106]. The kinetics of HIV-1 dissemination in human tissues during early infection are difficult to study and are not known precisely, but are likely analogous.

In the plasma of adult macaques, SIV and SHIV viral loads peak within the first 3 weeks following mucosal exposure and subsequently decrease to a steady state level, known as the set point, that is relatively stable over time but varies between individuals. Evidence from longitudinal and serial sacrifice NHP studies suggests that the viral reservoir is largely seeded in the first few days and weeks of acute infection[105-107]. In humans, acute HIV-1 infection follows a similar pattern, although on a longer timescale, with an eclipse period followed by several weeks of increasing viremia that peaks and subsequently decreases. HIV-1 viral loads typically peak around 10^5-10^6 viral RNA copies/ml plasma and stabilize around 10^2-10^4 copies/ml. Individual determinants of viral loads and disease progression are not fully understood, but likely depend on host genetics (especially CCR5 and MHC alleles)[108] as well as viral fitness[109]. Viremia caused by SIV and SHIV also varies between individuals, but tends to be higher, peaking at 10^7-10^8 copies/ml and stabilizing between 10^3-10^6 copies/ml in adult rhesus macaques.

One major difference between pathogenic SIV, SHIV, and HIV-1 infections is their respective time to disease. Pathogenic SIV strains, such as SIV_{mac239}, typically cause opportunistic infections and other signs of simian AIDS within 6 months to 2 years in adult macaques[36]. In contrast, while untreated HIV-1 is nearly uniformly lethal, the median survival time in adults is about a decade after seroconversion[110]. In the case of SHIV pathogenesis, outcomes can differ in different animals and run the gamut from severe terminal disease on a timeline similar to SIV_{mac239}[47,51,55] to spontaneous resolution by host immunity[111]. Importantly, pathogenesis of HIV in infants occurs more rapidly than

in adults. Infants who are vertically infected with HIV-1 have high viral loads[112] and a median survival time of < 2 years[113]. Analogously, in infant macaques exposed at 1 month of age, untreated $SHIV_{SF162P3}$ infection causes disease within weeks of exposure[105,114].

The acute infection period is marked by rapid viral dissemination and tissue reservoir seeding, with peak viremia accompanied by a transient dip in CD4+ T cells in peripheral blood. During this time, the immune system undergoes drastic and sweeping changes, including the acute and irreversible depletion of intestinal Th17 cells[41,115], permeabilization of the intestinal barrier and microbial translocation into the bloodstream[116,117], generalized immune activation[118], alterations in monocyte and CD8+ T cell subsets[119-121], and loss and dysregulation of plasmacytoid dendritic cells[122]. Hypergammaglobulinemia, expansion of transitional memory B cells, and dysregulation of the B cell compartment are also observed[123]. The systemic inflammation in turn leads to damage and fibrosis of lymphoid tissue architecture, hindering its ability to support the development of adaptive immune responses. In time, these changes lead to immune dysfunction, T cell exhaustion, loss of CD4+ T cells, and failure to control infection. Chronic immune activation also promotes viral replication and persistence, completing the vicious cycle[124].

In adult humans with HIV-1, AIDS is defined by the decline of CD4+ T cells in peripheral blood to <200 cells/μl, as well as the emergence of infection with opportunistic pathogens and certain malignancies like Kaposi's sarcoma. In infants, CD4 counts are naturally higher, and are therefore a poor measure of disease progression; the percentage of CD4+ T cells among peripheral blood leukocytes is used as a biomarker instead, with <15% CD4+ cells indicating AIDS. In rhesus macaques infected with SHIV or SIV, disease progression is associated with skin rashes and lesions, opportunistic bacterial infections, and loss of CD4+ T cells.

v. The persistent reservoir as an obstacle to HIV cure

The HIV-1 replication cycle relies on the synthesis and integration of a DNA copy of the viral genome—the provirus—into the chromosomal DNA of the infected cell. Once integrated, the provirus persists in the host cell's genome indefinitely. If the cell divides, the provirus is carried on in all of that cell's progeny. Even during suppressive ART treatment, the persistence of the viral reservoir may be maintained by several mechanisms, including low-level viral replication and integration into new target cells in select anatomic compartments, homeostatic proliferation of infected memory CD4+ T cells, and longevity of the CD4+ memory T cell pool[125]. CD4+ T cells harboring replication-competent proviruses may remain in a resting, or latent, state during which no viral production is taking place. Such latently infected cells comprise part of the HIV-1 reservoir in adults[126,127] and children[128] and are effectively invisible to the immune system, as they do not express viral mRNA or proteins and do not display viral peptides on MHC-I. Although CD32a has been suggested as a possible cell surface marker of latently infected CD4+ T cells[129], other groups have failed to replicate these findings[130-132], and no marker of the latent reservoir has been conclusively identified.

A curative strategy that can eliminate the persistent HIV-1 reservoir remains an unmet goal. Nonetheless, the development of antiretroviral therapy (ART) has effectively made HIV-1 a manageable chronic infection for those able to access treatment. These drugs are small molecules that halt virus production by inhibiting key steps of the viral replication cycle. Currently there are 6 classes of FDA-approved antiretroviral drugs: nucleoside analog reverse transcriptase inhibitors (NRTIs) and non-nucleoside reverse transcriptase inhibitors (NNRTIs) that block reverse transcription; integrase inhibitors that block proviral DNA integration; protease inhibitors that block the cleavage of Gag and Gag-Pol polyprotein, which is essential for virion maturation; and fusion inhibitors

and chemokine coreceptor antagonists that inhibit viral entry. Taken daily, ART is able to "turn off the faucet" and suppress viral replication in infected cells, reducing viremia to undetectable levels. However, ART interruption (ATI) in individuals with established reservoirs almost invariably results in viral rebound within days of treatment cessation. Once infection is established, the reservoir decays very slowly during ART; it has been estimated that 73.4 years of treatment would be needed to eliminate an HIV-1 reservoir of approximately 10^6 cells[127,133].

In addition to CD4+ T cells and possibly macrophages, HIV-infected astrocytes have been proposed to be a viral reservoir in the brain. A recent study of adoptive transfer of HIV-infected astrocytes into uninfected humanized mice demonstrated that astrocytes can transfer the virus to CD4+ T cells, leading to systemically disseminated infection when the T cells migrate to secondary lymphoid organs. This process occurs even in the presence of ART, further raising the barrier to HIV cure using ART alone[134].

E. Immune responses to HIV/SIV

i. Intrinsic and innate immunity

Anatomical barriers represent the first line of defense against viral pathogens, including HIV and SIV. For instance, unbroken skin effectively blocks these viruses from entering the blood. In addition, mucosal tissues such as the vagina, rectum, and gut are lined with epithelial cells that secrete thick mucus and antiviral molecules such as defensins, inhibiting most viral entry. Virions that make it across these barriers encounter the lamina propria, a subepithelial layer rich in blood vessels and immune cells. Here, host recognition of viral infection occurs through cell-intrinsic and cell-extrinsic innate immune mechanisms. In infected macrophages or CD4+ T cells, viral genomic RNA is sensed by RIG-I and/or MDA5, and nascent viral cDNA generated during reverse

transcription is sensed by IFI16 and/or cGAS. Sensing by RIG-I and MDA5 triggers a signal cascade mediated by the adapter MAVS and transcription factors IRF3, IRF7, and NFκB to induce the expression of inflammatory cytokines, such as TNF-α, IL-6, IL-12, and type I interferons like IFN-α and IFN-β. Similarly, IFI16 and cGAS signal through STING to activate IRF3 and NFκB. In addition, cells of the innate immune system—including macrophages, monocytes, dendritic cells, and granulocytes—can also take up HIV virions via endocytosis or macropinocytosis. In their endosomal compartments, Toll-like receptors 7 and 8 (TLR7 and TLR8) bind viral single-stranded RNA and signal through MyD88, leading to the NFκB- and IRF-mediated expression and secretion of type I IFNs. IFN then signals in an autocrine or paracrine manner by binding to IFN receptors (IFNARs) on the same cell or nearby cells, activating the JAK/STAT pathway to induce the expression of hundreds of interferon-stimulated genes (ISGs) with diverse functions that contribute to antiviral defense. Some of these ISGs, including TRIM5α, SAMHD1, tetherin, APOBEC3G, and MX2, are lentiviral restriction factors that specifically inhibit HIV and/or SIV replication[135].

The type I IFN response likely plays complex and opposing roles in HIV-1 control and disease progression[136]. Treating macaques with type I IFN suppresses acute SIV infection[137], and IFNα2 treatment of humans on ART improves viral control after treatment interruption[138], suggesting that this pathway is an important mechanism of viral control. There is also evidence of selective pressure driving HIV-1 and SHIV escape from type I IFN responses[139,140]. However, comparative studies of pathogenic and nonpathogenic SIV infection have demonstrated that, while type I IFN responses occur during acute infection regardless of pathogenicity, only in pathogenic infection do they persist during the chronic phase, in concert with greater immune activation[141,142]. These findings suggest that while the type I IFN system is important for initial control of

infection, sustained IFN responses may be deleterious and contribute to the ongoing immune activation that drives disease progression in HIV-1 and pathogenic SIV infection. Indeed, type I IFN expression is positively correlated with viremia[143] and is associated with CD4+ T cell dysfunction and loss during chronic HIV-1 infection[144]. With respect to the IFN response, there may be a tradeoff between effective control of chronic viral infection *versus* inflammatory damage and immune exhaustion.

In addition to cell-intrinsic responses, cell-extrinsic responses allow the effector cells and other components of the innate immune system to directly kill infected cells. Upon recognition of viral molecular patterns, pro-inflammatory cytokines, or opsonized antigen, effector cells become activated and increase in their ability to destroy pathogens. Each type of effector cell has a distinct mechanism. NK cells express various receptors that allow them to recognize virus-infected cells, which they destroy through perforin and granzyme-mediated lysis. Macrophages take up infected cells through phagocytosis and traffic them to lysosomal compartments for destruction. Neutrophils degranulate, releasing cytotoxic compounds. Finally, the complement system consists of soluble blood proteins that, when activated, undergo sequential cleavage steps that generate pro-inflammatory intermediates and culminate in the assembly of a membrane attack complex (MAC) that lyses the cell membrane. Complement can be activated by several distinct pathways that differ in the initial trigger: the binding of antibodies to a cell-surface antigen, binding of mannose-binding lectins to cell-surface sugar moieties, or the spontaneous cleavage of C3 into C3a and C3b. The importance of complement in controlling HIV/SIV infection is controversial, and complement activation products have been suggested to facilitate HIV-1 infectivity and spread *in vivo*[145].

ii. Adaptive immunity

Innate immunity recognizes general classes of pathogens with germline-encoded PRRs and can mobilize quickly to provide a first line of defense. In contrast, adaptive immune responses rely on the custom generation of exquisitely specific receptors on B and T cells, and provide strong and rapid protection on subsequent exposures to the same pathogen. Antigen-presenting cells, such as macrophages dendritic cells, bridge innate and adaptive immunity.

T cells express unique T cell receptors (TCR) that are produced by the recombination of germline-encoded V, D, and J segments chosen among many alleles of each gene. Naïve T cells become activated upon receiving two signals from antigen-presenting cells (APCs): 1) T cell receptor (TCR)-mediated recognition of viral peptides/MHC complexes, and 2) a costimulatory signal, such as CD28 binding to CD80/CD86, ICOS binding to ICOSL, or OX40 binding to OX40L. A third signal may be provided by the uptake of cytokines secreted by the APC. Following activation, the T cell proliferates and differentiates into effector or memory subsets. Most of the effector and memory T cells die, but a small number of long-lived memory T cells remain in a dormant state until their next antigen exposure.

CD4+ T cells recognize peptides on MHC-II. Upon activation, a CD4+ T cell proliferates and becomes polarized by the cytokine milieu to differentiate into one of several classes: Th1, Th2, Th17, Treg, or Tfh. Each class secretes a distinct set of cytokines that promote specific types of immune responses. Th1 cells secrete mainly IFNγ, which creates an antiviral state by enhancing the cell killing functions of CD8+ T cells, NK cells, and macrophages. Th2 cells make IL-4, IL-5, IL-9, and IL-13, driving increased IgE production and eosinophil activation, and are associated with anti-parasitic responses and allergies. Th17 cells make IL-17, IL-21, IL-22, and IL-23, which

are important for antibacterial and antifungal immunity. Tregs secrete IL-10 and TGF-β, which dampen inflammation and promote immune tolerance. Finally, Tfh cells localize to the B cell zone in secondary lymphoid organs, where they direct germinal center (GC) formation and modulate B cell responses by providing co-stimulation via CD40/CD40L and secreting IL-21. During HIV/SIV infection, Th1 responses are a critical part of the antiviral response[146], although excessive frequencies of Th1 CD4+ cells in mucosal tissues were detrimental to protection from SIV challenge in a recent vaccine study[147]. Given the vital role of Tfh cells in promoting B cell responses, boosting their function may also be an important strategy for therapies and vaccines aimed at inducing antibody-mediated protection or control of HIV[148]. However, HIV and SIV infection cause the acute loss of memory CD4+ T cells, especially Th17 cells in the gut[41,115,149,150], and induce gradual CD4+ T cell depletion over the long term. These changes impair the ability of the CD4+ T cell compartment to effectively respond to insults and eventually lead to AIDS, defined in human adults as CD4+ count below 200 cells/μl.

CD8+ T cells recognize viral peptides on MHC-I molecules, make IFNγ to amplify the antiviral response, and directly kill infected cells by secreting perforin and granzyme B. Numerous lines of evidence suggest that CD8+ T cell responses are critical for the post-acute control of HIV and SIV. For instance, CD8+ T cell depletion results in a transient increase in SIV viremia in macaques[151]. Moreover, certain MHC-I alleles in humans and macaques are strongly associated with superior long-term HIV and SIV control in the absence of ART[152-155]. CD8+ T cells recognize relatively conserved epitopes in the viral genome, for instance *Gag*, making them an attractive target for vaccine or therapy. Indeed, a vaccine approach using a cytomegalovirus vector to induce CD8+ T cell immunity has shown 50% efficacy in clearing SIV reservoirs in rhesus macaques[156]. However, T cell responses alone are unlikely to provide sterilizing

immunity. Moreover, during chronic infection, CD8+ T cells are persistently activated and become functionally exhausted, upregulating markers like PD-1, LAG3, TIM3, and TIGIT and losing their cytotoxic capacity[121,157-161]. CD8+ T cell exhaustion is associated with higher viral loads and more rapid disease progression in SIV and HIV infection, and its prevention or reversal is an important goal of HIV cure research.

Like T cells, naïve B cells also bear a unique antigen receptor (B cell receptor, BCR) on their surface, with diversity in the variable region generated by the recombination of several germline gene segments among many possible alleles. Naïve B cells express IgM and IgD BCRs. Upon binding of a cognate antigen to the BCR, B cells are able to take up the antigen by endocytosis, process it into peptides, and present the peptides to CD4+ T cells on MHC-II surface receptors. To become activated, naïve B cells bearing BCRs specific for a protein antigen require 1) crosslinking of the BCR by the antigen, and 2) a cytokine signal provided by T cells recognizing the peptide antigen presented by the B cell. Following activation, the naïve B cell may become a plasmablast, which is a short-lived cell that secretes its BCR (a soluble secreted BCR is an antibody). Alternatively, it may enter the GC, where the BCR is altered by the processes of class switching, somatic hypermutation, and affinity maturation. In the GC dark zone, B cells undergo clonal expansion and somatic hypermutation (SHM), in which the activation-induced cytidine deaminase (AID) randomly introduces C-G to A-T mutations into the BCR sequence, diversifying the BCR repertoire. In the light zone, the new BCRs compete to bind their cognate antigen expressed on follicular dendritic cells (FDCs). The B cell clones with the highest affinity survive, while weaker binders undergo apoptosis. Tfh cells may also provide co-stimulatory signals via CD40/CD40L and cytokines (IL-21) that direct the B cell to undergo class switching. In this process, the constant region of the B cell receptor is modified by rearrangement of the heavy chain locus. This process results in the surface expression of a different BCR class, such as

IgG (subclasses 1-4), IgE, or IgA (subclasses 1-2), instead of IgM and IgD. When secreted as antibodies, these Ig classes each have different structural properties that tune their functions and interactions with the innate immune system. The B cell can now re-enter the dark zone for another round of SHM, or it may exit the GC and differentiate into a memory B cell or a plasma cell. Memory B cells are long-lived quiescent cells that can quickly differentiate into antibody-secreting cells upon antigen exposure. Plasma cells are long-lived cells that reside in the bone marrow and constitutively secrete antibody, maintaining relatively constant levels of circulating antibody that can provide sterilizing protection.

The B cell compartment is profoundly altered during HIV infection, as evidenced by acute memory B cell loss, proliferation of immature transitional B cells and plasmablasts, increased cell turnover, and hypergammaglobulinemia[123,162]. Nonetheless, most people mount an antibody response to HIV within a few weeks of infection. Env is the main target of the antibody response, and only anti-Env antibodies have the potential to neutralize the virus. Initially, antibodies recognize only the transmitted/founder variant. However, the viral Env mutates rapidly and evolves in response to immune pressure, resulting in escape variants. The antibody response in turn evolves through SHM and affinity maturation to neutralize the new variants in circulation. NHP studies of B cell depletion prior to and during SIV infection showed that antibody responses are important in viral control during acute and/or early chronic infection[163,164]. However, the role of antibody responses in controlling chronic HIV-1 is less well established. In one case report, an HIV+ lymphoma patient treated with rituximab (anti-CD20 monoclonal antibody for B cell depletion) experienced a transient decrease in neutralizing antibody titers that was associated with an increase in plasma viremia[165]. Yet, because these changes occurred 16 weeks after the last rituximab treatment, and antibody-secreting plasma cells do not express CD20, these observations cannot be definitively attributed

to rituximab. More importantly, no statistical conclusions can be drawn from a case report with one participant. Larger, well-controlled studies of B cell depletion in people living with HIV have not been performed.

II. Perinatal HIV infection

A. The scale of the problem

Vertical acquisition of HIV-1 remains prevalent in many resource-limited regions. Through international initiatives to prevent vertical transmission, substantial progress has been made since 2000, when about 450,000 [estimates range 300,000 – 700,000] children acquired HIV. However, the rate of progress has largely stalled, with only a 20% decrease in infections in 2018 as compared with 2014. Approximately 160,000 [estimates range 110,000 – 260,000] children were newly infected in 2018[166]. Of these children, 86% were in the WHO African Region. In 2018, about 1.3 [estimates range 1.0 – 1.6] million pregnant women were living with HIV, of whom 82% [62% – 95%] were accessing ART (WHO Global Health Observatory data).

B. HIV infection in infants and children

i. Transmission

Nearly all children who become infected with HIV acquire it through vertical transmission. HIV can be transmitted from a pregnant woman with HIV to her infant during gestation, during labor and birth, and postpartum via breastfeeding. Intrauterine transmission is less common than peripartum or postpartum, and tends to occur later in pregnancy. In the absence of breastfeeding, about 30% of new infections occur *in utero*, and 70% peripartum. In breastfeeding populations, about 20-50% of new infections are

attributable to breastfeeding, with the relative proportion (and absolute risk) increasing with greater duration[167]. The overall risk of vertical HIV transmission ranges from 15% in non-breastfeeding populations to as high as 45% in the setting of extended breastfeeding. After 6 weeks of age, the risk of vertical transmission is about 1% per month of breastfeeding (WHO 2006). Nonetheless, the WHO, UNAIDS, and UNICEF guidelines recommend exclusive breastfeeding in low-resource settings, as mixed feeding with either solids or formula is associated with a higher risk of HIV transmission[168].

During breastfeeding, infants acquire HIV via oral exposure to virus in the breastmilk. Likewise, during labor and birth, infants are thought to become infected via mucosal (likely oral) exposure to virus in maternal blood and secretions. The risk of transmission is proportional to the mother's viral load in blood and breastmilk, as well as her clinical stage of HIV disease and immunologic status. Effective ART treatment during pregnancy, birth, and breastfeeding can therefore markedly reduce the risk of vertical transmission. Even small changes to the treatment regimen can have an impact. For example, in mother-infant pairs receiving zidovudine during late gestation and for one week postnatally, a single dose of nevirapine during labor can substantially reduce the risk of perinatal transmission[169].

A unique feature of vertical HIV transmission is that it occurs in conjunction with the transfer of maternal antibodies to the newborn during late gestation and breastfeeding. Maternal antibodies are thought to contribute to a viral bottleneck during transmission, although their role in limiting transmission is not straightforward. Viral variants established in the infant are commonly resistant to neutralization by maternal antibodies, suggesting selective pressure on the transmitted/founder virus[170-172]. In addition, vertically infected infants that received maternal antibodies with antiviral functions, such as antibody-dependent cellular cytotoxicity (ADCC), had a reduced risk

of mortality[173]. However, comparison of autologous neutralization titers in transmitting vs. non-transmitting mothers failed to show a link between neutralizing activity and transmission risk, suggesting that other factors may play a larger role[174]. Importantly, maternal HIV infection is associated with perturbations in transplacental transfer of maternal antibodies, including altered glycosylation profiles, Fc receptor binding activity, impaired functional (ADCC) activity, and reduced overall transfer[173,175].

ii. Viral loads, disease progression, and prognosis

In infants, HIV infection is characterized by high viral loads, weak control of post-acute viremia, and consequently rapid progression to disease[112]. Without treatment, >30% of infants die in their first year of life, and over half die by age 2[113]. Among infants who acquired HIV-1 vertically, age at the time of HIV-1 infection is correlated with survival rate, with mortality highest among those infected before 4 weeks of age and decreasing gradually over the first year of life[113,176,177]. This age-dependent decrease in mortality may be attributable at least in part to immune maturation during infancy, resulting in an increasing capacity for defense against viral pathogens and attenuated damage to the immune system.

Neonatal immunity is distinct from that of adults in ways that are presumed to hinder newborns' ability to control viral infection. Newborns have an immature immune system characterized by greater Treg-mediated suppression and Th2 bias, deficiency in Th1 responses, underdeveloped humoral immunity, and impairments in T cell priming and other innate effector functions[178,179]. Human and animal studies of HIV infection have identified CD8+ T cell responses as a major mechanism of viral control[180]. Weak CD8+ T cell responses are observed in HIV-infected children under 3 years of age, especially those with depleted or phenotypically altered CD4+ T cells in conjunction with

high viral loads[181]. Regulatory T cells (Tregs), an abundant anti-inflammatory T cell subset in newborns, are conjectured to play multifactorial and opposing roles in HIV-1 infection by suppressing either beneficial virus-specific CD8+ T cell responses, deleterious immune hyperactivation, or both[182]. Although the relationship between immune activation and pathogenesis in infants is not well characterized, in one study, CD8+ T cell activation in infants at 1-2 months of age was predictive of disease progression[183]. In addition to functional deficiencies that impede antiviral defense, infants and newborns are at a disadvantage due to elevated numbers of potential target cells. Newborn and infant rhesus macaques have greater counts and frequencies of CD4+ T cells[184], notably activated CD4+ CCR5+ memory T cells that are prime targets for infection with SIV[43,185]. These cells are likewise abundant in the human gut at birth, and may be a key target cell population during vertical HIV-1 acquisition[186].

C. Clinical care for HIV-exposed and -infected children

i. Diagnosis and treatment

Because transmission is most likely to occur late in pregnancy or peripartum, the risk is minimized by administering ART during pregnancy and to newborns as early as possible after birth. The seminal ACTG 076 study showed that, in high-resource settings, administration of the ART drug zidovudine to mothers during pregnancy and intrapartum, and to newborns for the first 6 weeks of life, reduced transmission risk by two thirds[187]. However, even when mothers were not treated, infection risk was reduced by treatment of the newborn with zidovudine beginning within 48 h of birth, although treatment beginning at 3 days of age or later was ineffective[188]. Based on these findings, the WHO recommends that HIV-exposed newborns receive ART as post-exposure prophylaxis for the first 4-6 weeks of life, beginning as early as possible—ideally within 6-12 hours of

birth. The exact ART regimen is determined based on several factors, including the mother's use of ART, her timing of infection, and her viral load and clinical status, as well as the infant feeding method. More aggressive prophylaxis regimens with multiple drugs and longer treatment durations are indicated for babies at higher risk.

Because lengthy, complex, and expensive interventions like the full ACTG 076 regimen are not always feasible in low-resource settings, clinical trials have also tested shorter or simplified ART regimens for prevention of vertical HIV-1 transmission. A trial in Thailand showed a 50% reduction in transmission when mothers received zidovudine late in pregnancy and during labor, without treatment of the newborn[189]. The participants in this study did not breastfeed, limiting the applicability of findings to settings where breastfeeding rates are high. Nonetheless, in the HIVNET 012 trial in Uganda, a single dose of nevirapine to the mother intrapartum and to the newborn postnatally was more effective than an intrapartum and one-week postnatal regimen of zidovudine[190]. The difference in HIV-free survival was sustained at 18 months despite moderate to high breastfeeding prevalence[191], suggesting that short intrapartum/postpartum ART regimens can significantly mitigate transmission risk even in breastfeeding populations.

Because of the presence of maternal HIV antibodies in the newborn during early life, a serological test cannot be used to detect HIV infection in the baby. Instead, both the World Health Organization and the US Department of Health and Human Services recommend using nucleic acid tests (NAT) to detect the presence of viral DNA or RNA through 18 months of age[192,193]. In the United States, the timing of testing is determined by the infant's risk of infection. Infants born to mothers with undetectable viral loads and who received ART during pregnancy are considered to be at low risk; for these infants, testing is performed at 2-3 weeks, 4-8 weeks, and 4-6 months of age[193]. Infants are considered at higher risk if the mother did not receive prenatal care, was not on ART (or only received ART during labor), acquired HIV infection during pregnancy, or had

detectable viremia. For these infants, NAT is performed at the same intervals as low-risk infants, in addition to a test as soon as possible after birth, and again 2-6 weeks after cessation of neonatal ART prophylaxis[193]. A positive result within 72 hours after birth indicates that the infant was infected *in utero*. A negative test result shortly after birth followed by a positive result 4-6 weeks later indicates that transmission likely occurred during labor, birth, or via breastfeeding shortly after birth. If the first positive test occurs after this time, it suggests that transmission probably occurred later in the postpartum period via breastfeeding. A positive NAT result that is confirmed with a repeat NAT indicates HIV-1 infection. Based on the findings from the CHER study, which showed that rapid ART initiation improves outcomes in children infected with HIV[194], ART is recommended to begin as soon as possible, ideally immediately upon diagnosis[195].

ii. Disadvantages of existing strategies

Post-exposure prophylaxis in newborns using ART has been indispensable for reducing vertical transmission of HIV-1. However, this intervention strategy has numerous disadvantages. First, ART can be cost-prohibitive in resource-limited settings, and many children have no or inadequate access to treatment; only 54% [estimates range 37% - 73%] of children living with HIV were accessing ART in 2018[166]. In addition, adherence is hindered by drug regimen complexity, frequent dosing intervals, and poor palatability. While ART drugs are commonly formulated as multi-drug combination pills for adults, this is not the case for infants, who must swallow bitter solutions of individual ART drugs orally. Doses must be carefully calculated and measured according to the child's weight. Depending on the regimen, newborns may be required to take multiple doses of different drugs at regular intervals throughout the day[196]. While ART is generally considered safe during pregnancy and in newborns, certain drug classes have

been associated with mitochondrial toxicity, especially during cumulative exposure[197]. Moreover, ART drugs are small molecules that have short half-lives *in vivo*, necessitating treatment daily or multiple times a day for ongoing protection during breastfeeding. All of these factors may work together to result in suboptimal or sporadic treatment, which raises the risk of viral resistance and treatment failure[196]. Finally, a key drawback is that ART does not destroy latently infected cells and cannot appreciably shrink the reservoir once infection is established. As a result, efficacy decreases sharply when treatment is delayed even by only a few days after viral exposure[188].

D. Notable cases of HIV remission in children

In the vast majority of cases, a positive HIV-1 diagnosis indicates lifelong infection, requiring uninterrupted daily ART for sustained virologic suppression and disease-free survival. However, there have been several notable exceptions. These unusual cases fall into three categories: 1) aviremic long-term non-progressors, also known as elite controllers, a rare subset of people who spontaneously control the virus through multiple mechanisms that are not yet fully elucidated; 2) individuals such as Timothy Ray Brown (the “Berlin patient”) and Adam Castillejo (the “London patient”), who achieved HIV-1 remission after undergoing cancer treatments involving an allogeneic hematopoietic stem cell transplant using donor cells bearing an HIV-1-resistant CCR5 allele[198,199]; and 3) spontaneous durable control or long-term remission in previously viremic children following ART cessation[200-202].

Among the cases of long-term remission in children who stopped ART, the best-known case is known as the Mississippi baby. This child was born to a mother living with HIV who had not received prenatal ART. HIV-1 RNA was detected in the baby’s blood within 24 hours of birth, indicating that infection occurred *in utero*. The baby was put on

ART beginning at 30 hours of age, reducing the viral load to below detection, and continued on ART until the mother discontinued the child's treatment at about 18 months old. Remarkably, rather than experiencing viral rebound after ART cessation, the child remained aviremic for 28 months, until just shy of her 4th birthday. Upon detection of viremia rebound, ART treatment was restarted and full viral suppression was again achieved[201,203].

E. Nonhuman primate models of HIV vertical infection

Infection of macaques with SIV or SHIV are established models for testing vaccines and therapies for HIV-1 in nonhuman primates (NHP). In adult rhesus macaques exposed to the pathogenic Tier 2 viral swarm $SHIV_{SF162P3}$, viremia tends to mirror the course of adult HIV-1 infection, with acute peak viremia soon decreasing to a set point that varies between individuals[55,204] and in some cases is controlled spontaneously[111]. In contrast, infant rhesus or pigtailed macaques infected orally with this SHIV recapitulate the high viral loads and weak post-acute control seen in perinatal HIV-1 infection, and rapidly progress to disease within several weeks[105,114,205,206]. In a study of vertical $SHIV_{SF162P3}$ transmission in pigtailed macaques, *in utero* and peripartum/postpartum infection were observed at a rate of ~45%, with transmission of neutralization-resistant variants indicating selective pressure from maternal antibodies[207].

Despite the finding that newborns have poorer outcomes and more rapid disease progression than infants just a few weeks older at the time of infection, many NHP studies intended to model peripartum HIV infection use macaques that are several weeks[105,114,205,206] to several months old[208]. The relative pathogenicity of SHIV infection in newborns compared with older infants has not been explored. Furthermore, immunologic

damage in infants as a result of infection with either HIV-1 or SHIV is not well characterized.

III. Antibodies as passive therapy for HIV

A. Antibody structure and function

Antibodies (also known as immunoglobulins) are the secreted form of the B cell receptor, and are the principal component of the humoral adaptive immune response. Each B cell clone makes one unique antibody. In most mammals including humans, a typical antibody contains two heavy chains (HC) and two light chains (LC). Humans have two types of LC, lambda (λ) and kappa (κ); each is comprised of a variable (VL) region and a constant (CL) region. The HC similarly has a variable (VH) and 2-3 constant (CH) regions, numbered in increasing order of distance from the VH. The overall shape of the antibody molecule is like a Y. Each 'arm' of the Y consists of the VH, CH1, VL, and CL regions and is known as a Fab (fragment antigen binding), and the 'stem' consists of the CH2 and CH3 (and possibly CH4) regions, collectively termed the Fc (fragment crystallizable). Disulfide bonds link each HC to one LC at the CH1 and CL regions in each Fab, and HCs are linked by disulfide bonds in the Fab/Fc 'hinge' between CH2 and CH3. The molecule is further stabilized by additional disulfide bonds within each of the variable and constant regions. Finally, each antibody bears two or more glycans; the number and locations of glycosylation sites vary by antibody class.

As its name suggests, the Fab—specifically the variable regions (VH and VL)—is involved in binding antigen. The combining site is the portion of the antibody that makes direct contacts with the antigen. Its structure is dictated by six highly variable loops in the complementarity-determining region (CDR), which are supported by less-variable framework regions in the VH and VL. Although the total number of B cells in an

individual is on the order of 10^{11}, of which 10^{9} are naïve, the antibody repertoire is exceptionally diverse: combinatorial estimates posit 10^{15}-10^{18} potential unique naïve B cell receptors in an individual[209]. The extraordinary diversity of the antibody repertoire arises from several processes during B cell maturation and affinity maturation. First, in immature B cell precursors in the bone marrow, VJ recombination in the light chain locus and VDJ recombination in the heavy chain locus is mediated by the enzymes RAG1 and RAG2 to generate a naïve B cell receptor (BCR). During this process, variable (V), diversity (D), and joining (J) gene segments are chosen from a set of many possible alleles in the germline, and the DNA is cut and then repaired using non-homologous end joining, further increasing diversity at the V(D)J junctions. Because the resulting BCR may recognize self-antigen and thus be detrimental to the host, multiple checkpoints exist in the bone marrow and peripheral lymphoid organs to maintain immune tolerance. An autoreactive B cell may die by apoptosis, undergo receptor editing in an attempt to generate a new BCR that is non-self-reactive, be rendered anergic (unreactive), or be suppressed by Tregs in the periphery. Finally, the B cell repertoire undergoes further diversification during affinity maturation in the GC, where successive rounds of somatic hypermutation and positive selection generate *de novo* variants that are not encoded in the germline. Together, these processes of gene rearrangement, error-prone DNA repair, receptor editing, and hypermutation generate an antibody repertoire theoretically capable of recognizing any antigen with exquisite specificity.

Humans have four antibody classes: immunoglobulin M (IgM), IgG, IgA, and IgE. A fifth class, IgD, exists as a B cell receptor on naïve B cells, but is not secreted as soluble antibody and is downregulated in memory B cells. These antibody classes differ in the ways they engage the innate immune system; except for IgM and IgD, they are generated by class switching in the germinal center, and their various specialized functions are largely determined by the heavy chain constant regions specific to each

class. The presence and composition of glycans in the constant regions also influence the properties of the antibody and its interactions with the immune system.

IgM is expressed as monomers on naïve B cells. In its secreted form, it is a 970 kDa pentamer covalently linked by disulfide bonds in the CH3 constant regions. IgM is the earliest antibody class secreted during the adaptive immune response, and its high valency of binding promotes efficient agglutination of pathogens—an important advantage for an antibody with no or very little affinity maturation. IgM is also a very potent activator of complement. However, its large size hinders its diffusion out of circulation and transport across tissues, especially the placenta, and it is not an effective opsonin for driving phagocytosis or cytotoxicity.

IgE, a 200 kDa monomeric antibody, has prominent roles in the pathology of allergies as well as host defense against parasites. Its primary function is to induce mast cell degranulation. It is the least abundant Ig class in the blood, does not activate complement or neutralize pathogens, and is not a major player in the antiviral immune response.

IgA exists predominantly as a 160 kDa monomer or a 600 kDa dimer, and rarely multimerizes beyond two subunits. Abundant in blood, breastmilk, and mucosal secretions, IgA primarily provides protection at mucosal tissue sites. In its dimeric form, it is efficiently transported across epithelial barriers by cells bearing polymeric Ig receptors (pIgR). Conversely, monomeric IgA more efficiently diffuses out of circulation into extravascular sites. It is a strong activator of complement and potently neutralizes pathogens, but does not mediate effector functions such as phagocytosis and cell killing, and does not cross the placenta. The two human IgA subclasses, IgA1 and IgA2, arose through gene duplication and are highly similar in sequence and function. IgA1 has a longer hinge region, which may allow it to bind widely spaced epitopes with higher

avidity, but comes at the cost of increased vulnerability to proteolytic cleavage by bacterial pathogens[210].

A monomer of ~150 kDa, IgG is by far the most abundant antibody class in blood. Being relatively small, IgG excels at diffusing across the endothelium into tissue and is efficiently transported across the placenta. There are four IgG subclasses in humans, IgG1 through IgG4; their structures and functions are comprehensively reviewed in [211]. All four subclasses have an N-linked glycan at position 297 within each CH1 that is involved in interactions with Fc γ receptors (FcγRs) and the neonatal Fc receptor (FcRn). The presence and composition of these glycans therefore have important consequences for antibody half-life, transplacental transfer, biodistribution, and effector function that are not yet fully understood. However, the four subclasses vary in their heavy chain structure as well as the number and locations of disulfide bonds, and these differences translate to distinct biophysical properties and functions within the immune system. IgG1 has just two disulfide bonds in the hinge region, making it relatively flexible. By contrast, IgG2 and IgG3 have more disulfide bonds and IgG3 has a longer hinge, resulting in a more rigid structure. IgG4 is similar to IgG1 in size and structure; however, a single amino acid difference in the hinge of IgG4 results in a dynamic equilibrium between hinge isoforms with disulfide bridges either between the two HCs or within the same HC. Once unpaired, a single HC can recombine with an HC from a different IgG4 antibody, generating a natural bispecific antibody in a process known as Fab arm exchange. Unlike IgG2 and IgG4, IgG1 and IgG3 antibodies are potent opsonins, and readily induce phagocytosis of the bound pathogen by macrophages or the release of cytotoxic granules by NK cells. Known as antibody-dependent cell phagocytosis (ADCP) and antibody-dependent cell cytotoxicity (ADCC), these functions are driven by the IgG Fc-mediated crosslinking of FcγRI/FcγRIIA and

FcγRIIIA respectively. Engagement of these activating FcγRs triggers the phosphorylation of an immunoreceptor tyrosine-based activation motif (ITAM) on the FcγR cytoplasmic domain, initiating a signal cascade that activates the effector cell to destroy the target via ADCP or ADCC. Finally, the four subclasses vary in their ability to bind C1q and fix complement, with IgG3 being most potent followed by IgG1, IgG2, and IgG4.

Because of their FcγR interactions, relatively rapid diffusion into extravascular tissues, stability, and ease of commercial production, the majority of biologic drugs are of the IgG1 subclass[212]. In addition, the IgG Fc region can be readily modified to tune, augment, or eliminate binding to FcγRs, FcRn, or C1q (complement) so as to precisely engineer the half-life of the drug and its interactions with the immune system[213].

B. Broadly neutralizing antibodies

i. Discovery and characterization

A hallmark of chronic HIV-1 infection is the diversification of both the viral quasispecies and the antiviral antibody response within an individual. The clinically relevant properties of antibodies against viral pathogens can be described in terms of their epitope, affinity/avidity, neutralization potency, and breadth. For antibodies to HIV-1, the antibody's epitope is the site on Env that is specifically recognized by the antibody, and its affinity and avidity refer to the strength of monovalent and multivalent epitope binding, respectively. Neutralization potency is the concentration of antibody required to block a given percentage (typically 50% or 80%) of infection events in cell culture, and usually correlates with binding affinity to the Env variant in question. Breadth refers to the proportion of globally circulating HIV-1 isolates that are neutralized by the

same antibody. Over time, as memory B cells undergo successive rounds of affinity maturation in germinal centers, the resulting antibodies increase in the degree of hypermutation from the germline sequence, as well as breadth and neutralizing potency. The breadth and potency of the antibody response vary between individuals, tend to increase over time, and correlate with higher plasma viremia[214-216]. At the extreme end of the breadth/potency continuum, rare individuals known as “elite neutralizers” have very potent antibodies that can neutralize numerous isolates across multiple clades[217]. Further analysis of the B cell repertoires of such individuals has shown that the exceptional breadth and potency of the sera may be conferred by just one or a few clones, known as “broadly neutralizing antibodies” (bNAbs). However, these antibodies do not confer viral control in their hosts, and viral escape continues.

Since the discovery of the first clinically relevant bNAb b12[218], over 200 bNAbs—some exceptionally potent and broad—have been discovered using various approaches. In hybridoma technology, a relatively slow and laborious method, plasma cells are fused with myeloma tumor cells to generate an immortal antibody-producing cell line[219,220]. Another traditional technique is phage display, which works by expressing a combinatorial library of donor VHs and VLs in phage and completing iterative rounds of panning for clones that bind to a target antigen on a plate[221]. One commonly used, but low-throughput, approach involves using FACS to identify and sort single memory B cells that bind to a recombinant antigen ‘bait’, amplifying the VH and VL transcripts by RT-PCR, and cloning them into HC and LC expression vectors with the constant regions to produce full-length recombinant monoclonal antibodies (mAbs) for functional characterization[222,223]. Alternatively, single antigen-specific memory B cells can first be sorted into 96 well plates and stimulated to secrete antibodies, allowing the supernatants to be screened for functional activity; this approach saves time by obviating the need to clone and express many uninteresting mAbs[224,225]. In a new technique called LIBRA-seq,

B cells are mixed with a library of DNA-barcoded antigens and single cell sorted, encapsulated in oil droplets with oligonucleotide-labeled beads for indexing the BCR and antigens together, and deep sequenced to generate a readout of numerous antigen-BCR interactions simultaneously[226]. In combining antibody VH/VL sequencing and functional readout, this new approach overcomes major hurdles that have limited the speed of antibody discovery.

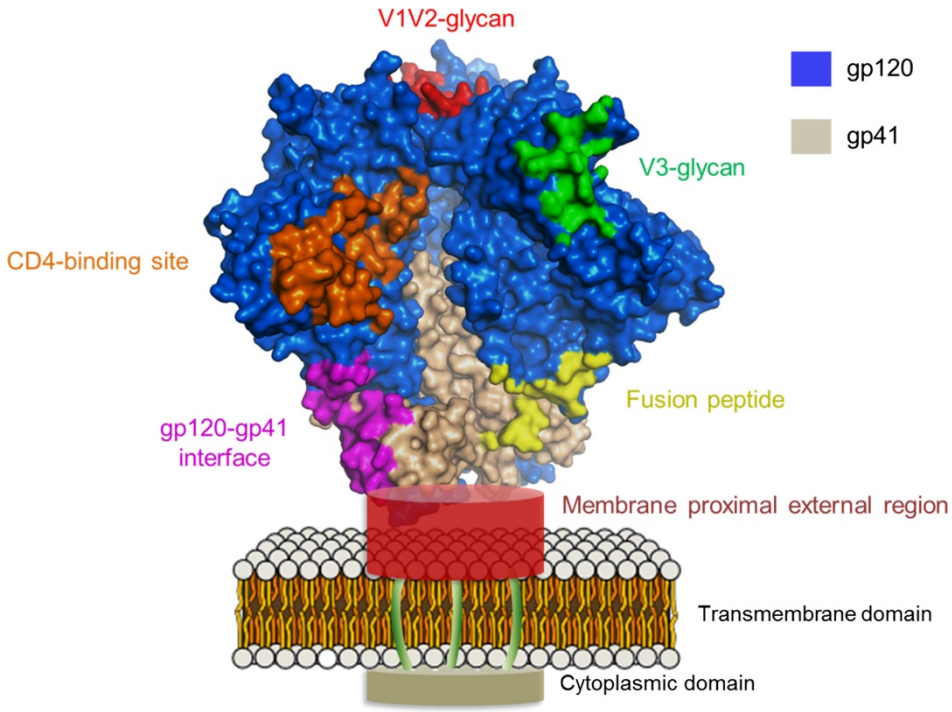

Figure 1.3. HIV-1 Envelope trimer structure and key sites of vulnerability targeted by broadly neutralizing antibodies. SU (gp120, blue) and TM (gp41, green) protein structures are shown in relation to the membrane. The membrane proximal external region (MPER) of the trimer is shown as a red cylinder due to lack of structural information available. Six sites of vulnerability commonly recognized by broadly neutralizing antibodies are indicated with individual colors and labeled accordingly. Figure is from Bonsignori, et al., 2017 *Immunol Rev*.

The characterization of the anti-HIV antibody response—especially bNAbs—has illuminated the potential sites of vulnerability on the Env trimer and informed strategies for rational vaccine design[227]. Broadly neutralizing antibodies differ from most HIV-1 Env antibodies in several respects. First, bNAbs target conserved epitopes that are poorly immunogenic due to being occluded by glycans or neighboring amino acid residues. To date, a number of bNAb epitopes have been discovered, including the V1/V2 glycan,

CD4 binding site (CD4bs), membrane-proximal external region (MPER), V3 glycan, and others (**Figure 1.3**)[228]. Notably, most antibodies that bind these conserved epitopes do not neutralize; for instance, the non-neutralizing antibody b13 binds the CD4bs similarly to the bNAb b12, yet subtle differences in the recognition site result in conformational shifts in gp120 that are incompatible with the trimeric Env, suggesting that recognition of these conserved epitopes must occur in a very specific way for neutralization to occur[229]. Second, many (though not all) bNAbs are highly diverged from the germline sequence, reflecting a complex evolutionary path over many years of chronic infection. Third, bNAbs often have unusually long CDRH3s that allow them to reach through the glycan shield and make direct contacts with conserved amino acid residues. Such long CDRH3s and the high rate of divergence from the germline sequence are associated with polyreactivity and autoreactivity, suggesting that central and peripheral tolerance mechanisms may exert selective pressure against the development of bNAbs in most people. This concept is supported by the finding that individuals who make bNAbs are more likely to have immunologic perturbations such as fewer Tregs and more autoantibodies[230]. Eliciting HIV-1 bNAbs by immunization has not yet been achieved in any animal except for cows, which naturally produce antibodies with exceptionally long CDRH3s[231]. Finally, the putative germline ancestor of some bNAbs does not bind HIV-1 Env at all[232,233]. The question of how these germline clones are initially selected and enriched remains unanswered, and is a vexing challenge for vaccine and immunogen design to elicit such bNAbs.

ii. Evidence of antiviral efficacy in human trials and animal studies

Although they cannot currently be elicited by any vaccine, passive transfer of bNAbs holds promise a prophylactic or therapeutic strategy. The role of neutralizing

antibodies in altering the course of HIV-1 infection is supported by NHP studies of polyclonal immune globulin transfer from SHIV- or SIV-infected donors (SHIVIG, SIVIG) before or shortly after infection with SHIV or SIV. In adult rhesus macaques, potently neutralizing SIVIG from a SIV_{smE660}-infected donor given at 1 and 14 days post-SIV_{smE660} infection resulted in faster development of endogenous neutralizing B cell responses and improved disease outcomes even 5 years later[234,235]. Another study in infant pigtailed macaques found that the presence of strain-matched neutralizing SHIVIG plus a non-protective dose of the bNAb IgG1-b12 at the time of $SHIV_{SF162P3}$ exposure was associated with reduced viremia and enhanced B cell immunity[206]. Similar outcomes were seen in infant rhesus macaques, and were associated with mitigated pathogenesis in this model[114]. These studies laid the groundwork for investigating passively administered monoclonal antibodies in the prevention and treatment of HIV.

Numerous studies have shown that passive immunization with bNAbs effectively protects macaques from single or repeated SHIV challenge[236-239]. In addition to neutralization, many bNAbs mediate antiviral activities such as ADCC and ADCP via FcγR engagement, and these functions may contribute to their protective efficacy[240]. Nonetheless, protection studies with non-NAbs and different antibody classes have demonstrated that neutralizing activity is required for protection[241-243]. Indeed, the potency of neutralization *in vitro* correlates with protective efficacy *in vivo*[244]. Based on the promising data from animal models, Antibody-Mediated Prevention (AMP) phase IIb clinical trials are now underway to test the bNAb VRC01 as PrEP in men and transgender people who have sex with men in the US and South America (HVTN 704/HPTN 085) and in high-risk women in sub-Saharan Africa (HVTN 703/HPTN 081).

The use of bNAbs as a therapy for HIV-1 has been explored as well, with mixed results. A trial of VRC01 in ART-untreated people with chronic HIV-1 achieved only transient decreases in viremia[245]. In comparison, a cocktail containing the more potent

bNAbs 10-1074 and 3BNC117 was able to achieve more substantial reductions in viremia for a longer period, with no evidence of viral resistance evolving to either antibody[246]. In ART-treated participants undergoing experimental treatment interruption (ATI), VRC01 delayed viral rebound only slightly compared with historical controls and exerted selective pressure on the rebounding viral variants, highlighting the risk of monotherapy for viral resistance[247]. Again, combination therapy with 10-1074 and 3BNC117 lengthened the duration of viral suppression after ATI to a median of 21 weeks, with no evidence of viral resistance to both bNAbs[248]. Notably, the bNAb therapy enhanced the development of T cell responses to HIV-1, although their contribution to viral control or clinical outcomes was unclear[249]. Taken together, these findings suggest that using potent bNAbs in combinations of two or more will maximize therapeutic efficacy and reduce the risk of viral escape.

Finally, with the potential for Fc-mediated functions like ADCC and ADCP, bNAbs may be effective as part of a strategy to reduce the viral reservoir. Because a major obstacle to viral clearance by the immune system is the establishment of latency, using latency-reversing agents (LRAs) alone or in combination with bNAbs has been proposed as an approach called “shock and kill”. Thus far, most “shock and kill” attempts have been foiled by inefficient latency reversal. However, a recent study showed delayed viral rebound upon ART interruption in a subset of macaques treated with a TLR7 agonist and PGT121[250], supporting the concept of using bNAbs as the “kill” component for reducing the latent reservoir.

C. Rationale for using broadly neutralizing antibodies in infants

Compared with traditional ART regimens, bNAbs are a promising alternative for preventing HIV-1 infection in exposed newborns for the following reasons: 1) the longer

half-life of an IgG would decrease dosing frequency, improve treatment adherence, and thus potentially allow for safer breastfeeding; 2) Fc-effector functions could help shrink the size of the newly established reservoir in the setting of post-exposure prophylaxis (PEP), as is the case when newborns receive treatment after being exposed to HIV-1 *in utero* or during birth; 3) monoclonal antibodies have an excellent safety record, and indeed, VRC01 was recently shown to be well-tolerated in newborn infants exposed to HIV-1[251]. PEP strategies with broadly neutralizing antibodies are now being evaluated in clinical trials, either alone or in conjunction with ART, in HIV-1 exposed infants through the IMPAACT trials network (P1112, P1115).

D. Recent key findings

In order for bNAbs to be a viable strategy for preventing infection in HIV-1 exposed newborns, they must be effective after viral exposure. Recent studies in macaques have shed light on the window of opportunity for effective bNAb therapy after SHIV challenge (**Table 1.1**). Using a rhesus macaque model of perinatal infection, our group presented the first evidence that treating infants with the bNAbs VRC07-523 and PGT121 beginning 24 hours after viral exposure resulted in clearance of infection and prevented reservoir establishment[105]. However, a similar study in which the bNAbs 10-1074 and 3BNC117 were given to adult macaques beginning on day 3 after SHIV exposure had a markedly different outcome, with the majority of animals becoming productively infected and, in about half of cases, eventually controlling viremia with T cell responses[252]. In contrast, treatment with PGT121 and VRC07-523 initiated on day 10, followed by 13 weeks of ART, was ineffective for clearing SHIV infection and did not alter the time to rebound or level of viral control after ATI, although CD4+ T cell-associated viral DNA was somewhat reduced[204]. Together, these findings suggest that

Table 1.1. NHP studies of bNAbs as post-exposure prophylaxis after SHIV infection

SHIV challenge	bNAbs	Treatment d.p.i.	Outcome	Reference
$SHIV_{SF162P3}$, intravaginal	PGT121 (2 mg/kg)	**-1**	12/12 **(100%) aviremic** for 6 months; distally disseminated virus cleared by day 10	Liu, et al., 2016 *Nature*
$SHIV_{SF162P3}$, oral (infants)	PGT121 and VRC07-523 (each 5 mg/kg **or** 20 mg/kg)	**1**, 4, 7, 10	12/12 **(100%) aviremic** for 6 months; distally disseminated virus cleared by day 7-14	Hessell, et al., 2016 *Nature Medicine*
$SHIV_{AD8EO}$, intrarectal **or** intravenous	10-1074 and 3BNC117 (each 10 mg/kg)	**3**, 10, 17	1/13 **(8%) aviremic** after bNAb decay; 6/12 viremic animals ultimately controlled virus by CD8+ immunity	Nishimura, et al., 2017 *Nature*
$SHIV_{SF162P3}$, intravenous	PGT121 and VRC07-523 (each 20 mg/kg)	**10** (followed by ART on days 21-112)	0/6 **(0%) aviremic** - all rebounded after ART cessation	Bolton, et al., 2015 *J Virol*

the window of opportunity for effective PEP with bNAbs is limited to the earliest days after exposure, and that efficacy drops off with the rapid seeding of the persistent reservoir during acute infection.

Chapter 2. Single-dose bNAb cocktail or abbreviated ART post-exposure regimens achieve tight SHIV control without adaptive immunity

I. Abstract

Vertical transmission accounts for most human immunodeficiency virus (HIV) infection in children, and treatments for newborns are needed to abrogate infection or limit disease progression. We showed previously that short-term broadly neutralizing antibody (bNAb) therapy given 24 hours after oral exposure cleared simian-human immunodeficiency virus (SHIV) in a macaque model of perinatal infection. Here, we report that all infants given either a single dose of bNAbs at 30 hours, or a 21-day triple-drug ART regimen at 48 hours, are aviremic with almost no virus in tissues. In contrast, bNAb treatment beginning at 48 hours leads to tight control without adaptive immune responses in half of animals. We conclude that both bNAbs and ART mediate effective post-exposure prophylaxis in infant macaques within 30-48 hours of oral SHIV exposure. Our findings suggest that optimizing the treatment regimen may extend the window of opportunity for preventing perinatal HIV infection when treatment is delayed.

II. Authors, Affiliations, Contributions, and Acknowledgements

Authors:

Mariya B. Shapiro[1], Tracy Cheever[2], Delphine C. Malherbe[2], Shilpi Pandey[2], Jason Reed[3], Eun Sung Yang[4], Keyun Wang[4], Amarendra Pegu[4], Xuejun Chen[4], Don Siess[5], David Burke[5], Heidi Henderson[2], Rebecca Lewinsohn[2], Miranda Fischer[2], Jeffrey J. Stanton[6], Michael K. Axthelm[2], Christoph Kahl[5], Byung Park[7], Anne D. Lewis[6], Jonah B. Sacha[1,2,3], John R. Mascola[4], Ann J. Hessell[2], Nancy L. Haigwood[1,2]*

*Corresponding author. Email: haigwoon@ohsu.edu

Affiliations:

[1]Department of Molecular Microbiology and Immunology, Oregon Health & Science University, Portland, OR, USA

[2]Division of Pathobiology & Immunology, Oregon National Primate Research Center, Oregon Health & Science University, Beaverton, OR, USA

[3]Vaccine & Gene Therapy Institute, Oregon Health & Science University, Beaverton, OR, USA

[4]Vaccine Research Center, NIAID/NIH, Bethesda, MD, USA

[5]Molecular Virology Core, Oregon National Primate Research Center, Oregon Health & Science University, Beaverton, OR, USA

[6]Division of Comparative Medicine, Oregon National Primate Research Center, Oregon Health & Science University, Beaverton, OR, USA

[7]Biostatistics & Bioinformatics Core, Oregon National Primate Research Center, Oregon Health & Science University, Beaverton, OR, USA

Contributions:

M.B.S., J.B.S., J.R.M., A.J.H., and N.L.H. designed the experiments. M.B.S. optimized SHIV stock production, performed viral outgrowth assays, and analyzed and interpreted data. T.C. managed tissue collection and databases, analyzed virology data, and performed antibody and viral outgrowth assays. D.C.M. designed and performed single genome cloning and bNAb escape studies. S.P. coordinated animal assignments, treatments, and procedures. M.B.S. and S.P. generated and titered the SHIVSF162P3 virus stock. J.R. performed ELISPOT assays and quantified peripheral T cells. E.S.Y., A.P., and K.W. performed and interpreted quantitative ELISAs for bNAb pharmacokinetics. X.C. provided the antibodies for in vivo use and proteins for performing the quantitative ELISAs. D.S. and D.B. measured virus in plasma and

tissues. H.H. and R.L. performed viral outgrowth and antibody binding and neutralization assays. M.F. collected samples from animals and performed T cell subset analyses. J.J.S. provided veterinary care and advice for animals. M.K.A. coordinated infectious disease resource animals. C.K. contributed molecular virology expertise and data analyses. B.P. performed statistical analyses. A.D.L. performed necropsies and described pathology. All authors discussed the results. M.B.S., A.J.H., and N.L.H. wrote the manuscript. N.L.H. supervised the research.

Acknowledgements:

We thank Dr. Ranajit Pal for discussions about quantitation of viral titer, and Drs. Gabriela Webb and Shaheed Abdulhaqq for discussions regarding virus stock production. We acknowledge technical assistance from Philip Barnette and William Sutton. We thank Dr. Rebecca M. Ducore, Lois M.A. Colgin and Heidi L. Pecoraro for performing necropsies and evaluating tissues for the study, and Dr. Peter Barry for kindly providing the cytomegalovirus detection antibody for pathology analyses. We acknowledge the veterinary and technical staff of the Division of Comparative Medicine at the Oregon National Primate Research Center for animal husbandry. This work was supported by NIH R01 HD080459 (N.L.H.), U42 OD023038 (M.K.A.), U42 OD010426 (M.K.A.), and P51 OD011092 (ONPRC), and by the intramural research program of the Vaccine Research Center, NIAID, NIH. M.B.S. was supported by NIH T32 AI007472.

III. Introduction

A hallmark of human immunodeficiency virus type 1 (HIV-1) infection is the early establishment of a persistent viral reservoir[253]. Daily antiretroviral therapy (ART), the current standard of care, can reduce plasma viral load (PVL) to undetectable levels, but treatment interruption results in viral rebound. Nonetheless, post-exposure prophylaxis

(PEP) with ART within 72 hours of exposure can reduce the likelihood of infection, although efficacy wanes the longer treatment is delayed[254]. Time of exposure can be determined with relative accuracy in the setting of mother-to-child transmission (MTCT), where over 180,000 children acquire HIV-1 each year (http://www.unaids.org/en/resources/documents/2018/unaids-data-2018) and, without treatment, half die before age two[255]. Because transmission is most likely to occur late in pregnancy or peripartum[167], risk is minimized by treating mothers during pregnancy and newborns at birth[187]. Nonetheless, even in infants born to untreated mothers, infection risk was reduced by treatment with the ART drug zidovudine beginning within 48 hours of birth, although treatment beginning at 3 days of age or later was ineffective[256]. Once virus is detected in the infant, lifelong ART is typically necessary to maintain suppression; however, there have been isolated cases of durable long-term remission in children following ART interruption[200,201,203]. The best-known case, the Mississippi baby, was already viremic when treatment began—evidence for infection *in utero* rather than peripartum[201]—and ultimately experienced viral rebound[203]. Thus, achieving remission in children perinatally infected with HIV may depend upon the time between earliest virus exposure and initiation of therapy; those infected *in utero* will likely be the most difficult to treat.

Nonhuman primate models of newborn and infant infection with simian immunodeficiency virus (SIV) and chimeric simian-human immunodeficiency virus (SHIV) have allowed in-depth investigations of viral dissemination and effectiveness of pre-exposure and post-exposure ART or broadly neutralizing antibody (bNAb) treatments[257]. SIV and SHIV disseminate rapidly in infant rhesus macaques, reaching distal tissues within one day of exposure[105,106]. Studies of early intervention using ART in both infant and adult macaques after SIV exposure have suggested that both timing and duration of treatment are critical for effective PEP[258-261]. Recently, Okoye *et al*. showed

evidence for durable tight control in adult macaques treated with ART for 600 days beginning 4-5 days after SIV infection and then released from ART, while delaying initiation of treatment to 6 days or longer led to viral rebound[107].

ART has been indispensable in reducing vertical transmission of HIV-1, yet many children have no access to treatment, and adherence is hindered by drug regimen complexity, frequent dosing intervals, and poor palatability[196]. Suboptimal treatment raises the risk of drug resistance[262], underscoring the need for more accessible interventions. Passive treatment with bNAbs offers several theoretical advantages over ART, including longer half-lives, simpler treatment regimens, and the potential for infected cell killing by Fc-mediated innate immune system engagement[240]. Potent bNAbs block SHIV infection in nonhuman primate models[263,264] and suppress viremia transiently in humans treated during chronic HIV-1 infection[246,248]. The use of bNAbs in the setting of vertical transmission is currently under evaluation in clinical trials[265,266]. Similar to human infants exposed to HIV-1 in maternal blood and cervico-vaginal secretions at birth, one-month-old infant macaques exposed orally to high doses of $SHIV_{SF162P3}$ develop high viremia and rapidly progress to disease[105,114,206]. This SHIV stock is a 'swarm' of variants that is classified as Tier 2 in neutralization sensitivity[263]. In this model of perinatal infection, we reported full clearance of viral foci and prevention of reservoir establishment with short-term bNAb cocktail treatment when treatment was initiated 1 day following SHIV exposure[105]. In contrast, a delay in treatment to 10 days[204] or even 3 days[267] after mucosal SHIV exposure in adult macaques resulted in viral resurgence after bNAb decay. However, the window of opportunity for PEP using bNAbs in young animals has not been strictly defined. Because treatment of an HIV-exposed newborn may be delayed by hours or days in a clinical setting, it is imperative to determine the time window for PEP using bNAbs and to examine which variables have the greatest impact on efficacy in the context of delayed PEP.

In the present study, we test the effect of extending the interval before bNAb treatment initiation time to 30 hours and 2 days post-exposure. Treatment with a single 40 mg/kg dose of bNAb cocktail at 30 hours is highly effective, with no evidence of virus in tissues at necropsy. In contrast, treatment with a 4-dose regimen of 10 mg/kg bNAb cocktail beginning at 48 hours results in durable control of plasma viremia in only half of treated animals. In comparison, we evaluate short-term ART beginning 2 days post-exposure in this model and find that a 21-day course beginning at 48 hours is also highly effective, with no viral rebound observed after ART cessation and little to no detectable virus in tissues. Regardless of treatment regimen, tight controllers do not mount long-lived adaptive immune responses and do not become viremic after $CD8^+$ T cell depletion, suggesting viral control by other mechanisms. Taken together, our findings begin to define the variables that impact the window of opportunity for PEP in this setting and show that viral clearance with either bNAbs or ART is an achievable outcome.

IV. Materials and Methods

Ethics statement. Macaque studies were performed at the Oregon National Primate Research Center (ONPRC) in Beaverton, OR, USA in compliance with all ethical regulations for animal testing and research. The ONPRC is accredited by the American Association for the Accreditation of Laboratory Animal Care (AAALAC) International, and adheres to the Guide for the Care and Use of Laboratory Animals and the U.S. Public Health Service Policy on the Humane Care and Use of Laboratory Animals. The study protocol was approved by the Oregon Health & Science University (OHSU) West Campus Institutional Animal Care and Use Committee (IACUC).

Animal model. For viral exposure and treatment studies in one-month-old infant rhesus macaques (*Macaca mulatta*), 31 male and female macaques were obtained from the

breeding colony at one week of age and raised in the ABSL-2 infant nursery for 3 weeks, during which time they were adapted to formula feeding. Infants were then transferred to ABSL-2+ containment for study procedures involving SHIV challenge. Animals were randomly assigned to study groups as they were born, and were excluded from the study if the animal, or its sire or dam, could not be confirmed negative for *Mamu*-B*08 and -B*17 MHC Class I alleles, which are associated with spontaneous lentiviral control[152,153]. Group sizes of six had previously been shown sufficient for statistically distinguishable measurements of plasma and cell-associated viral loads at 6 months as the primary study outcome for antibody treatment. Animals were housed in age-matched pairs throughout the study, and were monitored for clinical signs of disease by regular evaluation of body weight, peripheral lymph node size, appetite, behavior, and stool quality. Animals were euthanized under IACUC guidelines using standard methods consistent with the recommendations of the American Veterinary Medical Association (AVMA) Guidelines for Euthanasia[268].

SHIV virus challenge. For Group 2A, a challenge stock of $SHIV_{SF162P3}$ was obtained from the NIH AIDS Reagent Program, Division of AIDS, National Institute of Allergy and Infectious Diseases, National Institutes of Health ("$SHIV_{SF162P3}$ (NIH)", catalog number 6526; contributors J. Harouse, C. Cheng-Mayer, and R. Pal). Virus was diluted 4-fold in DMEM media just prior to oral challenge. Each animal received a total of 0.5 ml (885 $TCID_{50}$ measured in rhesus PBMC) of cell-free virus by swallowing, given as two 1 ml doses of diluted virus 15 minutes apart. For Groups 1, 2B, 3, and 4, a challenge stock of $SHIV_{SF162P3}$ virus ("$SHIV_{SF162P3}$ (OHSU-2017)" was generated in activated, magnetically-enriched $CD4^+$ macaque splenocytes inoculated with a stock of $SHIV_{SF162P3}$ obtained from the NIH AIDS Reagent Program (catalog number 6526; contributors J. Harouse, C. Cheng-Mayer, and R. Pal). See next section for detailed virus production methods. Cell-

free viral culture supernatant was harvested on day 7, and aliquots were stored in the liquid nitrogen gas phase until use in challenge experiments. Virus stock titer was quantified *in vitro* (see "Quantitation of Viral Stock Titer" section below). Animals received a total of 2 ml (4.1 x 10^4 $TCID_{50}$ measured in rhesus PBMC) of undiluted cell-free virus by swallowing, given as two 1 ml doses either 15 minutes apart (Group 2B) or 4 hours apart (Groups 1, 3, 4). Virus aliquots were transported on dry ice and thawed at room temperature or in hand just prior to animal challenge.

SHIV stock production. Spleens and blood from naïve rhesus macaques were processed to generate single cell suspensions, which were cryopreserved in the liquid nitrogen gas phase. To generate a stock of $SHIV_{SF162P3}$ for use in animals, a small-scale virus expansion was first performed using $SHIV_{SF162P3}$ stock obtained from the NIH AIDS Reagent Program (catalog number 6526) as inoculum; the day 7 supernatant of this small culture was subsequently used to inoculate a large-scale culture for virus stock production. For the small-scale expansion, a total of 8 x 10^7 PBMC from 3 different rhesus macaques were thawed and rested separately overnight, then enriched for $CD4^+$ cells by MACS using NHP CD4 MicroBeads (Miltenyi). CD4-enriched cells were pooled and activated for 24h in R15-100 media (RPMI1640, 15% FBS, 100 U/ml IL-2) containing a stimulation cocktail of Staphylococcal enterotoxin B (2 µg/ml, Toxin Technologies) and antibodies against CD3 (300 ng/ml, clone CD3-1, Mabtech), CD28 (1.5 µg/ml, clone L293, BD Biosciences), and CD49d (1.5 µg/ml, clone 9C10, BD Biosciences). The next day, cells were washed and incubated for 2 more days in fresh R15-100 media. A total of 2 x 10^7 cells were then spinoculated for 2h at 1600 x *g* at RT with 50 µL of $SHIV_{SF162P3}$ virus from an aliquot that had previously experienced one freeze-thaw cycle. Cells were washed the next day to remove free virus, and cultures were maintained by refreshing half of the media every other day until supernatant was

harvested and banked on day 7. Viral titer was quantified as described below. For the large-scale SHIV stock production, 2.5 x 10^9 rhesus splenocytes from a single animal were thawed and rested overnight, then subjected to $CD4^+$ enrichment by MACS and activation *in vitro,* as described above. Spinoculation was performed using the small-scale SHIV supernatant as inoculum, at an MOI = 0.08 as measured by $TCID_{50}$/ml in TZM-bl cells (NIH AIDS Reagent Program, catalog number 8129). Virus cultures were maintained until supernatant was harvested on day 7, aliquoted, and cryopreserved in liquid nitrogen for use *in vivo*. This stock is referred to as "$SHIV_{SF162P3}$ (OHSU-2017)". Viral titer was quantified as described below.

Quantitation of viral stock titer. $TCID_{50}$/ml was measured in rhesus PBMC using an assay adapted from Ranajit Pal (ABL, personal communication). Briefly, the viral stock was serially diluted 4-fold in a 96-well plate, beginning with a 1:2 dilution, making 7 replicates per dilution step. Viral dilutions were incubated with 2 x 10^5 PHA-stimulated naïve rhesus PBMC per well for 7 days at 37°C under 5% CO_2. Supernatants were then harvested and the presence or absence of virus in each well was determined by SIV p27 ELISA (RETROtek SIV p27 Antigen ELISA, ZeptoMetrix Corporation, Buffalo, NY). The positive cutoff value was determined by dividing the average OD_{450} of the lowest SIV p27 standard in the ELISA plate (63 pg/ml) by 2, and adding 0.05. $TCID_{50}$ was calculated using the Spearman-Karber method. For $SHIV_{SF162P3}$ (OHSU-2017), the challenge dose was chosen based on the results of *in vivo* titration by oral inoculation in infant rhesus macaques.

Monoclonal antibodies. IgG1 antibodies VRC07-523, VRC07-523LS, and PGT121[244,269] were produced by transient transfection in Expi293F cells (ThermoFisher

Scientific, Inc.) and affinity purified on Protein A columns to >95% purity. Antibodies were formulated in a cocktail and delivered subcutaneously around the dorsal cervical and thoracic regions according to the dosing regimens described in the text. For multiple-dose treatments, each dose was delivered at one site per day; the same or a different site may have been used on subsequent days.

Antiretroviral therapy (ART). Animals in Group 4 were given daily treatment with a triple-drug ART regimen[270]. The drugs were coformulated in a cocktail with 5.1 mg/ml tenofovir disoproxil fumarate (TDF, Gilead Sciences, Inc.), 40 mg/ml emtricitabine (FTC, Gilead Sciences, Inc.), and 2.5 mg/ml dolutegravir (DTG sodium salt and free base, Shanghai Medicilon, Inc.) dissolved in 15% Kleptose HPB Parenteral grade (Roquette) in sterile water, adjusted to pH 4.2, sterile filtered and stored frozen at -20°C. The cocktail was administered subcutaneously at 1 ml/kg each day for 21 days, beginning 48 hours after SHIV exposure.

Blood and tissue harvest and processing. Peripheral blood was collected into EDTA blood tubes prior to virus exposure on the day of challenge, on days 4, 7, 10, and 14, and weekly thereafter. Blood tubes were centrifuged at 1850 rpm for 25 minutes at 4°C with the brakes off in order to separate plasma from cells. The plasma supernatant was pipetted off and aliquots were stored at -80°C. The remaining blood fraction was resuspended in sterile PBS to double the original volume, and peripheral blood mononuclear cells (PBMC) were isolated by centrifugation in SepMate tubes (StemCell Technologies) over Lymphocyte Separation Medium (Corning). For viral DNA detection by quantitative PCR as described below, 3 x 10^6 PBMC were pelleted at ~20,000 x g in a benchtop microcentrifuge and frozen at -80°C; any remaining PBMC were

cryopreserved in liquid nitrogen. Inguinal or axillary lymph nodes were biopsied at various times post-exposure, and single cell suspensions were made by crushing the tissue through a 100 µm strainer. Lymph node cells were then frozen as pellets of 3 x 10^6 cells at -80°C for viral quantitation, and any remaining cells were cryopreserved in liquid nitrogen. At necropsy, blood, cerebrospinal fluid, and a panel of up to 31 solid tissues were harvested (see Supplementary Tables 2.2-2.6). Cerebrospinal fluid was collected into a 2 ml vial and stored at -80°C. From each solid tissue, 100 µg samples were excised and frozen at -80°C in 2 ml tubes pre-filled with 1.4 mm zirconia beads (Spex SamplePrep) to facilitate tissue homogenization with a bead beater, nucleic acid extraction, and viral DNA detection by quantitative PCR. For spleen and mixed mesenteric lymph nodes, any remaining tissue was processed to make single cell suspensions, which were cryopreserved in liquid nitrogen for use in viral outgrowth assays.

Viral nucleic acid detection in plasma, cells, and tissue homogenates. Nucleic acid from plasma, cerebrospinal fluid (CSF), or peripheral blood mononuclear cells (PBMC) was purified using a Maxwell 16 instrument (Promega, Madison, WI) per the manufacturer's protocol, using the LEV Viral Nucleic Acid Kit for plasma and CSF and the LEV Whole Blood Nucleic Acid Kit for cells. SHIV viral RNA in plasma and CSF was measured by quantitative RT-PCR with a detection limit of 50 copies/ml using a method developed by Cline, et al.[271] with minor modifications to the master mix to increase sample input. SHIV viral DNA in cellular DNA from PBMC or lymph node biopsy pellets was measured using quantitative PCR using Fast Advanced Mastermix on an Applied Biosystems QuantStudio 6 Flex instrument (Life Technologies, Carlsbad, CA). Reactions were performed with 2 µg nucleic acid input for 45 cycles using the FAST cycling

protocol (95°C for 1 s, 60°C for 20 s) in a 30 µl reaction volume. Virus copy numbers were estimated by comparison to a linearized pBSII-SIV*gag* standard curve and calculated per cell equivalent using the input nucleic acid mass and by assuming a DNA content of 6.5 µg per 10^6 cells, with a detection limit of 2 copies/µg DNA or 10 copies/10^6 cells. Primers and probe used for plasma and PBMC assays were those described by Cline, et al.[271]: SGAG21 forward (GTCTGCGTCATPTGGTGCATTC), SGAG22 reverse (CACTAGKTGTCTCTGCACTATPTGTTTTG), and pSGAG23 (5′-(FAM)-CTTCPTCAGTKTGTTTCACTTTCTCTTCTGCG-(BHQ1)-3′). Viral DNA was measured in necropsy tissue samples using an ultrasensitive nested quantitative PCR assay[156] targeting a highly conserved region of *gag* in SIV and SHIV with a detection limit of 0.02 copies/µg DNA or 1 copy/10^7 cells. Primers used for pre-amplification of viral DNA were SIVnestF01 (GATTTGGATTAGCAGAAAGCCTGTTG) and SIVnestR01 (GTTGGTCTACTTGTTTTTGGCATAGTTTC), and primers for quantitative PCR were SGAG21 forward, SGAG22 reverse, and pSGAG23 as described above. Samples were heated at 95°C for 5 min and then put on ice. Each sample was assayed in 12 replicates of 5 µg each. In order to assess PCR reaction efficiency, 10 copies of DNA containing the SIV *gag* target sequence were spiked into two of the reactions. None of the tested DNA samples showed significant amplification inhibition, defined as a 5-cycle delay relative to the amplification kinetics of reactions containing solely 10 copies of standard. The first round of amplification was performed in 12 cycles (95°C for 30 s, 60°C for 1 min) in a 50 µl reaction volume. For each pre-amplified replicate sample, 5 µl was used as input into quantitative PCR using the Fast Advanced Mastermix in the QuantStudio 6 Flex instrument. Reactions were performed for 45 cycles using the FAST cycling protocol described above in a 30 µl reaction volume. Virus copy numbers were calculated from the frequency of positive replicates using the Poisson distribution and

expressed as copies per µg DNA, or as copies per cell equivalent by assuming a DNA content of 6.5 µg DNA per 10^6 cells. Staff members performing the viral RNA and DNA assays were blinded to the experimental groups and conditions for all samples tested.

Flow cytometry and $CD4^+$ T cell counts. For each sample, 100 µl of whole blood was transferred from an EDTA blood collection tube into a cluster tube and washed twice with 1 ml PBS, aspirating and vortexing between washes. Surface stain antibodies and live/dead dye (Live/Dead Fixable Yellow Dead Cell Stain Kit, Life Technologies L34968, 0.1 µl/test) were then added, and samples were vortexed and incubated for 30 min at room temperature in the dark. Red blood cells were lysed with 1 ml of 1X FACSLyse (BD Biosciences 349202) for 8 min, followed by 3 washes in FACS buffer (PBS, 10% FBS, 1 mM EDTA). Samples were fixed in 100 µl of 2% paraformaldehyde. The following antibodies were used for surface staining: CD45 PE-Cy7 (clone D058-1283, BD Biosciences 561294, 0.1 µl/test), CD3 AlexaFluor 700 (clone SP34-2, BD Biosciences 561805, 1 µl/test), CD4 APC (clone M-T466, Miltenyi 130-113-250, 2.5 µl/test), CD8 Pacific Blue (clone DK25, Agilent Technologies PB98401-8, 2.5 µl/test), CD28 PE (clone 28.2, BD Biosciences 556622, 4 µl/test), CD95 FITC (clone DX2, BD Biosciences 556640, 5 µl/test), and CD20 PerCP-Cy5.5 (clone L27, BD Biosciences 340954, 1 µl/test). Prior to flow staining, a complete blood count (CBC) was performed on an aliquot of blood from the same day to obtain the absolute lymphocyte count per µl blood. The number of $CD4^+$ T cells per µl blood was calculated by multiplying the absolute lymphocyte count by the percentage of lymphocytes that were viable and $CD45^+$ $CD3^+$ $CD8^-$ $CD4^+$. See Supplementary Figure 2.8 for an example of the gating strategy used.

CD8α depletion and $CD8^+$ T cell counts. To evaluate the contribution of $CD8^+$ T cell immunity to control of viremia during post-acute infection in a subset of SHIV-exposed

and bNAb-treated animals, depleting anti-CD8α antibody (mouse/rhesus CDR-grafted IgG1, clone M-T807R1, NHP Reagent Resource, NIH) was administered subcutaneously in four doses. The initial dose was 10 mg/kg and three subsequent doses, 5 mg/kg each, were given 4, 8, and 11 days after the initial dose. Blood was drawn weekly thereafter, and peripheral $CD8^+$ T cell counts were monitored by complete blood counts in conjunction with flow cytometry using the staining protocol described above for $CD4^+$ T cells. The number of $CD8^+$ T cells per µl blood was calculated by multiplying the absolute lymphocyte count by the percentage of lymphocytes that were viable and $CD45^+$ $CD3^+$ $CD8^+$ $CD4^-$. See Supplementary Figure 2.8 for an example of the gating strategy used.

CD20 depletion. To evaluate the contribution of B cell immunity to viral control during chronic infection, animals 36505 and 36557 in Group 2B received a single dose of depleting anti-CD20 antibody (mouse/rhesus CDR-grafted IgG1, clone 2B8, NHP Reagent Resource, NIH) administered subcutaneously at 50 mg/kg.

Single-genome analysis (SGA). Viral RNA was isolated from plasma or viral stock samples using the QIAamp Viral RNA Mini kit (Qiagen, Valencia, CA), and cDNA was generated with BGenv3out (GGCCTCACTGATACCCCTACC) specific 3' primer using the SuperScript III first-strand synthesis system (Invitrogen, Carlsbad, CA). cDNA was subjected to limiting dilution such that <30% of wells yielded a PCR product after single-genome amplification. Single-genome amplification (SGA) of full-length gp160 Envelope was performed according to the CHAVI standard operating procedure[272] using high-fidelity platinum *Taq* (Invitrogen) and the following primer sets. First-round primers for gp160 SGA were BGenv5out (GCTATACCGCCCTCTAGAAGC) and BGenv3out (GGCCTCACTGATACCCCTACC). The first-round thermocycler program was (94°C x 2

min, [94°C x 15 s, 58°C x 30 s, 68°C x 4 min] x 35 cycles, 68°C x 15 min). Second-round primers for nested amplification were P3envB5in_NheI (GATCGCTAGCGTATGGGTCACAGTCT) and P3envB3in_MLuI (GATCGACGCGTATCCATATTGTAGGT); these primers introduced the restriction sites for NheI and MLuI to enable insertion of the gp160 product into the pEMC* vector for downstream pseudovirus construction. The second-round thermocycler program was (94°C x 2 min, [94°C x 15 s, 58°C x 30 s, 68°C x 4 min] x 45 cycles, 68°C x 15 min). Upon satisfying the SGA criteria for <30% positive results by gel electrophoresis, wells with a single genome were identified by Sanger sequencing analysis (elimination of sequences with early stop-codons or with double peaks) and the second round PCR was repeated on the positive samples. The resulting 2.5 kb fragments were purified on a 1% agarose gel and cleaned up using the Wizard SV Gel and PCR Cleanup System kit. DNAs were digested with MLuI and NheI, then ligated into the pEMC* vector, which had been previously digested with MLuI and NheI and SAP treated using exoSAP-IT (Affymetrix, Santa Clara, CA). Ligation was performed using the Thermo RapidDNA Ligation Kit. The resulting gp160/pEMC* vector was transformed into competent E. coli using the MAX Efficiency Stbl2 Competent Cell Kit and grown overnight at 30°C. Individual colonies were re-streaked and again grown overnight at 30°C to obtain clonal populations, which were then grown up in culture. To confirm presence of gp160 in the vector, colony PCR was performed using the Promega GoTaq Flexi DNA Polymerase kit and primers SK1 (GATCCTTAAGGCAGCGGCAGAAGAA) and SK6 (GATCGTGTATGGCTGATTATGATGAT). The thermocycler program was (95°C x 5 min, [95°C x 45 s, 60°C x 45 s, 72°C x 2.5 min] x 35 cycles, 72°C x 10 min). Products were run on a 1% agarose gel to confirm the presence of bands, and DNA was extracted from the confirmed cultures using the Promega PureYield Plasmid Miniprep System. To sequence the gp160, the following primers were used: 218

(ATCATTACACTTTAGAATCGC), ED5P3mod (ATGGGATCAAAGTCTAGAGCCATGTG), KK1 (GCACAGTACAATGTACACATGGAA), env8R (CACAATCCTCGCTGCAATCAAG), env6For (GAATTGGATAAGTGGGCAAG), SK5 (GATCGCCGTGAATTTAAGGGACGCTG), and SK6 (GATCGTGTATGGCTGATTATGATGAT). SHIV gp160/pEMC* vector DNA was stored at -20°C until use.

Env-pseudovirus construction. SHIV gp160/pEMC* vector DNA was co-transfected with pSG3ΔEnv HIV-1 backbone DNA into 293T cells (European Collection of Authenticated Cell Cultures, Sigma catalog number 12022001) using the jetPEI (Polyplus) transfection reagent. Supernatant containing pseudovirions was harvested after 2-3 days and frozen in 1 ml aliquots at -80°C. Pseudovirus stocks were titrated in TZM-bl cells (NIH AIDS Reagent Program, catalog number 8129) to determine the virus dilution required for 200,000 relative light units (RLU).

Env-pseudovirus neutralization assay. To determine whether emerging clones in bNAb-treated animals with breakthrough viremia were escape variants, a panel of bNAbs recognizing different epitopes were assayed in duplicate for neutralization against single round of entry $SHIV_{SF162P3}$ Env-pseudoviruses using TZM-bl reporter cells in which infection drives luciferase expression (NIH AIDS Reagent Program, catalog number 8129)[273]. Briefly, antibodies were serially diluted 3-fold in complete DMEM media (DMEM, 10% FBS, L-glutamine) and incubated with pseudovirus for 1 hour at 37°C in 96-well flat bottom plates. TZM-bl cells were harvested, mixed with DEAE dextran (7.5 μg/ml) to enhance viral uptake, and 10,000 cells were added to each well containing antibodies and virus. Additional control wells containing cells and virus only (no antibody) and cells only (no virus, no antibody) were included on each plate. Plates

were incubated at 37°C and 5% CO_2 for 48-72 hours. Bright-Glo (Promega) luciferase substrate was added to each well, and luciferase activity (relative light units, RLU) was measured on a luminometer. Wells containing only cells and virus defined 100% RLU signal, and cells-only wells defined 0% RLU signal. To calculate neutralization potency, the RLU in each well was divided by the RLU in the virus-only wells to give the percentage of viral infection not neutralized by antibody. This % RLU was plotted against antibody concentration to generate a dose-response curve for each antibody, from which 50% neutralization titer (IC_{50}) could be interpolated.

Pharmacokinetic determination. Plasma bNAb levels were quantified using plates coated with either RSC3[274] for specific detection of VRC07-523/VRC07-523LS or ST0A9[275] for specific detection of PGT121. Nunc MaxiSorp (Thermo Fisher) plates were coated overnight with 200 ng/well of RSC3 in PBS, washed with PBST five times, and blocked with TBST with 5% milk and 2% BSA for 1h at RT. Serial dilutions of all samples were plated in duplicate. Each bNAb (for standard curves) and positive and negative controls were included on each plate. Plasma was incubated for 1h at RT, followed by a PBST wash. Bound bNAbs were probed with a horseradish peroxidase-labeled goat antihuman IgG (1:5,000 dilution; Jackson Laboratories) for 30 min at RT. The plate was washed and TMB (Pierce) substrate was added. Once color was developed stopping buffer was added and the optical density at 450 nm was read. GraphPad Prism and Microsoft Office software was used to plot standard curves and calculate bNAb concentrations.

Measurement of anti-drug antibody responses. Plasma from macaques that had been administered PGT121 and VRC07-523/VRC07-523LS were diluted with PBS containing 5% skim milk, 2% BSA and 0.05% Tween 20. Five-fold serial dilutions

ranging from 1:50 to 1:781250 of these plasma samples were then added in duplicate wells to 96-well ELISA plates coated with 2 μg/ml of either PGT121 or VRC07-523/VRC07-523LS. The plate was incubated for 1 hour at room temperature followed by a PBS-T (PBS with 0.05% Tween-20) wash. Bound monkey IgGs were then probed with a horseradish peroxidase (HRP)-conjugated anti-monkey IgG, Fc-specific (Southern Biotech) for 30 minutes at room temperature. The plate was then washed and SureBlue TMB (Kirkegaard & Perry Laboratories, Gaithersburg, MD) substrate was added. Once color was developed (typically 15 to 20 min), stopping buffer (1N H_2SO_4) was added and the optical density at 450 nm was read. Endpoint titer was calculated by determining the lowest dilution that had optical density greater than five-fold of that in the background wells.

Viral outgrowth assay. To measure inducible replication-competent virus in tissues, the TZA assay was used as described[276] with the following modifications. Single cell suspensions were generated from spleen or mesenteric lymph nodes and cryopreserved in the liquid nitrogen gas phase. Aliquots of approximately 5 x 10^7 cells were thawed and rested overnight, then positively enriched for $CD4^+$ cells by magnetic-activated cell sorting (MACS) using NHP CD4 MicroBeads (Miltenyi). Bulk CD4-enriched cells were divided into two equal portions, and stimulated *in vitro* for 5 days in R15-100 media (RPMI1640, 15% FBS, 100 U/ml IL-2) using CD2/CD3/CD28 T cell stimulation beads (Miltenyi) at a 1:1 cell-to-bead ratio under two different culture conditions as follows. In the first condition, to block *de novo* cycles of replication during *in vitro* stimulation, tenofovir disoproxil fumarate (TDF, NIH AIDS Reagent Program, NIAID, NIH, catalog number 10198) was reconstituted in sterile PBS and added to cultures at a final concentration of 10 μM. In the second condition, TDF was omitted from the stimulation culture to permit *de novo* viral replication and thus increase assay sensitivity for

detecting small quantities of inducible virus in the sample. Because this condition permits additional infection during culture, the resulting viral outgrowth data overestimates the actual frequency of cells harboring inducible virus, and is therefore not strictly quantitative. On day 3 of stimulation, half of the cell culture supernatant volume was removed and replaced with fresh media. On the morning of the assay, 1 x 10^4 TZM-bl cells were plated into each well of a 96-well culture-treated flat bottom assay plate and allowed to adhere for 4-6 hours. Stimulated CD4-enriched cell samples were then plated in quadruplicate on top of the TZM-bl cells in a 4-fold dilution series starting with 2.5 x 10^5 cells/well. To detect the presence of infectious virus in each well, Bright-Glo (Promega) was added after 48 hours and luciferase activity was read out on a luminometer. Wells were considered positive for viral outgrowth if the luciferase signal exceeded the average plus 3 standard deviations of 12 replicate wells containing only TZM-bl cells (NIH AIDS Reagent Program, catalog number 8129). The number of infectious units per million $CD4^+$ cells (IUPM) in each sample was calculated using the IUPMStats v1.0 Infection Frequency Calculator available at http://silicianolab.johnshopkins.edu/.

Enzyme-linked immunosorbent assay (ELISA). Antibody responses were determined by measuring binding of plasma IgG to recombinant HIV-1 SF162 gp140 trimer. The gp140 trimer was produced as described[277] by transient transfection in Expi293F cells and purified over a *Galanthus nivalis* lectin-coupled agarose (GNA) column (Vector Laboratories, Burlingame, CA), followed by size exclusion chromatography on a Superdex 200 column (GE Healthcare Life Sciences) to separate trimer from monomer. The trimer fractions were pooled and concentrated, and aliquots were frozen at -20°C. Half-well ELISA plates (Costar) were coated with SF162 gp140 trimer at 0.5 µg/ml in carbonate/bicarbonate buffer and incubated overnight at 4°C. Plates were washed one

time in wash buffer (0.1% Triton X-100 in 1X PBS) and blocked with 1% normal goat serum/5% nonfat dried milk in PBS for 1h at RT. Serially diluted plasma samples were then incubated for 1h at RT followed by 3 washes. Plates were probed with a horseradish peroxidase-conjugated goat anti-human IgG Fc fragment-specific polyclonal antibody (1:5000, Jackson ImmunoResearch) for 1h at RT. After 5 washes, TMB substrate (SouthernBiotech) was added and incubated for 10 minutes before quenching with H_2SO_4. Optical density at 450 nm was read and 50% binding titers were calculated using GraphPad Prism and Microsoft Excel. Each sample was assayed in duplicate.

Enzyme-linked Immunospot Assay (ELISPOT). T cell responses in blood and tissues were tested in an interferon-γ (IFN-γ) enzyme-linked immunosorbent spot assay. Briefly, 1 x 10^5 mononuclear cells were incubated with antigen in duplicate wells of an anti-NHP IFN-γ coated ELISPOT plate (Mabtech) overnight at 37°C. To measure responses to Env, antigens tested were either HIV-1 SF162 Env (gp140) protein or pools of overlapping 15-mer peptides covering the length of the HIV-1 SF162 Env amino acid sequence. To detect anti-Gag responses, a pool of overlapping 15-mer peptides covering the entire SIV_{mac239} Gag open reading frame (ORF) was used. ELISPOT plates were then probed using a biotinylated anti-IFN-γ antibody followed by Streptavidin-Alkaline Phosphatase and developed with BCIP/NBT-plus substrate. Plates were read on an ELISPOT plate reader (Autoimmun Diagnostika GMBH). Cells incubated with Concanavalin A (Sigma-Aldrich) and Staphylococcal Enterotoxin B (Toxin Technologies) were used as positive controls, while antigens were omitted for a background control. The numbers of spots in duplicate wells were averaged and normalized to calculate the number of spot-forming cells per 1 x 10^6 cells. Wells with <50 spot-forming cells per 1 x 10^6 cells were considered negative. Positive responses were determined by using a one-tailed Student t test at $\alpha = 0.05$, where the null hypothesis was that the number of spots

in the treatment wells would be lower than or equal to the background. Values determined to be positive were reported as the average of duplicate test wells minus the average of all negative control wells.

Evaluation of pathology. At necropsy, rhesus macaque tissues and body fluids were collected fresh, frozen, or fixed in 10% formalin and subsequently processed for histologic evaluation. Necropsies and microscopic evaluation of tissues were performed by veterinary pathologists. Pathogens were identified and confirmed by H&E morphology and then histochemical stains, immunohistochemistry (IHC), and PCR. Adenovirus, cytomegalovirus, and *Enterocytozoon bieneusi* were all visualized by IHC using the Vectastain ABC Kit, Peroxidase Standard (Vector Laboratories, Burlingame, CA, USA). Adenovirus was detected with a mouse anti-adenovirus monoclonal antibody (MAB8052, 1:500 dilution, EMO Millipore, Temecula, CA, USA). Cytomegalovirus was detected using an antibody kindly gifted by Peter Barry (1:750 dilution) as previously reported[278]. *E. bieneusi* were visualized using a mouse anti-measles matrix protein monoclonal antibody (MAB8910, 1:1000 dilution, EMO Millipore, Temecula, CA, USA). *Spironucleus* species (sp) were confirmed in tissue by nested PCR amplification of small subunit ribosomal DNA using methods developed by Bailey et al.[279] (see Supplementary Table 2.13 for primer sequences). *Cryptosporidium* sp, SHIV giant cell disease, flagellated protozoa, *Pneumocystis* sp, *Malassezia* sp, and attaching and effacing *E. coli* were all diagnosed by H&E stain. Additional diagnostic methods included Gomori methenamine-silver stain for *Pneumocystis* sp and Periodic Schiff reaction for *Malassezia* sp. Intracellular agyrophilic bacteria were visualized by Warthin-Starry stain.

Statistical analysis. In Supplementary Figure 2.3, the percentage of aviremic animals in each treatment group was compared with the untreated control group using a Log-rank

test in which the threshold for significance was adjusted for multiple comparisons by the Dunnett-Hsu method. In the text discussing viral DNA copies in tissues (related to Figure 2.4), the ratio of DNA copies present in lymphoid vs. GI tract tissues in viremic animals was calculated by dividing the average of the copy numbers present in lymphoid tissues for each viremic animal by the average of the copy numbers present in GI tract tissues for that animal (n = 8). The mean and 95% confidence interval of these ratios is reported in the text. A D'Agostino and Pearson normality test was used to determine whether the ratios were derived from a normally distributed data set. Because the data were normally distributed (K^2 = 0.3989, p = 0.8192), a one-sample t test was used to test the hypothesis that the ratio of DNA copies present in lymphoid vs. GI tract tissues was equal to 0. Lymphoid tissues included all lymph nodes sampled (see Supplementary Table 2.1), as well as tonsil and spleen; GI tract tissues were duodenum, jejunum, ileum, cecum, colon descending, and rectum. For analysis of correlations between PVL AUC and viral DNA in tissues (Supplementary Table 2.7), PVL data was censored after 10 weeks in order to permit comparison between animals that remained on study for different lengths of time. All animals in Groups 1, 2B, 3, and 4 were included in the analysis except for 2 animals, 36206 and 36207, which were excluded because they were sacrificed prior to 10 weeks. All 23 animals in Groups 1, 2B, 3, and 4 were included in the analysis of correlations between tissue viral DNA and PVL peak or PVL final. Due to the skewed distribution of the data, nonparametric correlations were used. Statistical analyses were performed in GraphPad Prism 7 or in SAS 9.4.

V. Results

A. Study design

Previously, we tested bNAbs PGT121[269] and VRC07-523[244] together as PEP in infant macaques. Cocktails of either 10 mg/kg (each bNAb at 5 mg/kg) or 40 mg/kg (each bNAb at 20 mg/kg), given subcutaneously on days 1, 4, 7, and 10, initiated 24 hours after oral $SHIV_{SF162P3}$ exposure resulted in viral clearance and no evidence of persistent infection[105]. To test the impact of delaying bNAb treatment, we administered the same cocktail of bNAbs at 10 mg/kg (5 mg/kg each bNAb) subcutaneously to 2 groups of 6 infant macaques beginning 48 hours after high dose oral $SHIV_{SF162P3}$ challenge and again on days 4, 7, and 10 (**Figure 2.1**, Groups 2A and 2B). Animals in both groups received a SHIV challenge dose that reproducibly infected all untreated controls (**Supplementary Table 2.1**); however, a different SHIV challenge stock was used for Group 2A, an earlier pilot study. We also tested the outcome of a single bNAb cocktail dose at 30 hours, a more pragmatic clinical regimen. Because PGT121 persists longer *in vivo* than VRC07-523[105], and because mismatched decay kinetics of bNAbs in a cocktail have been shown to promote viral escape when only one bNAb remains[248], we replaced VRC07-523 with VRC07-523LS[244], which has mutations in the Fc at positions M428L and N434S that confer a longer half-life *in vivo*[280]. Six animals were exposed to SHIV orally followed by a single subcutaneous dose of bNAb cocktail containing PGT121 and VRC07-523LS at 40 mg/kg (20 mg/kg each bNAb) (**Figure 2.1**, Group 3). For comparison with the bNAb treatments, we exposed 6 animals to the same SHIV dose orally and treated with an ART cocktail of emtricitabine (FTC, 40 mg/kg/day), tenofovir disoproxil fumarate (TDF, 5.1 mg/kg/day), and dolutegravir (DTG, 2.5 mg/kg/day)[270] using an abbreviated 21-day regimen. The drugs were administered daily by subcutaneous injection beginning at 48 hours and continuing through day 23 (**Figure**

2.1, Group 4). Five age-matched animals exposed to the same SHIV dose were used as contemporaneous controls alongside Groups 2B, 3, and 4 (**Figure 2.1**, Group 1).

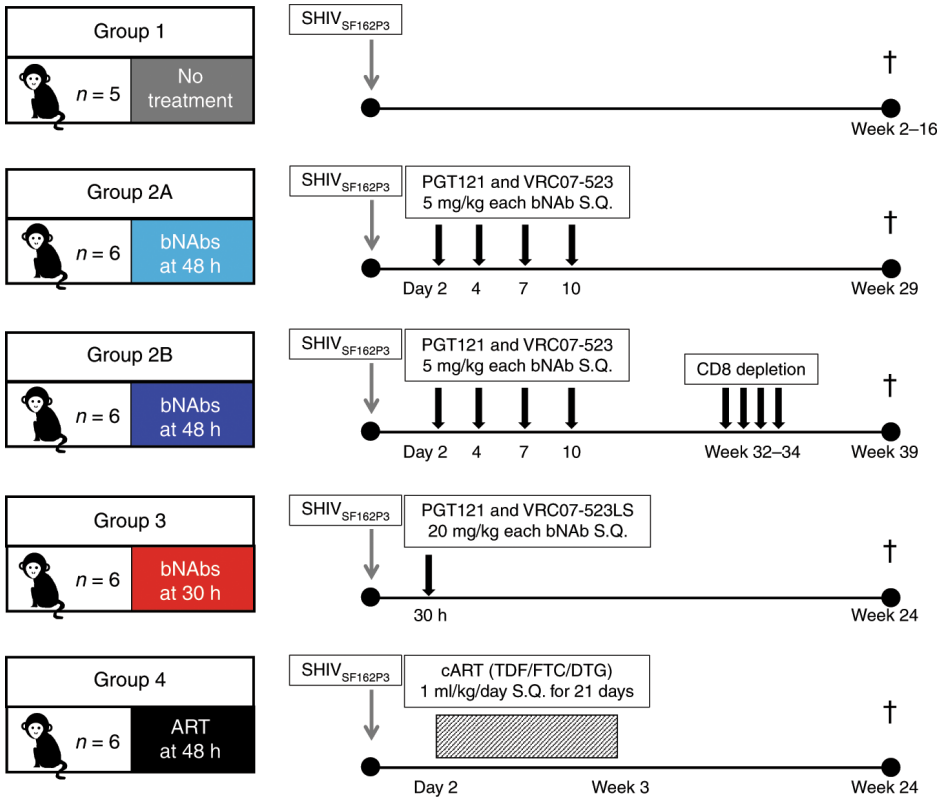

Figure 2.1. Study design. One-month-old infant rhesus macaques negative for *Mamu-B*08* and *Mamu-B*17* alleles were randomly assigned to groups. All animals were exposed to a single high dose $SHIV_{SF162P3}$ challenge by atraumatic oral inoculation. S.Q., subcutaneous delivery. TDF, tenofovir disoproxil fumarate (5.1 mg/kg). FTC, emtricitabine (40 mg/kg). DTG, dolutegravir (2.5 mg/kg). Gray arrows indicate SHIV infection. Black arrows indicate bNAb treatments. Rectangle with diagonal stripes indicates duration of daily ART treatment. Dagger indicates time of necropsy. Group colors are consistent throughout the manuscript. The number of animals (N) is indicated next to the monkey cartoon in each group.

B. Durable control of plasma viremia after bNAbs or ART

To compare the virologic outcomes of delaying bNAb treatment to 30 hours (Group 3) or 48 hours (Groups 2A and 2B), or short-term ART initiated at 48 hours (Group 4), we followed the animals for 24–39 weeks after SHIV exposure and quantified viral RNA in plasma and viral DNA (vDNA) in peripheral blood mononuclear cells

(PBMC). Initiation of bNAb treatment at 48 hours post-exposure (Group 2B) resulted in a delay in acquisition of sustained plasma and PBMC viremia compared with untreated controls (**Figure 2.2a-d**). In the 3/6 animals (50%) with breakthrough viremia, persistent viremia was first detected 5-6 weeks post-exposure, compared with 4-7 days in controls. The remaining 3/6 (50%) animals suppressed viremia to levels below detection in plasma and PBMC, except for isolated transient blips of viremia in plasma. Similar outcomes were observed in the pilot study (Group 2A) (**Supplementary Figure 2.1a-b**), but the corresponding control group of 2 animals precluded statistical analyses. The outcomes of full clearance when short-term treatment began at 24 hours[105] and viral suppression in 50% of infants when treatment began at 48 hours prompted us to test an intervening treatment time. A single-dose bNAb treatment at 30 hours (Group 3) resulted in a lack of detectable viremia in both plasma and PBMC of 6/6 animals, except for isolated blips at early time points (**Figure 2.2e-f**). These findings imply that a single high dose of bNAbs can prevent sustained viremia when administered as late as 30 hours after SHIV exposure.

To better understand the incomplete prevention of viremia by bNAb treatment at 48 hours, we asked whether viral breakthrough was due to escape mutations in the virus. Of the 3 animals in Group 2A that had breakthrough viremia, two (34215 and 34232) seroconverted 3-5 weeks after breakthrough viremia was first detected, while the third (34245) did not seroconvert (**Supplementary Figure 2.1c**). To determine whether emerging viruses in these animals were bNAb escape variants, we used single genome amplification (SGA) to clone full length *env* variants from plasma sampled shortly after viral breakthrough. Pseudoviruses made with these individual *env* clones were tested for sensitivity to neutralization by PGT121 and VRC07-523 (**Supplementary Figure 2.1d**). Several clones obtained by SGA from the $SHIV_{SF162P3}$ stock used in this experiment were also included in the analyses. There was no evidence of any bNAb-resistant clones in

either the stock or the plasma virus, suggesting that the bNAb cocktail could suppress virus expression, but that upon antibody decay virus grew out from reservoirs that had been seeded prior to bNAb therapy.

To determine whether control of viremia in bNAb-treated animals was mediated by $CD8^+$ T cells, we depleted $CD8^+$ cells in 2 moderately-viremic and 2 transiently-viremic animals in Group 2B. Anti-CD8α antibody was administered beginning at week 32 (36557, 36566) or week 34 (36494, 36505) after virus challenge (**Figure 2.2c-d**). $CD8^+$ T cells were undetectable in blood within one week of the first depleting antibody dose and remained below 200 cells/μL in all 4 animals until necropsy (**Supplementary Figure 2.2**). In the moderately-viremic animals, plasma viremia spiked within one week, increasing by 0.75 $\log_{10}$ and 2.77 $\log_{10}$ in 36505 and 36557 respectively. Viremia in 36505 decreased as $CD8^+$ T cells began to rebound, while viremia in 36557 remained high, coincident with a profound lack of $CD8^+$ T cell rebound in this animal. In contrast, viremia did not increase in either of the animals with transient viremia (**Figure 2.2c**). These data suggest that $CD8^+$ T cells play a role in controlling moderate viremia but are not required for maintaining tight control.

We next investigated treatment with a 3-week course of ART beginning at 48 hours after SHIV exposure (Group 4). In light of the incomplete viral blockade observed in animals treated with bNAbs at 48 hours, we hypothesized that this ART regimen would be less effective at clearing the nascent reservoir and preventing viral breakthrough. Unexpectedly, 0/6 animals experienced breakthrough after ART was discontinued (**Figure 2.2g-h**). Two animals, 37389 and 37480, had detectable plasma virus in the first 2-5 weeks, but subsequently controlled viremia (**Figure 2.2g**). For one animal, 37482, a low level of vDNA was detected in PBMC on day 0 prior to SHIV challenge, likely due to cross-contamination, but sample volume limitations prevented retesting (**Figure 2.2h**).

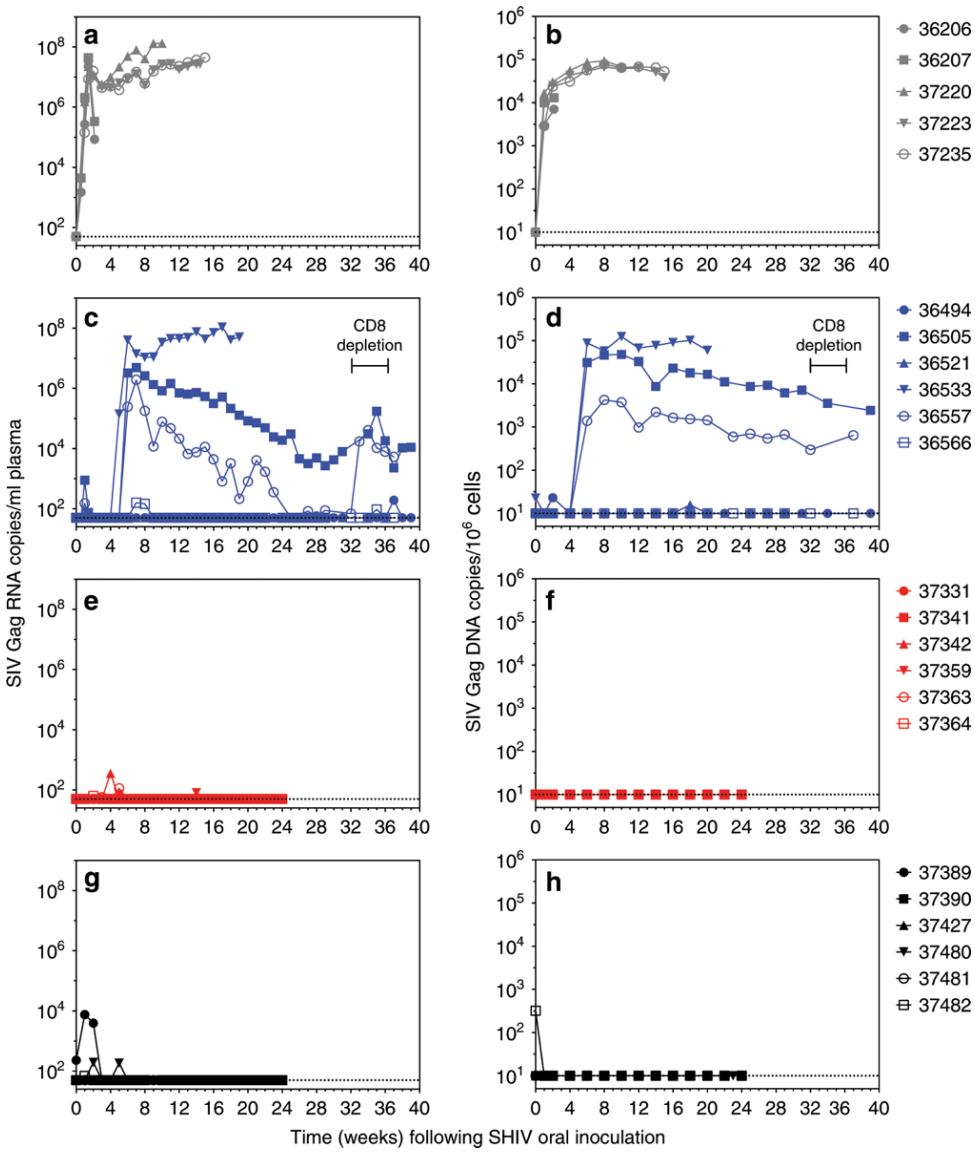

Figure 2.2. Viremia is attenuated by bNAbs or ART post-exposure. Plasma viral loads **(a**, **c**, **e**, **g)** and PBMC-associated viral loads **(b**, **d**, **f**, **h)** were measured longitudinally. **(a**, **b)** Group 1 (untreated controls). **(c**, **d)** Group 2B (bNAbs at 48 h). CD8α depletion was performed on two tight controllers (36494, 36566) and 2 viremic animals (36505, 36557) during the time frame indicated. **(e**, **f)** Group 3 (bNAbs at 30 h). **(g**, **h)** Group 4 (ART at 48 h). Group colors and individual animal symbols are consistent throughout the manuscript.

To determine the efficacy of each of the treatments relative to the untreated controls, we used Kaplan-Meier analysis to quantify the statistical differences between the number of animals that became persistently viremic in each treatment group compared with the control group. Compared with untreated controls (Group 1), persistent viremia occurred in a significantly smaller proportion of animals that received bNAbs at 30 hours (Group 3) or ART at 48 hours (Group 4) (Log-Rank test, adjusted p = 0.0002 for both comparisons, **Supplementary Figure 2.3**). While fewer animals became persistently viremic after receiving bNAbs at 48 hours (Group 2B) compared with the control group, the difference was not statistically significant (Log-Rank test, adjusted p = 0.0969). In summary, our findings indicate that bNAb or ART treatment initiated shortly after SHIV exposure can delay or prevent onset of sustained viremia.

C. bNAb pharmacokinetics and anti-drug antibody responses

Given the relatively short elapsed time of 18 hours between the times of bNAb initiation in Groups 2A and 2B (48 hours) and Group 3 (30 hours), the degree to which their virologic outcomes differed was remarkably large and warranted further investigation. We measured bNAb concentrations in plasma to determine whether the pharmacokinetics (PK) of the different human bNAb regimens contributed to this disparity. In Group 2B animals, which received 4 doses of each bNAb at 5 mg/kg, PGT121 concentrations in plasma reached an average peak of 86 μg/ml, peaking by day 14 and decaying to undetectable levels in most animals within 5-6 weeks of SHIV exposure, with an average half-life of 2.4 days; the exception was animal 36494, in which PGT121 had a much longer half-life of 15.9 days and remained detectable up to week 18 (**Figure 2.3a**). For VRC07-523, concentrations peaked on day 10, reaching an average of 17 μg/ml, and decayed within 3-4 weeks in all animals, with an average half-life of 2.9 days (**Figure 2.3b**). Not surprisingly, clearance of these human bNAbs from

the plasma was observed in conjunction with the development of robust anti-drug antibody (ADA) responses (**Figure 2.3c-d**). Notably, 36494 had weaker ADA against PGT121, consistent with the lengthy persistence of this bNAb in this animal's plasma. Unexpectedly, both bNAbs showed greater persistence in Group 3 animals, which received a single 20 mg/kg dose of each bNAb. Plasma concentrations of both PGT121 and VRC07-523LS were highest on day 4 after SHIV exposure—the first day of measurement—and declined thereafter with half-lives of 12.4 and 12.9 days respectively. PGT121 reached an average concentration of 151 μg/ml and was detectable for 6-18 weeks (median 15 weeks) (**Figure 2.3e**). Despite delivery at the same dose as PGT121, VRC07-523LS peaked at only 65 μg/ml, yet was detectable for a similar length of time as PGT121 (range 6-16 weeks, median 14 weeks) (**Figure 2.3f**). Because the bNAbs were given 30 hours after SHIV exposure, it is possible that plasma bNAb concentrations peaked before day 4, prior to sampling. Of the 6 animals in this group, only 3 mounted ADA responses against PGT121 and 4 against VRC07-523LS, coincident with more rapid clearance of each bNAb in these animals (**Figure 2.3g-h**).

To test whether the differences in peak bNAb concentration and bNAb half-life *in vivo* were determined by the treatment regimen, the specific bNAb, or both, we analyzed the data using a two-way ANOVA. Both bNAb ($p < 0.0001$) and treatment regimen ($p < 0.0001$) had a significant impact on the peak bNAb concentration in plasma; moreover, the interaction of bNAb and treatment regimen was significant ($p = 0.0395$), indicating that the treatment regimen affected the peak bNAb concentration differently for each bNAb (**Supplementary Figure 2.4a**). For bNAb half-life, neither the bNAb nor the interaction of bNAb and treatment regimen were significant determinants. However, the single-dose treatment at 30 hours (Group 3) resulted in a significantly longer half-life than the 4-dose treatment at 48 hours (Group 2B) regardless of the bNAb ($p < 0.0001$) (**Supplementary Figure 2.4b**).

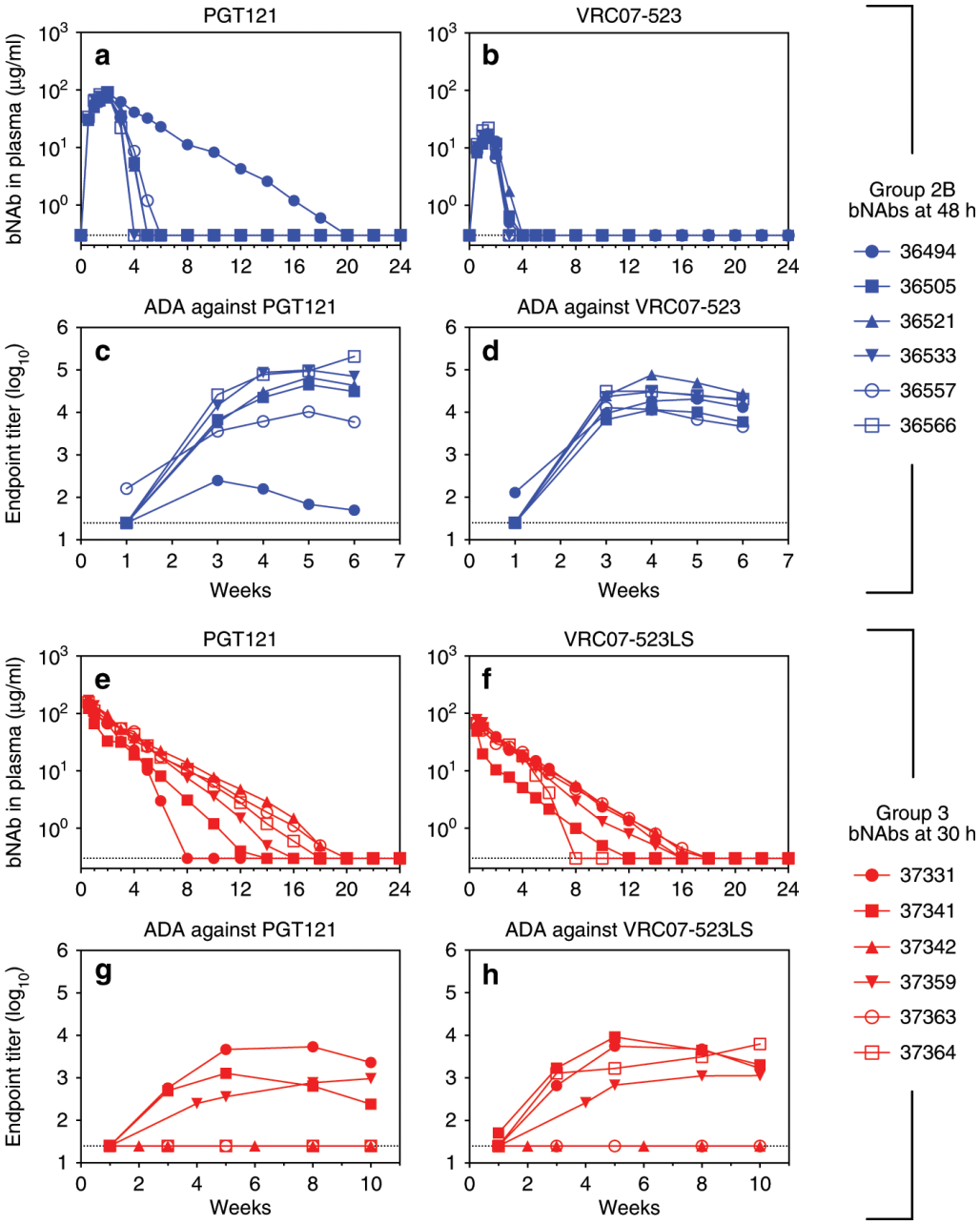

Figure 2.3. Pharmacokinetics of bNAb treatments. (a, b) Plasma concentrations of PGT121 and VRC07-523 in Group 2B animals (5 mg/kg each bNAb at 48 h and on days 4, 7, and 10). Except for 36494, no animal had detectable PGT121 or VRC07-523 in plasma after week 6. **(c, d)** Endogenous anti-drug antibody (ADA) responses against passively administered bNAbs for Group 2B animals. **(e, f)** Plasma concentrations of PGT121 and VRC07-523LS in Group 3 animals (20 mg/kg each bNAb at 30 h). **(g, h)** Endogenous ADA responses against passively administered bNAbs for Group 3 animals. Concentrations of each bNAb were measured by ELISA using binding to ST0A9 (PGT121) or RSC3 (VRC07-523 and VRC07-523LS). Dotted lines indicate limits of detection. Group colors and individual animal symbols are consistent throughout the manuscript.

D. Quantitation of viral reservoir seeding in tissues

We next asked how viral seeding in tissues was affected by post-exposure treatment with bNAbs or ART. Regardless of treatment, all persistently viremic animals—including 5/5 controls (Group 1) and 6/12 animals treated with bNAbs at 48 hours (Groups 2A and 2B)—had moderate to high levels of vDNA in all tissues tested at necropsy. Lymphoid tissues, which included tonsil, lymph nodes, and spleen (n = 9 tissues per animal) generally harbored more vDNA than gastrointestinal (GI) tract tissues, which included duodenum, jejunum, ileum, cecum, descending colon, and rectum (n = 6 tissues per animal), by a factor of 6.9 (95% CI: 3.7 - 10.2, one-sample t test, p = 0.0015, n = 11 animals) (**Figure 2.4a-b, Supplementary Tables 2.2-2.4**). This difference probably reflects greater abundance of target cells in lymphoid tissues versus the GI tract. It is likely that much of the vDNA in the GI tract localized within gut-associated lymphoid tissues (GALT) such as Peyer's patches, but we did not dissect these tissues to isolate GALT specifically. In tight controllers—including 6/12 animals treated with bNAbs at 48 hours (Groups 2A and 2B), and all animals treated with either bNAbs at 30 hours (Group 3) or ART at 48 hours (Group 4)—we detected no vDNA, or low levels in only a few tissues (**Figure 2.4b-d, Supplementary Tables 2.3-2.6**). Inguinal lymph node biopsies at various time points throughout the study demonstrated that vDNA levels in this tissue, like those in PBMC (**Figure 2.2**), remained stable over time in viremic animals and were undetectable in tight controllers (**Supplementary Figure 2.5**). For animals in Groups 1, 2B, 3, and 4, which all received the same virus stock and challenge dose, the number of vDNA copies in lymphoid and GI tract tissues at necropsy was strongly correlated with the area under the PVL curve (AUC), as well as with peak PVL and with final PVL at necropsy (**Supplementary Table 2.7**). Because

Group 2A animals were challenged with a different stock, they were excluded from this analysis.

Assays that measure vDNA within tissues give a theoretical maximum size for the viral reservoir, but the majority of vDNA is likely to be defective genomes[281,282]. To better estimate the size of the replication-competent viral reservoir, we adapted the TZA assay, a reporter-cell-based quantitative viral outgrowth assay that is well-suited for quantifying inducible replication-competent virus in small samples, such as those

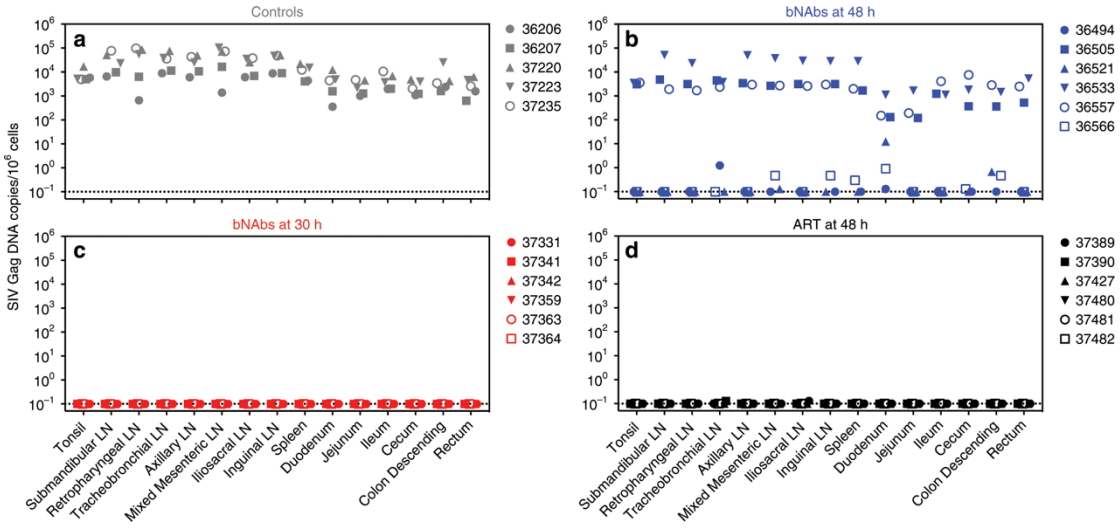

Figure 2.4. bNAb and ART treatments reduce virus in tissues. Tissues were harvested at time of death and total viral DNA was quantified using an ultrasensitive SIV DNA qPCR assay. Total viral DNA quantities are shown for the tissue types listed along the bottom of the figure. **(a)** Group 1 (untreated controls). **(b)** Group 2B (bNAbs at 48 h). **(c)** Group 3 (bNAbs at 30 h). **(d)** Group 4 (ART at 48 h). All data shown is from tissues harvested at time of death. Group colors and individual animal symbols are consistent throughout the manuscript. See Supplementary Tables 2.2–2.6 for numerical data from these and other tissues.

obtainable from infant and juvenile macaques[276]. Of the three control group animals from which spleen samples were available, viral outgrowth from stimulated $CD4^+$ cells was observed in two; the third was inconclusive due to microbial contamination (**Supplementary Figure 2.6**). In contrast, inducible virus was not detected in the tissues of the 12 animals treated either with bNAbs at 30 hours (Group 3) or with ART at 48 hours (Group 4), except for one animal (37482) in Group 4 that had very low levels in the mesenteric lymph nodes. However, omission of TDF from the stimulation culture to

permit *de novo* replication resulted in minimal but detectable outgrowth in several samples in Groups 3 and 4. In addition, a subset of animals treated with bNAbs at 48 hours (Groups 2A and 2B) had inducible virus in spleen and/or mesenteric lymph nodes. These results suggest that early bNAb or ART therapy not only limits the tissue vDNA, but may also reduce the size of the inducible replication-competent reservoir in lymphoid tissues, although sample sizes in each group were insufficient for statistical comparison.

E. Detection of adaptive immune responses to SHIV

Previous reports have suggested that bNAb treatment beginning 3 days after SHIV exposure can promote the development of endogenous antiviral immune responses[267]. To assess the development of adaptive immunity in treated and control animals, we measured Env-binding IgG antibody titers in plasma, as well as T cell responses to Env, Gag, and/or Vif. Among the untreated animals, only 2/5 animals (40%) developed HIV-1 Env-specific antibodies, and binding was weak and transient (**Figure 2.5a**), likely due to B cell dysfunction resulting from uncontrolled viremia and pathogenesis[283,284]. In contrast, in the group treated with bNAbs at 48 hours (Group 2B), moderately-viremic animals 36505 and 36557 developed persistent, increasing antibody responses, while highly viremic animal 36533 had transient seroconversion; the remaining three animals were tight controllers and did not seroconvert (**Figure 2.5b**). In order to examine the contribution of ongoing B cell responses to viral control during chronic infection, the two animals with strongest seroconversion, 36505 and 36557, were given a single dose of anti-CD20 depleting antibody 25 and 23 weeks after SHIV exposure respectively; no changes in viral load (**Figure 2.2b**) nor in plasma IgG binding titer (**Figure 2.5b**) were observed. Because antibody-producing plasma cells and plasmablasts do not express CD20[285], and thus were not effectively depleted, this

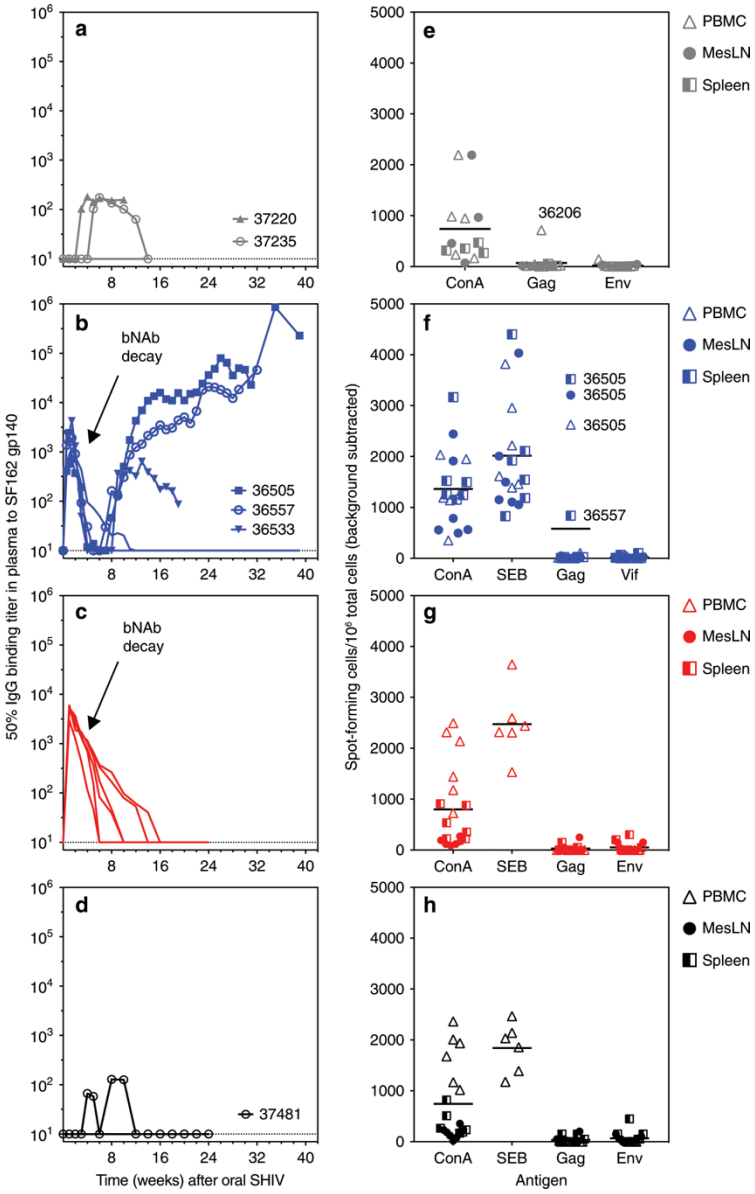

Figure 2.5. bNAbs and ART modulate adaptive immunity. (a–d) Plasma IgG binding titers to SF162 Env protein (gp140) were measured by ELISA. Group colors and individual animal symbols are consistent throughout the manuscript. The animal number is indicated for animals that had positive antibody responses to SF162 gp140. **(b**, **c)** In Groups 2B and 3, the period of bNAb decay (rather than endogenous antibody response) is indicated by arrows. **(e–h)** T cell responses to HIV-1 Env antigen, SIVmac239 Gag ORF 15-mer peptide pool, or SIVmac239 Vif ORF 15-mer peptide pool were measured by IFNγ ELISPOT. SF162 gp140 protein was used as the Env antigen for all samples except for peripheral blood mononuclear cells (PBMC) for Groups 3 and 4 **(g**, **h)**, for which Clade B consensus Env ORF 15-mer peptide pools were used. T cell responses in PBMC, mesenteric lymph nodes (MesLN), and spleen were quantified at time of death. Concanavalin A (ConA) and/or Staphylococcal Enterotoxin B (SEB) were used as positive stimulation controls. For each group, horizontal lines indicate the grand mean of ELISPOT responses to each antigen used for stimulation. Different tissue types (PBMC, MesLN, spleen) are indicated with individual symbols as shown. For specific tissue samples in which positive T cell responses to viral antigens were measured, the animal number is indicated next to the symbol. Group colors are consistent throughout the manuscript.

experiment was inconclusive. In animals treated either with bNAbs at 30 hours (Group 3) or ART at 48 hours (Group 4), transient or no seroconversion was observed, likely because none of these animals had a sufficient viral load to drive germinal center reactions (**Figure 2.5c-d**). T cell responses were likewise detectable only in the moderately-viremic animals in Group 2B (**Figure 2.5f**), and were weak or undetectable in both untreated animals with high viremia (**Figure 2.5e**) and in bNAb- or ART-treated tight controllers (**Figure 2.5f-h**). These data suggest that optimal adaptive immune responses depend on a moderate viral load, and that neither very high nor transient/undetectable viremia fosters B or T cell responses in this model.

F. SHIV pathogenesis and clinical outcomes

Finally, we evaluated pathology and clinical disease outcomes in treated and control infants (**Supplementary Tables 2.8-2.12**). Of the 5 untreated control animals (Group 1, **Supplementary Table 2.8**), 2 were sacrificed 15 days after SHIV exposure to confirm viral dissemination in tissues at this early time point (36206, 36207), and these did not have significant pathology. Of the remaining 3 controls, all had few to numerous opportunistic infections and lesions characteristic of SHIV disease. Among the viremic animals that received bNAbs at 48 hours (**Supplementary Tables 2.9-2.10**), only the highly viremic animal 34245 (Group 2A, **Supplementary Table 2.9**) progressed to disease. Regardless of group or treatment, pathological outcomes of the aviremic animals were consistent with those from age-matched uninfected animals in the colony. No lesions were observed in animals with moderate and low viremia, indicating the absence of disease due to SHIV infection (**Supplementary Tables 2.9-2.12**). Regardless of treatment, peripheral $CD4^+$ T cells did not decline precipitously in any animal over the course of the 6-month study timeline (**Supplementary Figure 2.7**),

consistent with observations that $CD4^+$ counts and percentages remain elevated in human infants during ART treatment failure[286]. However, $CD4^+$ counts were generally higher in animals with moderate and low viremia than in those with high and poorly controlled plasma viral loads.

VI. Discussion

The ability to suppress viremia using ART has made HIV-1 a manageable chronic infection for patients with access to treatment. However, even intensified ART regimens cannot clear the viral reservoir, necessitating continuous therapy once persistent infection is established. In the case of the Mississippi baby, positive at birth and treated beginning at 30 hours after birth, hopes for durable remission were dashed by the return of viremia[203]. Because this infant was likely infected *in utero*, the time between infection and treatment could not be determined. Recent and ongoing trials in newborns and children in the IMPAACT network as well as in young at-risk adults in the FRESH cohort[287] have focused on targeting primary viremia with ART as early as 1 day after the first positive viral test. The first such study in adults showed improvements in reducing both peak viremia and time to undetectable viremia, but it is not known if this has resulted in durable control[288]. In the present study, we have used a macaque model of perinatal HIV-1 infection to define the window of opportunity for intervention at known intervals after a single mucosal exposure with a high dose of SHIV that models exposure to a swarm of HIV-1 during birth and results in persistently high viremia and disease. Our data show that short-term therapy using either a single dose of bNAbs given within 30 hours or a 21-day course of ART started 48 hours after virus exposure can reliably prevent persistent viremia and limit viral DNA in tissues. However, PEP with bNAbs initiated 48 hours after SHIV exposure resulted in varying outcomes of reservoir establishment, shown by mitigated disease outcomes and tight control or clearance in

half of the treated infants, similar to the frequency of control and clearance observed with a powerful T cell vaccine[156]. We used viral DNA as a measure of the total virus because this is the most sensitive method for viral detection, and is standard for diagnosing HIV-1 infection in infants[289]. Testing of longitudinal lymph node biopsies showed that viral DNA copy number was stable in individual animals over time, mirroring the data in PBMCs and consistent with viral measures of plasma viral RNA and outgrowth of inducible virus from tissues.

A key advantage of bNAbs over ART is the possibility of Fc-mediated cell killing. Two studies have suggested that direct killing of infected cells may be a mechanism of bNAb-mediated SHIV clearance[105,239]. In contrast, ART is unable to kill infected cells directly; nonetheless, its effect *in vivo* is rapid, limiting viral replication and spread[290]. We hypothesized that the use of bNAbs in combination with a short-term ART regimen could therefore be a more effective PEP approach than either treatment alone, and might extend the window of opportunity for intervention after HIV-1 exposure. Before testing bNAbs and ART in combination, we tested an abbreviated regimen of ART alone. Our present findings show a highly abbreviated ART regimen is effective when commenced 48 hours after oral SHIV inoculation, suggesting that Fc-mediated killing of infected cells may not be required for bNAb PEP approaches. Instead, the data support a view that both ART and bNAbs act primarily by limiting viral replication and spread. The greater relative importance of neutralization over Fc function may be especially true in the case of highly potent bNAbs such as PGT121, which was able to protect monkeys from SHIV challenge despite abrogation of Fc receptor binding[291].

The finding that ART appeared to be more effective than bNAbs at the 48-hour time point was unexpected. While the specific kinetics of reservoir seeding are likely virus-specific, our findings are generally consistent with studies showing that while ART is able to limit initial seeding, its effectiveness wanes rapidly as the reservoir is seeded in

the first few days of SIVmac251 infection in adult macaques[261]. Moreover, we consider it likely that during the critical early window of rapid viral dissemination and reservoir seeding, the outcome of PEP depends as greatly on the speed and extent of drug biodistribution to the sites of viral replication as it does on the potency of viral blockade. Being small molecules, ART drugs rapidly diffuse to distal sites; for instance, DTG was detectable at therapeutically relevant concentrations in colorectal tissue within one hour of a single oral dose in a Phase I trial[292]. In contrast, monoclonal antibodies are much larger, and their rate of convection across interstitial space is influenced by antibody size and charge, tissue pore density, extracellular matrix structure, hydrostatic gradients, and the distribution of antigen and Fc receptors in tissue [293]. We showed previously that within 24 hours after a single 10 mg/kg subcutaneous dose of the bNAb cocktail used here, bNAbs were detectable in all tissue homogenates tested at a median concentration of 174.5 ng/ml (range 50 – 791 ng/ml), and in most cases had measurable neutralizing activity *in vitro*[105]; however, no time points before 24h were tested. Future studies of PEP with monoclonal antibodies should perform longitudinal tissue PK studies during the first hours after treatment to facilitate comparison with small-molecule ART regimens and to optimize treatment strategies.

Although bNAb treatment at 48 hours did not prevent persistent infection, viremia was attenuated in the majority of animals. Regardless of treatment regimen, infants that had tightly controlled or undetectable infection did not mount adaptive immune responses. The lack of viral resurgence after $CD8^+$ T cell depletion *in vivo* supported the idea that tight control was maintained independent of $CD8^+$ immunity, contrasting with previous reports in adult macaques[156,267]. In the current study, tight control may be actively maintained by other means, which may include localized innate immunity, low fitness of the transmitted/founder virus, cell-intrinsic resistance to infection, sequestration in distinct anatomical sites, or a combination of these mechanisms. Alternatively, tight

control may simply be a consequence of abortive infection due to potent blockade of establishment of a persistent replication-competent reservoir, with the rare detectable viral DNA likely being defective. We attempted to distinguish these two possibilities using a quantitative viral outgrowth assay. However, because a lack of inducible virus in tight controllers does not necessarily indicate the absence of a replication-competent reservoir *in vivo*, we cannot determine whether tight control is an active process on the basis of viral outgrowth data alone. Understanding the longevity of the earliest seeding events and kinetics of persistent reservoir establishment is critical to elucidating the mechanism of tight control after early intervention.

Finally, our findings support the concept that maximizing the effective concentration and persistence of passively delivered bNAbs is critical for reducing viral spread after exposure. In a study that used a cocktail of less-potent bNAbs for PEP in newborns, only partial control of viremia was observed[294], and we demonstrate here that the required antibody concentration is reduced and window of opportunity for intervention is extended by the greater potency of the bNAbs used. These studies also revealed that a single high dose of bNAbs resulted in longer antibody persistence *in vivo* than a 4-dose regimen—even for PGT121, which had no Fc modifications to extend half-life in either regimen. The strong inverse association between ADA responses and bNAb half-life suggests that drug immunogenicity has an important effect on PEP efficacy. Indeed, the single bNAb treatment regimen minimized ADA and was therefore sufficient to blanket the time of greatest vulnerability for viral spread. Further studies are needed to test whether increasing bNAb persistence and titer *in vivo*, either by single-dose treatment or Fc engineering, could improve outcomes when therapy is initiated 48 hours or later after exposure. Because the studies described here focused on SHIV infection at one month of age, during a time of rapid immune maturation, it will be important to test these concepts in newborn macaques to understand whether the immunological milieu

contributes to control. Combination therapy using both bNAbs and ART may also be a highly effective approach and should be explored, especially for newborns exposed to HIV infection during birth or breastfeeding.

VII. Supplementary Data

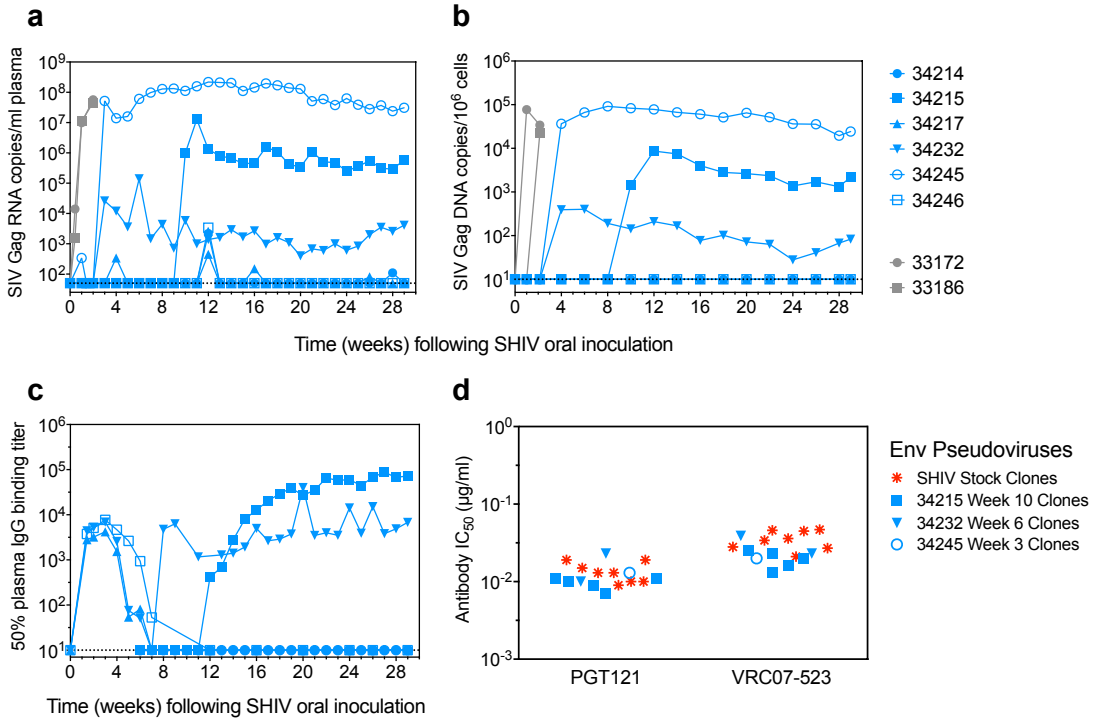

Supplementary Figure 2.1. Emergent virus is not resistant to bNAbs. One-month-old infant macaques (Group 2A, light blue symbols) were exposed orally with $SHIV_{SF162P3}$ and treated subcutaneously with 5 mg/kg PGT121 and 5 mg/kg VRC07-523 on days 2, 4, 7, and 10 after SHIV exposure. Contemporaneous age-matched control animals (gray symbols) were exposed with the same dose of SHIV and not treated with bNAbs. **(a)** Plasma viral loads over time. **(b)** Viral DNA in PBMC over time. Dotted lines indicate limits of detection. **(c)** Plasma IgG binding titers against SF162 gp140 protein. Plasma dilution at which 50% of antigen is bound is shown. **(d)** Neutralization of $SHIV_{SF162P3}$ stock and emergent clones from bNAb-treated animals. Env-pseudoviruses were cloned from the challenge SHIV stock (red symbols) or from plasma of three animals exposed to this SHIV stock and treated with 10 mg/kg bNAb cocktail on days 2, 4, 7, and 10 after exposure (light blue symbols). Time points were chosen based on sample availability and first detectable instance of plasma viremia in each animal. Env-pseudoviruses were tested for sensitivity to neutralization by the two bNAbs listed along the bottom. IC_{50}, concentration at 50% viral inhibition.

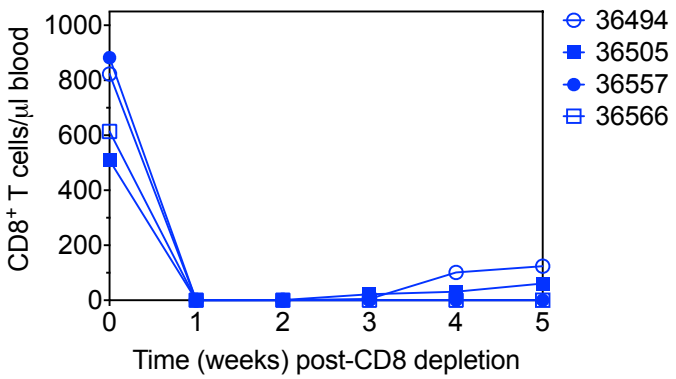

Supplementary Figure 2.2. CD8α depletion in four Group 2B animals (bNAbs at 48 hours). $CD8^+$ T cell counts in peripheral blood are shown for each animal. Time is measured in weeks after the first dose of depleting antibody. Group colors and individual animal symbols are consistent throughout the manuscript.

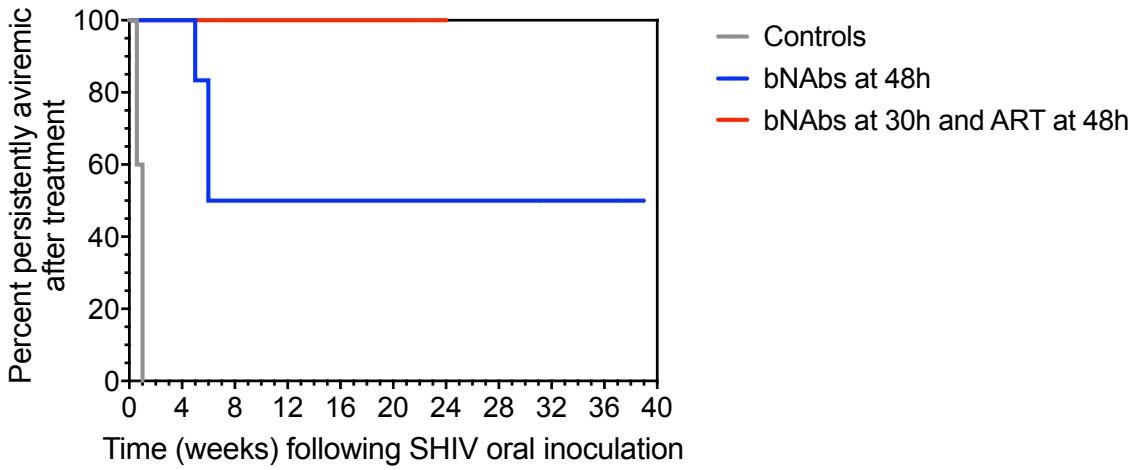

Supplementary Figure 2.3. Post-exposure bNAbs or ART prevent persistent viremia. Kaplan-Meier analysis of proportion of animals remaining persistently aviremic (defined as no more than one consecutive measurement of positive plasma viremia) after conclusion of treatment. Groups 3 (bNAbs at 30 hours, n = 6 animals) and 4 (ART at 48 hours, n = 6 animals) had a significantly smaller percentage of animals that became viremic than Group 1 (controls, n = 5 animals) (Log-rank test with Dunnett-Hsu correction for multiple comparisons, adjusted p = 0.0002 for both comparisons). Group 2B (bNAbs at 48 hours, n = 6 animals) was not significantly different from Group 1 (adjusted p = 0.0969).

a

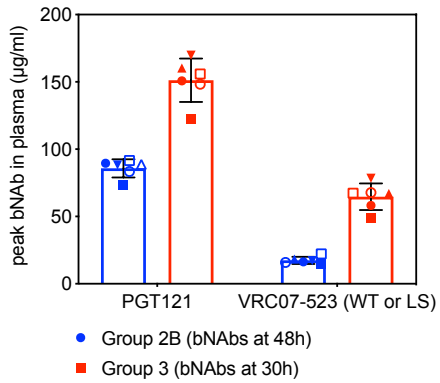

Source of Variation	% of total variation	P value	P value summary	Significant?	
Interaction	0.8632	0.0395	*	Yes	
bNAb	62.49	<0.0001	****	Yes	
Regimen	33.08	<0.0001	****	Yes	
ANOVA table	SS	DF	MS	F (DFn, DFd)	P value
Interaction	497.3	1	497.3	F (1, 20) = 4.851	P=0.0395
bNAb	36003	1	36003	F (1, 20) = 351.2	P<0.0001
Regimen	19060	1	19060	F (1, 20) = 185.9	P<0.0001
Residual	2051	20	102.5		

b

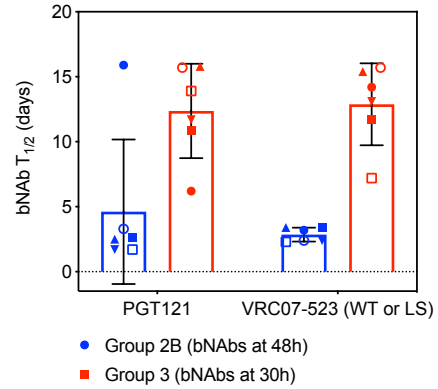

Source of Variation	% of total variation	P value	P value summary	Significant?	
Interaction	1.034	0.4568	ns	No	
bNAb	0.3099	0.6823	ns	No	
Regimen	62.73	<0.0001	****	Yes	
ANOVA table	SS	DF	MS	F (DFn, DFd)	P value
Interaction	7.820	1	7.820	F (1, 20) = 0.5757	P=0.4568
bNAb	2.344	1	2.344	F (1, 20) = 0.1725	P=0.6823
Regimen	474.4	1	474.4	F (1, 20) = 34.92	P<0.0001
Residual	271.7	20	13.58		

Supplementary Figure 2.4. Effects of bNAb and treatment regimen on concentration and half-life. The regimen factor includes 2 levels: the 4-dose regimen given starting at 48 hours and on days 4, 7, and 10 (Group 2B, n = 6 animals) and the single-dose regimen given at 30 hours (Group 3, n = 6 animals) after SHIV exposure. The bNAb factor includes 2 levels: PGT121 and VRC07-523 (wild-type [WT] for Group 2B, LS variant for Group 3). **(a)** Peak concentration in plasma for each bNAb in each treatment group. **(b)** bNAb half-life ($T_{1/2}$) in plasma for each bNAb in each treatment group. Blue symbols and bars, Group 2B. Red symbols and bars, Group 3. Individual animal values are plotted as symbols consistent with those used throughout the manuscript. The bar graph represents the mean. Error bars represent standard error of the mean (SEM). For peak concentration **(a)** and half-life **(b)**, results of the 2-way ANOVAs are shown in the tables at right. SS, sum of squares. DF, degrees of freedom. MS, mean squares. All statistical analyses are based on n = 6 animals per group.

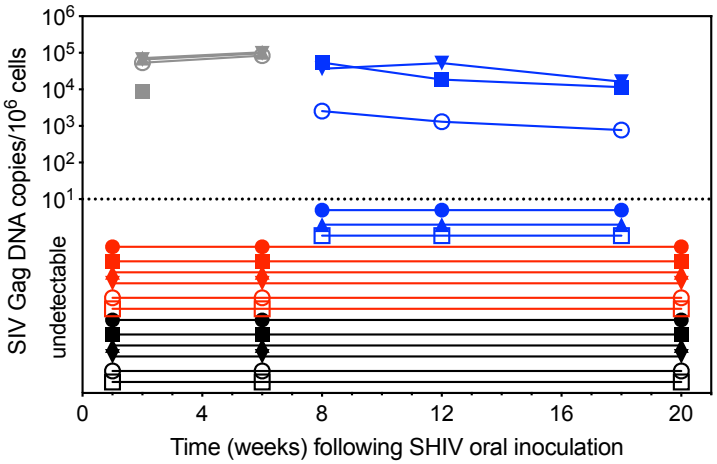

Supplementary Figure 2.5. Viral DNA in inguinal lymph nodes is stable over time. Gray, Group 1 (untreated controls). Blue, Group 2B (bNAbs at 48 hours). Red, Group 3 (bNAbs at 30 hours). Black, Group 4 (ART at 48 hours). Group colors and individual animal symbols are consistent throughout the manuscript. Total viral DNA levels were quantified in inguinal lymph nodes biopsied at the time points indicated. All samples shown below the dotted line at 10^1 DNA copies/10^6 cell equivalents were below the limit of detection.

		Spleen			Mixed Mesenteric Lymph Nodes		
Group	**Animal ID**	mean SIV gag DNA copies/million cells	IUPM (+TDF)	IUPM (-TDF)	mean SIV gag DNA copies/million cells	IUPM (+TDF)	IUPM (-TDF)
Group 1 (Controls)	36206	4408	*nd**	*nd**	1375	*nd**	*nd**
	36207	4053	*nd**	*nd**	16405	*nd**	*nd**
	37220	22021	*nd***	*nd***	71303	*nd***	*nd***
	37223	15148	375	718	105147	376	718
	37235	12307	9.0	29.0	73214	1668	2384
Group 2A (bNAbs at 48h)	34214	0.00	0.0	0.0	0.00	*nd*	*nd*
	34215	9760	4.7	718	7220	125	718
	34217	0.00	0.0	0.8	0.00	*nd*	*nd*
	34232	14	0.0	0.9	136	0.0	6.3
	34245	19159	5850	> 5851	54814	718	3521
	34246	0.13	0.0	0.0	0.00	*nd*	*nd*
Group 2B (bNAbs at 48h)	36494	0.00	0.0	0.0	0.00	4.0	0.0
	36505	1694	0.8	5850	2665	*nd***	*nd***
	36521	0.00	0.0	0.8	0.13	1.5	3.0
	36533	28432	718	1380	37780	2384	5850
	36557	1989	0.0	1.6	2724	0.0	2.7
	36566	0.30	0.0	0.0	0.47	0.0	0.0
Group 3 (bNAbs at 30h)	37331	0.00	0.0	0.0	0.00	0.0	0.0
	37341	0.00	0.0	0.0	0.00	0.0	0.8
	37342	0.00	0.0	0.0	0.00	0.0	0.0
	37359	0.00	0.0	0.0	0.00	0.0	0.8
	37363	0.00	0.0	0.0	0.00	0.0	0.0
	37364	0.00	0.0	0.0	0.00	0.0	0.0
Group 4 (ART at 48h)	37389	0.00	0.0	0.0	0.00	0.0	0.0
	37390	0.00	0.0	0.0	0.00	0.0	0.0
	37427	0.00	0.0	0.0	0.00	0.0	0.0
	37480	0.00	0.0	1.5	0.00	0.0	0.0
	37481	0.00	0.0	3.1	0.00	0.0	4.5
	37482	0.00	0.0	0.0	0.00	0.8	6.0

Supplementary Figure 2.6. Inducible replication-competent virus in spleen and lymph nodes. TDF, tenofovir disoproxil fumarate. IUPM, infectious units per million cells. Spleen and mixed mesenteric lymph nodes were collected at necropsy and replication-competent virus was measured in CD4-enriched single cell suspensions using a TZM-bl-based viral outgrowth (TZA) assay. Cells were stimulated in vitro either in the presence of TDF (+TDF) to limit de novo replication during cell stimulation, or in its absence (-TDF) to increase assay sensitivity. Values for the -TDF condition are an overestimate and not truly quantitative, and are only reported to give an idea of positivity relative to the +TDF condition. nd, not done. One asterisk (*), tissue sample not collected. Two asterisks (**), assay not possible due to microbial contamination.

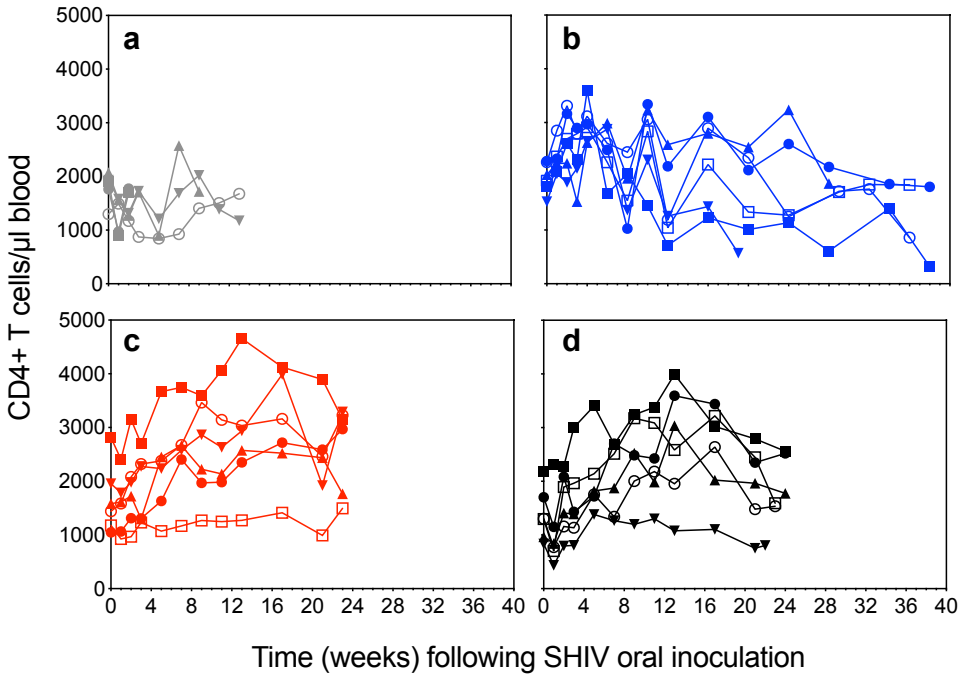

Supplementary Figure 2.7. Longitudinal CD4⁺ T cell counts. (a) Group 1 (untreated controls). **(b)** Group 2B (bNAbs at 48 hours). **(c)** Group 3 (bNAbs at 30 hours). **(d)** Group 4 (ART at 48 hours). Group colors and individual animal symbols are consistent throughout the manuscript.

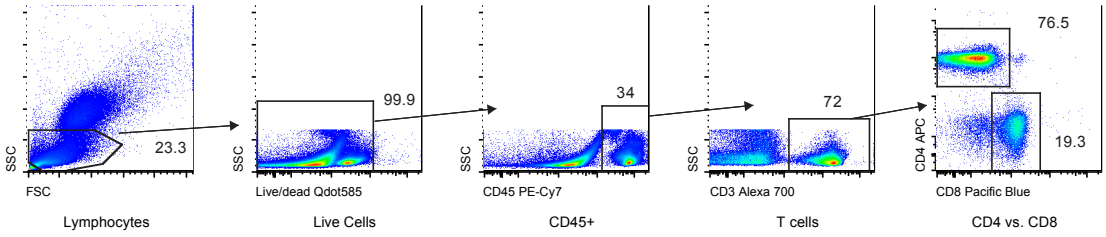

Supplementary Figure 2.8. Gating strategy for CD4⁺ and CD8⁺ T cell counts by flow cytometry. After gating on lymphocytes, singlets, and live cells, CD4⁺ T cells were defined as CD45⁺ CD3⁺ CD4⁺ CD8⁻, and CD8⁺ T cells were defined as CD45⁺ CD3⁺ CD4⁻ CD8⁺. Gating for a representative peripheral blood sample is shown.

Supplementary Table 2.1. Titration of $SHIV_{SF162P3}$ stocks *in vivo* by single dose oral challenge in infant rhesus macaques.

Study Groups	SHIV Virus Stock	Challenge Dose (ml virus)	Challenge Dose ($TCID_{50}$ measured in rhesus PBMC)	Of untreated control animals, number viremic/total (%)	Of untreated control animals, number with sustained high viremia/total (%)
2A	$SHIV_{SF162P3}$ (NIH)	0.5	885	2/2 (100%)	2/2 (100%)
1, 2B, 3, 4	$SHIV_{SF162P3}$ (OHSU-2017)	2	40960	5/5 (100%)	3/5 (60%)
x	$SHIV_{SF162P3}$ (OHSU-2017)	1	20480	2/2 (100%)	1/2 (50%)
x	$SHIV_{SF162P3}$ (OHSU-2017)	0.5	10240	4/6 (67%)	3/6 (50%)
x	$SHIV_{SF162P3}$ (OHSU-2017)	0.2	4096	0/2 (0%)	0/2 (0%)
x	$SHIV_{SF162P3}$ (OHSU-2017)	0.1	2048	1/4 (25%)	1/4 (25%)

x = this viral dose was not used in this study; it was only performed as part of an *in vivo* titration experiment to establish the appropriate viral dose to infect infant macaques for treatment studies including this one.

Supplementary Table 2.2. Viral DNA in tissues at time of death in Group 1 (untreated controls).

Animal ID (sex)	36206 (F)	36207 (M)	37220 (F)	37223 (M)	37235 (M)
Buccal Mucosa	262.54	63.17	x	x	x
Pharyngeal Mucosa	1108.26	1255.10	x	x	x
Esophagus	82.24	117.17	x	x	x
Stomach	604.22	2398.24	x	x	x
Duodenum	356.97	1569.49	12431.92	4920.54	4440.85
Jejunum	1011.80	1271.29	4499.76	2181.51	4676.33
Ileum	1947.42	1999.09	6788.91	3806.57	10624.47
Cecum	1081.90	1236.36	4916.87	3984.19	2029.65
Colon Ascending	1657.01	1537.68	x	x	x
Colon Transverse	1212.37	1427.19	x	x	x
Colon Descending	2394.72	1613.70	4208.47	25045.60	3424.81
Rectum	1571.66	634.25	6223.62	4642.02	2569.94
Tonsil	5760.80	4985.08	17060.22	5248.68	4952.87
Submandibular LN	6534.83	9782.95	51142.63	23191.66	77175.42
Retropharyngeal LN	658.26	6367.97	86092.38	55822.68	98429.89
Tracheobronchial LN	8868.62	11465.06	76229.20	39043.67	35993.26
Axillary LN	6008.74	10683.62	49678.89	25303.49	42952.55
Mixed Mesenteric LN	1374.58	16405.11	71303.26	105147.23	73214.19
Iliosacral LN	6136.82	6889.34	25386.19	35225.85	38236.22
Inguinal LN	8736.87	8999.33	49972.94	48075.27	47787.75
Spleen	4407.60	4053.21	22021.45	15148.00	12306.68
Mixed Repro Tract	107.86	47.51	x	x	x
Lungs	222.55	226.98	x	x	x
Thymus	83.10	38.59	x	x	x
Adrenal Gland	20.80	32.26	x	x	x
Pancreas	6389.00	6847.42	x	x	x
Kidney	33.69	24.57	x	x	x
Liver	x	x	x	x	x
Bladder	193.19	245.75	x	x	x
Thyroid	22.54	50.51	x	x	x
Cerebellum Brain	0.00	0.00	x	x	x
Cerebrospinal Fluid*	338.54	727.46	6530.54	41145.22	1716.50

Results are mean SIV Gag DNA copies per 10^6 total cells, except where indicated by a * symbol

x = not collected

* units are RNA copies/ml

Supplementary Table 2.3. Viral DNA in tissues at time of death in Group 2A (bNAbs at 48 hours).

Animal ID (sex)	34214 (F)	34215 (M)	34217 (F)	34232 (M)	34245 (M)	34246 (M)
Buccal Mucosa	0.00	7.97	0.00	0.13	34.45	0.00
Pharyngeal Mucosa	x	878.96	x	1.11	8695.22	x
Esophagus	0.00	1034.02	0.00	10.96	538.82	0.68
Stomach	0.00	12.27	0.13	7.67	961.13	0.00
Duodenum	0.00	493.03	0.00	9.99	7162.96	0.00
Jejunum	0.00	736.49	1.21	71.57	55182.56	1.21
Ileum	0.00	116.73	0.13	165.05	7605.49	0.00
Cecum	0.00	718.02	0.00	98.37	9979.20	0.00
Colon Ascending	0.00	3072.88	0.00	77.70	32202.49	0.00
Colon Transverse	0.00	4478.30	0.00	35.02	27767.40	0.13
Colon Descending	0.00	1866.49	0.00	26.77	29237.91	0.30
Rectum	0.00	2186.43	2.26	53.71	24165.32	0.00
Tonsil	0.00	22497.36	0.00	200.81	491.05	0.13
Submandibular LN	0.00	11322.05	0.00	514.18	59377.54	0.00
Retropharyngeal LN	0.00	13084.81	0.00	401.45	36491.34	0.00
Tracheobronchial LN	0.00	6864.54	0.00	139.44	79775.15	0.47
Axillary LN	0.00	9239.09	0.00	118.07	53829.92	32.56
Mixed Mesenteric LN	0.00	7220.38	0.00	135.70	54814.27	0.00
Iliosacral LN	0.00	9639.79	0.00	644.49	71868.11	0.13
Inguinal LN	0.00	12049.44	0.00	458.11	41839.97	0.00
Spleen	0.00	9759.76	0.00	13.76	19158.69	0.13
Mixed Repro Tract	0.00	194.51	0.00	0.00	254.45	0.13
Lungs	0.00	0.25	0.00	0.19	445452.25	0.13
Thymus	0.00	33.04	0.00	0.00	38110.55	0.00
Adrenal Gland	0.00	17.20	0.00	0.00	5040.59	0.00
Pancreas	0.00	4.41	0.00	0.00	3263.52	0.00
Kidney	0.00	18.68	0.00	0.00	592.71	0.00
Liver	0.00	15.51	0.00	0.00	5706.21	0.00
Bladder	0.00	31.64	0.00	2.08	361.87	0.00
Thyroid	0.00	24.41	x	0.00	1389.77	0.13
Cerebellum Brain	0.00	2.70	0.00	0.00	40.25	0.00
Cerebrospinal Fluid*	0.00	2805.95	0.00	153.34	1460.37	0.00

Results are mean SIV Gag DNA copies per 10^6 total cells, except where indicated by a * symbol

x = not collected

* units are RNA copies/ml

Supplementary Table 2.4. Viral DNA in tissues at time of death in Group 2B (bNAbs at 48 hours).

Animal ID (sex)	36494 (F)	36505 (F)	36521 (F)	36533 (F)	36557 (F)	36566 (F)
Buccal Mucosa	x	x	x	x	x	x
Pharyngeal Mucosa	x	x	x	x	x	x
Esophagus	x	x	x	x	x	x
Stomach	x	x	x	x	x	x
Duodenum	0.13	130.40	12.39	1129.32	150.63	0.91
Jejunum	0.00	120.62	0.00	1667.05	193.70	0.00
Ileum	0.00	1241.93	0.00	1140.22	4093.82	0.00
Cecum	0.00	371.14	0.00	1825.68	7591.03	0.13
Colon Ascending	x	x	x	x	x	x
Colon Transverse	x	x	x	x	x	x
Colon Descending	0.00	360.16	0.68	1468.65	2846.26	0.47
Rectum	0.00	524.89	0.00	5379.52	2478.46	0.00
Tonsil	0.00	3105.62	0.00	3486.99	3572.91	0.00
Submandibular LN	0.00	4831.04	0.00	51478.13	1905.10	0.00
Retropharyngeal LN	0.00	3133.38	0.00	23599.91	1700.90	0.00
Tracheobronchial LN	1.25	4456.31	0.00	3833.70	2377.28	0.00
Axillary LN	0.00	3431.00	0.00	50070.11	2973.55	0.00
Mixed Mesenteric LN	0.00	2665.00	0.13	37780.08	2723.72	0.47
Iliosacral LN	0.00	3154.65	0.00	29909.66	2591.30	0.00
Inguinal LN	0.00	3136.97	0.00	28897.06	3002.55	0.47
Spleen	0.00	1694.08	0.00	28431.70	1988.60	0.30
Mixed Repro Tract	x	x	x	x	x	x
Lungs	x	x	x	x	x	x
Thymus	x	x	x	x	x	x
Adrenal Gland	x	x	x	x	x	x
Pancreas	x	x	x	x	x	x
Kidney	x	x	x	x	x	x
Liver	x	x	x	x	x	x
Bladder	x	x	x	x	x	x
Thyroid	x	x	x	x	x	x
Cerebellum Brain	x	x	x	x	x	x
Cerebrospinal Fluid*	0.00	4315.11	0.00	1283.41	13830.52	0.00

Results are mean SIV Gag DNA copies per 10^6 total cells, except where indicated by a * symbol

x = not collected

* units are RNA copies/ml

Supplementary Table 2.5. Viral DNA in tissues at time of death in Group 3 (bNAbs at 30 hours).

Animal ID (sex)	37331 (M)	37341 (F)	37342 (F)	37359 (M)	37363 (M)	37364 (F)
Buccal Mucosa	x	x	x	x	x	x
Pharyngeal Mucosa	x	x	x	x	x	x
Esophagus	x	x	x	x	x	x
Stomach	x	x	x	x	x	x
Duodenum	0.00	0.00	0.00	0.00	0.00	0.00
Jejunum	0.00	0.00	0.00	0.00	0.00	0.00
Ileum	0.00	0.00	0.00	0.00	0.00	0.00
Cecum	0.00	0.00	0.00	0.00	0.00	0.00
Colon Ascending	x	x	x	x	x	x
Colon Transverse	x	x	x	x	x	x
Colon Descending	0.00	0.00	0.00	0.00	0.00	0.00
Rectum	0.00	0.00	0.00	0.00	0.00	0.00
Tonsil	0.00	0.00	0.00	0.00	0.00	0.00
Submandibular LN	0.00	0.00	0.00	0.00	0.00	0.00
Retropharyngeal LN	0.00	0.00	0.00	0.00	0.00	0.00
Tracheobronchial LN	0.00	0.00	0.00	0.00	0.00	0.00
Axillary LN	0.00	0.00	0.00	0.00	0.00	0.00
Mixed Mesenteric LN	0.00	0.00	0.00	0.00	0.00	0.00
Iliosacral LN	0.00	0.00	0.00	0.00	0.00	0.00
Inguinal LN	0.00	0.00	0.00	0.00	0.00	0.00
Spleen	0.00	0.00	0.00	0.00	0.00	0.00
Mixed Repro Tract	x	x	x	x	x	x
Lungs	x	x	x	x	x	x
Thymus	x	x	x	x	x	x
Adrenal Gland	x	x	x	x	x	x
Pancreas	x	x	x	x	x	x
Kidney	x	x	x	x	x	x
Liver	x	x	x	x	x	x
Bladder	x	x	x	x	x	x
Thyroid	x	x	x	x	x	x
Cerebellum Brain	x	x	x	x	x	x
Cerebrospinal Fluid*	0.00	0.00	0.00	0.00	0.00	0.00

Results are mean SIV Gag DNA copies per 10^6 total cells, except where indicated by a * symbol

x = not collected

* units are RNA copies/ml

Supplementary Table 2.6. Viral DNA in tissues at time of death in Group 4 (ART at 48 hours).

Animal ID (sex)	37389 (F)	37390 (M)	37427 (F)	37480 (F)	37481 (M)	37482 (M)
Buccal Mucosa	x	x	x	x	x	x
Pharyngeal Mucosa	x	x	x	x	x	x
Esophagus	x	x	x	x	x	x
Stomach	x	x	x	x	x	x
Duodenum	0.00	0.00	0.00	0.00	0.00	0.00
Jejunum	0.00	0.00	0.00	0.00	0.00	0.00
Ileum	0.00	0.00	0.00	0.00	0.00	0.00
Cecum	0.00	0.00	0.00	0.00	0.00	0.00
Colon Ascending	x	x	x	x	x	x
Colon Transverse	x	x	x	x	x	x
Colon Descending	0.00	0.00	0.00	0.00	0.00	0.00
Rectum	0.00	0.00	0.00	0.00	0.00	0.00
Tonsil	0.00	0.00	0.00	0.00	0.00	0.00
Submandibular LN	0.00	0.00	0.00	0.00	0.00	0.00
Retropharyngeal LN	0.00	0.00	0.00	0.00	0.00	0.00
Tracheobronchial LN	0.00	0.13	0.00	0.00	0.00	0.00
Axillary LN	0.00	0.00	0.00	0.00	0.00	0.00
Mixed Mesenteric LN	0.00	0.00	0.00	0.00	0.00	0.00
Iliosacral LN	0.13	0.00	0.00	0.00	0.00	0.00
Inguinal LN	0.00	0.00	0.00	0.00	0.00	0.00
Spleen	0.00	0.00	0.00	0.00	0.00	0.00
Mixed Repro Tract	x	x	x	x	x	x
Lungs	x	x	x	x	x	x
Thymus	x	x	x	x	x	x
Adrenal Gland	x	x	x	x	x	x
Pancreas	x	x	x	x	x	x
Kidney	x	x	x	x	x	x
Liver	x	x	x	x	x	x
Bladder	x	x	x	x	x	x
Thyroid	x	x	x	x	x	x
Cerebellum Brain	x	x	x	x	x	x
Cerebrospinal Fluid*	0.00	0.00	0.00	0.00	0.00	0.00

Results are mean SIV Gag DNA copies per 10^6 total cells, except where indicated by a * symbol

x = not collected

* units are RNA copies/ml

Supplementary Table 2.7. Spearman correlations between tissue viral DNA copies and plasma viremia for Groups 1, 2B, 3, and 4.

Tissue	PVL peak Spearman Rho	PVL peak p-value	PVL final Spearman Rho	PVL final p-value	PVL AUC Spearman Rho*	PVL AUC p-value*
Tonsil	0.83	<.0001	0.96	<.0001	0.82	<.0001
Submandibular LN	0.85	<.0001	0.99	<.0001	0.82	<.0001
Retropharyngeal LN	0.85	<.0001	0.89	<.0001	0.82	<.0001
Tracheobronchial LN	0.79	<.0001	0.99	<.0001	0.68	0.0007
Axillary LN	0.86	<.0001	0.92	<.0001	0.83	<.0001
Mixed Mesenteric LN	0.78	<.0001	1	<.0001	0.76	<.0001
Iliosacral LN	0.87	<.0001	0.92	<.0001	0.86	<.0001
Inguinal LN	0.85	<.0001	0.95	<.0001	0.83	<.0001
Spleen	0.85	<.0001	0.96	<.0001	0.83	<.0001
Lymphoid tissues average**	0.81	<.0001	0.88	<.0001	0.72	0.0002
Duodenum	0.79	<.0001	0.91	<.0001	0.71	0.0003
Jejunum	0.85	<.0001	0.99	<.0001	0.82	<.0001
Ileum	0.82	<.0001	0.95	<.0001	0.8	<.0001
Cecum	0.81	<.0001	0.92	<.0001	0.81	<.0001
Colon Descending	0.75	<.0001	0.9	<.0001	0.75	<.0001
Rectum	0.84	<.0001	0.99	<.0001	0.83	<.0001
GI tract tissues average***	0.77	<.0001	0.89	<.0001	0.7	0.0004

PVL, plasma viral load (RNA copies/ml)
PVL peak, maximum plasma viral load (RNA copies/ml) for each animal.
PVL AUC, area under the curve for plasma viral load.
LN, lymph node.
GI tract, gastrointestinal tract.
Except for PVL AUC (see below), data from a total of n = 23 animals were included in the correlation analyses.
* For PVL AUC analysis, data after 10 weeks was censored for all animals, and animals 36206 and 36207 were excluded because they were sacrificed prior to 10 weeks. A total of 21 animals were included in the PVL AUC analysis.
** Lymphoid tissues include tonsil, all lymph nodes listed in the table, and spleen.
*** GI tract tissues include duodenum, jejunum, ileum, cecum, colon descending, and rectum.

Supplementary Table 2.8. Clinical histories and pathologic findings for Group 1 (untreated controls).

Animal ID (Sex)	Age at termination (days)	Opportunistic infections, pathologic diagnoses, and clinical history
36206 (F)	38	Gross and microscopic findings normal for age. Unremarkable clinical history.
36207 (M)	36	Mild pharyngitis and interstitial pneumonia consistent with mild viral respiratory infection. Clinical history of periocular erythema, ventral abdominal rash, single episode of diarrhea.
37220 (F)	100	Minimal pancreatic duct cryptosporidiosis, mild membranous glomerulopathy, mild portal hepatitis. Chronic-active typhlocolitis. Clinical episode of diarrhea associated with *Campylobacter coli*.
37223 (M)	128	Multiple opportunistic infections and SHIV-related pathology including SHIV giant cell pneumonia; acute bronchopneumonia; cytomegaloviral interstitial pneumonia, orchitis, and sialoadenitis; proliferative choledochitis/cholecystitis attributed to *Enterocytozoon bieneusi*; mild membranous glomerulopathy. Chronic-active typhlocolitis. Thymic depletion. Clinical history of diarrhea, abdominal bloating, cough, and facial rash. Early termination due to clinical pneumonia.
37235 (M)	129	Several opportunistic infections including enteric and pancreatic duct cryptosporidiosis; proliferative choledochitis attributed to *Enterocytozoon bieneusi*, mild membranous glomerulopathy. Mild chronic-active typhlocolitis. Unremarkable clinical history.

Supplementary Table 2.9. Clinical histories and pathologic findings for Group 2A (bNAbs at 48 hours).

Animal ID (Sex)	Age at termination (days)	Opportunistic infections, pathologic diagnoses and clinical history
34214 (F)	250	Gross and microscopic findings normal for age. Unremarkable clinical history.
34215 (M)	246	Mild eosinophilic and granulomatous mediastinitis, thymitis. Unremarkable clinical history.
34217 (F)	246	Gross and microscopic findings normal for age. Unremarkable clinical history.
34232 (M)	236	Gross and microscopic findings normal for age. Unremarkable clinical history.
34245 (M)	237	Multiple opportunistic infections and SHIV-related pathology including flagellate gastritis; proliferative choledochitis and cholecystitis due to *Enterocytozoon bieneusi*; Pneumocystis pneumonia; adenoviral enteritis; intracytoplasmic agyrophilic bacteria in stomach and duodenum; enteropathy with attaching and effacing *Escherichia coli*; proliferative proctitis with flagellated protozoa; necrotizing granulomatous lymphadenitis due to *Spironucleus* sp.; mild membranous glomerulopathy; and SHIV giant cells in lymph nodes and lung. Chronic-active proliferative typhlocolitis. Widespread lymphoid depletion. Clinical history of erythematous rash; delayed growth and weight gain (35% below norm).
34246 (M)	240	Dermatitis with Malassezia sp yeast. Unremarkable clinical history.

Supplementary Table 2.10. Clinical histories and pathologic findings for Group 2B (bNAbs at 48 hours).

Animal ID (Sex)	Age at termination (days)	Opportunistic infections, pathologic diagnoses and clinical history
36494 (F)	305	Gross and microscopic findings normal for age. Unremarkable clinical history.
36505 (F)	303	Focal lymphocytic perivascular infiltrate in brainstem and cellulitis of chin. Moderate chronic-active typhlocolitis. Clinical history of intermittent diarrhea associated with *Campylobacter coli* and delayed growth.
36521 (F)	243	Gross and microscopic findings normal for age. Unremarkable clinical history.
36533 (F)	173	Mild membranous glomerulopathy. Moderate chronic-active typhlocolitis. Clinical history of delayed growth, maculopapular rash in inguinal region and ventral abdomen.
36557 (F)	293	Mild inflammation in meninges, kidney, liver, and large intestine. Unremarkable clinical history.
36566 (F)	289	Mild chronic-active typhlocolitis. Clinical history of diarrhea with positive fecal culture for Campylobacter coli and mildly delayed growth rate

Supplementary Table 2.11. Clinical histories and pathologic findings for Group 3 (bNAbs at 30 hours).

Animal ID (Sex)	Age at termination (days)	Opportunistic infections, pathologic diagnoses and clinical history
37331 (M)	187	Mild segmental chronic-active typhlocolitis. Unremarkable clinical history.
37341 (F)	183	Gross and microscopic findings normal for age. Unremarkable clinical history.
37342 (F)	183	Mild inflammation in lung, liver, and large intestine. Clinical history of intermittently delayed growth.
37359 (M)	194	Moderate chronic-active typhlocolitis. Clinical history of intermittent diarrhea, emesis and delayed growth rate.
37363 (M)	196	Mild multifocal granulomatous pneumonia. Unremarkable clinical history.
37364 (F)	193	Gross and microscopic findings normal for age. Unremarkable clinical history.

Supplementary Table 2.12. Clinical histories and pathologic findings for Group 4 (ART at 48 hours).

Animal ID (Sex)	Age at termination (days)	Opportunistic infections, pathologic diagnoses and clinical history
37389 (F)	199	Mild chronic-active typhlocolitis. Single episode of diarrhea.
37390 (M)	198	Gross and microscopic findings normal for age. Unremarkable clinical history.
37427 (F)	195	Gross and microscopic findings normal for age. Unremarkable clinical history.
37480 (F)	184	Mild chronic-active typhlocolitis. Clinical episode of diarrhea associated with *Campylobacter jejuni*.
37481 (M)	195	Gross and microscopic findings normal for age. Unremarkable clinical history.
37482 (M)	198	Gross and microscopic findings normal for age. Clinical history of mild papular rash.

Supplementary Table 2.13. List of primers used in this study.

Primer Name	Primer Sequence (5' – 3')	Purpose
SGAG21 forward	GTCTGCGTCATPTGGTGCATTC	Viral load quantitation in plasma, PBMC, tissues
SGAG22 reverse	CACTAGKTGTCTCTGCACTATPTGTTTTG	Viral load quantitation in plasma, PBMC, tissues
pSGAG23	(FAM)-CTTCPTCAGTKTGTTTCACTTTCTCTTCTGCG-(BHQ1)	Viral load quantitation in plasma, PBMC, tissues
SIVnestF01	GATTTGGATTAGCAGAAAGCCTGTTG	Viral load quantitation in tissues (pre-amplification)
SIVnestR01	GTTGGTCTACTTGTTTTTGGCATAGTTTC	Viral load quantitation in tissues (pre-amplification)
BGenv3out	GGCCTCACTGATACCCCTACC	Single genome analysis (cDNA synthesis, first round of PCR)
BGenv5out	GCTATACCGCCCTCTAGAAGC	Single genome analysis (first round of PCR)
P3envB5in_NheI	GATCGCTAGCGTATGGGTCACAGTCT	Single genome analysis (second round of PCR)
P3envB3in_MLuI	GATCGACGCGTATCCATATTGTAGGT	Single genome analysis (second round of PCR)
SK1	GATCCTTAAGGCAGCGGCAGAAGAA	Single genome analysis (colony PCR)
SK6	GATCGTGTATGGCTGATTATGATGAT	Single genome analysis (colony PCR, gp160 sequencing)
218	ATCATTACACTTTAGAATCGC	Single genome analysis (gp160 sequencing)
ED5P3mod	ATGGGATCAAAGTCTAGAGCCATGTG	Single genome analysis (gp160 sequencing)
KK1	GCACAGTACAATGTACACATGGAA	Single genome analysis (gp160 sequencing)
env8R	CACAATCCTCGCTGCAATCAAG	Single genome analysis (gp160 sequencing)
env6For	GAATTGGATAAGTGGGCAAG	Single genome analysis (gp160 sequencing)
SK5	GATCGCCGTGAATTTAAGGGACGCTG	Single genome analysis (gp160 sequencing)
HTTS2-FW	GCCTYATYGCGTTAACGAGC	Evaluation of pathology – detection of *Spironucleus* sp. (first round of PCR)
HTTS2-RV	GACGGGCGGTGTRTACAAAR	Evaluation of pathology – detection of *Spironucleus* sp. (first round of PCR)
Ssp3-FW	AGACGGCCAGCCCCCCGGGC	Evaluation of pathology – detection of *Spironucleus* sp. (second round of PCR)
Ssp3-RV	GGTGTGGCCGCGGCCGGAGC	Evaluation of pathology – detection of *Spironucleus* sp. (second round of PCR)

CHAPTER 3: Immune Perturbation is More Profound in Newborn than in Infant Macaques during Acute SHIV Infection

I. Abstract

Progress in preventing vertical HIV-1 transmission has stalled, with 160,000 infants infected annually. Newborns and infants exhibit higher viral loads and more rapid disease progression than adults and older children, with the lowest survival rates in those infected as newborns. While immunologic immaturity likely promotes pathogenesis and poor viral control, little is known about immune damage in infants. Here we examined virologic and immunologic outcomes in rhesus macaques exposed to $SHIV_{SF162P3}$ at 1-2 weeks or 4 months of age. Although differences in plasma viremia and seeded reservoirs during acute infection were minimal, we observed age-dependent alterations in leukocyte subsets and gene expression. Compared with infants, newborns had stronger skewing of monocytes and CD8+ T cells toward differentiated subsets and little evidence of type I interferon responses by transcriptomic analysis. These findings suggest that acute SHIV infection causes distinct immunological alterations in newborn and older infant macaques, laying groundwork for studies of how immune maturation affects pathogenesis in pediatric HIV-1 infection.

II. Authors, Affiliations, Contributions, and Acknowledgements

Authors:

Mariya B. Shapiro[1], Tracy Cheever[2], Shilpi Pandey[2], Eisa Mahyari[2,4], Kosiso Onwuzu[2,4], Jason Reed[2,3], Heather Sidener[5], Jeremy Smedley[5], Lois Colgin[5], Amanda Johnson[5], Anne D. Lewis[5], Benjamin Bimber[2,4], Jonah B. Sacha[1,2,3], Ann J. Hessell[2], Nancy L. Haigwood[1,2]*

*Corresponding author. Contact: haigwoon@ohsu.edu

Affiliations:

[1]Department of Molecular Microbiology and Immunology, Oregon Health & Science University, Portland, OR, USA

[2]Division of Pathobiology & Immunology, Oregon National Primate Research Center, Oregon Health & Science University, Beaverton, OR, USA

[3]Vaccine & Gene Therapy Institute, Oregon Health & Science University, Beaverton, OR, USA

[4]Genetics Division, Oregon National Primate Research Center, Oregon Health & Science University, Beaverton, OR, USA

[5]Division of Comparative Medicine, Oregon National Primate Research Center, Oregon Health & Science University, Beaverton, OR, USA

Contributions:

M.B.S., B.B., J.B.S., A.J.H., and N.L.H. designed the experiments. M.B.S. optimized SHIV stock production, designed and performed the flow cytometry experiments, isolated RNA, and analyzed and interpreted data. T.C. managed tissue collection and databases, isolated RNA, analyzed virology data, and performed ELISA and neutralization assays. S.P. coordinated animal assignments, treatments, and procedures. M.B.S. and S.P. generated and titrated the $SHIV_{SF162P3}$ virus stock used for Newborns and Infants. E.M. performed RNA-seq bioinformatics analysis and made heatmaps. K.O. developed and used the GeneSetVis program to facilitate gene ontology and pathway enrichment analysis of transcriptomic datasets. J.R. performed ELISPOT assays. H.S. provided veterinary care and advice for animals. J.S. performed biopsies and advised on surgical procedures. L.C., A.J., and A.D.L. performed necropsies and

described pathology. All authors discussed the results. M.B.S. and N.L.H. wrote the manuscript. N.L.H. supervised the research.

Acknowledgements:

We acknowledge technical assistance from Philip Barnette and William Sutton, as well as ONPRC Molecular Virology Core staff members Don Siess, David Burke, Jeff Torgerson, Travis Giobbi, and Greg Dissen. We thank Drs. Julie Mitchell and Lydie Trautmann for their advice regarding flow cytometry data analysis. We also thank Dr. Peter Barry for kindly providing the cytomegalovirus detection antibody for pathology analyses. We acknowledge the veterinary and technical staff of the Division of Comparative Medicine at the Oregon National Primate Research Center for animal husbandry. This work was supported by NIH R01 AI133712 (N.L.H.), U42 OD023038, U42 OD010426, and P51 OD011092. M.B.S. was supported by NIH T32 AI007472. The authors declare no competing financial interests.

III. Introduction

Vertical HIV-1 acquisition remains prevalent in resource-limited settings, particularly where access to antiretroviral therapy (ART) during pregnancy is inadequate. An estimated 160,000 infants were newly infected in 2018[166]. Transmission occurs predominantly during labor and birth, and also occurs during gestation or breastfeeding[167]. In infants, HIV infection is characterized by high viral loads, weak control of post-acute viremia, and consequently rapid progression to disease[112]. Without treatment, over 30% of infants die in their first year of life, and over half die by age 2[113].

Studies of HIV-1 in humans and animal models have demonstrated that lentiviral pathogenesis is associated with a “vicious cycle” of chronic immune activation, impaired immunological function, and persistence of the viral reservoir[124]. Beginning early in

infection, damage to the intestinal barrier results in microbial translocation into the blood[117]. Uptake of microbial products by myeloid antigen-presenting cells stimulates pro-inflammatory cytokine secretion, leading to systemic inflammation and immune activation[118]. In adults with HIV-1, activation and proliferation of CD8+ T cells occurs in a largely antigen-independent manner, and is driven by pro-inflammatory cytokines, especially IL-15[295]. Studies of untreated and ART-treated HIV infection in children and adults have identified inversion of the ratio of CD4+ to CD8+ T cells as a marker of immune activation, immune senescence, and poor prognosis[296-298]. The B cell compartment is also perturbed, with acute memory B cell loss, proliferation of immature transitional B cells and plasmablasts, increased cell turnover, and hypergammaglobulinemia[162]. Finally, alterations to the monocyte compartment during infection are associated with disease progression in humans infected with HIV-1 as well as animal models[120,299,300]. Monocytes exist on a spectrum of differentiation from classical (CD14+CD16-) through intermediate (CD14+CD16+) to nonclassical (CD14-CD16+) subsets, varying in their cell surface marker expression, cytokine production, and phagocytic activity[301,302]. Increased frequencies of intermediate monocytes have been found to correlate with systemic immune activation markers and negatively correlate with CD4+ T cell counts during HIV-1 infection[120].

Microarray and deep sequencing studies of gene expression have complemented these findings by identifying distinct transcriptomic signatures associated with different outcomes of HIV-1 infection. Untreated infection is characterized by an innate antiviral response mediated by type I IFN signaling and upregulation of interferon-stimulated genes (ISGs). These changes occur early; even during acute HIV-1 infection, transcriptional differences may be useful for predicting the viral set point[303]. Rapid disease progression is marked by the upregulation of certain microRNAs[304]. In contrast, elite controllers and long-term non-progressors have attenuated type I IFN responses

during the chronic stage, as well as other alterations[305,306]. Similarly, nonhuman primate (NHP) studies of acute infection with simian (SIV) and simian-human immunodeficiency viruses (SHIV) have revealed inflammasome activation, type I IFN, and IFN-γ responses in tissues within days of mucosal exposure[239,307]. Additionally, comparison of pathogenic and nonpathogenic SIV infection revealed that only pathogenic SIV infection drives sustained type I IFN responses during chronic infection[308], mirroring findings in human HIV-1 controllers.

Neonatal immunity is distinct from that of adults in ways that are presumed to hinder newborns' ability to control viral infection. Newborns have an immature immune system characterized by greater Treg-mediated suppression and Th2 bias, deficiency in Th1 responses, underdeveloped humoral immunity, and impairments in T cell priming and other innate effector functions[178,179]. Human and animal studies of HIV infection have identified CD8+ T cell responses as a major mechanism of viral control[180]. Weak CD8+ T cell responses are observed in HIV-infected children under 3 years of age, especially those with depleted or phenotypically altered CD4+ T cells in conjunction with high viral loads[181]. Regulatory T cells (Tregs), an abundant anti-inflammatory T cell subset in newborns, are conjectured to play multifactorial and opposing roles in HIV-1 infection by suppressing either beneficial virus-specific CD8+ T cell responses, deleterious immune hyperactivation, or both[182]. Although the relationship between immune activation and pathogenesis in infants is not well characterized, CD8+ T cell activation in infants at 1-2 months of age was predictive of disease progression in one study[183]. In addition to functional deficiencies that impede antiviral defense, infants and newborns are at a disadvantage due to elevated numbers of potential target cells. Newborn and infant rhesus macaques have greater counts and frequencies of CD4+ T cells[184], notably activated CD4+ CCR5+ memory T cells that are prime targets for

infection with SIV[43,185]. These cells are likewise abundant in the human gut at birth, and may be a key target cell population during vertical HIV-1 acquisition[186].

Infection of macaques with SIV or SHIV are established models for studying HIV-1 pathogenesis and testing vaccines and therapies. In adult macaques exposed to the pathogenic Tier 2 viral swarm $SHIV_{SF162P3}$, viremia tends to mirror the course of adult HIV-1 infection, with acute peak viremia soon decreasing to a set point that varies between individuals[55,204] and in some cases is controlled spontaneously[111]. In contrast, infant macaques infected with this SHIV recapitulate the high viral loads and weak post-acute control seen in perinatal HIV-1 infection, and progress to disease within weeks[105,114,205,206].

Among infants who acquired HIV-1 vertically, age at the time of HIV-1 infection is correlated with survival rate, with mortality highest among those infected before 4 weeks of age and decreasing gradually over the first year of life[113,176,177]. This age-dependent decrease in mortality may be attributable at least in part to immune maturation during infancy, resulting in an increasing capacity for defense against viral pathogens and attenuated damage to the immune system. Notably, however, many NHP studies intended to model peripartum HIV infection have assigned macaques that are several weeks[105,114,205,206] to several months old[208]. The relative pathogenicity of SHIV infection in newborns compared with older infants has not been explored. Furthermore, immunologic damage in infants as a result of infection with either HIV-1 or SHIV is not well characterized.

Here, we asked whether SHIV infection dynamics, immune responses, and outcomes in infant macaques are influenced by age at the time of exposure. To answer this question, we compared virologic outcomes, adaptive immune responses, frequencies and phenotypes of key leukocyte subsets, and transcriptome profiles during pathogenic SHIV infection in Newborn (1-2 weeks old) and Infant (15-16 weeks old)

rhesus macaques that were lacking the two major MHC-I alleles for post-acute viral control[152,153]. Taken together, our longitudinal data highlight subtle age-dependent quantitative and qualitative differences in the developing infant macaque immune system, providing a baseline for comparison to model the effect of novel HIV therapies on viral pathogenesis in the pediatric setting.

IV. Materials and Methods

Ethics statement. Macaque studies were performed at the Oregon National Primate Research Center (ONPRC) in Beaverton, OR, USA in compliance with all ethical regulations for animal testing and research. The ONPRC is accredited by the American Association for the Accreditation of Laboratory Animal Care International (AAALACi), and adheres to the Guide for the Care and Use of Laboratory Animals and the U.S. Public Health Service Policy on the Humane Care and Use of Laboratory Animals. The study protocol was approved by the Oregon Health & Science University (OHSU) West Campus Institutional Animal Care and Use Committee (IACUC).

Animal model. Twelve newborn male and female rhesus macaques of Indian origin (*Macaca mulatta*) were obtained from the breeding colony within days of birth, underwent veterinary evaluation, adapted to bottle feeding in the ABSL-2 infant nursery, and transferred to ABSL-2+ containment as soon as possible after 1 week of age. Animals were excluded from the study if the dam was positive for *Mamu*-B*08 and -B*17 MHC Class I alleles, which are associated with spontaneous post-acute lentiviral control[152,153]. Based on historical studies using this animal model, group sizes of six were considered sufficient to provide 80% power to detect a 1-$\log_{10}$ difference in plasma viral loads. Animals were housed in age-matched pairs throughout the study, and were

monitored for clinical signs of disease by regular evaluation of body weight, peripheral lymph node size, appetite, behavior, and stool quality. Animals were euthanized under IACUC guidelines using standard methods consistent with the recommendations of the American Veterinary Medical Association (AVMA) Guidelines for Euthanasia[309].

Hepatitis B immunization. For Newborns (Group 1), Hepatitis B vaccine Recombivax HB (Merck) was administered by intramuscular injection just prior to SHIV exposure on the first day of the study. For Infants (Group 2), the vaccine was given on the first day of the study, followed by a second dose at week 6.

SHIV stock production. Spleens and blood from naïve rhesus macaques were processed to generate single cell suspensions, which were cryopreserved in the liquid nitrogen gas phase. To generate a stock of $SHIV_{SF162P3}$ for use in Newborns (Group 1) and Infants (Group 2), a small-scale virus expansion was first performed using $SHIV_{SF162P3}$ stock obtained from the AIDS Reagent Program, Division of AIDS, National Institute of Allergy and Infectious Diseases, National Institutes of Health (catalog number 6526; contributors J. Harouse, C. Cheng-Mayer, and R. Pal) as inoculum. The day 7 supernatant of this small culture was subsequently used to inoculate a large-scale culture for virus stock production. For the small-scale expansion, a total of 8×10^7 peripheral blood mononuclear cells (PBMC) from three different rhesus macaques were thawed and rested separately overnight, then enriched for $CD4^+$ cells by MACS using NHP CD4 MicroBeads (Miltenyi). CD4-enriched cells were pooled and activated for 24 h in R15-100 media (RPMI1640, 15% FBS, 100 U/ml IL-2) containing a stimulation cocktail of Staphylococcal enterotoxin B (2 µg/ml, Toxin Technologies) and antibodies against CD3 (300 ng/ml, clone CD3-1, Mabtech), CD28 (1.5 µg/ml, clone L293, BD Biosciences), and CD49d (1.5 µg/ml, clone 9C10, BD Biosciences). The next day, cells were washed

and incubated for 2 more days in fresh R15-100 media. A total of 2×10^7 cells were then spinoculated for 2 h at 1600 × g at RT with 50 µL of $SHIV_{SF162P3}$ virus from an aliquot that had previously experienced one freeze-thaw cycle. Cells were washed the next day to remove free virus, and cultures were maintained by refreshing half of the media every other day until supernatant was harvested and banked on day 7. Viral titer was quantified as described below. For the large-scale SHIV stock production, 2.5×10^9 rhesus splenocytes from a single animal were thawed and rested overnight, then subjected to $CD4^+$ enrichment by magnetic cell separation (MACS) and activation *in vitro*, as described above. Spinoculation was performed using the small-scale SHIV supernatant as inoculum, at a multiplicity of infection (MOI) = 0.08 as measured by $TCID_{50}$/ml in TZM-bl cells (NIH AIDS Reagent Program, catalog number 8129). Virus cultures were maintained until supernatant was harvested on day 7, aliquoted, and cryopreserved in liquid nitrogen for use *in vivo*. Viral infectious titer was quantified in rhesus PBMC as described previously[205].

SHIV virus exposure. For Groups A, B, and C (preliminary study, Figure 3.1), a challenge stock of $SHIV_{SF162P3}$ was obtained from the AIDS Reagent Program (catalog number 6526) and stored at -80°C. Virus was diluted 4-fold in DMEM media just prior to oral challenge. Each animal received a total of 0.5 ml (644 $TCID_{50}$ measured in rhesus PBMC) of cell-free virus by swallowing, given as two 1 ml doses of diluted virus 15 minutes apart. Animals in Group A (n = 6) were exposed to SHIV at 6-9 weeks of age, resulting in productive infection in 3/6. Group B animals (n = 6) were initially exposed to SHIV at 5-10 weeks of age, followed by 3 weeks of daily subcutaneous ART. All 6 were aviremic until re-challenge with SHIV 47 days after the final ART dose, resulting in 4/6 becoming productively infected. Group C animals (n = 6) were initially exposed to SHIV at 5-8 weeks of age and then received a short treatment course of ART and broadly

neutralizing antibodies (bNAbs). Like Group B, these animals remained aviremic until SHIV re-challenge 69 days after the last ART treatment and 81 days after the last bNAb treatment, causing productive infection in all 6 animals. Because the focus of our subsequent study was age-dependent differences in post-acute control of infection, only the persistently viremic animals from Groups A-C are included in Figure 3.1. For the Newborns and Infants in the main study (Groups 1 and 2), a challenge stock of $SHIV_{SF162P3}$ virus was generated in activated, magnetically-enriched CD4+ macaque splenocytes inoculated with a stock of $SHIV_{SF162P3}$ obtained from the AIDS Reagent Program (catalog number 6526). Virus production methods are described in detail in the preceding section. Cell-free viral culture supernatant was harvested on day 7, and aliquots were stored in the liquid nitrogen gas phase until use in challenge experiments. Virus stock titer was quantified *in vitro* as previously described [205]. Each animal received a total of 2 ml (4.1×10^4 $TCID_{50}$ measured in rhesus PBMC) of undiluted cell-free $SHIV_{SF162P3}$ virus by swallowing, given as two 1 ml doses 10-15 min apart. Virus aliquots were transported on dry ice and thawed at room temperature or in hand just prior to animal challenge. Newborns were exposed to SHIV at 1-2 weeks of age, at the day 0 study time point. Infants were exposed at 15-16 weeks of age, corresponding to the week 14 study time point. See Figure 3.2 for study schedule and Table 3.1 for animal ages at key study time points.

Blood and tissue harvest and processing. Peripheral blood was collected into EDTA blood tubes prior to virus exposure on the day of challenge, on days 4, 7, 10, and 14, and weekly thereafter. When needed, aliquots of 500 µl and 100 µl whole blood were taken out for RNA isolation and flow cytometry, respectively, following the sampling schedule shown in Figure 1. The remaining blood was centrifuged in the collection tubes at 750 x *g* for 30 min at 4 °C with the brakes off in order to separate plasma from cells.

The plasma supernatant was pipetted off and aliquots were stored at −80 °C. The remaining blood fraction was resuspended in sterile PBS to double the original volume, and PBMC were isolated by centrifugation in SepMate tubes (StemCell Technologies) over Lymphocyte Separation Medium (Corning) and cryopreserved in liquid nitrogen. Inguinal lymph nodes were biopsied at weeks 1 and 6 post-SHIV exposure. At each biopsy, two adjacent lymph nodes were taken. One node was preserved in 4% paraformaldehyde and then transferred to 80% EtOH for paraffin embedding and imaging. The second node was crushed through a 100 µm strainer to generate a cell suspension. Pellets of 3×10^6 cells were frozen at −80 °C for viral quantitation, and any remaining cells were cryopreserved in liquid nitrogen. At necropsy, blood, cerebrospinal fluid (CSF), and a panel of solid tissues were harvested. CSF was collected into a 2 ml vial and stored at −80 °C. From each solid tissue, 100 µg samples were excised and frozen at −80 °C in 2 ml tubes pre-filled with 1.4 mm zirconia beads (Spex SamplePrep) to facilitate tissue homogenization with a bead beater, nucleic acid extraction, and vDNA detection by quantitative PCR. For spleen and mixed mesenteric lymph nodes, any remaining tissue was processed to make single cell suspensions, which were cryopreserved in liquid nitrogen.

Viral nucleic acid quantitation in plasma, cells, and tissue homogenates. Nucleic acid from plasma, CSF, or lymph node biopsy cell pellets was purified using a Maxwell 16 instrument (Promega, Madison, WI) per the manufacturer's protocol, using the LEV Viral Total Nucleic Acid Kit for plasma and CSF and the LEV Whole Blood DNA Kit for lymph node cells. The quantitative PCR and RT-PCR protocols for viral RNA, viral DNA in cell pellets, and viral DNA in tissues are described below. The following primers and probe were used for all protocols to amplify and detect a conserved region in SIV*gag*: SGAG21 forward primer (GTCTGCGTCATPTGGTGCATTC), SGAG22 reverse primer

(CACTAGKTGTCTCTGCACTATPTGTTTTG), and pSGAG23 probe (5′-6-carboxyfluorescein [FAM]-CTTCPTCAGTKTGTTTCACTTTCTCTTCTGCG-black hole quencher [BHQ1]-3′) [271]. Staff members performing the viral RNA and DNA assays were blinded to the experimental groups and conditions for all samples tested.

Viral RNA RT-qPCR assay: SHIV viral RNA in plasma and CSF was measured by quantitative RT-PCR (RT-qPCR) using the TaqMan® Fast Virus 1-Step Master Mix (Applied Biosystems #4444434). RT-qPCR reactions were set up in duplicate with 20 µl RNA per reaction, with 900 nM SGAG21, 900 nM SGAG22, and 250 nM pSGAG23 in a 30 µl total volume. SIV-positive plasma RNA was used for positive controls, and nuclease free water was used for no-template controls. Reactions were run on an Applied Biosystems QuantStudio 6 Flex instrument (Life Technologies, Carlsbad, CA) using the following protocol: 50°C for 5 min; 95°C for 20 sec; [95°C for 3 sec, 60°C for 30 sec] x 45 cycles. Virus RNA copies were calculated based on a standard curve of SIV*gag* RNA serially diluted in 5 ng/µl yeast tRNA (Sigma R5636, 10mg/ml) in 10mM TRIS pH 8.0. The limit of detection in this assay is 50 copies/ml.

Viral DNA qPCR assay for cell pellets: SHIV viral DNA in lymph node biopsy cell pellets was measured by quantitative PCR (qPCR) using the TaqMan® Fast Advanced Master Mix (Life Technologies #4444964). Reactions were performed with 2 µg DNA per reaction, with 600 nM SGAG21, 600 nM SGAG22, and 100 nM pSGAG23 in a 30 µl total volume. Nuclease free water was used for no template controls. Reactions were run on an Applied Biosystems QuantStudio 6 Flex instrument using the following protocol: 50°C for 2 min; 95°C for 20 sec; [95°C for 1 sec, 60°C for 20 sec] x 45 cycles. Virus DNA copies were estimated by comparison to a standard curve of linearized pBSII-SIV*gag* DNA serially diluted in TE buffer containing carrier DNA, and calculated per cell

equivalent using the input nucleic acid mass and by assuming a DNA content of 6.5 µg per 10^6 cells, with a detection limit of 2 copies/µg DNA or 10 copies/10^6 cells.

Viral DNA qPCR assay for tissues: Viral DNA was measured in necropsy tissue samples using the same qPCR assay described above for cell pellets, with the following changes. Tissue DNA was heated to 95°C for 5 min, then placed on ice, prior to adding to PCR reaction tubes. Reactions were performed with 2.5 µg total DNA input per reaction in a 20 µl total volume, and were run on an Applied Biosystems ABI 7500 instrument. This assay has a detection limit of 1 copy/µg DNA or 7 copies/10^6 cells.

Evaluation of pathology. At necropsy, rhesus macaque tissues and body fluids were collected fresh, frozen, or fixed in 10% formalin and subsequently processed for histologic evaluation. Necropsies and microscopic evaluation of tissues were performed by veterinary pathologists blinded to animal group assignments and viral load data. Pathogens were identified and confirmed by H&E morphology and then histochemical stains, immunohistochemistry (IHC), and PCR. Adenovirus, cytomegalovirus, and *Enterocytozoon bieneusi* were all visualized by IHC using the Vectastain ABC Kit, Peroxidase Standard (Vector Laboratories, Burlingame, CA, USA). Adenovirus was detected with a mouse anti-adenovirus monoclonal antibody (MAB8052, 1:500 dilution, EMO Millipore, Temecula, CA, USA). Cytomegalovirus was detected using an antibody kindly gifted by Peter Barry (1:750 dilution) as previously reported[278]. *E. bieneusi* were visualized using a mouse anti-measles matrix protein monoclonal antibody (MAB8910, 1:1000 dilution, EMO Millipore, Temecula, CA, USA). *Spironucleus* species (sp) were confirmed in tissue by nested PCR amplification of small subunit ribosomal DNA using methods developed by Bailey et al.[279]. *Cryptosporidium* sp, SHIV giant cell disease, flagellated protozoa, *Pneumocystis* sp, *Malassezia* sp, and attaching and effacing *E. coli*

were all diagnosed by H&E stain. Additional diagnostic methods included Gomori methenamine-silver stain for *Pneumocystis* sp and Periodic Schiff reaction for *Malassezia* sp. Intracellular argyrophilic bacteria were visualized by Warthin-Starry stain. Disease scores of 0, 1, or 2 were assigned to each animal according to the criteria outlined in Table 3.1.

Enzyme-linked immunosorbent assay (ELISA). Antibody responses were determined by measuring binding of plasma IgG to recombinant HIV-1 SF162 gp140 trimer. The gp140 trimer was produced as described[277] by transient transfection in Expi293F cells and purified over a *Galanthus nivalis* lectin-coupled agarose (GNA) column (Vector Laboratories, Burlingame, CA), followed by size exclusion chromatography on a Superdex 200 column (GE Healthcare Life Sciences) to separate trimer from monomer. The trimer fractions were pooled and concentrated, and aliquots were frozen at −20 °C. Half-well ELISA plates (Costar) were coated with SF162 gp140 trimer at 0.5 μg/ml in carbonate/bicarbonate buffer and incubated overnight at 4 °C. Plates were washed one time in wash buffer (0.1% Triton X-100 in 1X PBS) and blocked with 1% normal goat serum/5% nonfat dried milk in PBS for 1 h. Serially diluted plasma samples were then incubated for 1 h followed by three washes. Plates were probed with a horseradish peroxidase-conjugated goat anti-human IgG Fc fragment-specific polyclonal antibody (1:5000, Jackson ImmunoResearch) for 1 h. After five washes, TMB substrate (SouthernBiotech) was added and incubated for 10 min before quenching with1 N H_2SO_4. Optical density at 450 nm was read and 50% binding titers were calculated using GraphPad Prism and Microsoft Excel. Each sample was assayed in duplicate.

Env-pseudovirus construction. SHIV gp160/pEMC* vector DNA was co-transfected with pSG3ΔEnv HIV-1 backbone DNA into 293T cells (European Collection of

Authenticated Cell Cultures, Sigma catalog number 12022001) using the jetPEI (Polyplus) transfection reagent. Supernatant containing pseudovirions was harvested after 2–3 days and frozen in 1 ml aliquots at −80 °C. Pseudovirus stocks were titrated in TZM-bl cells (NIH AIDS Reagent Program, catalog number 8129) to determine the virus dilution required for 200,000 relative light units (RLU).

Env-pseudovirus neutralization assay. To measure neutralizing antibody titers, heat-inactivated plasma samples with measurable SF162 gp140 binding titers by ELISA were assayed in duplicate for neutralization against single round of entry $SHIV_{SF162P3}$ Env-pseudoviruses using TZM-bl reporter cells in which infection drives luciferase expression (NIH AIDS Reagent Program, catalog number 8129)[273]. Briefly, plasma samples were serially diluted 3-fold in complete DMEM media (DMEM, 10% FBS, L-glutamine) from a starting dilution of 1:50 and incubated with pseudovirus for 1 h at 37 °C in 96-well flat bottom plates. TZM-bl cells were harvested, mixed with DEAE dextran (7.5 µg/ml) to enhance viral uptake, and 10,000 cells were added to each well containing antibodies and virus. Additional control wells containing cells and virus only (no antibody) and cells only (no virus, no antibody) were included on each plate. As a positive control, a cocktail of the broadly neutralizing monoclonal antibodies PGT121[225] and VRC07-523[244] was included on every other plate in a multi-plate experiment, and serially diluted 3-fold from a starting concentration of 1 µg/ml. Plates were incubated at 37 °C and 5% CO_2 for 48–72 h. Bright-Glo (Promega) luciferase substrate was added to each well, and luciferase activity was measured on a luminometer. Wells containing only cells and virus defined 100% RLU signal, and cells-only wells defined 0% RLU signal. To calculate neutralization potency, the RLU in each well was divided by the RLU in the virus-only wells to give the percentage of viral infection not neutralized by antibody. This % RLU

was plotted against antibody concentration to generate a dose-response curve for each antibody, from which 50% neutralization titer (IC_{50}) could be interpolated.

Enzyme-linked immunospot assay (ELISPOT). T cell responses in blood and tissues were tested in an interferon-γ (IFN-γ) enzyme-linked immunosorbent spot assay. Briefly, 1×10^5 mononuclear cells were incubated with antigen in duplicate wells of an ELISPOT plate coated with anti-NHP IFN-γ antibody (Mabtech) overnight at 37 °C. To measure responses to Env, pools of overlapping 15-mer peptides covering the length of the HIV-1 SF162 Env amino acid sequence were used as antigens. To detect anti-Gag responses, pools of overlapping 15-mer peptides covering the length of SIV_{mac239} Gag were used. ELISPOT plates were then probed using a biotinylated anti-IFN-γ antibody followed by Streptavidin-Alkaline Phosphatase and developed with BCIP/NBT-plus substrate. Plates were read on an ELISPOT plate reader (Autoimmun Diagnostika GMBH). Cells incubated with Concanavalin A (Sigma-Aldrich) and Staphylococcal Enterotoxin B (Toxin Technologies) were used as positive controls, while antigens were omitted for a background control. The numbers of spots in duplicate wells were averaged and normalized to calculate the number of spot-forming cells per 1×10^6 cells. Wells with <50 spot-forming cells per 1×10^6 cells were considered negative. Positive responses were determined by using a one-tailed Student t test at $\alpha = 0.05$, where the null hypothesis was that the number of spots in the treatment wells would be lower than or equal to the background. Values determined to be positive were reported as the average of duplicate test wells minus the average of all negative control wells.

Flow cytometry. For each sample, 100 µl of fresh whole blood were transferred from an EDTA blood collection tube into each of 2 cluster tubes, one for each staining panel, and washed once with 1 ml PBS. Surface stain antibodies for Panel 1 or Panel 2, as well as

live/dead dye (Live/Dead Fixable Yellow Dead Cell Stain Kit, Life Technologies L34968, 0.1 µl/test) were then added, and samples were vortexed and incubated for 30 min at room temperature in the dark in a total volume of 100-150 µl. Red blood cells were lysed with 1 ml of 1X FACSLyse (BD Biosciences 349202) for 8 min, followed by one wash in FACS buffer (PBS, 10% FBS, 1 mM EDTA). Samples were then fixed in 150 µl of 2% paraformaldehyde and stored at 4□C. Samples were run on a Becton-Dickinson LSR II flow cytometer as soon as possible, within 3 days of staining. Data were analyzed in Flowjo according to the gating strategies defined in Supplementary Figures 3.3 and 3.4 for Panels 1 and 2 respectively. The following antibodies were used for surface staining for Panel 1: CD3 Pacific Blue (clone SP34-2, BD Biosciences 558124, 1 µl/test), CD8 PerCP-Cy5.5 (clone SK1, BD Biosciences 565310, 2.5 µl/test), CD11c AlexaFluor 700 (clone 3.9, eBioscience 50-112-9413, 1 µl/test), CD14 ECD (clone RMO52, Beckman Coulter IM2707U, 2.5 µl/test), CD16 PE-Cy7 (clone 3G8, BD Biosciences 560716, 0.5 µl/test), CD20 APC-Cy7 (clone 2H7, Biolegend 302314, 1 µl/test), CD45 FITC (clone D058-1283, BD Biosciences 557803, 2.5 µl/test), CD123 APC (clone 6H6, eBioscience 50-150-65, 2.5 µl/test), HLA-DR PE (clone G46-6, BD Biosciences 555561, 3 µl/test). The following antibodies were used for surface staining for Panel 2: CD3 Pacific Blue (clone SP34-2, BD Biosciences 558124, 1 µl/test), CD4 APC-Cy7 (clone OKT4, Biolegend 317418, 2.5 µl/test), CD8 PerCP-Cy5.5 (clone SK1, BD Biosciences 565310, 2.5 µl/test), CD25 PE (clone BC96, eBioscience 50-112-9575, 5 µl/test), CD28 PE-Cy7 (clone CD28.2, BD Biosciences 560684, 2.5 µl/test), CD45 FITC (clone D058-1283, BD Biosciences 557803, 2.5 µl/test), CD69 PE-CF594 (clone FN50, BD Biosciences 562617, 2 µl/test), CD95 APC (clone DX2, BD Biosciences 558814, 7.5 µl/test), HLA-DR AlexaFluor 700 (clone G46-6, BD Biosciences 560743, 2.5 µl/test).

RNA isolation and deep sequencing (RNA-seq). From 500 µl peripheral whole blood collected in EDTA tubes, total cellular RNA was isolated using the QIAamp RNA Blood Mini Kit (Qiagen, catalog number 52304). RNA was eluted in 30 µl nuclease free water, split into two aliquots of 23 µl and ~5 µl, and immediately frozen at -80C. Frozen RNA aliquots were shipped on dry ice to MedGenome (Foster City, CA) for sample quality control, barcoded cDNA library construction, and bulk deep sequencing (RNA-seq) using the Illumina platform. Barcoded cDNA libraries were built using the Illumina TruSeq Stranded Total RNA kit with globin removal. Sequencing was performed with an Illumina NovaSeq instrument using a 100 bp paired-end read protocol for a read depth of ~50 million total reads (~25 million paired end reads) per sample. A total of 56 samples were processed to generate 56 readsets, of which 54 were used in downstream transcriptome analysis. The remaining 2 samples were included as backups for a particular sample of interest (Control Newborn 38371 42 DPB) that had low RNA quality, in case the library preparation or sequencing failed for that sample. However, because the sample in question successfully yielded a barcoded library and good quality sequence data, the backup readsets were not analyzed further.

RNA-seq computational pipeline and statistical analysis. RNA-seq readsets were analyzed for read quality, aligned to the rhesus Mmul10 reference genome, and genes were enumerated by the STAR method. Downstream processing of the count matrix data was performed in R (3.6.3)[310]. Data were normalized with the centered log-ratio method[311] and differential expression (DE) between contrasts of interest were analyzed using DESeq2[312]. Contrasts of interest are summarized in Figure 3.9a. Genes were considered significantly DE if adjusted p value < 0.1 using the FDR method to correct for multiple comparisons. Only significantly DE genes were displayed in the heatmaps and included in the transcriptomic signatures for each contrast. In order to increase power to

detect differences, direct comparisons between groups were performed without setting up multi-factor models, because the study was designed to control for the potentially confounding factors of sex, age, and environment. Pair-wise clustered heatmaps were generated using the pheatmap package using complete clustering on Euclidean distances[313]. Venn diagrams were constructed using the VennDiagram package[314] to visualize DE gene sets that overlap between different contrasts. For Venn diagrams, genes were considered significantly DE if adjusted p-value < 0.1. To obtain insight into biological functions and pathways of DE gene signatures, we used GeneSetVis, a custom-built bioinformatics tool, to mine the MSigDB, StringDB (Gene Ontology [GO] and Kyoto Encyclopedia of Genes and Genomes [KEGG]), and Reactome databases for functional annotation of significant genes, in order to identify pathways and cellular processes that are DE in contrasts of interest. Significantly enriched terms (adjusted p value < 0.1) that were represented by at least 3 query genes were reported in Figure 3.9 and Supplementary Figure 3.5.

V. Results

A. Study design

We showed previously that single high-dose oral exposure to $SHIV_{SF162P3}$ causes high uncontrolled viremia and rapid disease development in infant macaques exposed in the first 4 weeks of life[105,114,205,206]. In contrast, this virus is spontaneously controlled in most juvenile or adult rhesus macaques exposed by single or by repeated, titered mucosal exposure, with post-acute viral loads declining by several logs in the absence of treatment[55,111,204]. For an unrelated study of antibody and ART combination therapies, we infected three groups of infant rhesus macaques, ranging in age from 7-20 weeks, with $SHIV_{SF162P3}$ *via* oral inoculation using 644 $TCID_{50}$ (50% tissue culture infectious doses).

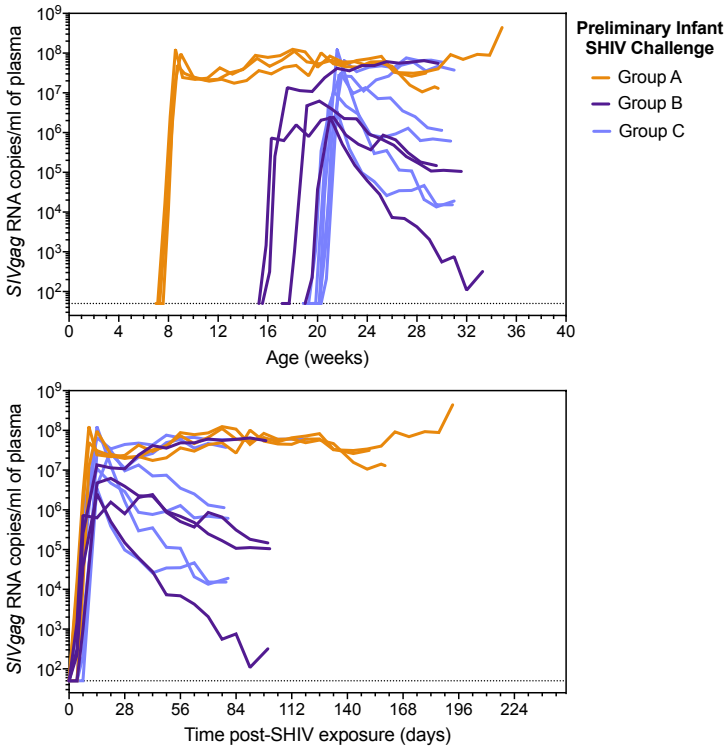

Figure 3.1. Moderate dose oral SHIV infection in infant rhesus macaques shows differences in viremia by age at time of challenge. Animals in the three different experimental groups became persistently infected upon oral $SHIV_{SF162P3}$ challenge with 644 $TCID_{50}$ at 7-8 (Group A) or 15-20 (Groups B and C) weeks of age. Plasma viral load (PVL) was measured longitudinally in each animal until the time of necropsy. Top, viral load data is shown for each animal by age at the time of the SHIV exposure that resulted in productive infection. Bottom, viral load data is shown by time since SHIV exposure.

In these three groups, treatment was either not given or had decayed to undetectable levels by the time of the viral challenge that resulted in productive infection. Intriguingly, although the viral challenge dose was the same in all three groups, only the animals exposed at <8 weeks of age displayed the high persistent post-acute viremia typical of infant infection; the other two groups exhibited adult-like patterns of post-acute viral control, despite still being infants at 15-20 weeks of age (**Figure 3.1**). Because this prior study was not designed to examine age-dependent differences in virologic outcomes, we designed an experiment to test the hypothesis that older infants, unlike newborns, are capable of controlling SHIV viremia. We also asked how age at the time of SHIV exposure affects viral reservoir seeding, immune responses, and the nature and extent of immunologic damage caused by SHIV infection.

To answer these questions, we exposed two groups of six rhesus macaques each to a single oral high dose ($4.1x10^4$ $TCID_{50}$) of $SHIV_{SF162P3}$ during different stages of infancy (**Figure 3.2**). Animals in Group 1 (hereafter referred to as “Newborns”) were exposed to SHIV at 1-2 weeks of age, while those in Group 2 (referred to as “Infants”)

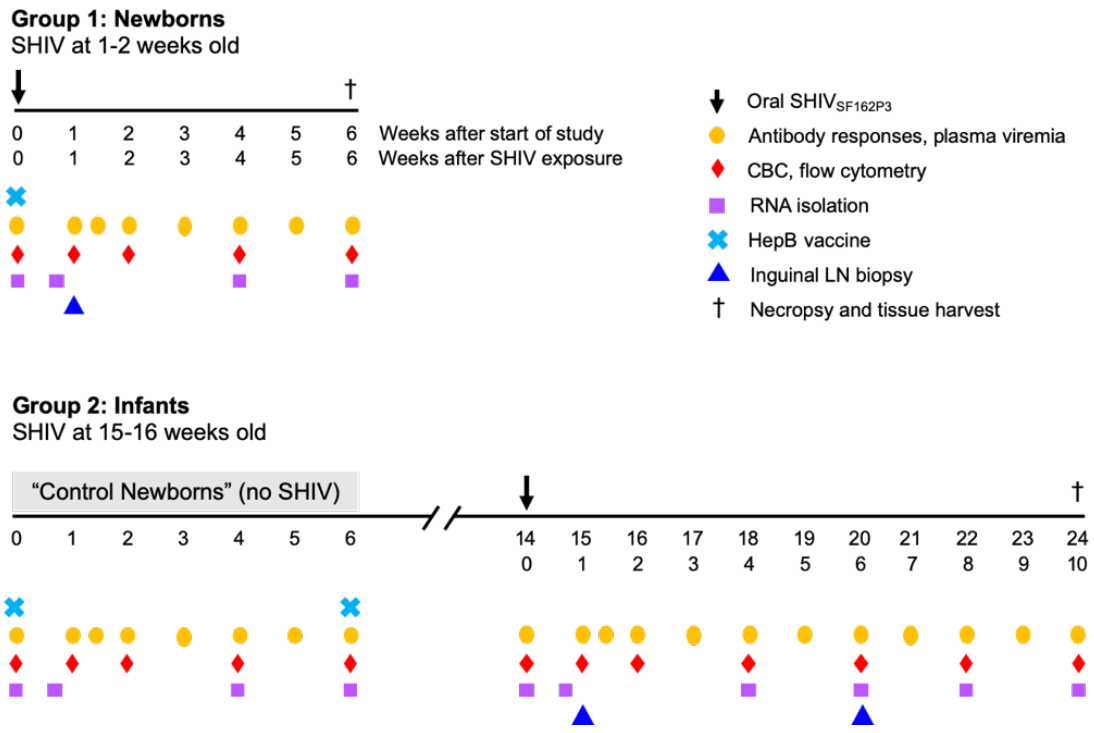

Figure 3.2. Study design. Twelve newborn rhesus macaques were transferred to containment housing as soon as possible after birth. Infants in Group 1 ("Newborns", n = 6 animals) were orally exposed to a single high dose of SHIV$_{SF162P3}$ at 1-2 weeks of age, while those in Group 2 ("Infants", n = 6 animals) were exposed at 15-16 weeks of age. During the first 6 weeks of the study, Infants, which had not yet been exposed to SHIV, served as uninfected age-matched controls for comparison with Newborns (these samples are termed "Control Newborns" in the manuscript). To test how SHIV infection affects the development of B cell responses, all animals were given the hepatitis B (HepB) vaccine (light blue X) on the first day of the study and, for Infants, a second dose 6 weeks later. Blood was sampled at the time points indicated in order to measure antibody responses and, for those infected, plasma viral loads (orange ovals), as well as complete blood counts and leukocyte phenotyping by flow cytometry (red diamonds), and RNA isolation for transcriptome analysis (purple squares). Inguinal lymph node biopsies (blue triangles) were taken at 1 week and, for Infants, 6 weeks after SHIV exposure. Animals were euthanized at the indicated time points (dagger) after SHIV exposure, or sooner if clinical endpoints were met due to onset of SHIV disease, and tissues were harvested for viral load quantitation and measurement of T cell responses.

were exposed at 15-16 weeks of age (see **Table 3.1** for individual animals' ages at key study timepoints). Because the microbiome may influence susceptibility to mucosal SHIV infection by modulating target cell activation[315], we took steps to minimize environmental differences between Newborns and Infants that might alter the microbiome. For this reason, both Newborns and Infants were adapted to bottle formula feeding and transferred to ABSL-2+ containment housing in pairs or triplets at approximately 1 week of age. Newborns were exposed to SHIV the following week, whereas Infants were exposed to SHIV 14 weeks later. Blood and lymph node biopsies were sampled at

intervals during the first few weeks of SHIV infection in order to track viral dynamics and immune responses by flow cytometry, *in vitro* immunological assays, and transcriptome profiling. Blood was also collected from Infants at age-matched time points during the newborn period in order to provide baseline measurements for comparison to the SHIV-infected Newborns; these samples are hereafter referred to as “Control Newborns”. To facilitate measurement of how SHIV infection might impact adaptive responses to unrelated antigens not present in the SHIV, all animals were immunized with a hepatitis B (HepB) vaccine during the newborn period using a regimen modeled after the routine HepB immunization schedule for infants in the United States. Finally, lymphoid and gastrointestinal tract tissues were harvested at the end of the study for spatial analysis of viral reservoir seeding in these key tissues of interest.

Table 3.1. Study demographics and pathology summary.

ID (Sex)	Group	Age at Start of Study (days)[a]	Age at SHIV exposure (days)	Age at necropsy (days)	Days from SHIV exposure to necropsy	Clinical history, opportunistic infections and pathologic diagnoses	Disease score[b]
37619 (F)	Newborns[c]	14	14	39	25	Weight loss and diarrhea. Lymphoid depletion; enteric cryptospridiosis; neutrophilic colitis and proctitis; mild bronchointerstitial pneumonia.	2
37650 (M)	Newborns[c]	7	7	32	25	Weight loss, diarrhea, and erythematous rash on abdomen. Lymphoid depletion; enteric, pharyngeal, and salivary gland cryptosporidiosis; segmental necroulcerative colitis. Chronic-active typhlocolitis.	2
38248 (M)	Newborns	12	12	51	39	Intermittent regurgitation and weight loss. Mild lymphoid depletion. Chronic-active typhlocolitis.	1
38275 (F)	Newborns	12	12	54	42	Unremarkable clinical history. Mild chronic-active typhlocolitis.	0
38276 (F)	Newborns	12	12	54	42	Chronic diarrhea and abdominal erythematous rash. Mild chronic-active typhlocolitis.	1
38317 (F)	Newborns	11	11	55	44	Weight loss, poor appetite, and abdominal erythematous rash. Variable lymphoid depletion. Chronic-active typhlocolitis.	1
38221 (M)	Infants	14	112	171	59	Dermatitis, weight loss, and diarrhea. Tracheal, tonsillar, enteric and colonic cryptosporidiosis; colonic attaching and effacing *E. coli;* membranoproliferative glomerulopathy.	2
38242 (F)	Infants	8	106	173	67	Dermatitis and diarrhea. Mild multifocal lymphoid hyperplasia; mild tonsillar and enteric cryptosporidiosis.	2
38362 (M)	Infants	14	112	181	69	Transient vesicular cheilitis. Mild membranoproliferative glomerulopathy. Minimal chronic-active typhlocolitis.	1
38371 (M)	Infants	14	112	180	68	No significant clinical history. Minimal chronic-active typhlocolitis.	0
38395 (F)	Infants	13	111	177	66	Diarrhea. Variable lymphoid depletion; pharyngeal, enteric, and salivary gland cryptosporidiosis. Mild chronic-active typhlocolitis.	2
38423 (M)	Infants	10	108	173	65	Intermittent weight loss. Bronchointerstitial pneumonia; pharyngeal cryptosporidiosis; ulcerative cheilitis; minimal glomerulopathy.	2

[a] The start of the study is defined as the first timepoint at which blood was collected from each animal. For Newborns, this is the day of SHIV exposure (day 0). For Infants, this is the day they would have been exposed to SHIV had they been assigned as Newborns – i.e., the day 0 sample from the age-matched uninfected control group ("Control Newborns").
[b] Disease score criteria: 0 - No significant lesions and clinical history OR diarrhea and typhlocolitis consistent with colony infants without SHIV. 1 - One or more non-specific findings such as rash or minimal or mild glomerular change. Findings cannot be definitively assigned to SHIV-related immune suppression. 2 - One or more of the following: opportunistic infections, lymphoid depletion, glomerulonephropathy consistent with SHIV-related disease in infant macaques.
[c] Like the other four Newborns, animals 37619 and 37650 were orally exposed to a single high dose of $SHIV_{SF162P3}$ at 1-2 weeks old. However, except for CD4, CD8, and CD20 counts, detailed longitudinal monitoring by flow cytometry was not performed for these two animals.

B. SHIV infection dynamics and reservoir seeding

To track viral production during acute and post-acute infection, we measured viral RNA copies in each animal's plasma over time (**Figure 3.3**). In contrast to the first study (**Figure 3.1**) most animals exposed to the high oral dose of SHIV in both age groups maintained high post-acute viral loads, with only a transient decrease in viremia from the peak level on day 10 post-infection (p.i.) (**Figure 3.3a**). Although one animal in the Infant group, 38242, appeared to be developing some partial control at 8-10 weeks p.i., there was no significant difference in cumulative plasma viral loads between Newborns and Infants during the first 6 weeks (**Figure 3.3b-c**). One salient difference between this study and our pilot study was that the Newborns and Infants in the present

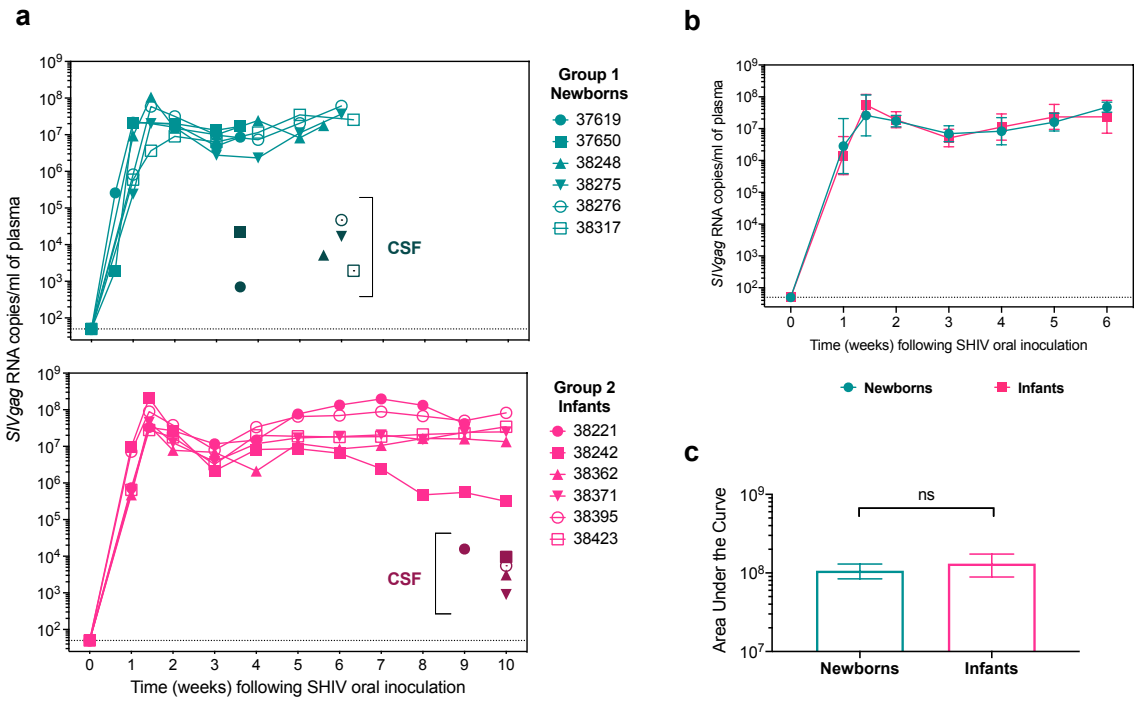

Figure 3.3. Viral loads during the acute phase following high dose challenge with SHIV do not vary by age at time of exposure in infant macaques. a) Top, plasma viral load (PVL) data for Newborns (exposed to $SHIV_{SF162P3}$ at 1-2 weeks of age). Bottom, PVL data for Infants (exposed to $SHIV_{SF162P3}$ at 15-16 weeks of age). Individual animals are represented by unique symbols. Symbols shown in darker colors indicate each animal's viral load in cerebrospinal fluid (CSF) at the time of necropsy. **b)** For statistical comparison of PVL between Newborns and Infants, data were censored at 6 weeks, and time points were excluded from analysis if PVL was measured for only one group. Error bars are SEM. **c)** Area under the curve was computed for each group by taking the mean PVL measurement at each timepoint during the first 6 weeks after SHIV exposure. There was no significant difference between the groups (unpaired t test with Welch's correction, two-tailed $p > 0.05$, $n = 6$ animals per group).

study received a different, higher titer SHIV stock, resulting in a 63-fold higher dose of viral inoculum (4.1×10^4 $TCID_{50}$ compared with 644 $TCID_{50}$). It is possible that such a high dose obscured any subtle age-dependent differences in immune-mediated viral control, which may have been evident if a lower dose had been used.

We also quantified viral DNA in inguinal lymph nodes at day 7 and at week 6 p.i. and found that both Newborns and Infants had more viral DNA at the latter time point (**Figure 3.4a-b**), likely reflecting ongoing tissue seeding in the first 2-3 weeks of infection. Viral DNA levels were similar in both groups on day 7 and at week 6 (**Figure 3.4c-d**). However, pairwise comparison of viral DNA in lymphoid and gut tissues at necropsy revealed a small but significant 0.36-log_{10} increase in viral seeding in Newborns compared to Infants (**Figure 3.4e**). As the necropsy tissue samples were collected at week 9 or 10 for Infants and at week 3 or 6 for Newborns (see **Table 1**), we were unable to compare viral seeding in the full tissue panel at matched time points. However, we consider it likely that lymphoid tissue viral DNA quantities were similar between weeks 6 and 10 in the Infants, because we previously demonstrated that viral DNA levels are stable during post-acute infection in this infant model[205].

Finally, we evaluated each animal's clinical history, assigning a disease score from 0-2 to indicate disease severity. In both the Newborn and Infant groups, 5/6 animals developed some degree of renal glomerular change or rash (disease score 1), with 2/6 Newborns and 4/6 Infants exhibiting lesions or opportunistic infections directly attributable to SHIV infection (disease score 2) (**Table 3.1**). However, there was no significant difference in disease score between groups (Mann Whitney U test, two-tailed $p = 0.53$, $n = 6$ animals per group).

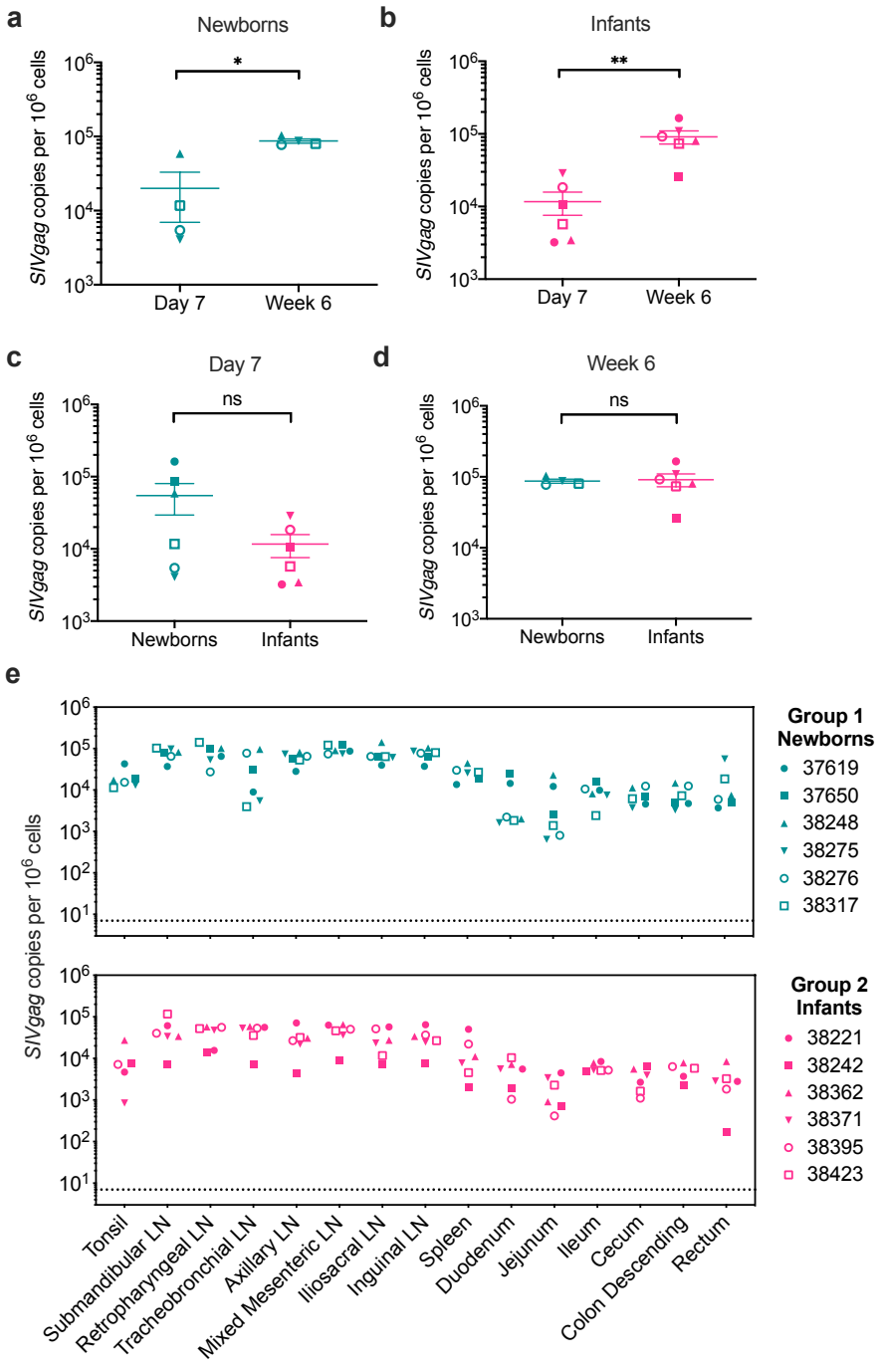

Figure 3.4. Viral DNA in tissues of Newborns and Infants. a-b) Newborns and Infants both had significantly more viral DNA copies in inguinal LN at week 6 compared with day 7 after SHIV exposure. **a)** Newborns: paired t test, two-tailed p = 0.0333, n = 6 animals per time point. **b)** Infants: paired t test, two-tailed p = 0.0053, n = 6 animals per time point). **c-d)** Viral DNA copies in inguinal LN did not significantly differ between age groups at either day 7 or week 6 after SHIV exposure. **c)** Day 7: unpaired t test, two-tailed p = 0.1744, n = 6 animals per group. **d)** Week 6: unpaired t test, two-tailed p = 0.8048, n = 6 animals per group. **e)** Viral DNA quantitation in lymphoid and gut tissues at time of death. Newborns had a median of 0.36 logs more viral DNA copies per 10^6 cells in each tissue than Infants (Wilcoxon matched-pairs signed rank test on $\log_{10}$-transformed data, two-tailed p = 0.0006). **, $p < 0.01$. *, $p < 0.05$. Symbols used for each animal are consistent throughout the manuscript. Error bars are SEM.

C. Adaptive immune responses

To examine the effect of SHIV infection on adaptive immunity, we administered the HepB vaccine Recombivax HB to all animals on the first day of the study, followed by a second dose at week 6 for those animals still alive, in a regimen similar to the recommended HepB immunization schedule for US infants[316]. We then measured plasma antibody responses to the hepatitis B surface antigen (HBsAg) protein in each animal over time (**Figure 3.5a**). Strikingly, while all 6 Infants made antibodies after their first vaccine dose, with 5/6 (83%) responding by week 3, the majority of Newborns (4/6) did not respond at all (**Figure 3.5b**). Because the major difference between the Newborns and Infants over this time period was the presence or absence of SHIV infection, this finding suggested that acute SHIV infection hampered newborn B cell responses to HepB vaccination, as HIV does in human infants[317]. While we only measured binding to HBsAg and therefore cannot generalize to B cell immunity globally, it is probable that SHIV weakens humoral responses to other vaccine antigens, given that reductions in vaccine-induced antibody titer after HepB, pneumococcal, tetanus, diphtheria, pertussis, oral polio, and measles vaccination have been reported in HIV-infected infants[318].

While the HepB immunization schedule precluded evaluation of primary HepB responses in Infants after SHIV infection as in Newborns, we nonetheless were able to measure the effect of SHIV on preexisting HepB immunity by comparing the SHIV-infected Infants with an aviremic control group (**Figure 3.5a, c**). The animals in this control group were matched to the Infants by age and HepB vaccination history, but they

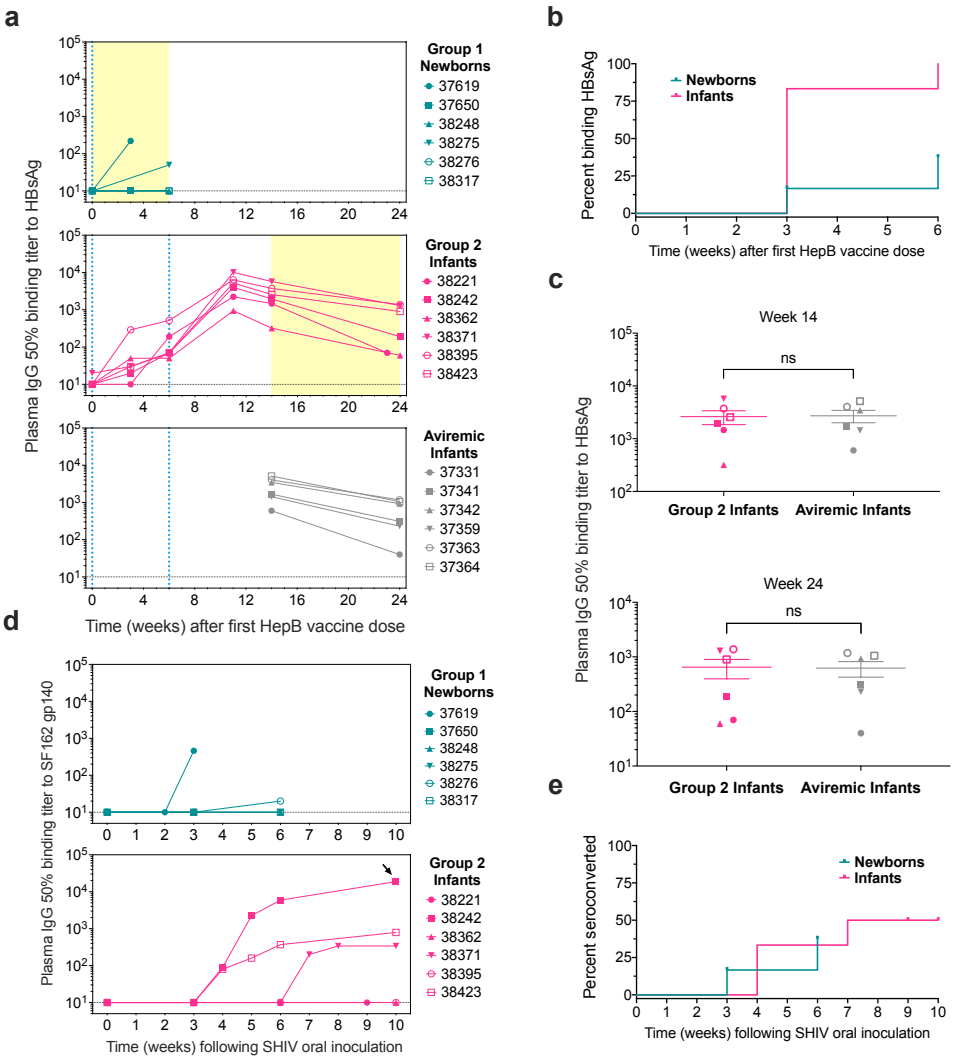

Figure 3.5. Acute SHIV infection impairs humoral responses to Hepatitis B vaccine in Newborns. a) Plasma IgG binding titers to hepatitis B (HepB) surface antigen recombinant protein measured over time in Newborns (top), Infants (middle), and a comparison group of approximately age-matched infants without detectable SHIV viremia (bottom). The animals in this comparison group, termed "Aviremic Infants", were exposed to $SHIV_{SF162P3}$ on the same day as their first HepB vaccine dose, followed 30 hours later by a broadly neutralizing antibody treatment that halted infection, resulting in undetectable viral loads in all 6 animals. Light blue dotted lines at x = 0 and x = 6 denote the first and second doses of hepatitis B vaccine; Newborns only received the first dose. Yellow shaded areas indicate time periods after SHIV exposure for Newborns and Infants. **b)** Kaplan-Meier analysis of the percentage of animals in each group that have antibodies to HepB surface antigen by the indicated time points. In this analysis, while the two groups are matched in age, they differ in that the Newborns were exposed to SHIV on study day 0, whereas the Infants were not. A significantly smaller percentage of Newborns than Infants mounted antibody responses to HepB antigen after a single dose of HepB vaccine (Log-rank test, p = 0.0115, n = 6 animals per group). **c)** Binding titers to HepB surface antigen were not significantly different between Group 2 Infants and Aviremic Infants at either 14 weeks (top) or 24 weeks (bottom) after the first dose of HepB vaccine (unpaired t tests, two-tailed p = 0.8225 and p = 0.8473 for weeks 14 and 24 respectively, n = 6 animals per group for each comparison). Symbols used for each animal are consistent throughout the manuscript. Error bars are SEM. **d)** Plasma IgG binding titers to SF162 Env gp140 glycoprotein measured over time in Newborns (top) and Infants (bottom). Black arrow indicates the only plasma sample with neutralizing activity against $SHIV_{SF162P3}$ pseudovirus in a TZM-bl neutralization assay (ID_{50} = 1200). **e)** Kaplan-Meier analysis of the percentage of animals in each group that have seroconverted (i.e. developed binding antibodies to SF162 gp140) by the indicated time points. There is no significant difference between the two groups (Log-rank test, p = 0.8354, n = 6 animals per group).

had been exposed to SHIV followed by prompt treatment with potent broadly neutralizing monoclonal antibodies, resulting in durable tight control of infection and an absence of viremia during the period of comparison[205]. We found no differences between HepB plasma antibody titers in the two groups, suggesting that persistent SHIV viremia did not diminish preexisting antibody immunity to HepB in infants (**Figure 3.5c**), although it is possible that comparison with a true SHIV-unexposed control group would have yielded a different outcome.

In order to investigate how age at the time of SHIV infection influences antiviral immune responses, we tracked the kinetics and potency of anti-SHIV IgG responses in newborns and infants. Seroconversion was observed in 2/6 (33%) Newborns and 3/6 (50%) Infants (**Figure 3.5d**). Among the Newborns, 37619 seroconverted by week 3 but did not survive beyond day 25; all other animals remained negative except for 38276, which had low binding titers just above the limit of detection at week 6 (**Figure 3.5d**, top). In contrast, the Infants that seroconverted tended to achieve stronger binding responses, with 38242 reaching a 50% binding titer of 10^4 by week 6 and developing moderate neutralizing activity by week 10 (**Figure 3.5d**, bottom). However, the time until seroconversion was similar among Newborns and Infants (**Figure 3.5e**). We also measured the breadth of T cell responses against pools of SIV_{mac239} Gag and HIV-1 Clade B consensus Env peptides by IFN-□ ELISPOT. No responses were detected in any animal except for Newborn 37619 and Infant 38242, and their responses were narrowly focused on just one or two peptide pools (**Figure 3.6**). A weak positive signal was also observed for Infant 38362 in the spleen, though not in LN and PBMC, against one Env peptide pool (**Figure 3.6d**). Overall, T cell responses to Gag and Env were weak or absent in both groups. However, the possibility of T cells recognizing other SHIV epitopes or making cytokines other than IFN-□ cannot be ruled out. Indeed, HIV-

specific CD8+ T cells have been found to produce low IFN-□ levels in adult women with acute infection[319].

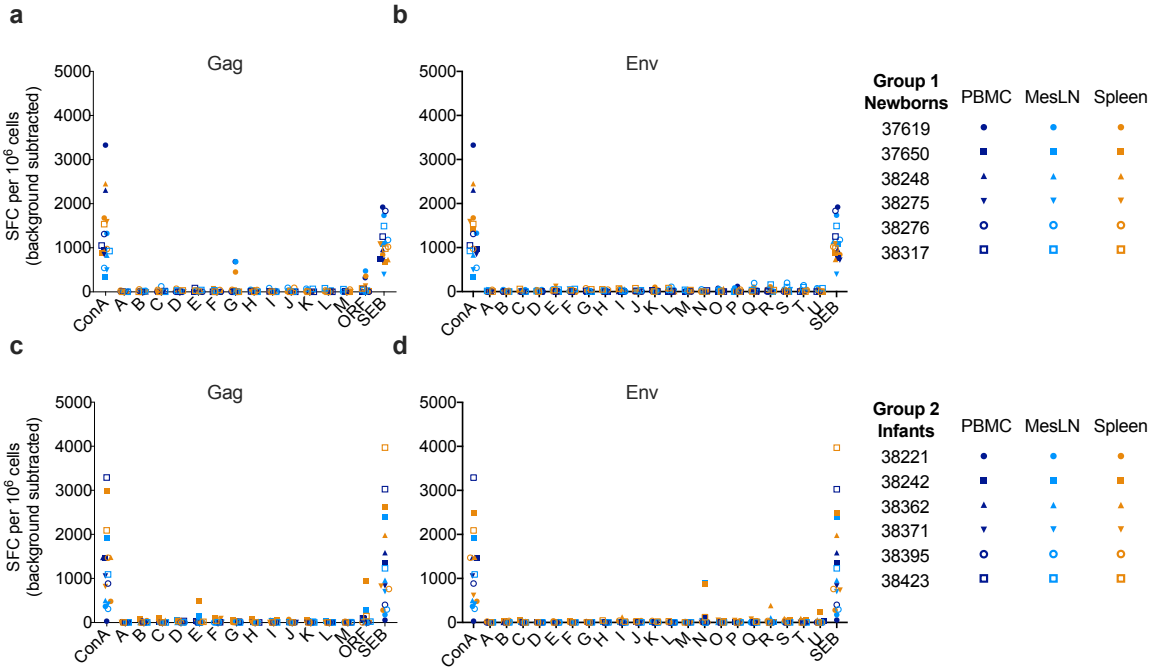

Figure 3.6. T cell responses to Gag and Env peptide pools. a-b) T cell responses to SIVmac239 Gag **(a)** and Clade B consensus Env **(b)** 15-mer peptide pools were measured by IFNγ ELISPOT for Newborns at the time of death. Symbol shapes correspond to individual animals and colors indicate tissue type, as indicated in the key. **c-d)** T cell responses to SIV_{mac239} Gag **(c)** and Clade B consensus Env **(d)** 15-mer peptide pools were measured by IFNγ ELISPOT for Infants at the time of death. Symbol shapes correspond to individual animals and colors indicate tissue type, as indicated in the key. Concanavalin A (ConA) and/or Staphylococcal Enterotoxin B (SEB) were used as positive stimulation controls. Background signal was determined using no-antigen controls. MesLN, mixed mesenteric lymph nodes. SFC, spot-forming centers.

D. Leukocyte dynamics in peripheral blood

To probe the impact of SHIV infection on major immune cell populations, we performed longitudinal analysis of peripheral blood leukocytes using flow cytometry. One staining panel was designed to enumerate B cells, natural killer (NK) cells, natural killer T (NKT) cells, and monocyte subsets (**Supplementary Figure 3.1**), and a second panel was used to track naïve and memory T cell subsets and their activation marker phenotypes (**Supplementary Figure 3.2**). A complete blood count (CBC) was also performed for each sample to facilitate the quantitation of absolute cell counts from flow

percentages. To analyze differences due to SHIV infection status in the newborn period, data for Newborns and Infants were aligned according to time after the start of the study, such that animals were matched in age but only the Newborns had been inoculated with SHIV (in other words, we compared Newborns with Control Newborns). Conversely, to determine the impact of age at SHIV exposure on immune subsets, the two groups were instead aligned according to time after SHIV exposure. For each immune parameter, the groups were statistically compared both at each individual timepoint using Sidak's multiple comparisons test to examine differences due to age and/or SHIV.

There were no significant differences in absolute counts of white blood cells, neutrophils, lymphocytes, B cells, T cells, or monocytes between groups during either the first 6 weeks of the study or the first 6 weeks of SHIV infection (**Supplementary Figure 3.3a-c, e-f, h**). We detected significantly higher platelet and NKT cell counts in Newborns than in Infants on day 4 after SHIV exposure, although the differences were marginal (**Supplementary Figure 3.3d, g**). We also observed a gradual increase in B cell numbers in both groups during the first 6 weeks of the study (**Supplementary Figure 3.3e**, top), consistent with previous findings in both human and rhesus macaque newborns[184,320]. Interestingly, while we observed a drop in B cell counts during acute infection in Infants, we saw no such pattern in Newborns (**Supplementary Figure 3.3e**, bottom). One explanation for the difference could be the preferential loss of memory B cells[321,322], which in human infants comprise a greater share of total B cells than in newborns[320], but we did not examine B cell phenotypes in detail.

Acute SHIV infection was also associated with a transient dip in NK cell count to < 200 NK cells/μl blood in both Infants and Newborns on day 10 p.i. that was strikingly consistent between individuals (**Supplementary Figure 3.3i,** bottom), although high individual variability in NK cell counts obscured differences between infected and uninfected newborns (**Supplementary Figure 3.3i**, top). We also observed a small but

distinct population of $CD3^-$ $CD8^+$ $CD20^{dim}$ cells that we provisionally refer to as $CD20^{dim}$ NK cells, although we did not test for expression of any additional NK markers such as NKG2A or CD56 (**Supplementary Figure 3.3j**). We noted lower levels of these putative $CD20^{dim}$ NK cells in Newborns than Infants at baseline (day 0 just before SHIV infection) and during acute infection (**Supplementary Figure 3.3j**, bottom), although no differences were found between SHIV-infected and Control Newborns (**Supplementary Figure 3.3j**, top). We next examined CD16 expression on classical $CD20^-$ NK cells as well as the $CD20^{dim}$ NK cell subset. In general, a smaller fraction of $CD20^{dim}$ NK cells were $CD16^+$ than the $CD20^-$ NK cells. While no age- or SHIV-dependent differences were observed in CD16 expression on $CD20^-$ NK cells (**Supplementary Figure 3.3k**), $CD20^{dim}$ NK cells expressed higher levels of CD16 at week 4 in SHIV-infected Newborns compared with Control Newborns (**Supplementary Figure 3.3l**, top). As the detection of a $CD20^{dim}$ $CD8^+$ $CD3^-$ putative NK subset was unexpected, the implications of these observations are unclear and merit further study.

Next, we examined monocyte phenotypes in greater detail. Consistent with a previous study[299], absolute monocyte counts were largely stable regardless of SHIV infection status or age (**Supplementary Figure 3.3h**). However, the relative frequencies of classical, intermediate, and nonclassical monocytes were altered in both Newborns and Infants during acute SHIV infection (**Figure 3.7a**). The proportion of classical monocytes was significantly reduced on day 10 of SHIV infection in Newborns, yet was unchanged in Control Newborns (**Figure 3.7b**, top). The magnitude of this reduction was greater in Newborns than in Infants at the same timepoint after SHIV exposure (**Figure 3.7b**, bottom), suggesting an age-dependent difference in the impact of SHIV on monocyte differentiation. The decrease in classical monocytes accompanied increases

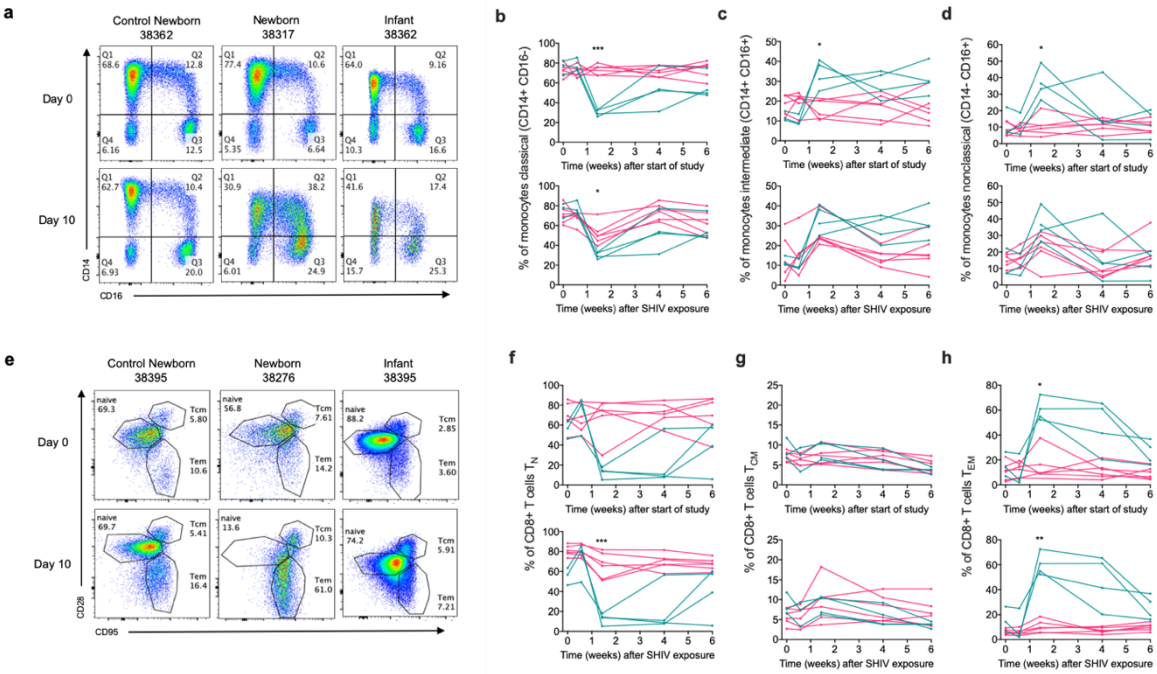

Figure 3.7. Newborn CD8+ T cells and monocytes are strongly skewed toward differentiated phenotypes during acute SHIV infection. Monocytes **(a-d)** and CD8+ T cells **(e-h)** were monitored longitudinally in peripheral blood by flow cytometry. **a)** Within the CD20- CD3- CD8- population, classical (Q1), intermediate (Q2), and nonclassical (Q3) monocyte subsets were resolved by expression of CD14 and CD16. Representative plots are shown from Newborns and Infants just before and on day 10 of SHIV infection, and from Control Newborns on study days 0 and 10. **b-d)** Percentages of monocytes with a **(b)** classical phenotype (CD14+ CD16-), **(c)** intermediate phenotype (CD14+ CD16+), and **(d)** nonclassical phenotype (CD14- CD16+). Newborns are shown in teal and Infants/Control Newborns in pink. **e)** Within the CD3+ CD4- CD8+ population, naïve (TN), central memory (TCM), and effector memory (TEM) CD8+ T cell subsets were resolved by expression of CD28 and CD95. Representative plots are shown from Newborns and Infants just before and on day 10 of SHIV infection, and from Control Newborns on study days 0 and 10. **f-h)** Percentages of CD8+ T cells with a **(f)** naïve (CD28+ CD95-), **(g)** central memory (CD28+ CD95+), and **(h)** effector memory (CD28- CD95+) phenotype. Newborns are shown in teal and Infants/Control Newborns in pink. For each set of graphs, the top graph shows measurements after the beginning of the study, so any differences between the groups are due to SHIV infection status (teal: SHIV+ Newborns, pink: SHIV- Control Newborns). The bottom graph shows measurements after SHIV infection, so any differences between the groups are due to age at the time of SHIV exposure (teal: 1-2 weeks, pink: 15-16 weeks). Pairwise statistical comparisons at each time point were performed using Sidak's multiple comparisons test. *, $p < 0.05$. **, $p < 0.01$. ***, $p < 0.001$.

in both intermediate and nonclassical monocytes (**Figure 3.7c-d**) during SHIV infection in Newborns as well as Infants. However, unlike classical monocytes, neither intermediate nor nonclassical monocytes differed significantly in frequency based on age at the time of SHIV exposure (**Figure 3.7c-d**, bottom).

To analyze T cell population dynamics in Newborns and Infants, we measured CD4+ and CD8+ T cell counts and examined the proportions of naïve and memory T cell subsets longitudinally. We did not find alterations in absolute CD4+ and CD8+ T cell

counts in either group (**Supplementary Figure 3.4a-b**). In contrast to adult rhesus macaques, which experience CD4/CD8 inversion 2-3 weeks after vaginal infection with $SHIV_{SF162P3}$[111], the Newborn and Infant macaques in our study did not exhibit inversion of the CD4/CD8 ratio (**Supplementary Figure 3.4c**). However, we did note a significant decrease in the CD4/CD8 ratio in Newborns at weeks 4 and 6 after SHIV exposure compared with Control Newborns, consistent with a study showing that human infants vertically infected with HIV-1 have CD4/CD8 ratios that gradually decline from normal levels of >2, but remain >1 during the first year of life[323].

To track CD4+ and CD8+ T cell subset dynamics, we defined naïve (T_N), central memory (T_{CM}), and effector memory (T_{EM}) T cells based on differential surface expression of CD28 and CD95[324]. As previously reported for SIV-infected and uninfected neonatal rhesus macaques[324], the CD4+ compartment was predominantly naïve in all animals regardless of infection status, although Infants had somewhat lower CD4+ T_N frequencies than Newborns 6 weeks p.i. (**Supplementary Figure 3.4d**). T_{CM} cells comprised ~10-20% of CD4+ T cells in Control Newborns, and their frequency decreased gradually during SHIV infection in both Newborns and Infants, reaching ~5% by week 6 p.i. (**Supplementary Figure 3.4e**). In contrast, CD4+ T_{EM} cells—the smallest subset in Control Newborns—increased significantly during SHIV infection in Infants, but not Newborns, with significant differences between groups evident as early as day 4 p.i. (**Supplementary Figure 3.4f**).

Unlike the relatively modest changes in the CD4+ compartment, CD8+ T cell naïve and memory subsets were strongly altered during SHIV infection (**Figure 3.7e**). In agreement with a previous study[324], the majority of CD8+ T cells were also naïve in the absence of infection (**Figure 3.7f**, top). However, in Newborns but not Infants, SHIV infection heavily skewed the CD8+ T cell compartment away from naïve and towards effector memory, inverting the T_N/T_{EM} ratio by day 10 p.i. (**Figure 3.7f and h**). The

magnitude of these rapid changes was maintained in most Newborns through week 4 and were still altered at week 6 p.i. In contrast, no changes in the frequencies of CD8+ T_{CM} were noted (**Figure 3.7g**).

The striking observation that acute SHIV infection causes profound expansion of CD8+ T_{EM} cells in Newborns, but not Infants, led us to ask whether immune activation phenotypes differ between age groups. To answer this question, we monitored expression of the activation markers CD69, CD25, and HLA-DR on the surface of naïve, central memory, and effector memory CD4+ and CD8+ T cells. Surprisingly, SHIV infection did not result in increased expression of any of these activation markers on the surface of most T cell subsets (**Supplementary Figure 3.4g-x,** top row of each set of graphs), with several minor exceptions as described below.

In both the CD4+ and CD8+ T cell compartments, cells expressing CD69 were most frequent within the T_{EM} subsets, less frequent in T_{CM}, and rarest among T_N (**Supplementary Figure 3.4g-l**). There was a trend toward greater CD69 expression on CD4 T_{EM} cells in Newborns than Infants during SHIV infection (**Supplementary Figure 3.4i**), despite more robust expansion of this subset in Infants than in Newborns (**Supplementary Figure 3.4f**), but the difference in CD69 expression was not significant. In SHIV-infected Newborns compared with Control Newborns, CD69 expression was significantly higher in naïve CD8+ T cells at week 4 (**Supplementary Figure 3.4j**, top).

Unlike CD69, patterns of CD25 expression were distinct for CD4+ and CD8+ T cells. CD25+ cells were most frequent among the CD4+ T_{EM}, less frequent within the CD4+ and CD8+ T_{CM} populations, and comprised <5% of other subsets examined (**Supplementary Figure 3.4m-r**). We observed sustained decreases in CD25 expression on CD4+ T_N subsets after SHIV infection in both Newborns and Infants (**Supplementary Figure 3.4m**) as well as a transient decrease in CD25+ CD4+ T_{CM} that was more pronounced in Infants (**Supplementary Figure 3.4n**). CD25+ CD4+ T_{EM} cell

frequencies were maintained at higher levels during SHIV infection in Newborns than in Infants, but were unaffected by the presence or absence of neonatal SHIV infection, suggesting an age-dependent difference in the frequency of this subset (**Supplementary Figure 3.4o**). Because Tregs are characterized as CD25+ CD4+, our data may reflect age-dependent differences in Treg depletion dynamics during acute SHIV infection, as previously reported for intestinal Tregs in neonates infected with SIV[325]. In contrast, no differences in CD25 expression on CD8+ T cell subsets were observed (**Supplementary Figure 3.4p-r**).

Finally, we examined HLA-DR expression on T cell subsets. HLA-DR+ cells were present at modest or low frequencies in all subsets, with a greater proportion of T_{EM} and T_{CM} cells bearing HLA-DR compared with T_N (**Supplementary Figure 3.4s-x**). Surprisingly, with the exception of slightly higher expression on CD8+ T_{EM} in Infants than in Newborns at week 4 p.i. (**Supplementary Figure 3.4x**, bottom), no differences between groups were noted. Given the highly variable HLA-DR expression between time points as well as individual animals, the extent to which this small difference is biologically meaningful is uncertain.

Cumulative differences in blood leukocyte phenotypes

To obtain a summative profile of immunological differences between Newborns and Infants, we calculated the mean area under the curve (AUC) for each parameter measured longitudinally by flow cytometry during the first 6 weeks of the study as well as the first 6 weeks of SHIV infection. For each parameter, AUCs in Newborns and Infants were directly compared using t tests, with separate analyses done to test for differences during the first 6 weeks of the study (SHIV-infected Newborns vs. Control Newborns) and the first 6 weeks of infection (Newborns vs. Infants). A false discovery rate (FDR)

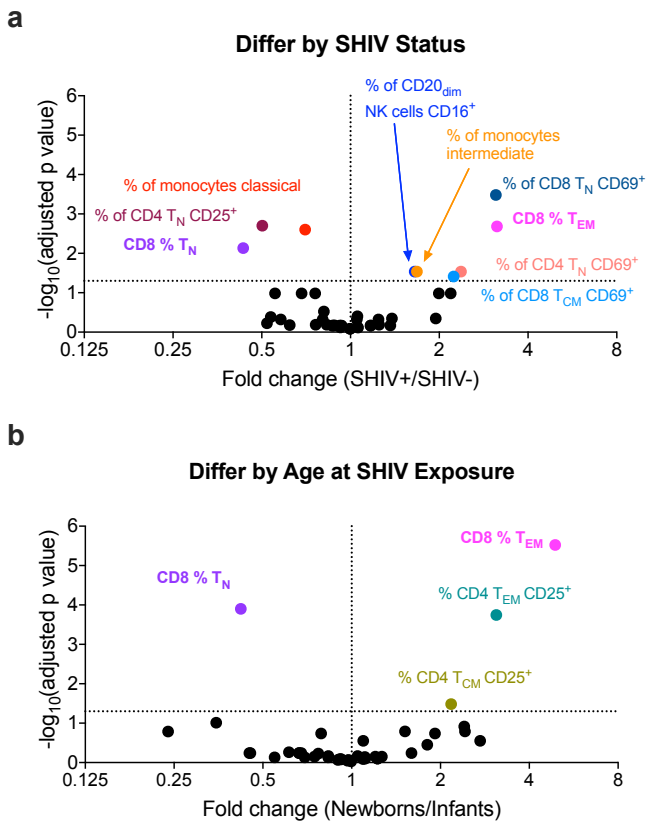

Figure 3.8. Between-group differences in leukocyte counts and phenotypes during SHIV infection in early life. a) For each of 42 parameters measured by flow cytometry, area under the curve (AUC) during the first 6 weeks of the study was computed for each group. Groups were compared by one t test per AUC comparison (total t tests: 42) and p values were adjusted for multiple comparisons by the False Discovery Rate (FDR) approach. **b)** For each of 42 parameters measured by flow cytometry, AUC during the first 6 weeks of SHIV infection was computed for each group. Groups were compared by one t test per AUC comparison (total t tests: 42) and p values were adjusted for multiple comparisons by the FDR approach. For **(a)** and **(b)**, discoveries were determined using the two-stage linear step-up procedure of Benjamini, Krieger and Yekutieli, with Q = 5%. Each parameter was analyzed individually, without assuming a consistent SD. Discoveries are denoted by colored symbols and corresponding labels. In each plot, the horizontal line indicates the –log10 transformed threshold of significance at the Q = 0.05 level.

approach was used to determine which parameters were significantly different between groups. If AUCs for a parameter differed significantly between SHIV Newborns and Control Newborns during the first 6 weeks of the study, the difference was attributed to SHIV infection status because the groups were matched in age. Conversely, if AUCs differed significantly between Newborns and Infants during the first 6 weeks of SHIV infection, the difference was attributed to age at the time of SHIV exposure.

Using this analysis strategy, we identified 9 parameters for which AUCs differed significantly between groups as a function of SHIV infection status during the newborn period (**Figure 3.8a**). In line with our findings that SHIV infection skewed CD8+ T cell and monocyte subset frequencies, especially around day 10 p.i. (**Figure 3.7**), the AUC analysis showed that the cumulative percentages of classical and intermediate monocytes were 25% lower and 70% higher respectively in SHIV-infected Newborns compared with Control Newborns. CD8+ T cells were even

more strongly skewed, with >2-fold lower cumulative frequencies of CD8+ T_N and >3-fold higher frequencies of CD8+ T_{EM} over the first 6 weeks of SHIV infection. Interestingly, despite the paucity of significant intergroup differences in activation marker expression at any particular time point (**Supplementary Figure 3.4g-x**), AUC analysis revealed that SHIV-infected Newborns had significantly greater cumulative frequencies of CD69+ cells within several T cell subsets than their uninfected counterparts. In line with timepoint-specific comparisons, CD25+ CD4+ T_N cell frequencies were significantly decreased during SHIV infection. Because this cell subset has been reported to express high levels of lymphoid tissue homing markers CD62L and CCR7[326], their disappearance from peripheral blood may have been due to migration into lymphoid tissues during SHIV infection. Finally, SHIV infection was associated with a significant enrichment of $CD20_{dim}$ NK cells expressing CD16; the biological importance of this observation is unknown.

In a parallel FDR analysis of intergroup differences during the 6 weeks after SHIV infection, we identified 4 parameters for which AUCs differed significantly between groups as a function of age at the time of SHIV exposure (**Figure 3.8b**). Importantly, two of these parameters—the frequencies of CD8+ T_N and T_{EM} cells—were found to differ as a function of both SHIV infection status and age at SHIV exposure, indicating an age-dependent difference in the effect of SHIV. In addition, cumulative frequencies of CD25+ CD4+ T_{CM} and T_{EM} were 2- and 3-fold greater in Newborns than in Infants, possibly reflecting the relatively greater abundance of Tregs in the neonatal immune system.

E. Transcriptome analysis

To determine how innate responses to SHIV infection may differ between Newborns and Infants, we performed transcriptome analysis in the peripheral blood using bulk RNA sequencing (RNA-seq). For Newborns and Infants, we analyzed samples on day 0 just prior to SHIV exposure, as well as day 4 and (when available) day

42 of SHIV infection (0, 4, and 42 DPI [days post-infection]). For a SHIV-unexposed age-matched baseline for comparison with the Newborns, we also included Control Newborn samples on days 0, 4, and 42 from the beginning of the study (0, 4, and 42 DPB [days post-beginning]) (**Figure 3.9a**). The design of our study allowed differential expression (DE) analyses to be performed across multiple contrasts, designed to measure different facets of infection (**Figure 3.9a**). Contrasts at time points before SHIV exposure measure age-dependent differences or cohort/batch effects. Within-group contrasts after SHIV exposure measure the impact of SHIV infection in Newborns and in Infants. Across-group contrasts at matched time points after SHIV exposure evaluate age-dependent responses to SHIV infection.

We began our analysis by examining DE genes in contrasts prior to SHIV exposure to measure baseline/background differences in gene expression. As expected, there was little difference between the two groups of animals at the beginning of the study, with only three genes significantly DE (adjusted $p < 0.1$) between Newborns on 0 DPI and Control Newborns on 0 DPB (**Supplementary Figure 3.5a**). As no meaningful differences were found, these groups were combined into a single "0 DPB_{pooled}" group for subsequent contrasts. No genes were significantly DE between 0 DPB_{pooled} and Control Newborns 4 DPB. However, a signature of 187 DE genes was noted for Control Newborns at 42 DPB vs. 0 DPB_{pooled} (**Supplementary Figure 3.5b**). An even stronger signature with 477 DE genes was found for Infants at 0 DPI contrasted with 0 DPB_{pooled} (**Supplementary Figure 3.5c**). Given that 'Control Newborns' and 'Infants' are the same animals sampled at different ages, this result is consistent with age-dependent transcriptomic changes as these animals grew older in the absence of SHIV infection. In both contrasts, Gene Ontology (GO) and Kyoto Encyclopedia of Genes and Genomes (KEGG) revealed differential expression of genes associated with various processes

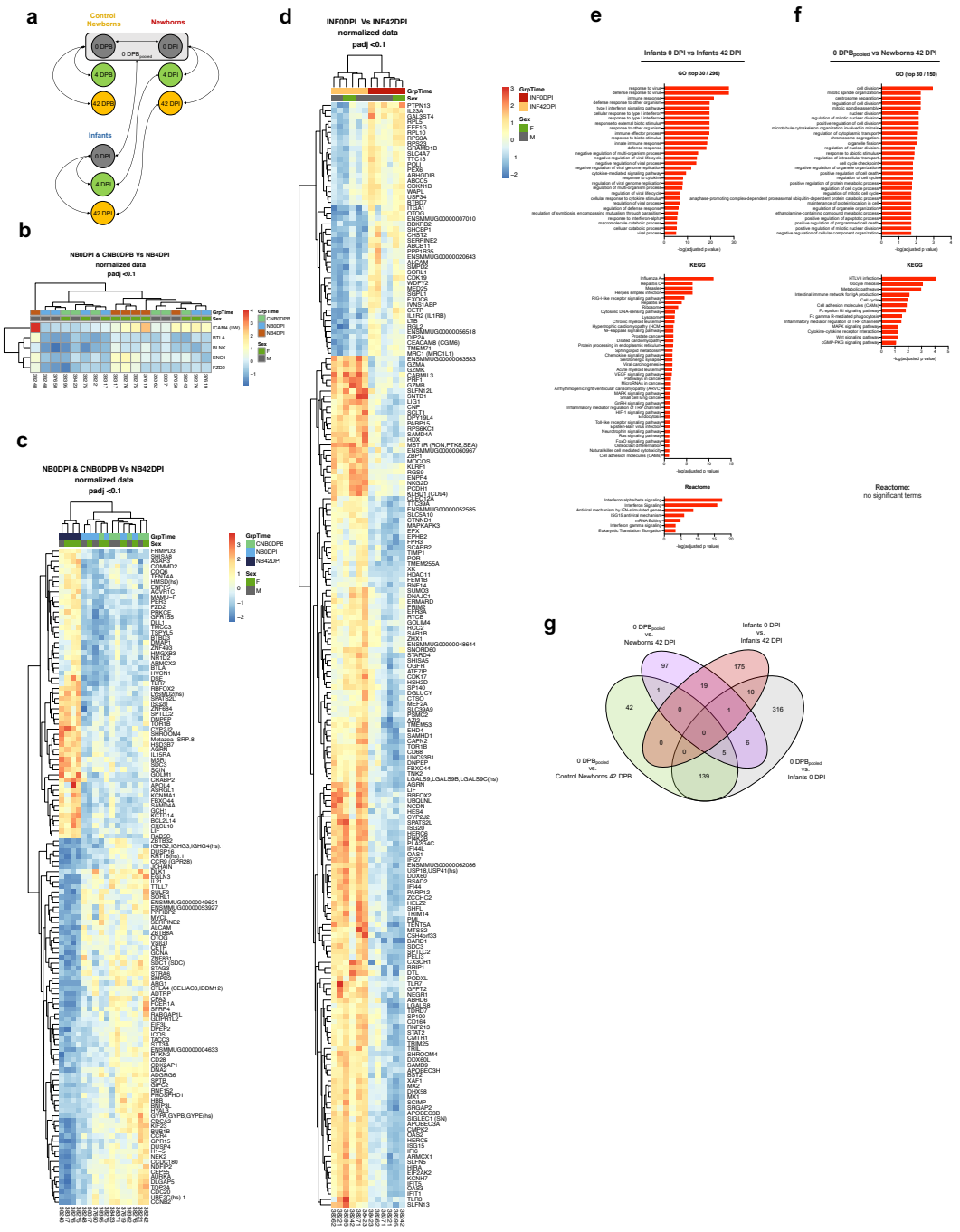

Figure 3.9. RNA-seq reveals distinct transcriptomic signatures in Newborns and Infants on day 42 of SHIV infection. a) Contrasts of interest are shown with arrows. DPB, days post-beginning of study. DPI, days post-SHIV infection. 0 DPB_{pooled} is the combined sample group of all uninfected newborns at the beginning of the study (N = 12 animals). **b)** DE genes in Newborns on 4 DPI vs. 0 DPB_{pooled} (adjusted $p < 0.1$). **c)** Differentially expressed genes in Newborns 42 DPI vs. 0 DPB_{pooled} (adjusted $p < 0.1$). **d)** DE genes in Infants on 42 DPI vs. Infants 0 DPI (adjusted $p < 0.1$). Animal IDs are listed along the bottom of each heatmap in **b-d**. **e)** Gene ontology (GO), Kyoto Encyclopedia of Genes and Genomes (KEGG), and Reactome analyses of DE genes in Infants on 42 DPI vs. 0 DPI (adjusted $p < 0.1$). Where many terms were significant (adjusted $p < 0.1$), top significant terms are shown. **f)** GO and KEGG analyses of DE genes in Newborns on 42 DPI vs. 0 DPB_{pooled}. No pathways were significantly enriched in the Reactome database. Where many terms were significant (adjusted $p < 0.1$), top significant terms are shown. **g)** Venn diagram of DE genes in Newborns 42 DPI vs. 0 DPB_{pooled} (purple), Infants 42 DPI vs. Infants 0 DPI (pink), and background transcriptional signatures in Control Newborns (green) and Infants (gray) at different timepoints in the absence of SHIV infection.

related to immune system development and signaling (**Supplementary Figure 3.5d-e**), likely reflecting normal immunological maturation during early life.

Next, we evaluated within-group differences in gene expression for Newborns and Infants during SHIV infection. Similar to Control Newborns, only five genes were found significantly DE between 0 DPI and 4 DPI in Newborns, suggesting that gene expression in peripheral blood is not yet substantially altered at this early time point in acute infection (**Figure 3.9b**). However, by 42 DPI, we detected 129 genes DE, of which 57 (44%) were upregulated and 72 (56%) were downregulated relative to 0 DPB_{pooled} (**Figure 3.9c**). Similarly, for intra-group contrasts among Infants, we compared gene signatures in Infants 0 DPI with those on 4 DPI and 42 DPI. No significant genes were identified as DE in 0 DPI vs. 4 DPI. However, on 42 DPI of SHIV infection in Infants, 205 genes were DE, of which 158 (77%) were upregulated and 47 (23%) were downregulated relative to 0 DPI (**Figure 3.9d**).

In Infants, GO analysis revealed differential regulation of gene networks involved in antiviral immune responses mediated by type I IFN signaling (**Figure 3.9e**). Genes contributing to enriched terms containing the phrase “type I interferon” included *ADAR, BST2, IFI6, IFI27, IFIT1, IFIT3, ISG15, ISG20, MX1, MX2, OAS1, OAS2, OAS3, RSAD2, SAMHD1, SP100, STAT2, USP18, and XAF1*. Notably, many of these are lentiviral restriction factors, and most were significantly upregulated on 42 DPI. In contrast, GO analysis showed that the DE signature in Newborns consisted largely of genes involved in cell division, cell cycle regulation, and metabolism (**Figure 3.9f**). Genes in the most significantly enriched term “cell division” were *AURKA*, *ECT2*, *KIF23*, *KIF11*, *BUB1B*, *CCNB2*, *BIRC5*, *PRKCE*, *CDC20*, *CDCA2*, *PTTG1*, *NEK2*, *CEP55*, *ZWINT*, and *TOP2A*; most were significantly downregulated on 42 DPI compared with 0 DPB_{pooled}. We did observe upregulation of several genes, including *TLR7*, *ISG20*, *CXCL10*, and *LIF*, which were part of the significantly enriched GO term “immune response” (adjusted p value =

0.048), although they did not seem to cluster with any specific pathway. CXCL10 in particular is a biomarker for high viremia and rapid HIV-1 disease progression[306,327,328], as well as immune dysfunction in infectious diseases more broadly[329]. Thus, the finding that this gene was significantly DE in Newborns but not in Infants suggests a possible role for CXCL10 in age-dependent mechanisms of SHIV pathogenesis. Newborn and Infant transcriptional signatures were very distinct, with 97/129 (75%) of genes DE in Newborns and 175/205 (85%) of genes DE in Infants specific to each group's SHIV response on 42 DPI (**Figure 3.9g**). Of the 291 total genes DE in either group specifically on day 42 of SHIV infection relative to that group's 0 DPI baseline, only 19 genes (6.5%) were common to both groups (**Figure 3.9g**). Taken together, these findings reveal stark differences in transcriptomic signatures associated with SHIV infection in Newborns and Infants, and raise the possibility that antiviral immunity is impaired in Newborns due in part to underdeveloped type I IFN responses, which we found intact and readily detectable in Infants infected at 15-16 weeks of age.

Finally, we examined between-group differences in gene expression at matched time points during SHIV infection. As previously noted, 477 genes were DE on 0 DPI in Infants vs. 0 DPBpooled in Newborns, indicating a substantial age-dependent difference in transcriptomic profiles at baseline (**Supplementary Figure 3.5c**). By 4 DPI, only 237 genes were found to be DE in Newborns vs. Infants (**Supplementary Figure 3.5f**). On 42 DPI, only 38 genes were DE (**Supplementary Figure 3.5g**). GO and KEGG analysis suggested DE of genes involved in metabolism, porphyrin synthesis, and erythrocyte development on 4 DPI (**Supplementary Figure 3.5h**). Yet, on 42 DPI there was no clear enrichment for particular biological processes or signaling pathways (**Supplementary Figure 3.5i**). Taken together, and in light of the results from the within-group comparisons (**Figure 3.9**), these data paradoxically suggest that, although SHIV responses differ by age, SHIV infection ultimately reduces age-dependent differences in

gene expression. Intriguingly, this phenomenon is detectable as early as 4 DPI, a time point when SHIV infection has little effect on gene expression in Newborns (**Figure 3.9b**) and no significant effect in Infants.

VI. Discussion

Without treatment, HIV-1 is likely to cause severe disease in infants that acquire the virus vertically, with especially poor outcomes in those infected *in utero* or peripartum. Here, we show in a macaque model using high dose oral inoculation that despite similar degrees of viral seeding in lymphoid tissues at day 7 and plasma viral loads, newborns exhibit features consistent with increased immune damage and defective antiviral innate immunity during acute infection compared with infants infected at 4 months of age. We did observe a small, yet statistically significant, 0.36-$\log_{10}$ reduction in viral DNA in lymphoid and gut tissues sampled at necropsy in infants compared with newborns. However, because tissues were sampled from infants at 9-10 weeks p.i. and from newborns at 3-6 weeks p.i., we cannot make a direct comparison, as the seeded reservoir could conceivably have decreased by 0.36 $\log_{10}$ in the infants between 6 and 10 weeks after infection. In support of this idea, viral DNA in inguinal LN did not differ between infants and newborns at week 6, reflecting the similar levels of viral RNA in plasma in both groups. This lack of detectable age-dependent differences in viral load was unexpected, given that previous comparisons by our group of virus loads in newborns and infants infected at different ages had shown larger differences. However, the earlier studies were performed with a different stock of $SHIV_{SF162P3}$ produced several years earlier and used a 63-fold lower exposure dose, which could have obscured more subtle age-dependent differences in immune function and viral control. Indeed, two studies in untreated adult macaques challenged with a single dose of this SHIV demonstrated stark differences in immune-mediated viral control, with

animals given a higher dose[55] faring worse than those given a lower dose[111]. These study results prompted the current, tightly controlled comparative study using the same virus stock and high dose challenge to discriminate differences due to age at time of exposure.

In agreement with previous studies showing impaired vaccine responses in HIV-infected children, we observed weaker antibody responses to HepB vaccine in newborns infected with SHIV compared with age-matched uninfected newborns. Our data suggest that this SHIV model recapitulates this important aspect of HIV-1 pathogenesis in the pediatric setting. In contrast, we found that adaptive responses arose with similar kinetics in infants and newborns, although the study timeline was too short to compare the potency of antibody responses, which typically take months to acquire and reach a plateau.

Longitudinal analysis of leukocyte subsets revealed that the monocyte and T cell compartments were markedly altered during SHIV infection, especially in newborns. First, we found that SHIV infection skewed monocytes toward intermediate and nonclassical phenotypes, and this skewing was more pronounced in newborns than in infants. We also detected profound alterations in T cell subsets, with an inverted ratio of naïve to effector memory CD8+ T cells in both age groups. Though we did not determine what proportion of these CD8+ T_{EM} cells were specifically recognizing SHIV epitopes, we did measure T cell responses to Gag and Env peptide pools at the time of death and found no detectable responses in most animals in both groups, suggesting that this increase reflected antigen-independent activation and expansion of CD8+ T cells as seen in adults with HIV[295]. The age-dependent increases in differentiated monocytes and CD8+ T cells in newborns may be indicative of greater levels of systemic immune activation. However, unexpectedly, we did not detect clear age- or infection-dependent differences in activation marker expression on T cell subsets, in contrast with studies

documenting HLA-DR upregulation on CD8+ T cells during acute HIV-1 infection in adults and infants[183,319]. It is possible that other measures of systemic immune activation would have been informative; for instance, soluble CD14 is secreted by monocytes and macrophages stimulated by lipopolysaccharide, and is a biomarker of microbial translocation resulting from gut epithelial barrier damage[118]. In addition, because our study was limited to acute infection, we did not examine the functional significance of these alterations for long-term clinical outcomes.

Complementing our flow cytometry findings, analysis of peripheral blood cellular transcriptomes illuminated striking differences in gene expression signatures associated with SHIV infection in newborns and infants. Infants had evidence of a robust antiviral program mediated by type I IFN responses. In contrast, newborns had a transcriptional signature dominated by the downregulation of genes involved in mitotic, cell cycle, and activation processes; the near-absence of a viral infection response; and upregulation of *CXCL10*, a biomarker of greater disease severity. Given the central importance of type I IFN signaling in mounting an effective innate antiviral defense during acute infection, its presence in 4-month-old macaques yet profound lack in newborns may explain, in part, the age-dependent difference in pathogenesis seen in children infected with HIV-1 *in utero* or at birth compared with those infected at older ages. The timing of the development of type I IFN-mediated immune function during infancy should be defined more precisely in future studies.

Using a well-established rhesus macaque model of vertical HIV acquisition, we examined the relationship between immune maturation over the course of early infancy and damage associated with pathogenic lentiviral infection. The strengths of our study lie primarily in the comprehensive immunologic and transcriptomic profiling, as well as the study design and protocol with attention to age-matched controls. First, we gathered detailed longitudinal data on many different immune cell populations, allowing a

comprehensive look into the influence of SHIV on immune dynamics in newborns and infants. Second, to our knowledge, this study is the first to examine and compare transcriptome profiles during lentiviral infection in newborns and infants at different ages. Finally, by closely matching newborns and infants in age at the start of the study and housing them together in the same environment, we strove to minimize the influence of confounding variables that might influence immune function and create noise in the data. In particular, we tried to minimize differences in microbiome composition and diversity by feeding all animals the same formula, housing them in pairs and triplets, and providing opportunities to interact closely with other pairs. However, we did not characterize the microbiota in these animals. Given the importance of the microbiome in neonatal immune system development[330] and its role in modulating immune activation and HIV persistence[331], future studies should directly examine the influence of the microbiome on lentiviral pathogenesis in newborns and infants.

Despite these strengths, our study had some limitations. First, we chose the SHIV dose based on an *in vivo* titration to determine the dose required for high uncontrolled viremia in 4-week-old infant macaques. As a result, the dose of SHIV was likely much higher than the HIV dose a human infant might receive from exposure to maternal blood, vaginal secretions, or breastmilk. Second, in order to prevent the consequences of advanced SHIV disease, we terminated the study within 6 weeks of SHIV exposure for newborns and 10 weeks for infants. Consequently, we cannot determine from our findings how virologic outcomes and disease severity may compare between age groups over a longer period of observation. Finally, we did not examine leukocyte frequencies, phenotypes, or transcriptomes in gut and lymphoid tissues, the major sites of viral replication and host defense. Age-dependent dynamics of immunopathology at these anatomic sites should be elucidated in future studies.

Understanding why disease progression is so rapid in the setting of vertical HIV transmission remains a critical question, because the answers could inform strategies for the treatment of pathology and clearance of viral reservoirs in this vulnerable population. Taken together, our findings suggest a role for defective innate defenses and elevated immune activation in age-dependent differences in pathogenesis. We conclude that SHIV, like HIV-1, wreaks greater havoc in newborns than in infants infected at older ages, reinforcing the validity of this model for understanding mechanisms of pathogenesis in vertically-acquired HIV infection. Furthermore, this study lays the groundwork for future work to evaluate the effectiveness of antiretroviral and passive antibody therapies for children perinatally exposed to HIV. Ultimately, therapeutic intervention as early as possible after birth is more likely to have a durable effect on disease progression by limiting damage to the immune system.

VII. Supplementary Data

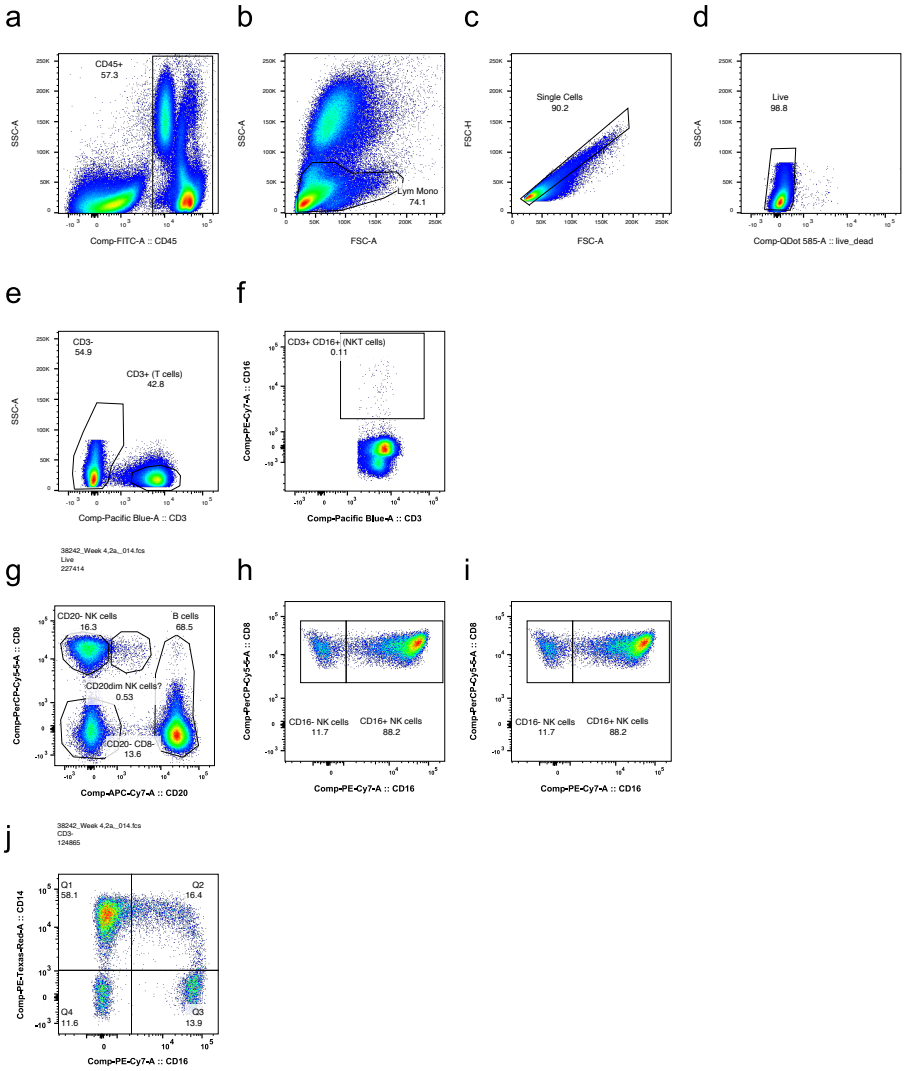

Supplementary Figure 3.1. Flow cytometry gating strategy for Panel 1 (B cells, NK cells, NKT cells, monocytes). Populations of interest were analyzed after gating on CD45+ **(a)** lymphocytes and monocytes by forward and side scatter profile **(b)**, then excluding doublets **(c)** and dead cells **(d)**. T cells were defined as CD3+ **(e)**, and NKT cells were defined as CD3+ CD16+ **(f)**. Within the CD3- gate, B cells as well as two populations of NK cells (CD20- and CD20dim) were defined based on CD20 and CD8 expression **(g)**. In some animals, a sizeable fraction of CD20+ cells expressed CD8. Follow-up experiments showed that these CD20+ CD8+ cells were true singlets, stained positive with antibodies to different CD8 epitopes, had a NKG2A- CD56- CD8b- CD19+ CD79a+ phenotype, and were present at relatively constant frequencies in individual animals longitudinally. Thus, we included them in the absolute B cell count. Expression of CD16 was measured on **h)** CD20- NK cells and **i)** CD20dim NK cells. Within the CD8- CD20- population, three monocyte subsets were defined based on their expression of CD14 and/or CD16; cells in the double-negative gate were not analyzed further **(j)**. HLA-DR was not used in the gating strategy for monocytes because replacement and recalibration of the green laser during the study resulted in inconsistent signal strength for HLA-DR PE during the longitudinal sampling period. Each blood sample was collected, stained, and analyzed individually. Antibody stain mixes and flow cytometer voltage settings were kept the same for the duration of the study. Where possible, gates were drawn based on obvious divisions between positive and negative populations; if the separation of populations was indistinct, positive cutoffs were determined based on a cell subset known to be negative for the marker in question.

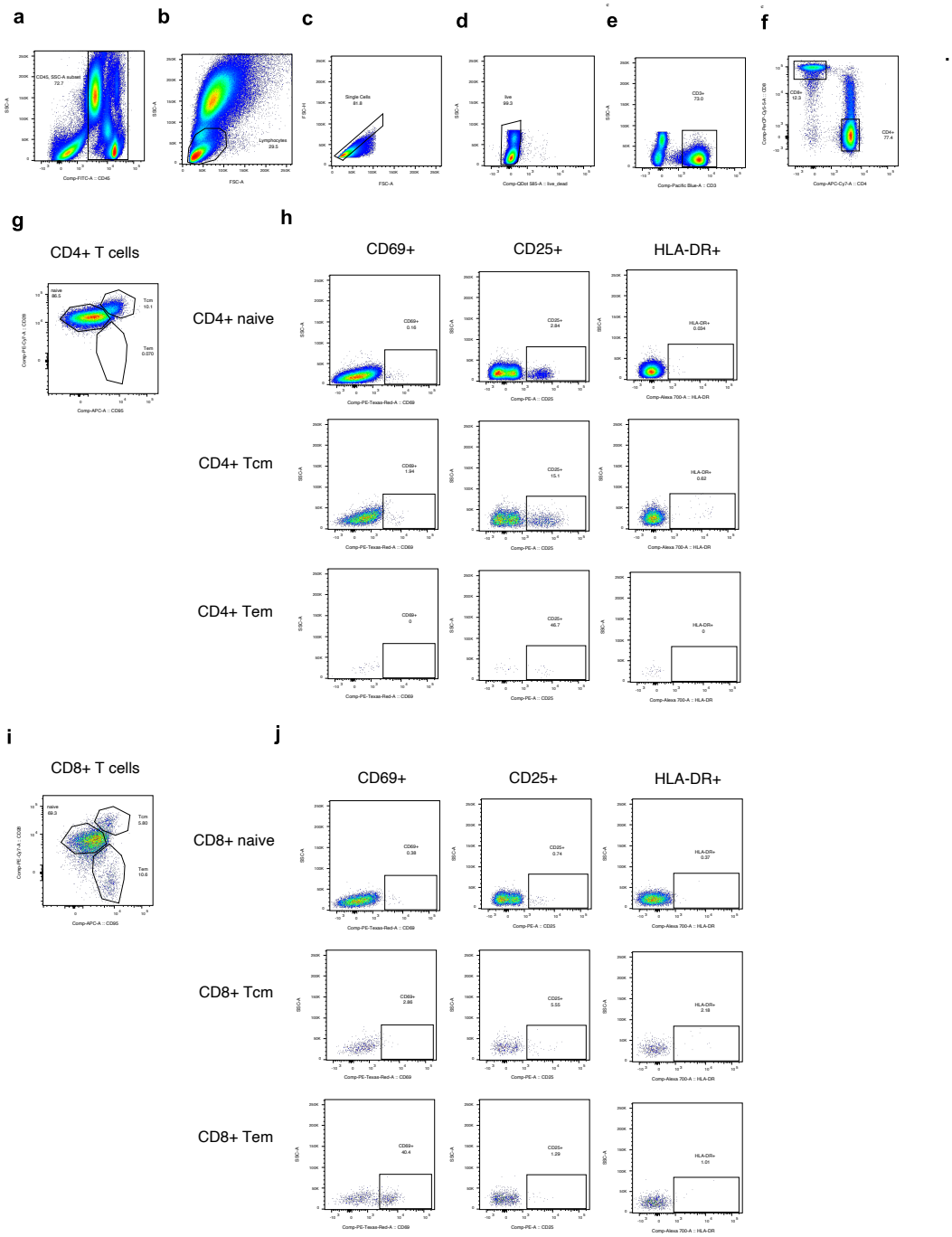

Supplementary Figure 3.2. Flow cytometry gating strategy for Panel 2 (T cells). Populations of interest were analyzed after gating on CD45+ cells **(a)**, then lymphocytes by forward and side scatter profile **(b)**, then excluding doublets **(c)** and dead cells **(d)**. T cells were defined as CD3+ **(e)**, and within the CD3+ gate, CD4+ and CD8+ T cells were discriminated **(f)**. CD4+ T cells were further subdivided into naïve, central memory (Tcm), and effector memory (Tem) subsets on the basis of CD28 and CD95 expression **(g)**. Each of these subsets was evaluated for expression of the activation markers CD69, CD25, and HLA-DR **(h)**. The same strategy was applied to the analysis of CD8+ T cell subsets and their activation marker profiles **(i-j)**. Each blood sample was collected, stained, and analyzed individually. Gates were drawn based on clear divisions between positive and negative populations, where possible. If the separation of populations was indistinct, positive and negative cutoffs were determined based on a cell subset known to be negative for the marker in question.

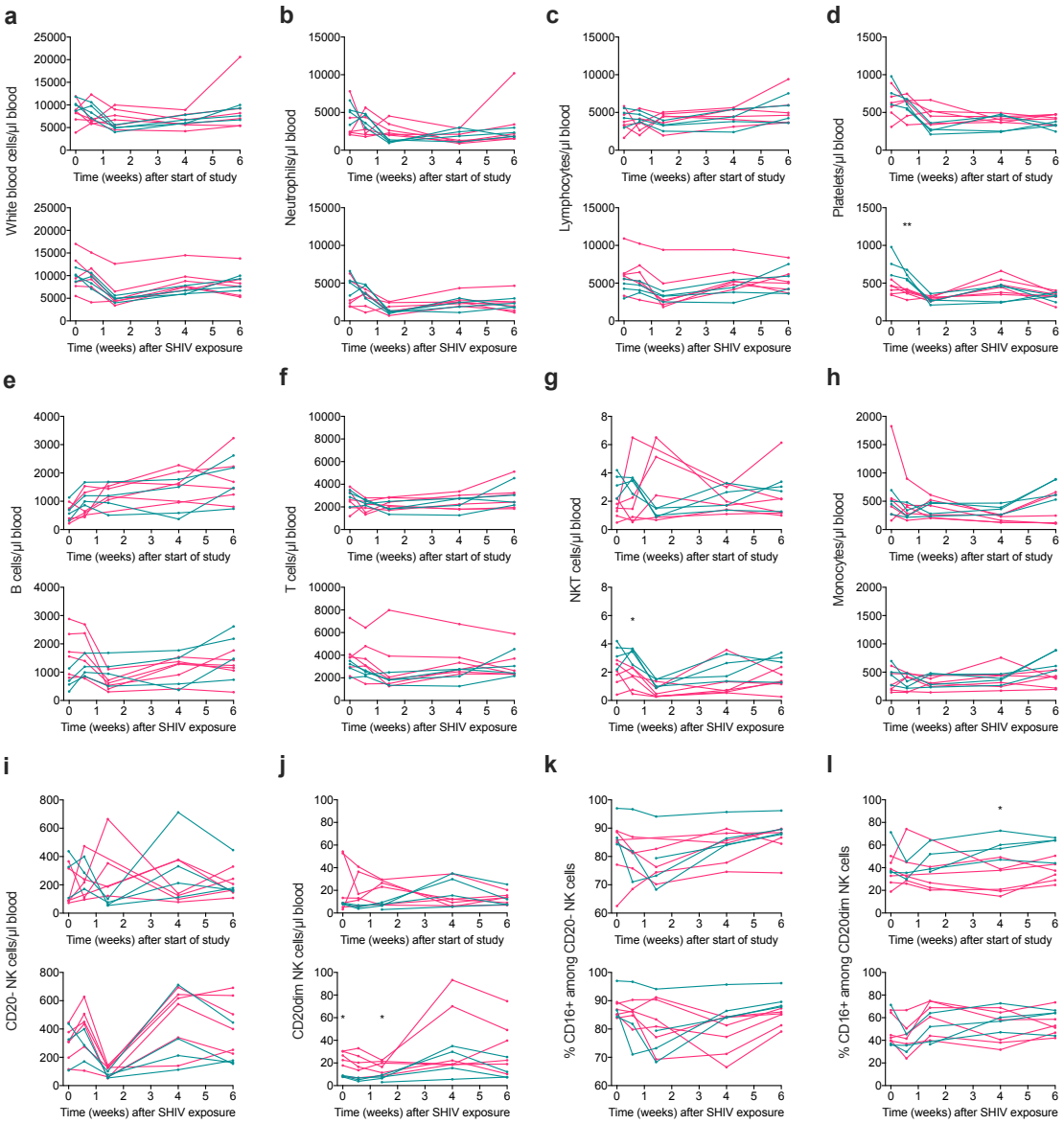

Supplementary Figure 3.3. Major leukocyte populations in newborns and infants before and during SHIV infection. Leukocyte populations in blood were monitored longitudinally by flow cytometry and complete blood count (CBC). Newborns are shown in teal and Infants (or Control Newborns) in pink. For each set of graphs, the top graph shows measurements after the start of the study, so any differences between the groups are due to SHIV infection status (teal: SHIV+ Newborns, pink: SHIV- Control Newborns). The bottom graph shows measurements after SHIV infection, so any differences between the groups are due to age at the time of SHIV exposure (teal: Newborns at 1-2 weeks, pink: Infants at 15-16 weeks). **a)** Absolute white blood cell counts. **b)** Absolute neutrophil counts. **c)** Absolute lymphocyte counts. **d)** Absolute platelet counts. **e)** Absolute B cell counts. **f)** Absolute T cell counts. **g)** Absolute NKT cell counts. **h)** Absolute monocyte counts. **i)** Absolute counts of CD20- NK cells. **j)** Absolute counts of CD20dim NK cells. **k)** Percentages of CD20- NK cells that express CD16. **l)** Percentages of CD20dim NK cells that express CD16. Pairwise statistical comparisons at each time point were performed using Sidak's multiple comparisons test. *, $p < 0.05$. **, $p < 0.01$.

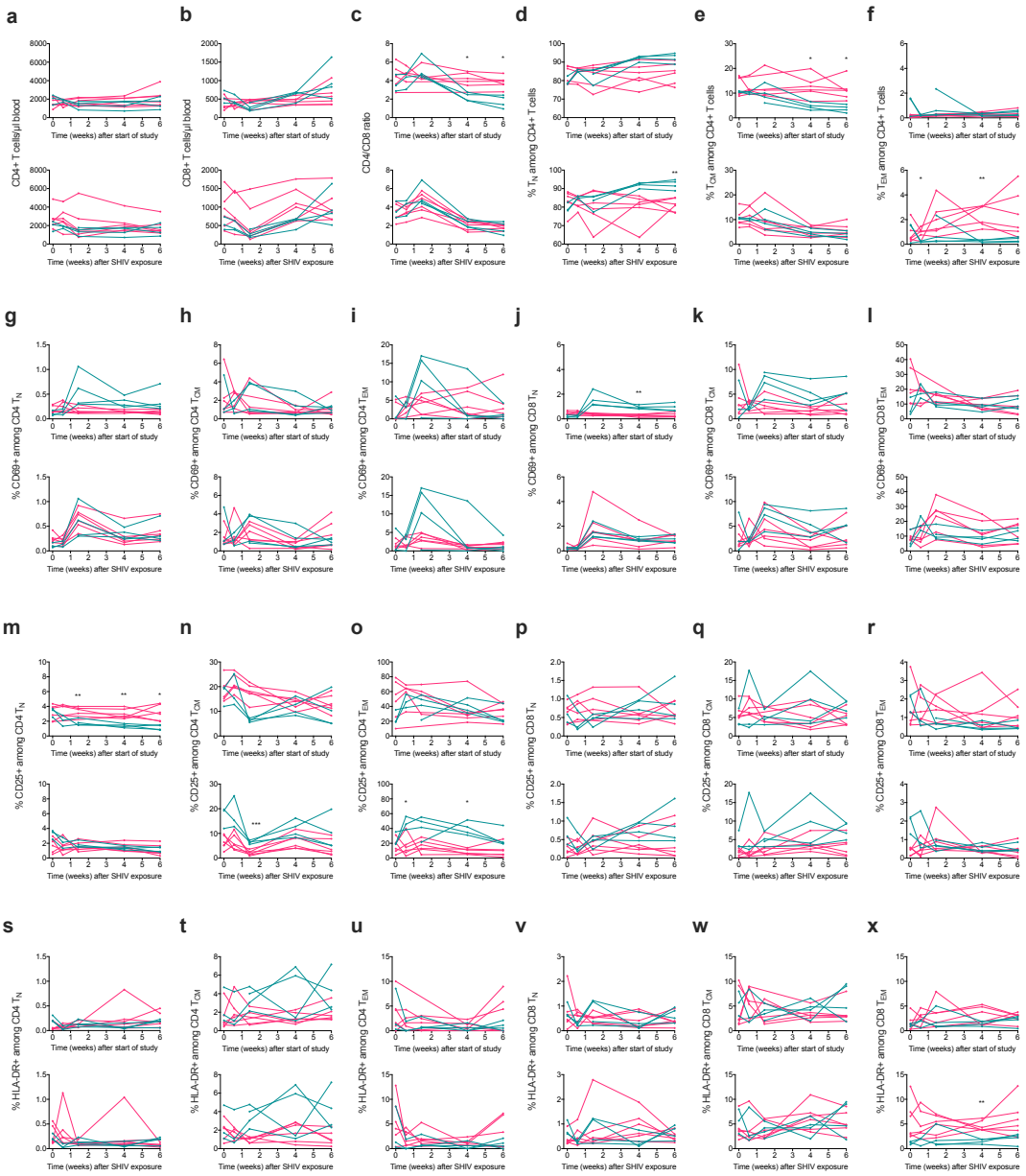

Supplementary Figure 3.4. T cell counts, CD4+ subsets, and activation phenotypes in newborns and infants before and during SHIV infection. Peripheral blood T cell populations and activation markers were monitored longitudinally by flow cytometry. Newborns are shown in teal and Infants (or Control Newborns) in pink. For each set of graphs, the top graph shows measurements after the start of the study, so any differences between the groups are due to SHIV infection status (teal: SHIV+ Newborns, pink: SHIV- Control Newborns). The bottom graph shows measurements after SHIV infection, so any differences between the groups are due to age at the time of SHIV exposure (teal: Newborns at 1-2 weeks, pink: Infants at 15-16 weeks). **a)** Absolute counts of CD4+ T cells. **b)** Absolute counts of CD8+ T cells. **c)** Ratio of CD4+ to CD8+ T cells. **d)** Percentages of naïve CD4+ T cells (CD28+ CD95-). **e)** Percentages of central memory CD4+ T cells (CD28+ CD95+). **f)** Percentages of effector memory CD4+ T cells (CD28- CD95+). **g-i)** Percentages of naïve, central memory, and effector memory CD4+ T cells expressing CD69. **j-l)** Percentages of naïve, central memory, and effector memory CD8+ T cells expressing CD69. **m-o)** Percentages of naïve, central memory, and effector memory CD4+ T cells expressing CD25. **p-r)** Percentages of naïve, central memory, and effector memory CD8+ T cells expressing CD25. **s-u)** Percentages of naïve, central memory, and effector memory CD4+ T cells expressing HLA-DR. **v-x)** Percentages of naïve, central memory, and effector memory CD8+ T cells expressing HLA-DR. Pairwise statistical comparisons at each time point were performed using Sidak's multiple comparisons test. *, $p < 0.05$. **, $p < 0.01$. ***, $p < 0.001$.

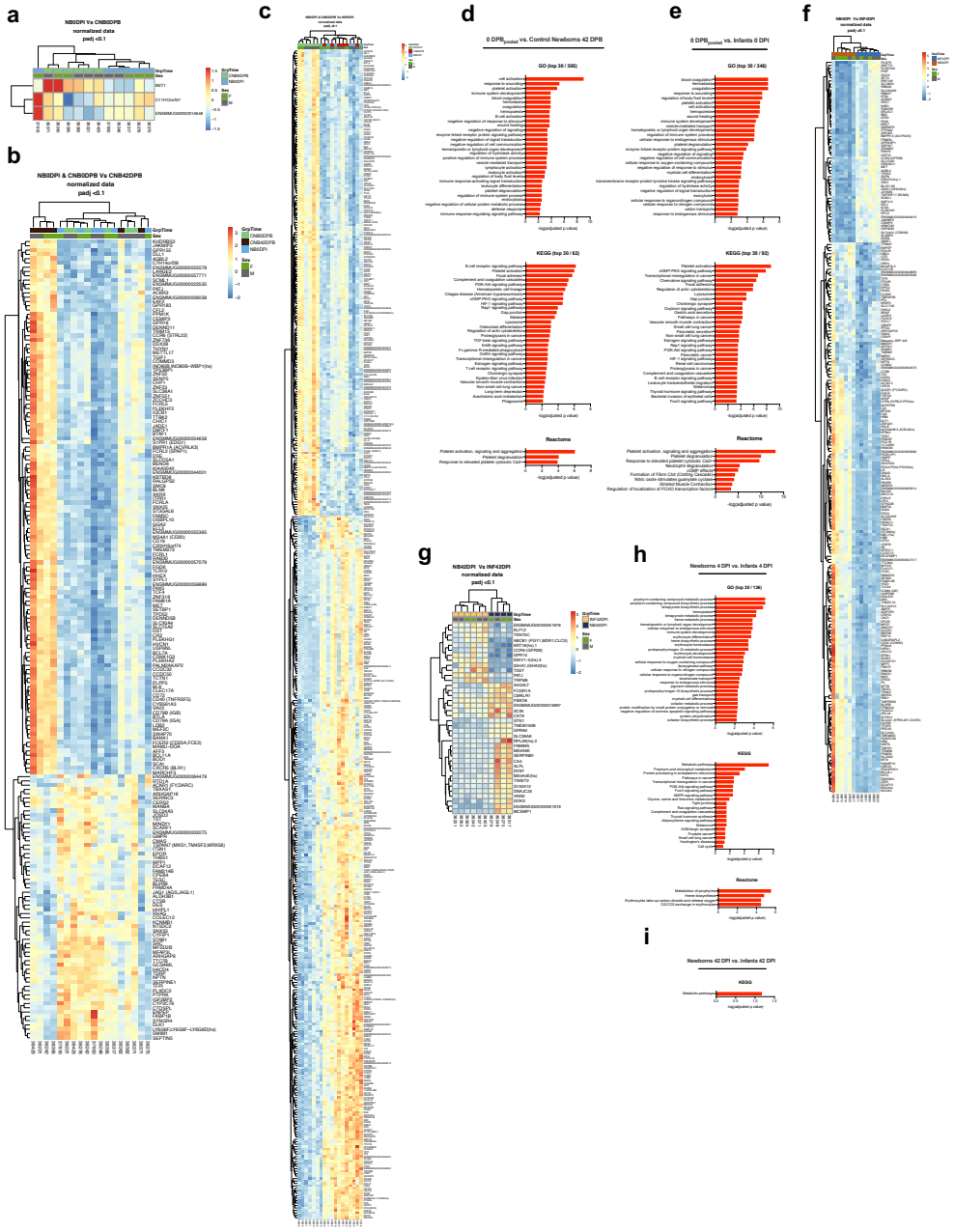

Supplementary Figure 3.5. Transcriptional signatures in background and between-group contrasts. a) Differentially expressed genes in Newborns vs. Control Newborns on study day 0 (adjusted p < 0.1). The only significantly DE genes were BET1 (higher in Control Newborns), which encodes a Golgi vesicular trafficking protein; C11H12orf57 (higher in Newborns), which encodes the ubiquitously expressed C10 protein that is involved in brain development; and ENSMMUG00000014648 (higher in Newborns), coding for 40S ribosomal protein S18. **b)** DE genes in Control Newborns at 42 DPB vs. 0 DPB_{pooled} (adjusted p < 0.1). **c)** DE genes in Infants at 0 DPI—which is also study day 98 (98 DPB)—vs. 0 DPB_{pooled} (adjusted p < 0.1). **d)** GO, KEGG, and Reactome analyses of DE genes in Control Newborns at 42 DPB vs. 0 DPB_{pooled}. Where many terms were significant (adjusted p < 0.1), top significant terms are shown. **e)** GO, KEGG, and Reactome analyses of DE genes in Infants at 0 DPI—which is also study day 98 (98 DPB)—vs. 0 DPB_{pooled}. Where many terms were significant (adjusted p < 0.1), top significant terms are shown. **f)** DE genes at 4 DPI in Newborns vs. Infants (adjusted p < 0.1). **g)** DE genes at 42 DPI in Newborns vs. Infants (adjusted p < 0.1). **h)** GO, KEGG, and Reactome analyses of DE genes at 4 DPI in Newborns vs. Infants. Where many terms were significant (adjusted p < 0.1), top significant terms are shown. **i)** KEGG analysis of DE genes of DE genes at 42 DPI in Newborns vs. Infants (adjusted p < 0.1). No significant terms were found in GO or Reactome analyses.

CHAPTER 4: Implications and Future Directions

I. Implications

A. "Hit early, hit hard": the importance of early intervention to limit reservoir seeding

The clinical importance of early ART for limiting HIV-1 disease progression is well appreciated. In the 1990s, it was found that initiating ART during the asymptomatic period of HIV infection could prolong AIDS-free survival by limiting virus replication and thereby slowing the erosion of the immune system. In pediatric infection, earlier ART has been conclusively shown to have a significant impact on infant mortality [194], leading to the current recommendation to initiate ART immediately upon diagnosis of HIV infection. In both humans and NHP, studies of post-exposure prophylaxis using ART have consistently shown clear benefits to beginning treatment as early as possible after exposure [107,188]. Because ART does not clear the reservoir, the importance of prompt treatment is consistent with the necessity to limit seeding during active viral replication and spread. Even initiation of ART during Fiebig I—the earliest stage of diagnosable HIV infection, when RNA is first detectable in plasma—is too late to prevent viral rebound upon treatment interruption [332].

Unlike ART, antibodies offer the hope of directly impacting reservoir size via Fc effector functions that can provide clearance of virion antibody complexes or potentially the killing of infected cells. Passive administration of neutralizing antibodies (matched SIVIG/SHIVIG, bNAbs) can lead to T-cell-mediated control when given within 3 days of exposure [252], and even as late as day 10 can alter certain measures of reservoir size [204]. However, prior to the work described in this dissertation, full viral clearance with bNAbs had only been achieved with treatment beginning 24 hours or earlier after exposure [105].

In the work described here, we tested the same bNAb treatment regimen that was effective at 24 hours, beginning at 48 hours, allowing us to define the rate at which bNAb efficacy decreases with treatment delay. Whereas clearance of virus from tissues was observed in all treated infants at 24 hours, beginning the same treatment at 48 hours resulted in variable levels of viral seeding in tissues, with only 50% of infants durably controlling viremia. In addition, we tested a modified treatment regimen of only a single large dose of the bNAb cocktail, equivalent to the amount in the multidosing regimen, beginning at 30 hours; this treatment resulted in full clearance of virus from tissues, extending the window of opportunity for full bNAb-mediated clearance from 24 hours to 30 hours. We are currently in the process of testing the single-dose bNAb treatment at 48 hours in order to enable head-to-head comparison of single-dose bNAbs given at 30 vs. 48 hours, as well as single- vs. multi-dose regimens beginning at 48 hours. Taken together, these studies fill a knowledge gap regarding the window of opportunity for bNAb-mediated viral clearance after exposure, and begin to shed light on the determinants of efficacy for bNAbs as PEP.

In addition to testing bNAbs at 30 and 48 hours, we have tested a 3-week ART regimen starting at 48 hours for comparison. To our surprise, these animals had similar outcomes to those treated with a single dose of bNAbs at 30 hours: nearly undetectable plasma viremia and virus in tissues, and a lack of measurable adaptive immune responses. Because we know that the virus is widely disseminated within 1-2 days of exposure [105], and ART cannot directly kill infected cells, our findings suggest that early ART mediates clearance indirectly, by blocking viral replication and seeding and allowing the small nascent reservoir to be extinguished by the innate immune system. In a subsequent as yet unpublished study, we tested the same ART regimen beginning at 72 hours and found that 4/6 animals experienced viral breakthrough after treatment cessation—similar to the outcomes of multi-dose bNAbs beginning at 48 hours.

Together, our findings are consistent with the idea that the outcomes of PEP using either bNAbs or ART are limited primarily by the rapid rate of reservoir seeding during early infection. Therefore, early treatment is paramount for antibody strategies as well as for ART—perhaps even more so for antibodies, as they take longer than ART to reach distal sites of viral replication.

B. Considerations for optimizing antibody treatment regimens

Many studies of passive antibody therapy have administered the treatment in multiple doses, ostensibly to extend the duration of antibody persistence *in vivo* [105,250,252]. However, we found unexpectedly that giving the bNAb cocktail as a single 40 mg/kg dose resulted in a considerably longer period of detection in plasma, compared with the same cocktail given as four 10 mg/kg doses spread out over 8 days. The half-life of each antibody was inversely correlated with the presence of anti-drug antibody (ADA) responses in each animal, suggesting that ADAs sped up drug clearance and could be limited by giving the bNAbs as a single large dose instead of several smaller injections. Our findings are consistent with previous work showing that ADA responses to infliximab were inversely correlated with dose in rheumatoid arthritis patients, suggesting that higher doses promote immunologic tolerance [333]. We speculate that giving a single large bNAb dose promotes tolerance by inhibiting memory B cell differentiation into antibody-secreting plasma cells, a mechanism thought to be important for tolerance to high-dose factor VIII used to treat Hemophilia A [334]. Although the role of ADAs in bNAb clearance is likely exacerbated in this model due to the species mismatch of the human bNAb and the macaque immune system [335], ADAs have also been reported in humans treated with human monoclonal antibodies and other biologics [336], and are a vexing concern in biotherapeutic development. Although Phase I trials of bNAbs VRC01, 10-1074, and

3BNC117 given at relatively high doses in the 30-50 mg/kg range have thus far found little evidence of ADA responses [337,338], adeno-associated virus (AAV)-vector delivery of bNAbs in macaques is associated with strong ADAs contributing to rapid drug clearance, especially when the IgG1 subclass is used [339-342]. Various strategies to reduce drug immunogenicity and modulate immune responses to mitigate ADAs are being explored, and these are important avenues of investigation [343]. However, our data suggest that a relatively simple modification to a bNAb therapy—altering the dose size and frequency—may have a profound impact on ADAs and drug pharmacokinetics, and ultimately treatment efficacy.

In addition to their potential for use in newborns as PEP, bNAbs have been proposed as a therapy given to the mother during late gestation, so as to reach the fetus at risk of infection *in utero*. Because using a mammalian expression system to generate the large quantities of bNAbs required for treatment of the mother would be cost-prohibitive, bNAb production in a different, higher-throughput expression system may be cheaper and thus make this approach more feasible. Our collaborator, Dr. Yvonne Rosenberg (PlantVax Inc.), has produced bNAbs in bulk using a transient transfection system in plants (*Nicotiana benthamiana*) with similar neutralizing potency to their mammalian-produced counterparts. The plant-produced bNAbs were protective in SHIV challenge studies in macaques, yet their capacity to transfer across the placenta is unknown. Because FcRn mediates transplacental transfer, variants of the bNAbs were engineered with Fc mutations (LS or YTE) to increase FcRn affinity. To test the degree of transplacental transfer of wild-type and Fc-variant bNAbs given passively, we injected bNAbs made either in mammalian cells or in *N. benthamiana* (“plant mAbs”) into pregnant rhesus macaques within 1-2 weeks of parturition, and then measured mAb concentrations in the dam and in the newborn over time. This set of experiments clearly demonstrated that while the mammalian antibodies crossed the placenta with varying

efficiency of 5-18%, the plant bNAbs failed to transfer with greater than 1% efficiency, despite mutations to enhance FcRn binding (**Figure 4.1**).

Transplacental transfer is mediated by FcRn in the trophoblast and FcγRs in the villous tissues [175,344], and alterations in Fc glycosylation and FcγR binding modulate transfer [175,345]. Thus, we hypothesized that the plant bNAbs had altered FcγR interactions. To test this hypothesis, we used flow cytometry to measure the binding of plant and mammalian-produced bNAbs to TZM-bl cell lines expressing human FcγRI, FcγRIIa, or FcγRIIIa. This assay showed that, compared with mammalian bNAbs, the plant bNAbs bound poorly to human FcγRI-expressing TZM-bl cells when tested at 1 μg/ml (**Figure 4.2**). However, the FcγRIIa and FcγRIIIa TZM-bl experiments were inconclusive due to poor monovalent affinity for all bNAbs

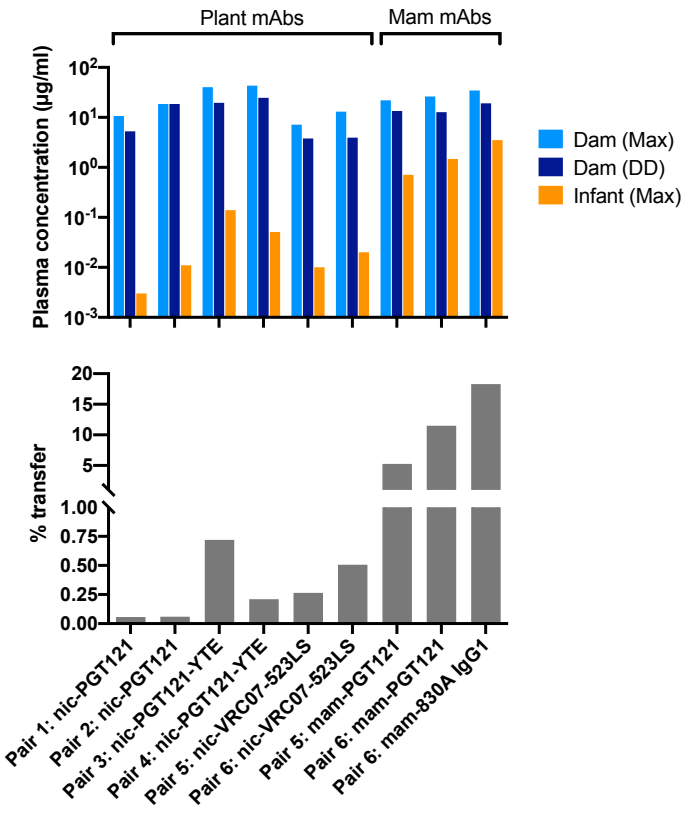

Figure 4.1. Monoclonal antibodies produced in *N. benthamiana* cross the placenta less efficiently than antibodies produced in mammalian cells. HIV antibodies produced in plants (nic-) or in CHO or HEK293 cells (mam-) were subcutaneously administered to pregnant dams in 1-2 doses of 5 mg/kg near the time of delivery. Pairs 1-6 denote individual dam-infant pairs. Concentrations of each antibody in the plasma of each pair of infants and dams were measured by ELISA, using plates coated with ST0A9 for PGT121 and its variants, RSC3 for VRC07-523 and its variants, and V1V2 peptide for 830A. Percent transfer was calculated by dividing the maximum (Max) concentration in the infant by the concentration in the dam on the delivery day (DD). Pair 1: dam 27435, infant 36611 (nic-PGT121, 1 dose, 4d before DD). Pair 2: dam 30060, infant 36648 (nic-PGT121, 2 doses, 5d and 1d before DD). Pair 3: dam 27455, infant 36176 (nic-PGT121-YTE, 2 doses, 15d and 1d before DD). Pair 4: dam 25961, infant 36310 (nic-PGT121-YTE, 2 doses, 9d and 5d before DD). Pair 5: dam 31561, infant 38294 (nic-VRC07-523LS + mam-PGT121, 1 dose, 6d before DD). Pair 6: dam 31306, infant 38579 (nic-VRC07-523LS + mam-PGT121 + mam-830A IgG1, 1 dose, 6d before DD).

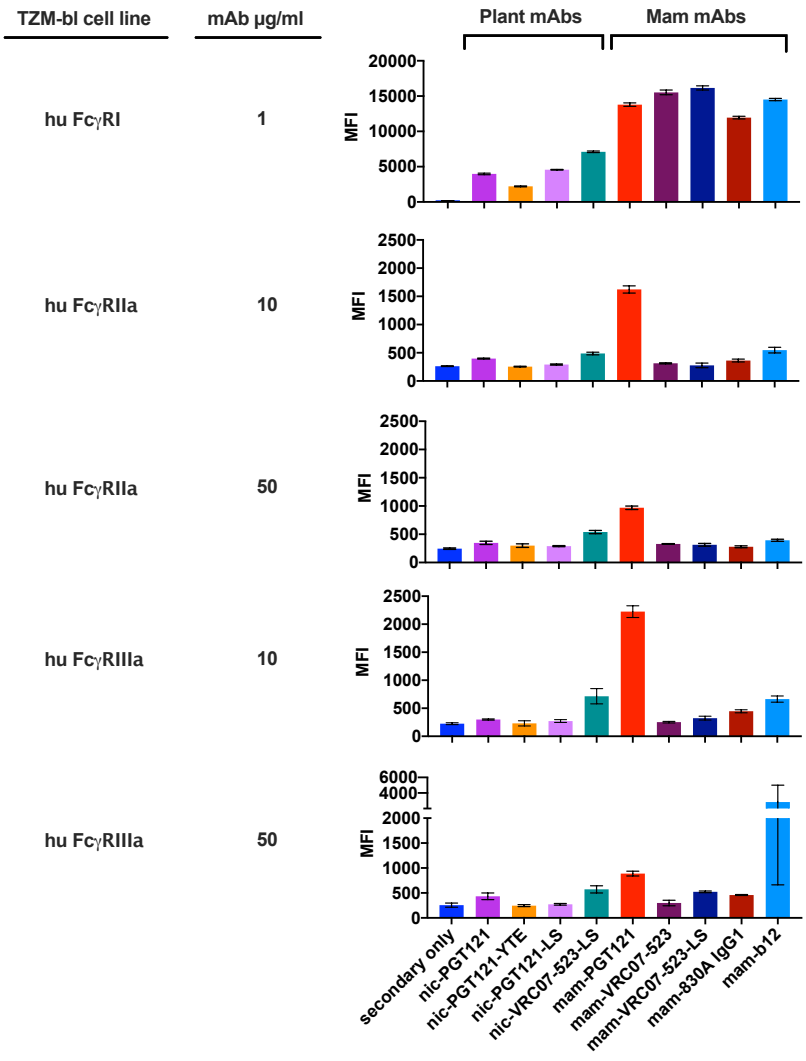

Figure 4.2. Antibodies produced in *N. benthamiana* bind poorly to human FcγRI-expressing cells compared with mammalian-produced antibodies. Monoclonal HIV antibodies produced in plants (nic-) or in CHO or HEK293 cells (mam-) were incubated in cluster tubes for 30 minutes with 1 x 10^5 TZM-bl cells expressing one of three human FcγRs, as indicated under the "TZM-bl cell line" heading. For each cell line, antibodies were tested at the concentrations indicated under the "mAb µg/ml" heading. Bound antibodies were detected by flow cytometry using a goat anti-human IgG PE secondary. Each test was done in triplicate. MFI, mean fluorescence intensity. Error bars represent SD.

tested at 10 or even 50 µg/ml (**Figure 4.2**). As an alternative readout of FcγRIIIa binding, we used an ADCC assay because ADCC activity requires FcγRIIIa binding and crosslinking. We tested each bNAb for ADCC activity mediated by a rhesus FcγRIIIa-expressing effector cell line against SHIV-infected luciferase reporter cells using an assay developed in David Evans' lab [346]. This experiment showed that ADCC activity was abrogated for plant bNAbs (**Figure 4.2**). Binding affinity to rhesus FcγRI, human FcγRIIIa, and either human or rhesus FcγRIIa, FcγRIIb, and FcRn, have not yet been determined.

Our preliminary findings lead us to speculate that the impairments in Fc receptor binding and functional activity of the plant-produced mAbs may be due to altered

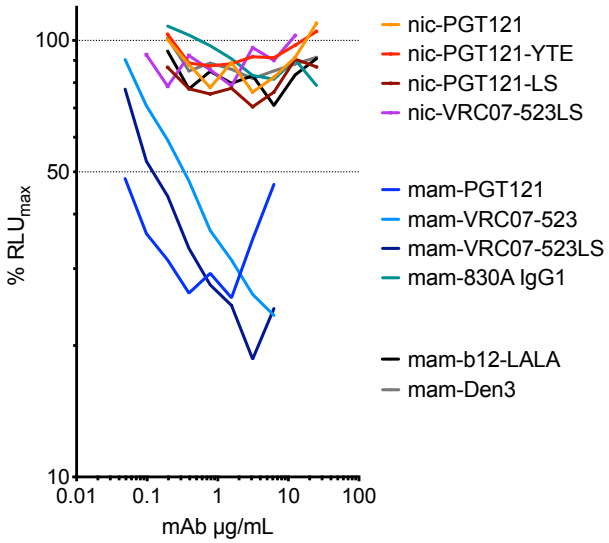

Figure 4.3. Plant-produced bNAbs do not mediate ADCC against SHIV-infected target cells. Luciferase reporter target cells (NKR24 cell line) were spinoculated with $SHIV_{SF162P3}$ to induce the Tat-driven expression of luciferase off the LTR promoter. Infected target cells were combined with effector cells (KHYG-1 rhCD16, a human FcγRIIIa- NK cell line transduced to stably express rhesus FcγRIIIa) in 96-well plates at an effector-target ratio of 10:1. Serially diluted plant- or mammalian-produced monoclonal antibodies were added to each well, and plates were incubated for 8 hours at 37°C. BrightGlo luciferase substrate was then added, and plates were read on a luminometer. RLU, relative light units. RLU_{max} is defined by control wells containing SHIV-infected target cells and effector cells only (no antibody). % RLUmax is the percentage of the maximum RLU remaining in each well after 8 hours; a dose-response decrease in RLU indicates death of infected target cells due to ADCC. Mam-b12-LALA and mam-Den3 are negative control antibodies.

glycosylation and/or M252 oxidation in the IgG1 Fc. The N297 glycan is known to affect IgG binding to FcγRs, and VRC01 glycovariants produced in glycoengineered transgenic *N. benthamiana* had varied FcγR binding affinities [347]. In contrast, FcRn binding is unaffected by the N297 glycan, but is impaired for all plant-produced VRC01 glycovariants due to oxidation of Met252 in the IgG1 Fc [347]. The glycan composition of our plant bNAbs is currently being studied by Dr. Rosenberg. The Met252 oxidation status is unknown. Thus, although much more work needs to be done, our data point to a possible role for altered Fc-FcγR interactions in impairing the transplacental transfer of plant-produced bNAbs. The fact that HIV infection is associated with reduced and altered IgG transplacental transfer [175] suggests that transfer of passively administered plant bNAbs could be even less efficient in pregnant women living with HIV than in uninfected pregnant women. Despite the disappointing results, the findings from our study have important implications for the use of antibodies in pregnancy: even if plant-produced bNAbs may not be a feasible intervention for preventing vertical transmission, the defective transplacental transfer of plant antibodies could be an advantage in settings where transfer to the fetus

is strongly contraindicated, such as immunotherapy for cancer, inflammatory bowel disease, or other maladies. If Fc aberrations in the plant mAbs are indeed responsible for reduced transfer, introducing these modifications intentionally could be a strategy to limit unwanted transplacental transfer of therapeutic antibodies.

C. Antibody therapy as a strategy to reduce the "effective" viral dose

The dogma of lentiviral infection is that the outcomes of viral exposure are binary: either infection a) occurs, with viral load following a predictable pattern of peaking in acute infection and subsequently reducing to a set point, or b) does not occur, resulting in no detectable virus in plasma or tissues. However, our observations in the infant macaque/SHIV model challenge this dogma. After depletion of a reliable stock of $SHIV_{SF162P3}$ virus provided by NIH in 2016, our lab was forced to switch to a different NIH-provided stock. This stock failed to establish high viremia reproducibly in all control animals, rendering many concurrent treatment experiments inconclusive. Deep sequencing of each of the stocks did not reveal obvious differences in viral variant composition, suggesting the problem was low infectious viral titer rather than some intrinsic property of the viral swarm. In order to establish a SHIV stock that would be appropriate for use in treatment studies, we optimized a method for SHIV production in CD4-enriched rhesus splenocytes that were stimulated *in vitro*, and used the low-quality SHIV stock as inoculum to generate a high-titer stock of this virus (henceforth termed OHSU-2017) for use *in vivo*. Using various assays to titer the OHSU-2017 stock *in vitro*, we found that its titer was comparable to or higher than the reliable SHIV stock we had successfully used in the past. We then performed an *in vivo* titration to determine the challenge dose required to achieve robust infection in infants after a single oral exposure. We tested a range of doses, from 2 ml (4.1×10^4 $TCID_{50}$) down to 0.2 ml (4.1

x 10^3 $TCID_{50}$). We predicted that infants would be either viremic or aviremic after challenge, depending on the inoculum size; however, we found that intermediate SHIV doses of 1 ml (2 x 10^4 $TCID_{50}$) and 0.5 ml (1 x 10^4 $TCID_{50}$) resulted in intermediate viral loads in plasma and in tissues, challenging the dogma that the dynamics of lentiviral infection are all-or-none (**Figure 4.4**). The titration study had group sizes too small for meaningful statistical inferences. Nonetheless, we have observed similar phenomena in two groups of 6 animals each that were treated with multiple doses of bNAbs beginning 48 hours after exposure to a single high dose of SHIV (see Chapter 2, data for Groups 2A and 2B). Like the viral titration study, these treated animals also exhibited a wide range of peak and setpoint viral loads in both plasma and tissues. Using the TZA assay [348] (a modified quantitative viral outgrowth assay) to quantify replication-competent virus in mesenteric lymph nodes and spleen from SHIV-infected untreated infants in the titration study and other untreated control groups, as well as bNAb-treated infants, we

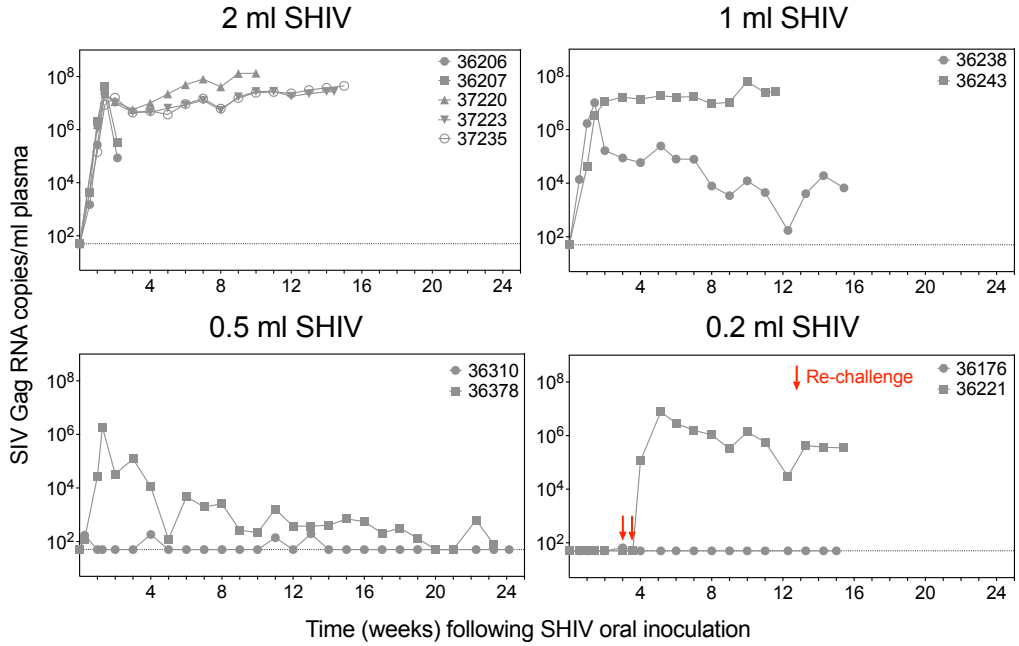

Figure 4.4. Oral SHIV infection in infants is dose-dependent. Infant macaques less than 4 weeks old were challenged with the OHSU-2017 stock of $SHIV_{SF162P3}$ a single time, except where re-challenge is indicated, via oral inoculation. Infants received 2 ml (*n* = 5), 1 ml (*n* = 2), 0.5 ml (*n* = 2), or 0.2 ml (*n* = 2) of SHIV and were not treated. Plasma viral load was measured weekly using a qRT-PCR assay.

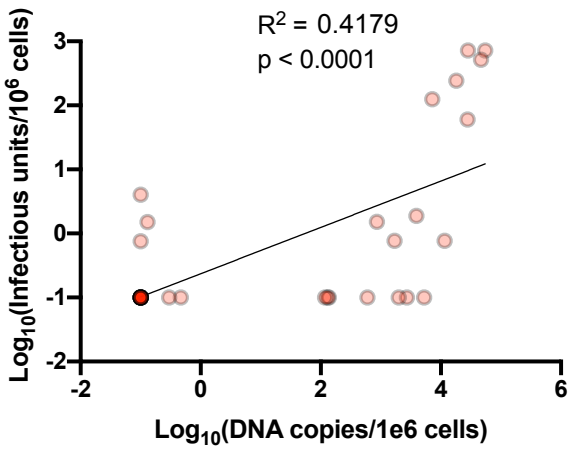

Figure 4.5. Replication-competent inducible virus correlates with total viral DNA copies in spleens and mesenteric LNs of SHIV-infected infants. Viral DNA copies were measured in homogenized tissues using either a standard or an ultrasensitive qPCR assay with a limit of detection of 0.1 copies/10^6 cells. Infectious units were measured in magnetically purified CD4+ cells using a modified TZA assay with a limit of quantification of ~0.8 infectious units/10^6 cells. A total of 35 tissues collected at necropsy were included in the linear regression analysis (20 LNs and 15 spleens) from 15 bNAb-treated and 9 untreated infants. Darker colored data points represent overlapping samples. There were 13 samples negative for both infectious virus and viral DNA; exclusion of these samples from the analysis gives $R^2 = 0.2377$ and $p = 0.0214$.

found that the replication-competent inducible viral reservoir in purified CD4+ cells was strongly correlated with the amount of viral DNA in these tissues (**Figure 4.5**). We are collaborating with scientists who are experts in mathematical modeling, Drs. Joshua Schiffer and Daniel Reeves, at the Fred Hutchinson Cancer Research Center in Seattle, Washington to analyze the relationship between viral inoculum dose and resulting plasma viremia and tissue virus in infants after oral SHIV exposure, with and without bNAb treatment. We hypothesize that bNAbs given as PEP act as a "sink" for the virus, in effect reducing the "viral dose" that seeds the reservoir early after exposure. In other words, bNAb treatment after high dose exposure results in equivalent reservoir seeding dynamics as does a lower exposure dose without bNAb treatment. If so, these findings would shed light on the mechanism of action for bNAbs and inform the rational design of interventions to reduce seeding and thereby modulate the long-term outcomes of infection.

D. Validity and utility of the macaque/SHIV model for understanding HIV transmission and treatment in human newborns

Oral SHIV infection in infant macaques is an invaluable model for recapitulating the virology, immunology, and pathogenesis of vertical HIV infection. Our lab has established a model of peripartum HIV exposure in which uninfected newborn rhesus macaques (*Macaca mulatta*) of Indian origin are exposed at <4 weeks of age to a single dose of $SHIV_{SF162P3}$ by the oral route, which is thought to be the primary route of perinatal exposure. Like transmitted/founder HIV isolates, this SHIV is CCR5-tropic and replicates rapidly in infants, reaching peak plasma virus titers of 10^7 copies/ml within 10-14 days of exposure. The exposure dose of 4×10^4 $TCID_{50}$ was chosen based on animal titration experiments in which all animals became highly viremic and exhibited rapid disease progression and opportunistic infections, mirroring the severe course of HIV-1 infection in human newborns exposed at or near birth. Notably, as in human infants infected with HIV-1, viremia remains at the peak level with no evidence of post-acute control, accompanied by weak or absent adaptive immune responses.

Nonetheless, no model is perfect; SHIV infection in infant macaques differs from human infant HIV-1 infection in a number of important ways. First, while SHIV infection of macaques at birth is theoretically possible, it is logistically challenging. Before they can be experimentally exposed to SHIV, the newborns must undergo a physical examination by a veterinarian, confirmed sufficiently healthy to be assigned to a SHIV challenge study, and stabilized in the nursery, including adaptation to formula feeding. These prerequisites typically take 1-2 weeks to complete. We showed previously that in pigtailed macaques (*M. nemestrina*), a closely related species, vertical transmission of SHIV occurs with similar frequency to that of HIV-1 in humans [207]; however, because the transmission rate is <50%, infection of newborns by infecting the pregnant dams is

expensive and unethical. For these reasons, we use oral inoculation with cell-free virus (swallowing) to infect newborn macaques as soon as possible after birth, ideally within 4 weeks. Another difference between this model and HIV-1 infection is that most animals infected at <4 weeks of age progress to AIDS and require euthanasia within 2-16 weeks. This timeline represents a faster course of disease than in human infants infected with HIV-1, who survive to a median 2 years of age, with higher mortality rates among those infected at younger ages. In addition, HIV-1 viremia in human newborns is typically 1-2 $\log_{10}$ lower than SHIV viremia in infant macaques.

Finally, a key caveat in our studies is the use of what may be a higher dose of viral inoculum than the exposure dose human infants would receive from their mothers during birth. The amount of virus that gets into the baby from cervicovaginal secretions during birth is not known and is difficult to measure accurately. Indeed, infectious viral titer is difficult to measure *in vitro*, and different measures of viral titer often correlate poorly with each other and with rates of infection *in vivo*. However, since the absolute rate of peripartum HIV infection is ~10-20% [167], and we observe a wide range of infection probabilities and outcomes from less than a 10-fold difference in the SHIV inoculum dose, we believe our high-dose inoculum is likely a modest overestimate of the dose received by a baby during birth, but not outside the realm of possibility. In addition, the necessity for a high dose stems from the relatively small group sizes that must be used in NHP studies due to cost and ethical reasons. To maximize statistical power to detect any therapeutic benefit of bNAbs or other interventions, we must use a sufficiently large viral dose to ensure that the challenge results in reproducible infection of all untreated control animals. To the extent that virologic outcomes are dose-dependent, our use of such large challenge doses may actually be creating a “worst case scenario,” stacking the deck against us and setting a higher bar for therapeutic efficacy than would likely be needed in a clinical setting.

II. Future directions

A. Designing combination therapies to deploy different mechanisms of action

The studies described in this dissertation have added to the body of knowledge regarding the mechanisms of action of bNAb and ART therapies for HIV. It is clear that there is ample room for improvement to extend the window of opportunity for delayed treatment. While ART does not directly kill infected cells, we showed that ART given early enough after SHIV exposure can effectively block viral replication and seeding, stacking the deck in favor of clearance of the nascent unstable reservoir via cell-intrinsic and innate immune mechanisms. In addition, ART has the advantage of more rapid dissemination than bNAbs to sites of viral replication, and therefore can act sooner to block the virus. However, bNAbs have clear advantages over ART in terms of half-life, as well as the ability to neutralize free virions, acting as a sink for infectious viral particles and thereby reducing the number of virions available to seed new infectious centers. Combining ART and bNAbs, therefore, could be a potent strategy for extending the window of opportunity for viral clearance and/or durable control after exposure.

In addition to bNAbs and ART, the anti-CCR5 IgG4 monoclonal antibody leronlimab (PRO 140) has emerged as a promising tool for HIV treatment and prevention. Leronlimab is a competitive inhibitor of Env-CCR5 binding, and when bound to CCR5 blocks viral entry. In addition to its other potential therapeutic applications in the treatment of cancer and COVID-19, leronlimab is now entering clinical trials for use as HIV PrEP in high-risk individuals in Thailand. Work in the lab of our collaborator, Dr. Jonah Sacha, recently showed that leronlimab treatment initiated 3 weeks after intravenous SHIV infection was able to reduce viral loads in plasma and viral DNA in tissues in adult macaques. Moreover, preventative treatment with leronlimab protected macaques from multiple SHIV challenges, recapitulating the effect of the CCR5Δ32

mutation that confers resistance to HIV infection. However, neither of these studies tested the efficacy of leronlimab as a short-term PEP intervention to limit reservoir seeding and persistence. We are planning to test leronlimab alone, and in combination with ART and/or bNAbs, in our NHP model of perinatal infection. We predict that the distinct mechanisms of action mediated by leronlimab, ART, and bNAbs will synergize to extend the window of opportunity for viral clearance and durable control.

In contrast to monovalent monoclonal antibodies, bispecifics and trispecifics that engage 2 or 3 distinct targets at once are being explored for HIV prevention and treatment. Borrowing a strategy from cancer immunotherapy, these molecules could be leveraged to enhance infected cell killing by bridging effectors (such as CD8+ T cells) and infected target cells. For instance, bispecific antibodies targeting CD3 and Env are being tested by TeneoBio, Inc., a project on which we collaborated with them to test their constructs *in vitro*. Another approach involves engineering bispecifics that leverage distinct mechanisms of viral inhibition by neutralizing Env with one Fab and blocking cell entry by binding the CD4 or CCR5 receptor with the other Fab. Bispecifics combining an HIV-1 bNAb and iMab (binds CD4) or leronlimab (binds CCR5) often had greater breadth and potency than the parental mAbs alone; one construct, $10E8_{v2.0}$/iMab, was tested *in vivo* and found to protect humanized mice from HIV-1 infection and reduce viral loads in infected mice [349]. Alternatively, combining multiple bNAb specificities for different epitopes into one antibody molecule can increase the breadth and potency of the engineered antibody. For instance, trispecifics targeting the CD4bs, the MPER, and V1V2 glycan sites were shown to provide superior protection from challenge with a mixture of SHIVs in macaques compared with individual bNAbs [350]. In the context of treating nascent or established infection, such an approach might also help to overcome the risk of viral escape due to ‘monotherapy’ resulting from unequal rates of decay of bNAbs in a cocktail. However, issues of immunogenicity and ADA for these unnatural

constructs *in vivo* may limit their application to short-term treatments, or they may need to be used serially to avoid clearance by ADA.

Finally, future studies should consider testing combination treatment using bNAbs and an anti-inflammatory agent, such as an anti-tumor necrosis alpha (TNFα) biologic, to limit lentiviral pathogenesis. Abundant evidence exists for a link between inflammatory damage to the GI tract barrier during acute infection, mucosal immune dysfunction, loss of epithelial barrier integrity, microbial translocation, chronic systemic inflammation, and immunopathology and pathogenesis. In macaques infected with SIV, intestinal damage was shown to occur before immune dysfunction, suggesting that inflammatory GI tract damage plays a key role in initiating pathogenesis [116]. Intriguingly, TNFα blockade using the monoclonal antibody adalimumab was able to limit lymph node inflammation and damage during pathogenic SIV infection, supporting a role for TNFα in driving inflammatory processes that promote disease progression [351]. It is likely that adalimumab and other TNFα inhibitors also dampen GI tract inflammation, since they are FDA-approved to treat inflammatory diseases in the gut, including ulcerative colitis and Crohn's disease. Thus, one possible strategy for improving the efficacy of delayed bNAb treatment could be to combine them with a targeted anti-inflammatory treatment, such as a TNFα inhibitor. If blocking the pro-inflammatory pathways driven by TNFα can help preserve GI tract barrier integrity and limit immunologic damage during inadequately-controlled SHIV infection, we may be able to buy time for the infant immune system to mature and mount more effective adaptive immune responses to control the nascent infection that has already taken hold before bNAb treatment. Future studies should examine the degree to which inhibition of TNFα may be able to synergize with bNAbs to preserve GI tract homeostasis and enhance viral control compared with bNAbs alone in the context of treatment delay.

A wide variety of innovative strategies are being explored to block viral seeding and to effect durable HIV remission. In light of the heterogeneity of the viral reservoir and the complexity of its persistence and pathogenesis mechanisms, multiple approaches—including but not limited to ART, antibodies, bispecifics, as well as targeted modulation of immune responses—may need to be used in combination for effective intervention, functional cure, and eradication of HIV.

B. Examining the impact of dose- and age-dependent immunologic differences on viral infection and treatment outcomes in newborns

In vertically HIV infected infants, differences in severity of disease and mortality rates as a function of age at infection are well appreciated. Newborns undergo extensive immunologic maturation during the first days and weeks of life, and the increased immunologic maturity likely accounts for improved outcomes in infants infected at older ages. However, the specific determinants of differential pathogenesis in newborns and older infants are poorly defined. Our study of single high dose SHIV infection in newborn and older infant macaques pinpointed distinct alterations in leukocyte subsets and innate immune responses that differ by age independent of the viral dose, which was the same in all animals, thus removing the confounding factor of different viral doses received during birth compared to breastfeeding.

Our findings may have important implications for optimizing therapies in infants infected at birth in contrast to those infected at older ages. For instance, our finding that newborns, unlike infants, fail to mount a robust type I IFN response during acute infection suggests that strategies that rely primarily on the host innate immune system to eliminate the nascent reservoir, such as very early ART, may not be as effective in newborns as in older infants with their improved type I IFN function. In younger infants,

more potent PEP interventions may be needed to achieve clearance; if it is important to "hit early, hit hard" in adults exposed to HIV, it may be necessary to "hit even harder" in exposed newborns to compensate for their weaker innate immunity. The kinetics of type I IFN maturation during infancy, as well as the specific signaling defect(s) leading to this transcriptomic phenotype, remain to be elucidated and may be important considerations when designing optimal interventions for infants exposed at different stages of growth and development. Because many strategies for limiting persistence and pathogenesis involve modulating or taking advantage of host immunity to varying extents, future animal studies of PEP for infants exposed to HIV before or at birth should be performed in newborns so as to better model the stage of immunologic immaturity at this age.

III. Concluding Thoughts

Vertical HIV-1 transmission remains a global health challenge with complex social, economic, and scientific factors standing in the way of reducing transmission and improving infant health and survival. In the absence of a protective vaccine, passive administration of broadly neutralizing antibodies offers hope for protection or treatment of HIV-1 in this vulnerable population. The work described in this dissertation employs a validated nonhuman primate model of HIV-1 peripartum infection to shed light on the kinetics of viral reservoir seeding and mechanisms of pathogenesis, informing strategies for effective treatment. We also demonstrate, for the first time, that a single dose of broadly neutralizing antibodies given 30 hours after SHIV exposure can prevent the establishment of a persistent reservoir in treated infant macaques. Our findings open the door to future studies of potent combinations of antibodies, antiretrovirals, and other interventions to further extend the window of opportunity for effective prevention of lifelong infection in infants exposed to HIV-1 at birth.

References

1 Faria, N. R. *et al.* HIV epidemiology. The early spread and epidemic ignition of HIV-1 in human populations. *Science* **346**, 56-61, doi:10.1126/science.1256739 (2014).

2 Worobey, M. *et al.* 1970s and 'Patient 0' HIV-1 genomes illuminate early HIV/AIDS history in North America. *Nature* **539**, 98-101, doi:10.1038/nature19827 (2016).

3 Centers for Disease, C. Pneumocystis pneumonia--Los Angeles. *MMWR Morb Mortal Wkly Rep* **30**, 250-252 (1981).

4 Centers for Disease, C. Kaposi's sarcoma and Pneumocystis pneumonia among homosexual men--New York City and California. *MMWR Morb Mortal Wkly Rep* **30**, 305-308 (1981).

5 Durack, D. T. Opportunistic infections and Kaposi's sarcoma in homosexual men. *N Engl J Med* **305**, 1465-1467, doi:10.1056/NEJM198112103052408 (1981).

6 Centers for Disease, C. Pneumocystis carinii pneumonia among persons with hemophilia A. *MMWR Morb Mortal Wkly Rep* **31**, 365-367 (1982).

7 Masur, H. *et al.* An outbreak of community-acquired Pneumocystis carinii pneumonia: initial manifestation of cellular immune dysfunction. *N Engl J Med* **305**, 1431-1438, doi:10.1056/NEJM198112103052402 (1981).

8 Centers for Disease, C. Unexplained immunodeficiency and opportunistic infections in infants--New York, New Jersey, California. *MMWR Morb Mortal Wkly Rep* **31**, 665-667 (1982).

9 Centers for Disease, C. Opportunistic infections and Kaposi's sarcoma among Haitians in the United States. *MMWR Morb Mortal Wkly Rep* **31**, 353-354, 360-351 (1982).

10 Centers for Disease, C. Immunodeficiency among female sexual partners of males with acquired immune deficiency syndrome (AIDS) - New York. *MMWR Morb Mortal Wkly Rep* **31**, 697-698 (1983).

11 Broder, S. & Gallo, R. C. A pathogenic retrovirus (HTLV-III) linked to AIDS. *N Engl J Med* **311**, 1292-1297, doi:10.1056/NEJM198411153112006 (1984).

12 Barre-Sinoussi, F. *et al.* Isolation of a T-lymphotropic retrovirus from a patient at risk for acquired immune deficiency syndrome (AIDS). *Science* **220**, 868-871, doi:10.1126/science.6189183 (1983).

13 Levy, J. A. *et al.* Isolation of lymphocytopathic retroviruses from San Francisco patients with AIDS. *Science* **225**, 840-842, doi:10.1126/science.6206563 (1984).

14 Jacobs, M. M. HIV or HTLV-III? *Arch Surg* **122**, 959, doi:10.1001/archsurg.1987.01400200109031 (1987).

15 Fitzgerald, D. W. *et al.* An Ad5-vectored HIV-1 vaccine elicits cell-mediated immunity but does not affect disease progression in HIV-1-infected male subjects: results from a randomized placebo-controlled trial (the Step study). *J Infect Dis* **203**, 765-772, doi:10.1093/infdis/jiq114 (2011).

16 Rerks-Ngarm, S. *et al.* Vaccination with ALVAC and AIDSVAX to prevent HIV-1 infection in Thailand. *N Engl J Med* **361**, 2209-2220, doi:10.1056/NEJMoa0908492 (2009).

17 Centers for Disease, C. Update: acquired immunodeficiency syndrome (AIDS)--United States. *MMWR Morb Mortal Wkly Rep* **32**, 465-467 (1983).

18 Centers for Disease, C. Possible transfusion-associated acquired immune deficiency syndrome (AIDS) - California. *MMWR Morb Mortal Wkly Rep* **31**, 652-654 (1982).

19 Ziegler, J. B., Cooper, D. A., Johnson, R. O. & Gold, J. Postnatal transmission of AIDS-associated retrovirus from mother to infant. *Lancet* **1**, 896-898, doi:10.1016/s0140-6736(85)91673-3 (1985).
20 Scott, G. B., Buck, B. E., Leterman, J. G., Bloom, F. L. & Parks, W. P. Acquired immunodeficiency syndrome in infants. *N Engl J Med* **310**, 76-81, doi:10.1056/NEJM198401123100202 (1984).
21 Centers for Disease, C. Recommendations for assisting in the prevention of perinatal transmission of human T-lymphotropic virus type III/lymphadenopathy-associated virus and acquired immunodeficiency syndrome. *MMWR Morb Mortal Wkly Rep* **34**, 721-726, 731-722 (1985).
22 Kolata, G. FDA approves AZT. *Science* **235**, 1570, doi:10.1126/science.3469754 (1987).
23 FDA approves AZT for pediatric AIDS patients under 13. *Oncology (Williston Park)* **4**, 96 (1990).
24 Ho, D. D. Time to hit HIV, early and hard. *N Engl J Med* **333**, 450-451, doi:10.1056/NEJM199508173330710 (1995).
25 Holmes, D. FDA paves the way for pre-exposure HIV prophylaxis. *Lancet* **380**, 325, doi:10.1016/s0140-6736(12)61235-5 (2012).
26 Sharp, P. M. & Hahn, B. H. Origins of HIV and the AIDS pandemic. *Cold Spring Harb Perspect Med* **1**, a006841, doi:10.1101/cshperspect.a006841 (2011).
27 Van Heuverswyn, F. *et al.* Human immunodeficiency viruses: SIV infection in wild gorillas. *Nature* **444**, 164, doi:10.1038/444164a (2006).
28 Hirsch, V. M., Zack, P. M., Vogel, A. P. & Johnson, P. R. Simian immunodeficiency virus infection of macaques: end-stage disease is characterized by widespread distribution of proviral DNA in tissues. *J Infect Dis* **163**, 976-988, doi:10.1093/infdis/163.5.976 (1991).
29 Hahn, B. H., Shaw, G. M., De Cock, K. M. & Sharp, P. M. AIDS as a zoonosis: scientific and public health implications. *Science* **287**, 607-614, doi:10.1126/science.287.5453.607 (2000).
30 Bbosa, N., Kaleebu, P. & Ssemwanga, D. HIV subtype diversity worldwide. *Curr Opin HIV AIDS* **14**, 153-160, doi:10.1097/COH.0000000000000534 (2019).
31 Korber, B. *et al.* Evolutionary and immunological implications of contemporary HIV-1 variation. *Br Med Bull* **58**, 19-42, doi:10.1093/bmb/58.1.19 (2001).
32 Hatziioannou, T. & Evans, D. T. Animal models for HIV/AIDS research. *Nat Rev Microbiol* **10**, 852-867, doi:10.1038/nrmicro2911 (2012).
33 Melkus, M. W. *et al.* Humanized mice mount specific adaptive and innate immune responses to EBV and TSST-1. *Nat Med* **12**, 1316-1322, doi:10.1038/nm1431 (2006).
34 Rhesus Macaque Genome, S. *et al.* Evolutionary and biomedical insights from the rhesus macaque genome. *Science* **316**, 222-234, doi:10.1126/science.1139247 (2007).
35 Mansfield, K. G., Lerch, N. W., Gardner, M. B. & Lackner, A. A. Origins of simian immunodeficiency virus infection in macaques at the New England Regional Primate Research Center. *J Med Primatol* **24**, 116-122, doi:10.1111/j.1600-0684.1995.tb00156.x (1995).
36 Kestler, H. *et al.* Induction of AIDS in rhesus monkeys by molecularly cloned simian immunodeficiency virus. *Science* **248**, 1109-1112, doi:10.1126/science.2160735 (1990).
37 Desrosiers, R. C. *et al.* Macrophage-tropic variants of SIV are associated with specific AIDS-related lesions but are not essential for the development of AIDS. *Am J Pathol* **139**, 29-35 (1991).

38 Puffer, B. A. *et al.* CD4 independence of simian immunodeficiency virus Envs is associated with macrophage tropism, neutralization sensitivity, and attenuated pathogenicity. *J Virol* **76**, 2595-2605, doi:10.1128/jvi.76.6.2595-2605.2002 (2002).
39 Keele, B. F. *et al.* Low-dose rectal inoculation of rhesus macaques by SIVsmE660 or SIVmac251 recapitulates human mucosal infection by HIV-1. *J Exp Med* **206**, 1117-1134, doi:10.1084/jem.20082831 (2009).
40 Strickland, S. L. *et al.* Significant genetic heterogeneity of the SIVmac251 viral swarm derived from different sources. *AIDS Res Hum Retroviruses* **27**, 1327-1332, doi:10.1089/aid.2011.0100 (2011).
41 Brenchley, J. M. *et al.* Differential Th17 CD4 T-cell depletion in pathogenic and nonpathogenic lentiviral infections. *Blood* **112**, 2826-2835, doi:10.1182/blood-2008-05-159301 (2008).
42 Huot, N. *et al.* Natural killer cells migrate into and control simian immunodeficiency virus replication in lymph node follicles in African green monkeys. *Nat Med* **23**, 1277-1286, doi:10.1038/nm.4421 (2017).
43 Chahroudi, A. *et al.* Target cell availability, rather than breast milk factors, dictates mother-to-infant transmission of SIV in sooty mangabeys and rhesus macaques. *PLoS Pathog* **10**, e1003958, doi:10.1371/journal.ppat.1003958 (2014).
44 Ambrose, Z., KewalRamani, V. N., Bieniasz, P. D. & Hatziioannou, T. HIV/AIDS: in search of an animal model. *Trends Biotechnol* **25**, 333-337, doi:10.1016/j.tibtech.2007.05.004 (2007).
45 Jiang, Y. *et al.* RT-SHIV, an infectious CCR5-tropic chimeric virus suitable for evaluating HIV reverse transcriptase inhibitors in macaque models. *AIDS Res Ther* **6**, 23, doi:10.1186/1742-6405-6-23 (2009).
46 Hatziioannou, T. *et al.* A macaque model of HIV-1 infection. *Proc Natl Acad Sci U S A* **106**, 4425-4429, doi:10.1073/pnas.0812587106 (2009).
47 Reimann, K. A. *et al.* A chimeric simian/human immunodeficiency virus expressing a primary patient human immunodeficiency virus type 1 isolate env causes an AIDS-like disease after in vivo passage in rhesus monkeys. *J Virol* **70**, 6922-6928 (1996).
48 Igarashi, T. *et al.* Emergence of a highly pathogenic simian/human immunodeficiency virus in a rhesus macaque treated with anti-CD8 mAb during a primary infection with a nonpathogenic virus. *Proc Natl Acad Sci U S A* **96**, 14049-14054, doi:10.1073/pnas.96.24.14049 (1999).
49 Song, R. J. *et al.* Molecularly cloned SHIV-1157ipd3N4: a highly replication-competent, mucosally transmissible R5 simian-human immunodeficiency virus encoding HIV clade C Env. *J Virol* **80**, 8729-8738, doi:10.1128/JVI.00558-06 (2006).
50 Harouse, J. M., Gettie, A., Tan, R. C., Blanchard, J. & Cheng-Mayer, C. Distinct pathogenic sequela in rhesus macaques infected with CCR5 or CXCR4 utilizing SHIVs. *Science* **284**, 816-819 (1999).
51 Nishimura, Y. *et al.* Generation of the pathogenic R5-tropic simian/human immunodeficiency virus SHIVAD8 by serial passaging in rhesus macaques. *J Virol* **84**, 4769-4781, doi:10.1128/JVI.02279-09 (2010).
52 Keele, B. F. *et al.* Identification and characterization of transmitted and early founder virus envelopes in primary HIV-1 infection. *Proc Natl Acad Sci U S A* **105**, 7552-7557, doi:10.1073/pnas.0802203105 (2008).

53 Richman, D. D. & Bozzette, S. A. The impact of the syncytium-inducing phenotype of human immunodeficiency virus on disease progression. *J Infect Dis* **169**, 968-974, doi:10.1093/infdis/169.5.968 (1994).
54 Harouse, J. M. *et al.* Mucosal transmission of pathogenic CXCR4-utilizing SHIVSF33A variants in rhesus macaques. *Virology* **248**, 95-107, doi:10.1006/viro.1998.9236 (1998).
55 Harouse, J. M. *et al.* Mucosal transmission and induction of simian AIDS by CCR5-specific simian/human immunodeficiency virus SHIV(SF162P3). *J Virol* **75**, 1990-1995, doi:10.1128/JVI.75.4.1990-1995.2001 (2001).
56 Ho, S. H., Shek, L., Gettie, A., Blanchard, J. & Cheng-Mayer, C. V3 loop-determined coreceptor preference dictates the dynamics of CD4+-T-cell loss in simian-human immunodeficiency virus-infected macaques. *J Virol* **79**, 12296-12303, doi:10.1128/JVI.79.19.12296-12303.2005 (2005).
57 Endo, Y. *et al.* Short- and long-term clinical outcomes in rhesus monkeys inoculated with a highly pathogenic chimeric simian/human immunodeficiency virus. *J Virol* **74**, 6935-6945, doi:10.1128/jvi.74.15.6935-6945.2000 (2000).
58 Seaman, M. S. *et al.* Tiered categorization of a diverse panel of HIV-1 Env pseudoviruses for assessment of neutralizing antibodies. *J Virol* **84**, 1439-1452, doi:10.1128/JVI.02108-09 (2010).
59 Barre-Sinoussi, F., Ross, A. L. & Delfraissy, J. F. Past, present and future: 30 years of HIV research. *Nat Rev Microbiol* **11**, 877-883, doi:10.1038/nrmicro3132 (2013).
60 Klaver, B. & Berkhout, B. Comparison of 5' and 3' long terminal repeat promoter function in human immunodeficiency virus. *J Virol* **68**, 3830-3840 (1994).
61 Wetzel, K. S. *et al.* CXCR6-Mediated Simian Immunodeficiency Virus SIVagmSab Entry into Sabaeus African Green Monkey Lymphocytes Implicates Widespread Use of Non-CCR5 Pathways in Natural Host Infections. *J Virol* **91**, doi:10.1128/JVI.01626-16 (2017).
62 Elliott, S. T. *et al.* Dualtropic CXCR6/CCR5 Simian Immunodeficiency Virus (SIV) Infection of Sooty Mangabey Primary Lymphocytes: Distinct Coreceptor Use in Natural versus Pathogenic Hosts of SIV. *J Virol* **89**, 9252-9261, doi:10.1128/JVI.01236-15 (2015).
63 Wetzel, K. S. *et al.* Loss of CXCR6 coreceptor usage characterizes pathogenic lentiviruses. *PLoS Pathog* **14**, e1007003, doi:10.1371/journal.ppat.1007003 (2018).
64 Wilen, C. B., Tilton, J. C. & Doms, R. W. HIV: cell binding and entry. *Cold Spring Harb Perspect Med* **2**, doi:10.1101/cshperspect.a006866 (2012).
65 Hao, H. N. & Lyman, W. D. HIV infection of fetal human astrocytes: the potential role of a receptor-mediated endocytic pathway. *Brain Res* **823**, 24-32, doi:10.1016/s0006-8993(98)01371-7 (1999).
66 Liu, Y. *et al.* CD4-independent infection of astrocytes by human immunodeficiency virus type 1: requirement for the human mannose receptor. *J Virol* **78**, 4120-4133, doi:10.1128/jvi.78.8.4120-4133.2004 (2004).
67 Hu, W. S. & Hughes, S. H. HIV-1 reverse transcription. *Cold Spring Harb Perspect Med* **2**, doi:10.1101/cshperspect.a006882 (2012).
68 Craigie, R. & Bushman, F. D. HIV DNA integration. *Cold Spring Harb Perspect Med* **2**, a006890, doi:10.1101/cshperspect.a006890 (2012).
69 Sloan, R. D. & Wainberg, M. A. The role of unintegrated DNA in HIV infection. *Retrovirology* **8**, 52, doi:10.1186/1742-4690-8-52 (2011).

70 Donahue, D. A. & Wainberg, M. A. Cellular and molecular mechanisms involved in the establishment of HIV-1 latency. *Retrovirology* **10**, 11, doi:10.1186/1742-4690-10-11 (2013).
71 Rice, A. P. The HIV-1 Tat Protein: Mechanism of Action and Target for HIV-1 Cure Strategies. *Curr Pharm Des* **23**, 4098-4102, doi:10.2174/1381612823666170704130635 (2017).
72 Tazi, J. *et al.* Alternative splicing: regulation of HIV-1 multiplication as a target for therapeutic action. *FEBS J* **277**, 867-876, doi:10.1111/j.1742-4658.2009.07522.x (2010).
73 Jacks, T. *et al.* Characterization of ribosomal frameshifting in HIV-1 gag-pol expression. *Nature* **331**, 280-283, doi:10.1038/331280a0 (1988).
74 Shehu-Xhilaga, M., Crowe, S. M. & Mak, J. Maintenance of the Gag/Gag-Pol ratio is important for human immunodeficiency virus type 1 RNA dimerization and viral infectivity. *J Virol* **75**, 1834-1841, doi:10.1128/JVI.75.4.1834-1841.2001 (2001).
75 Sundquist, W. I. & Krausslich, H. G. HIV-1 assembly, budding, and maturation. *Cold Spring Harb Perspect Med* **2**, a006924, doi:10.1101/cshperspect.a006924 (2012).
76 Checkley, M. A., Luttge, B. G. & Freed, E. O. HIV-1 envelope glycoprotein biosynthesis, trafficking, and incorporation. *J Mol Biol* **410**, 582-608, doi:10.1016/j.jmb.2011.04.042 (2011).
77 Votteler, J. & Sundquist, W. I. Virus budding and the ESCRT pathway. *Cell Host Microbe* **14**, 232-241, doi:10.1016/j.chom.2013.08.012 (2013).
78 Tedbury, P. R. & Freed, E. O. The role of matrix in HIV-1 envelope glycoprotein incorporation. *Trends Microbiol* **22**, 372-378, doi:10.1016/j.tim.2014.04.012 (2014).
79 Haffar, O. K. *et al.* Two nuclear localization signals in the HIV-1 matrix protein regulate nuclear import of the HIV-1 pre-integration complex. *J Mol Biol* **299**, 359-368, doi:10.1006/jmbi.2000.3768 (2000).
80 Paxton, W., Connor, R. I. & Landau, N. R. Incorporation of Vpr into human immunodeficiency virus type 1 virions: requirement for the p6 region of gag and mutational analysis. *J Virol* **67**, 7229-7237 (1993).
81 Gottlinger, H. G., Dorfman, T., Sodroski, J. G. & Haseltine, W. A. Effect of mutations affecting the p6 gag protein on human immunodeficiency virus particle release. *Proc Natl Acad Sci U S A* **88**, 3195-3199, doi:10.1073/pnas.88.8.3195 (1991).
82 Datta, S. A. *et al.* Dimerization of the SP1 Region of HIV-1 Gag Induces a Helical Conformation and Association into Helical Bundles: Implications for Particle Assembly. *J Virol* **90**, 1773-1787, doi:10.1128/JVI.02061-15 (2016).
83 Coren, L. V. *et al.* Mutational analysis of the C-terminal gag cleavage sites in human immunodeficiency virus type 1. *J Virol* **81**, 10047-10054, doi:10.1128/JVI.02496-06 (2007).
84 de Marco, A. *et al.* Role of the SP2 domain and its proteolytic cleavage in HIV-1 structural maturation and infectivity. *J Virol* **86**, 13708-13716, doi:10.1128/JVI.01704-12 (2012).
85 Sheehy, A. M., Gaddis, N. C., Choi, J. D. & Malim, M. H. Isolation of a human gene that inhibits HIV-1 infection and is suppressed by the viral Vif protein. *Nature* **418**, 646-650, doi:10.1038/nature00939 (2002).
86 Stopak, K., de Noronha, C., Yonemoto, W. & Greene, W. C. HIV-1 Vif blocks the antiviral activity of APOBEC3G by impairing both its translation and intracellular stability. *Mol Cell* **12**, 591-601, doi:10.1016/s1097-2765(03)00353-8 (2003).

87 Kogan, M. & Rappaport, J. HIV-1 accessory protein Vpr: relevance in the pathogenesis of HIV and potential for therapeutic intervention. *Retrovirology* **8**, 25, doi:10.1186/1742-4690-8-25 (2011).
88 Goh, W. C. *et al.* HIV-1 Vpr increases viral expression by manipulation of the cell cycle: a mechanism for selection of Vpr in vivo. *Nat Med* **4**, 65-71, doi:10.1038/nm0198-065 (1998).
89 Roshal, M., Kim, B., Zhu, Y., Nghiem, P. & Planelles, V. Activation of the ATR-mediated DNA damage response by the HIV-1 viral protein R. *J Biol Chem* **278**, 25879-25886, doi:10.1074/jbc.M303948200 (2003).
90 Douglas, J. L. *et al.* Vpu directs the degradation of the human immunodeficiency virus restriction factor BST-2/Tetherin via a {beta}TrCP-dependent mechanism. *J Virol* **83**, 7931-7947, doi:10.1128/JVI.00242-09 (2009).
91 Willey, R. L., Maldarelli, F., Martin, M. A. & Strebel, K. Human immunodeficiency virus type 1 Vpu protein induces rapid degradation of CD4. *J Virol* **66**, 7193-7200 (1992).
92 Willey, R. L., Maldarelli, F., Martin, M. A. & Strebel, K. Human immunodeficiency virus type 1 Vpu protein regulates the formation of intracellular gp160-CD4 complexes. *J Virol* **66**, 226-234 (1992).
93 Garcia, J. V. & Miller, A. D. Serine phosphorylation-independent downregulation of cell-surface CD4 by nef. *Nature* **350**, 508-511, doi:10.1038/350508a0 (1991).
94 Schwartz, O., Marechal, V., Le Gall, S., Lemonnier, F. & Heard, J. M. Endocytosis of major histocompatibility complex class I molecules is induced by the HIV-1 Nef protein. *Nat Med* **2**, 338-342, doi:10.1038/nm0396-338 (1996).
95 Basmaciogullari, S. & Pizzato, M. The activity of Nef on HIV-1 infectivity. *Front Microbiol* **5**, 232, doi:10.3389/fmicb.2014.00232 (2014).
96 Sawai, E. T., Hamza, M. S., Ye, M., Shaw, K. E. & Luciw, P. A. Pathogenic conversion of live attenuated simian immunodeficiency virus vaccines is associated with expression of truncated Nef. *J Virol* **74**, 2038-2045, doi:10.1128/jvi.74.4.2038-2045.2000 (2000).
97 Learmont, J. C. *et al.* Immunologic and virologic status after 14 to 18 years of infection with an attenuated strain of HIV-1. A report from the Sydney Blood Bank Cohort. *N Engl J Med* **340**, 1715-1722, doi:10.1056/NEJM199906033402203 (1999).
98 Churchill, M. J. *et al.* Longitudinal analysis of human immunodeficiency virus type 1 nef/long terminal repeat sequences in a cohort of long-term survivors infected from a single source. *J Virol* **80**, 1047-1052, doi:10.1128/JVI.80.2.1047-1052.2006 (2006).
99 Pollard, V. W. & Malim, M. H. The HIV-1 Rev protein. *Annu Rev Microbiol* **52**, 491-532, doi:10.1146/annurev.micro.52.1.491 (1998).
100 Hrecka, K. *et al.* Vpx relieves inhibition of HIV-1 infection of macrophages mediated by the SAMHD1 protein. *Nature* **474**, 658-661, doi:10.1038/nature10195 (2011).
101 Su, J. *et al.* HIV-2/SIV Vpx targets a novel functional domain of STING to selectively inhibit cGAS-STING-mediated NF-kappaB signalling. *Nat Microbiol* **4**, 2552-2564, doi:10.1038/s41564-019-0585-4 (2019).
102 Coquel, F. *et al.* SAMHD1 acts at stalled replication forks to prevent interferon induction. *Nature* **557**, 57-61, doi:10.1038/s41586-018-0050-1 (2018).
103 Chen, S. *et al.* SAMHD1 suppresses innate immune responses to viral infections and inflammatory stimuli by inhibiting the NF-kappaB and interferon pathways. *Proc Natl Acad Sci U S A* **115**, E3798-E3807, doi:10.1073/pnas.1801213115 (2018).

104 Xu, H., Wang, X. & Veazey, R. S. Mucosal immunology of HIV infection. *Immunol Rev* **254**, 10-33, doi:10.1111/imr.12072 (2013).
105 Hessell, A. J. *et al.* Early short-term treatment with neutralizing human monoclonal antibodies halts SHIV infection in infant macaques. *Nat Med* **22**, 362-368, doi:10.1038/nm.4063 (2016).
106 Milush, J. M. *et al.* Rapid dissemination of SIV following oral inoculation. *AIDS* **18**, 2371-2380 (2004).
107 Okoye, A. A. *et al.* Early antiretroviral therapy limits SIV reservoir establishment to delay or prevent post-treatment viral rebound. *Nat Med* **24**, 1430-1440, doi:10.1038/s41591-018-0130-7 (2018).
108 McLaren, P. J. & Carrington, M. The impact of host genetic variation on infection with HIV-1. *Nat Immunol* **16**, 577-583, doi:10.1038/ni.3147 (2015).
109 Claiborne, D. T. *et al.* Replicative fitness of transmitted HIV-1 drives acute immune activation, proviral load in memory CD4+ T cells, and disease progression. *Proc Natl Acad Sci U S A* **112**, E1480-1489, doi:10.1073/pnas.1421607112 (2015).
110 Todd, J. *et al.* Time from HIV seroconversion to death: a collaborative analysis of eight studies in six low and middle-income countries before highly active antiretroviral therapy. *AIDS* **21 Suppl 6**, S55-63, doi:10.1097/01.aids.0000299411.75269.e8 (2007).
111 Pahar, B., Wang, X., Dufour, J., Lackner, A. A. & Veazey, R. S. Virus-specific T cell responses in macaques acutely infected with SHIV(sf162p3). *Virology* **363**, 36-47, doi:10.1016/j.virol.2007.01.010 (2007).
112 Shearer, W. T. *et al.* Viral load and disease progression in infants infected with human immunodeficiency virus type 1. Women and Infants Transmission Study Group. *N Engl J Med* **336**, 1337-1342, doi:10.1056/NEJM199705083361901 (1997).
113 Newell, M.-L. *et al.* Mortality of infected and uninfected infants born to HIV-infected mothers in Africa: a pooled analysis. *The Lancet* **364**, 1236-1243, doi:10.1016/s0140-6736(04)17140-7 (2004).
114 Jaworski, J. P. *et al.* Neutralizing polyclonal IgG present during acute infection prevents rapid disease onset in simian-human immunodeficiency virus SHIVSF162P3-infected infant rhesus macaques. *J Virol* **87**, 10447-10459, doi:10.1128/JVI.00049-13 (2013).
115 Bixler, S. L. & Mattapallil, J. J. Loss and dysregulation of Th17 cells during HIV infection. *Clin Dev Immunol* **2013**, 852418, doi:10.1155/2013/852418 (2013).
116 Hensley-McBain, T. *et al.* Intestinal damage precedes mucosal immune dysfunction in SIV infection. *Mucosal Immunol* **11**, 1429-1440, doi:10.1038/s41385-018-0032-5 (2018).
117 Estes, J. D. *et al.* Damaged intestinal epithelial integrity linked to microbial translocation in pathogenic simian immunodeficiency virus infections. *PLoS Pathog* **6**, e1001052, doi:10.1371/journal.ppat.1001052 (2010).
118 Brenchley, J. M. *et al.* Microbial translocation is a cause of systemic immune activation in chronic HIV infection. *Nat Med* **12**, 1365-1371, doi:10.1038/nm1511 (2006).
119 Otani, I. *et al.* Phenotypic changes in peripheral blood monocytes of cynomolgus monkeys acutely infected with simian immunodeficiency virus. *AIDS Res Hum Retroviruses* **14**, 1181-1186, doi:10.1089/aid.1998.14.1181 (1998).
120 Chen, P. *et al.* Perturbations of Monocyte Subsets and Their Association with T Helper Cell Differentiation in Acute and Chronic HIV-1-Infected Patients. *Front Immunol* **8**, 272, doi:10.3389/fimmu.2017.00272 (2017).

121 Hoffmann, M. *et al.* Exhaustion of Activated CD8 T Cells Predicts Disease Progression in Primary HIV-1 Infection. *PLoS Pathog* **12**, e1005661, doi:10.1371/journal.ppat.1005661 (2016).
122 Fitzgerald-Bocarsly, P. & Jacobs, E. S. Plasmacytoid dendritic cells in HIV infection: striking a delicate balance. *J Leukoc Biol* **87**, 609-620, doi:10.1189/jlb.0909635 (2010).
123 Moir, S. & Fauci, A. S. Pathogenic mechanisms of B-lymphocyte dysfunction in HIV disease. *J Allergy Clin Immunol* **122**, 12-19; quiz 20-11, doi:10.1016/j.jaci.2008.04.034 (2008).
124 Klatt, N. R., Chomont, N., Douek, D. C. & Deeks, S. G. Immune activation and HIV persistence: implications for curative approaches to HIV infection. *Immunol Rev* **254**, 326-342, doi:10.1111/imr.12065 (2013).
125 Pierson, T., McArthur, J. & Siliciano, R. F. Reservoirs for HIV-1: mechanisms for viral persistence in the presence of antiviral immune responses and antiretroviral therapy. *Annu Rev Immunol* **18**, 665-708, doi:10.1146/annurev.immunol.18.1.665 (2000).
126 Finzi, D. *et al.* Identification of a reservoir for HIV-1 in patients on highly active antiretroviral therapy. *Science* **278**, 1295-1300 (1997).
127 Chun, T. W. *et al.* Quantification of latent tissue reservoirs and total body viral load in HIV-1 infection. *Nature* **387**, 183-188, doi:10.1038/387183a0 (1997).
128 Persaud, D. *et al.* A stable latent reservoir for HIV-1 in resting CD4(+) T lymphocytes in infected children. *J Clin Invest* **105**, 995-1003, doi:10.1172/JCI9006 (2000).
129 Descours, B. *et al.* CD32a is a marker of a CD4 T-cell HIV reservoir harbouring replication-competent proviruses. *Nature*, doi:10.1038/nature21710 (2017).
130 Perez, L. *et al.* Conflicting evidence for HIV enrichment in CD32(+) CD4 T cells. *Nature* **561**, E9-E16, doi:10.1038/s41586-018-0493-4 (2018).
131 Bertagnolli, L. N. *et al.* The role of CD32 during HIV-1 infection. *Nature* **561**, E17-E19, doi:10.1038/s41586-018-0494-3 (2018).
132 Osuna, C. E. *et al.* Evidence that CD32a does not mark the HIV-1 latent reservoir. *Nature* **561**, E20-E28, doi:10.1038/s41586-018-0495-2 (2018).
133 Siliciano, J. D. *et al.* Long-term follow-up studies confirm the stability of the latent reservoir for HIV-1 in resting CD4+ T cells. *Nat Med* **9**, 727-728, doi:10.1038/nm880 (2003).
134 Silvestri, G. *et al.* HIV infects astrocytes in vivo and egresses from the brain to the periphery. *PLOS Pathogens* **16**, doi:10.1371/journal.ppat.1008381 (2020).
135 Altfeld, M. & Gale, M., Jr. Innate immunity against HIV-1 infection. *Nat Immunol* **16**, 554-562, doi:10.1038/ni.3157 (2015).
136 Utay, N. S. & Douek, D. C. Interferons and HIV Infection: The Good, the Bad, and the Ugly. *Pathog Immun* **1**, 107-116, doi:10.20411/pai.v1i1.125 (2016).
137 Sandler, N. G. *et al.* Type I interferon responses in rhesus macaques prevent SIV infection and slow disease progression. *Nature* **511**, 601-605, doi:10.1038/nature13554 (2014).
138 Azzoni, L. *et al.* Pegylated Interferon alfa-2a monotherapy results in suppression of HIV type 1 replication and decreased cell-associated HIV DNA integration. *J Infect Dis* **207**, 213-222, doi:10.1093/infdis/jis663 (2013).
139 Boyd, D. F., Sharma, A., Humes, D., Cheng-Mayer, C. & Overbaugh, J. Adapting SHIVs In Vivo Selects for Envelope-Mediated Interferon-alpha Resistance. *PLoS Pathog* **12**, e1005727, doi:10.1371/journal.ppat.1005727 (2016).

140 Fenton-May, A. E. *et al.* Relative resistance of HIV-1 founder viruses to control by interferon-alpha. *Retrovirology* **10**, 146, doi:10.1186/1742-4690-10-146 (2013).
141 Harris, L. D. *et al.* Downregulation of robust acute type I interferon responses distinguishes nonpathogenic simian immunodeficiency virus (SIV) infection of natural hosts from pathogenic SIV infection of rhesus macaques. *J Virol* **84**, 7886-7891, doi:10.1128/JVI.02612-09 (2010).
142 Mandl, J. N. *et al.* Divergent TLR7 and TLR9 signaling and type I interferon production distinguish pathogenic and nonpathogenic AIDS virus infections. *Nat Med* **14**, 1077-1087, doi:10.1038/nm.1871 (2008).
143 Hardy, G. A. *et al.* Interferon-alpha is the primary plasma type-I IFN in HIV-1 infection and correlates with immune activation and disease markers. *PLoS One* **8**, e56527, doi:10.1371/journal.pone.0056527 (2013).
144 Sedaghat, A. R. *et al.* Chronic CD4+ T-cell activation and depletion in human immunodeficiency virus type 1 infection: type I interferon-mediated disruption of T-cell dynamics. *J Virol* **82**, 1870-1883, doi:10.1128/JVI.02228-07 (2008).
145 Yu, Q., Yu, R. & Qin, X. The good and evil of complement activation in HIV-1 infection. *Cell Mol Immunol* **7**, 334-340, doi:10.1038/cmi.2010.8 (2010).
146 Vingert, B. *et al.* HIV controllers maintain a population of highly efficient Th1 effector cells in contrast to patients treated in the long term. *J Virol* **86**, 10661-10674, doi:10.1128/JVI.00056-12 (2012).
147 Chamcha, V. *et al.* Strong TH1-biased CD4 T cell responses are associated with diminished SIV vaccine efficacy. *Sci Transl Med* **11**, doi:10.1126/scitranslmed.aav1800 (2019).
148 Niessl, J. & Kaufmann, D. E. Harnessing T Follicular Helper Cell Responses for HIV Vaccine Development. *Viruses* **10**, doi:10.3390/v10060336 (2018).
149 Favre, D. *et al.* Critical loss of the balance between Th17 and T regulatory cell populations in pathogenic SIV infection. *PLoS Pathog* **5**, e1000295, doi:10.1371/journal.ppat.1000295 (2009).
150 Raffatellu, M. *et al.* Simian immunodeficiency virus-induced mucosal interleukin-17 deficiency promotes Salmonella dissemination from the gut. *Nat Med* **14**, 421-428, doi:10.1038/nm1743 (2008).
151 Jin, X. *et al.* Dramatic rise in plasma viremia after CD8(+) T cell depletion in simian immunodeficiency virus-infected macaques. *J Exp Med* **189**, 991-998, doi:10.1084/jem.189.6.991 (1999).
152 Yant, L. J. *et al.* The high-frequency major histocompatibility complex class I allele Mamu-B*17 is associated with control of simian immunodeficiency virus SIVmac239 replication. *J Virol* **80**, 5074-5077, doi:10.1128/JVI.80.10.5074-5077.2006 (2006).
153 Loffredo, J. T. *et al.* Mamu-B*08-positive macaques control simian immunodeficiency virus replication. *J Virol* **81**, 8827-8832, doi:10.1128/JVI.00895-07 (2007).
154 Kaslow, R. A. *et al.* Influence of combinations of human major histocompatibility complex genes on the course of HIV-1 infection. *Nat Med* **2**, 405-411, doi:10.1038/nm0496-405 (1996).
155 Goulder, P. J. & Walker, B. D. HIV and HLA class I: an evolving relationship. *Immunity* **37**, 426-440, doi:10.1016/j.immuni.2012.09.005 (2012).
156 Hansen, S. G. *et al.* Immune clearance of highly pathogenic SIV infection. *Nature* **502**, 100-104, doi:10.1038/nature12519 (2013).

157 Chew, G. M. *et al.* TIGIT Marks Exhausted T Cells, Correlates with Disease Progression, and Serves as a Target for Immune Restoration in HIV and SIV Infection. *PLoS Pathog* **12**, e1005349, doi:10.1371/journal.ppat.1005349 (2016).
158 Wherry, E. J. T cell exhaustion. *Nat Immunol* **12**, 492-499, doi:10.1038/ni.2035 (2011).
159 Tian, X. *et al.* The upregulation of LAG-3 on T cells defines a subpopulation with functional exhaustion and correlates with disease progression in HIV-infected subjects. *J Immunol* **194**, 3873-3882, doi:10.4049/jimmunol.1402176 (2015).
160 Jones, R. B. *et al.* Tim-3 expression defines a novel population of dysfunctional T cells with highly elevated frequencies in progressive HIV-1 infection. *J Exp Med* **205**, 2763-2779, doi:10.1084/jem.20081398 (2008).
161 Day, C. L. *et al.* PD-1 expression on HIV-specific T cells is associated with T-cell exhaustion and disease progression. *Nature* **443**, 350-354, doi:10.1038/nature05115 (2006).
162 Moir, S. & Fauci, A. S. B cells in HIV infection and disease. *Nat Rev Immunol* **9**, 235-245, doi:10.1038/nri2524 (2009).
163 Miller, C. J. *et al.* Antiviral antibodies are necessary for control of simian immunodeficiency virus replication. *J Virol* **81**, 5024-5035, doi:10.1128/JVI.02444-06 (2007).
164 Schmitz, J. E. *et al.* Effect of Humoral Immune Responses on Controlling Viremia during Primary Infection of Rhesus Monkeys with Simian Immunodeficiency Virus. *Journal of Virology* **77**, 2165-2173, doi:10.1128/jvi.77.3.2165-2173.2003 (2003).
165 Huang, K. H. *et al.* B-cell depletion reveals a role for antibodies in the control of chronic HIV-1 infection. *Nat Commun* **1**, 102, doi:10.1038/ncomms1100 (2010).
166 UNAIDS. UNAIDS Fact Sheet. (2019).
167 De Cock, K. M. *et al.* Prevention of mother-to-child HIV transmission in resource-poor countries: translating research into policy and practice. *JAMA* **283**, 1175-1182, doi:10.1001/jama.283.9.1175 (2000).
168 Coovadia, H. M. *et al.* Mother-to-child transmission of HIV-1 infection during exclusive breastfeeding in the first 6 months of life: an intervention cohort study. *Lancet* **369**, 1107-1116, doi:10.1016/S0140-6736(07)60283-9 (2007).
169 Lallemant, M. *et al.* Single-dose perinatal nevirapine plus standard zidovudine to prevent mother-to-child transmission of HIV-1 in Thailand. *N Engl J Med* **351**, 217-228, doi:10.1056/NEJMoa033500 (2004).
170 Wu, X. *et al.* Neutralization escape variants of human immunodeficiency virus type 1 are transmitted from mother to infant. *J Virol* **80**, 835-844, doi:10.1128/JVI.80.2.835-844.2006 (2006).
171 Dickover, R. *et al.* Role of maternal autologous neutralizing antibody in selective perinatal transmission of human immunodeficiency virus type 1 escape variants. *J Virol* **80**, 6525-6533, doi:10.1128/JVI.02658-05 (2006).
172 Kliks, S. C., Wara, D. W., Landers, D. V. & Levy, J. A. Features of HIV-1 that could influence maternal-child transmission. *JAMA* **272**, 467-474 (1994).
173 Milligan, C., Richardson, B. A., John-Stewart, G., Nduati, R. & Overbaugh, J. Passively acquired antibody-dependent cellular cytotoxicity (ADCC) activity in HIV-infected infants is associated with reduced mortality. *Cell Host Microbe* **17**, 500-506, doi:10.1016/j.chom.2015.03.002 (2015).
174 Milligan, C. *et al.* Maternal Neutralization-Resistant Virus Variants Do Not Predict Infant HIV Infection Risk. *mBio* **7**, e02221-02215, doi:10.1128/mBio.02221-15 (2016).

175 Martinez, D. R. *et al.* Fc Characteristics Mediate Selective Placental Transfer of IgG in HIV-Infected Women. *Cell*, doi:10.1016/j.cell.2019.05.046 (2019).
176 Becquet, R. *et al.* Children who acquire HIV infection perinatally are at higher risk of early death than those acquiring infection through breastmilk: a meta-analysis. *PLoS One* **7**, e28510, doi:10.1371/journal.pone.0028510 (2012).
177 Marston, M. *et al.* Net survival of perinatally and postnatally HIV-infected children: a pooled analysis of individual data from sub-Saharan Africa. *Int J Epidemiol* **40**, 385-396, doi:10.1093/ije/dyq255 (2011).
178 Basha, S., Surendran, N. & Pichichero, M. Immune responses in neonates. *Expert Rev Clin Immunol* **10**, 1171-1184, doi:10.1586/1744666X.2014.942288 (2014).
179 Abel, K. The rhesus macaque pediatric SIV infection model - a valuable tool in understanding infant HIV-1 pathogenesis and for designing pediatric HIV-1 prevention strategies. *Curr HIV Res* **7**, 2-11, doi:10.2174/157016209787048528 (2009).
180 Walker, B. & McMichael, A. The T-cell response to HIV. *Cold Spring Harb Perspect Med* **2**, doi:10.1101/cshperspect.a007054 (2012).
181 Sandberg, J. K. *et al.* HIV-specific CD8+ T cell function in children with vertically acquired HIV-1 infection is critically influenced by age and the state of the CD4+ T cell compartment. *J Immunol* **170**, 4403-4410, doi:10.4049/jimmunol.170.8.4403 (2003).
182 Chevalier, M. F. & Weiss, L. The split personality of regulatory T cells in HIV infection. *Blood* **121**, 29-37, doi:10.1182/blood-2012-07-409755 (2012).
183 Paul, M. E. *et al.* Predictors of immunologic long-term nonprogression in HIV-infected children: implications for initiating therapy. *J Allergy Clin Immunol* **115**, 848-855, doi:10.1016/j.jaci.2004.11.054 (2005).
184 DeMaria, M. A., Casto, M., O'Connell, M., Johnson, R. P. & Rosenzweig, M. Characterization of lymphocyte subsets in rhesus macaques during the first year of life. *Eur J Haematol* **65**, 245-257, doi:10.1034/j.1600-0609.2000.065004245.x (2000).
185 Wang, X. *et al.* Simian immunodeficiency virus selectively infects proliferating CD4+ T cells in neonatal rhesus macaques. *Blood* **116**, 4168-4174, doi:10.1182/blood-2010-03-273482 (2010).
186 Bunders, M. J. *et al.* Memory CD4(+)CCR5(+) T cells are abundantly present in the gut of newborn infants to facilitate mother-to-child transmission of HIV-1. *Blood* **120**, 4383-4390, doi:10.1182/blood-2012-06-437566 (2012).
187 Connor, E. M. *et al.* Reduction of maternal-infant transmission of human immunodeficiency virus type 1 with zidovudine treatment. Pediatric AIDS Clinical Trials Group Protocol 076 Study Group. *N Engl J Med* **331**, 1173-1180, doi:10.1056/NEJM199411033311801 (1994).
188 Wade, N. A. *et al.* Abbreviated regimens of zidovudine prophylaxis and perinatal transmission of the human immunodeficiency virus. *N Engl J Med* **339**, 1409-1414, doi:10.1056/NEJM199811123392001 (1998).
189 Shaffer, N. *et al.* Short-course zidovudine for perinatal HIV-1 transmission in Bangkok, Thailand: a randomised controlled trial. Bangkok Collaborative Perinatal HIV Transmission Study Group. *Lancet* **353**, 773-780, doi:10.1016/s0140-6736(98)10411-7 (1999).
190 Guay, L. A. *et al.* Intrapartum and neonatal single-dose nevirapine compared with zidovudine for prevention of mother-to-child transmission of HIV-1 in Kampala, Uganda: HIVNET 012 randomised trial. *The Lancet* **354**, 795-802, doi:10.1016/s0140-6736(99)80008-7 (1999).

191 Jackson, J. B. *et al.* Intrapartum and neonatal single-dose nevirapine compared with zidovudine for prevention of mother-to-child transmission of HIV-1 in Kampala, Uganda: 18-month follow-up of the HIVNET 012 randomised trial. *Lancet* **362**, 859-868, doi:10.1016/S0140-6736(03)14341-3 (2003).
192 Organization, W. H. WHO Recommendations on the Diagnosis of HIV Infection in Infants and Children. (2010).
193 Services, U. D. o. H. a. H. Diagnosis of HIV Infection in Infants and Children. (2019).
194 Violari, A. *et al.* Early antiretroviral therapy and mortality among HIV-infected infants. *N Engl J Med* **359**, 2233-2244, doi:10.1056/NEJMoa0800971 (2008).
195 HIV, P. o. A. T. a. M. M. o. C. L. w. Guidelines for the Use of Antiretroviral Agents in Pediatric HIV Infection. (2020).
196 Schlatter, A. F., Deathe, A. R. & Vreeman, R. C. The Need for Pediatric Formulations to Treat Children with HIV. *AIDS Res Treat* **2016**, 1654938, doi:10.1155/2016/1654938 (2016).
197 Foster, C. & Lyall, H. HIV and mitochondrial toxicity in children. *J Antimicrob Chemother* **61**, 8-12, doi:10.1093/jac/dkm411 (2008).
198 Gupta, R. K. *et al.* HIV-1 remission following CCR5Delta32/Delta32 haematopoietic stem-cell transplantation. *Nature* **568**, 244-248, doi:10.1038/s41586-019-1027-4 (2019).
199 Allers, K. *et al.* Evidence for the cure of HIV infection by CCR5Delta32/Delta32 stem cell transplantation. *Blood* **117**, 2791-2799, doi:10.1182/blood-2010-09-309591 (2011).
200 Frange, P. *et al.* HIV-1 virological remission lasting more than 12 years after interruption of early antiretroviral therapy in a perinatally infected teenager enrolled in the French ANRS EPF-CO10 paediatric cohort: a case report. *Lancet HIV* **3**, e49-54, doi:10.1016/S2352-3018(15)00232-5 (2016).
201 Persaud, D. *et al.* Absence of detectable HIV-1 viremia after treatment cessation in an infant. *N Engl J Med* **369**, 1828-1835, doi:10.1056/NEJMoa1302976 (2013).
202 Violari, A. *et al.* A child with perinatal HIV infection and long-term sustained virological control following antiretroviral treatment cessation. *Nat Commun* **10**, 412, doi:10.1038/s41467-019-08311-0 (2019).
203 Luzuriaga, K. *et al.* Viremic relapse after HIV-1 remission in a perinatally infected child. *N Engl J Med* **372**, 786-788, doi:10.1056/NEJMc1413931 (2015).
204 Bolton, D. L. *et al.* Human Immunodeficiency Virus Type 1 Monoclonal Antibodies Suppress Acute Simian-Human Immunodeficiency Virus Viremia and Limit Seeding of Cell-Associated Viral Reservoirs. *J Virol* **90**, 1321-1332, doi:10.1128/JVI.02454-15 (2015).
205 Shapiro, M. B. *et al.* Single-dose bNAb cocktail or abbreviated ART post-exposure regimens achieve tight SHIV control without adaptive immunity. *Nat Commun* **11**, 70, doi:10.1038/s41467-019-13972-y (2020).
206 Ng, C. T. *et al.* Passive neutralizing antibody controls SHIV viremia and enhances B cell responses in infant macaques. *Nat Med* **16**, 1117-1119, doi:10.1038/nm.2233 (2010).
207 Jayaraman, P. *et al.* Evidence for persistent, occult infection in neonatal macaques following perinatal transmission of simian-human immunodeficiency virus SF162P3. *J Virol* **81**, 822-834, doi:10.1128/JVI.01759-06 (2007).
208 Mavigner, M. *et al.* Simian Immunodeficiency Virus Persistence in Cellular and Anatomic Reservoirs in Antiretroviral Therapy-Suppressed Infant Rhesus Macaques. *J Virol* **92**, doi:10.1128/JVI.00562-18 (2018).

209 Rees, A. R. Understanding the human antibody repertoire. *MAbs* **12**, 1729683, doi:10.1080/19420862.2020.1729683 (2020).
210 Woof, J. M. & Kerr, M. A. IgA function--variations on a theme. *Immunology* **113**, 175-177, doi:10.1111/j.1365-2567.2004.01958.x (2004).
211 Vidarsson, G., Dekkers, G. & Rispens, T. IgG subclasses and allotypes: from structure to effector functions. *Front Immunol* **5**, 520, doi:10.3389/fimmu.2014.00520 (2014).
212 Irani, V. *et al.* Molecular properties of human IgG subclasses and their implications for designing therapeutic monoclonal antibodies against infectious diseases. *Mol Immunol* **67**, 171-182, doi:10.1016/j.molimm.2015.03.255 (2015).
213 Wang, X., Mathieu, M. & Brezski, R. J. IgG Fc engineering to modulate antibody effector functions. *Protein Cell* **9**, 63-73, doi:10.1007/s13238-017-0473-8 (2018).
214 Hraber, P. *et al.* Prevalence of broadly neutralizing antibody responses during chronic HIV-1 infection. *AIDS* **28**, 163-169, doi:10.1097/QAD.0000000000000106 (2014).
215 Sather, D. N. *et al.* Factors associated with the development of cross-reactive neutralizing antibodies during human immunodeficiency virus type 1 infection. *J Virol* **83**, 757-769, doi:10.1128/JVI.02036-08 (2009).
216 Doria-Rose, N. A. *et al.* Frequency and phenotype of human immunodeficiency virus envelope-specific B cells from patients with broadly cross-neutralizing antibodies. *J Virol* **83**, 188-199, doi:10.1128/JVI.01583-08 (2009).
217 Simek, M. D. *et al.* Human immunodeficiency virus type 1 elite neutralizers: individuals with broad and potent neutralizing activity identified by using a high-throughput neutralization assay together with an analytical selection algorithm. *J Virol* **83**, 7337-7348, doi:10.1128/JVI.00110-09 (2009).
218 Burton, D. R. *et al.* Efficient neutralization of primary isolates of HIV-1 by a recombinant human monoclonal antibody. *Science* **266**, 1024-1027, doi:10.1126/science.7973652 (1994).
219 Buchacher, A. *et al.* Generation of human monoclonal antibodies against HIV-1 proteins; electrofusion and Epstein-Barr virus transformation for peripheral blood lymphocyte immortalization. *AIDS Res Hum Retroviruses* **10**, 359-369, doi:10.1089/aid.1994.10.359 (1994).
220 Purtscher, M. *et al.* A broadly neutralizing human monoclonal antibody against gp41 of human immunodeficiency virus type 1. *AIDS Res Hum Retroviruses* **10**, 1651-1658, doi:10.1089/aid.1994.10.1651 (1994).
221 Burton, D. R. *et al.* A large array of human monoclonal antibodies to type 1 human immunodeficiency virus from combinatorial libraries of asymptomatic seropositive individuals. *Proc Natl Acad Sci U S A* **88**, 10134-10137, doi:10.1073/pnas.88.22.10134 (1991).
222 Wu, X. *et al.* Rational design of envelope identifies broadly neutralizing human monoclonal antibodies to HIV-1. *Science* **329**, 856-861, doi:10.1126/science.1187659 (2010).
223 Scheid, J. F. *et al.* Broad diversity of neutralizing antibodies isolated from memory B cells in HIV-infected individuals. *Nature* **458**, 636-640, doi:10.1038/nature07930 (2009).
224 Walker, L. M. *et al.* Broad and potent neutralizing antibodies from an African donor reveal a new HIV-1 vaccine target. *Science* **326**, 285-289, doi:10.1126/science.1178746 (2009).
225 Walker, L. M. *et al.* Broad neutralization coverage of HIV by multiple highly potent antibodies. *Nature* **477**, 466-470, doi:10.1038/nature10373 (2011).

226 Setliff, I. *et al.* High-Throughput Mapping of B Cell Receptor Sequences to Antigen Specificity. *Cell* **179**, 1636-1646 e1615, doi:10.1016/j.cell.2019.11.003 (2019).
227 Mascola, J. R. & Haynes, B. F. HIV-1 neutralizing antibodies: understanding nature's pathways. *Immunol Rev* **254**, 225-244, doi:10.1111/imr.12075 (2013).
228 Bonsignori, M. *et al.* Antibody-virus co-evolution in HIV infection: paths for HIV vaccine development. *Immunol Rev* **275**, 145-160, doi:10.1111/imr.12509 (2017).
229 Chen, L. *et al.* Structural basis of immune evasion at the site of CD4 attachment on HIV-1 gp120. *Science* **326**, 1123-1127, doi:10.1126/science.1175868 (2009).
230 Moody, M. A. *et al.* Immune perturbations in HIV-1–infected individuals who make broadly neutralizing antibodies. *Sci Immunol*, doi:10.1126/sciimmunol.aag0851 (2016).
231 Sok, D. *et al.* Rapid elicitation of broadly neutralizing antibodies to HIV by immunization in cows. *Nature* **548**, 108-111, doi:10.1038/nature23301 (2017).
232 Hoot, S. *et al.* Recombinant HIV envelope proteins fail to engage germline versions of anti-CD4bs bNAbs. *PLoS Pathog* **9**, e1003106, doi:10.1371/journal.ppat.1003106 (2013).
233 McGuire, A. T., Glenn, J. A., Lippy, A. & Stamatatos, L. Diverse recombinant HIV-1 Envs fail to activate B cells expressing the germline B cell receptors of the broadly neutralizing anti-HIV-1 antibodies PG9 and 447-52D. *J Virol* **88**, 2645-2657, doi:10.1128/JVI.03228-13 (2014).
234 Haigwood, N. L. *et al.* Passive immunotherapy in simian immunodeficiency virus-infected macaques accelerates the development of neutralizing antibodies. *J Virol* **78**, 5983-5995, doi:10.1128/JVI.78.11.5983-5995.2004 (2004).
235 Haigwood, N. L. *et al.* Passive immune globulin therapy in the SIV/macaque model: early intervention can alter disease profile. *Immunol Lett* **51**, 107-114, doi:10.1016/0165-2478(96)02563-1 (1996).
236 Gautam, R. *et al.* A single injection of anti-HIV-1 antibodies protects against repeated SHIV challenges. *Nature* **533**, 105-109, doi:10.1038/nature17677 (2016).
237 Julg, B. *et al.* Protection against a mixed SHIV challenge by a broadly neutralizing antibody cocktail. *Sci Transl Med* **9**, doi:10.1126/scitranslmed.aao4235 (2017).
238 Julg, B. *et al.* Broadly neutralizing antibodies targeting the HIV-1 envelope V2 apex confer protection against a clade C SHIV challenge. *Sci Transl Med* **9**, doi:10.1126/scitranslmed.aal1321 (2017).
239 Liu, J. *et al.* Antibody-mediated protection against SHIV challenge includes systemic clearance of distal virus. *Science* **353**, 1045-1049, doi:10.1126/science.aag0491 (2016).
240 Hessell, A. J. *et al.* Fc receptor but not complement binding is important in antibody protection against HIV. *Nature* **449**, 101-104, doi:10.1038/nature06106 (2007).
241 Burton, D. R. *et al.* Limited or no protection by weakly or nonneutralizing antibodies against vaginal SHIV challenge of macaques compared with a strongly neutralizing antibody. *Proc Natl Acad Sci U S A* **108**, 11181-11186, doi:10.1073/pnas.1103012108 (2011).
242 Astronomo, R. D. *et al.* Neutralization Takes Precedence Over IgG or IgA Isotype-related Functions in Mucosal HIV-1 Antibody-mediated Protection. *EBioMedicine* **14**, 97-111, doi:10.1016/j.ebiom.2016.11.024 (2016).

243 Cheeseman, H. M. *et al.* Broadly Neutralizing Antibodies Display Potential for Prevention of HIV-1 Infection of Mucosal Tissue Superior to That of Nonneutralizing Antibodies. *J Virol* **91**, doi:10.1128/JVI.01762-16 (2017).
244 Rudicell, R. S. *et al.* Enhanced potency of a broadly neutralizing HIV-1 antibody in vitro improves protection against lentiviral infection in vivo. *J Virol* **88**, 12669-12682, doi:10.1128/JVI.02213-14 (2014).
245 Lynch, R. M. *et al.* Virologic effects of broadly neutralizing antibody VRC01 administration during chronic HIV-1 infection. *Sci Transl Med* **7**, 319ra206, doi:10.1126/scitranslmed.aad5752 (2015).
246 Bar-On, Y. *et al.* Safety and antiviral activity of combination HIV-1 broadly neutralizing antibodies in viremic individuals. *Nat Med* **24**, 1701-1707, doi:10.1038/s41591-018-0186-4 (2018).
247 Bar, K. J. *et al.* Effect of HIV Antibody VRC01 on Viral Rebound after Treatment Interruption. *N Engl J Med* **375**, 2037-2050, doi:10.1056/NEJMoa1608243 (2016).
248 Mendoza, P. *et al.* Combination therapy with anti-HIV-1 antibodies maintains viral suppression. *Nature* **561**, 479-484, doi:10.1038/s41586-018-0531-2 (2018).
249 Niessl, J. *et al.* Combination anti-HIV-1 antibody therapy is associated with increased virus-specific T cell immunity. *Nat Med*, doi:10.1038/s41591-019-0747-1 (2020).
250 Borducchi, E. N. *et al.* Antibody and TLR7 agonist delay viral rebound in SHIV-infected monkeys. *Nature* **563**, 360-364, doi:10.1038/s41586-018-0600-6 (2018).
251 Cunningham, C. K. *et al.* Safety, Tolerability, and Pharmacokinetics of the Broadly Neutralizing HIV-1 Monoclonal Antibody VRC01 in HIV-Exposed Newborn Infants. *J Infect Dis*, doi:10.1093/infdis/jiz532 (2019).
252 Nishimura, Y. *et al.* Early antibody therapy can induce long-lasting immunity to SHIV. *Nature*, doi:10.1038/nature21435 (2017).
253 Siliciano, J. M. & Siliciano, R. F. The Remarkable Stability of the Latent Reservoir for HIV-1 in Resting Memory CD4+ T Cells. *J Infect Dis*, doi:10.1093/infdis/jiv219 (2015).
254 Sultan, B., Benn, P. & Waters, L. Current perspectives in HIV post-exposure prophylaxis. *HIV AIDS (Auckl)* **6**, 147-158, doi:10.2147/HIV.S46585 (2014).
255 Newell, M. L. *et al.* Mortality of infected and uninfected infants born to HIV-infected mothers in Africa: a pooled analysis. *Lancet* **364**, 1236-1243 (2004).
256 Wade, N. A. *et al.* Abbreviated regimens of zidovudine phrophylaxis and perinatal transmission of the human immunodeficiency virus. *New England Journal of Medicine* **339**, 1409-1414 (1998).
257 Hessell, A. J. & Haigwood, N. L. Animal models in HIV-1 protection and therapy. *Curr Opin HIV AIDS*, doi:10.1097/COH.0000000000000152 (2015).
258 Whitney, J. B. *et al.* Rapid seeding of the viral reservoir prior to SIV viraemia in rhesus monkeys. *Nature* **512**, 74-77, doi:10.1038/nature13594 (2014).
259 Tsai, C. C. *et al.* Effectiveness of postinoculation (R)-9-(2-phosphonylmethoxypropyl) adenine treatment for prevention of persistent simian immunodeficiency virus SIVmne infection depends critically on timing of initiation and duration of treatment. *J Virol* **72**, 4265-4273 (1998).
260 van Rompay, K. K. *et al.* Early short-term 9-[2-(R)-(phosphonomethoxy)propyl]adenine treatment favorably alters the subsequent disease course in simian immunodeficiency virus-infected newborn Rhesus macaques. *J Virol* **73**, 2947-2955 (1999).

261 Whitney, J. B. *et al.* Prevention of SIVmac251 reservoir seeding in rhesus monkeys by early antiretroviral therapy. *Nat Commun* **9**, 5429, doi:10.1038/s41467-018-07881-9 (2018).
262 Mofenson, L. M. & Watts, D. H. Safety of pediatric HIV elimination: the growing population of HIV- and antiretroviral-exposed but uninfected infants. *PLoS Med* **11**, e1001636, doi:10.1371/journal.pmed.1001636 (2014).
263 Pegu, A., Hessell, A. J., Mascola, J. R. & Haigwood, N. L. Use of broadly neutralizing antibodies for HIV-1 prevention. *Immunol Rev* **275**, 296-312, doi:10.1111/imr.12511 (2017).
264 Hessell, A. J., Malherbe, D. C. & Haigwood, N. L. Passive and active antibody studies in primates to inform HIV vaccines. *Expert Rev Vaccines* **17**, 127-144, doi:10.1080/14760584.2018.1425619 (2018).
265 International Maternal, P., Adolescent AIDS Clinical Trials Network. IMPAACT 2008 (DAIDS ID 20735): Phase I/II Multisite Randomized Controlled Study of Monoclonal Antibody VCR01 Combined with Antiretroviral Therapy to Promote Clearance of HIV-1 Infected Cells in Infants. (2019).
266 Network, I. M. P. A. A. C. T. P1112 (DAIDS ID 11903): Open-Label, Dose-Escalating, Phase I Study to Determine Safety and Pharmacokinetic Parameters of Subcutaneous (SC) VRC01, VRC01LS, and VRC07-523LS, Potent Anti-HIV Neutralizing Monoclonal Antibodies, in HIV-1-Exposed Infants. (2019).
267 Nishimura, Y. *et al.* Early antibody therapy can induce long-lasting immunity to SHIV. *Nature* **543**, 559-563, doi:10.1038/nature21435 (2017).
268 Association, A. V. M. AVMA Guidelines for the Euthanasia of Animals. (U.S. Veterinary Medical Association, 2013).
269 Walker, L. M. *et al.* Broad neutralization coverage of HIV by multiple highly potent antibodies. *Nature*, doi:10.1038/nature10373 (2011).
270 Del Prete, G. Q. *et al.* Short Communication: Comparative Evaluation of Coformulated Injectable Combination Antiretroviral Therapy Regimens in Simian Immunodeficiency Virus-Infected Rhesus Macaques. *AIDS Res Hum Retroviruses* **32**, 163-168, doi:10.1089/AID.2015.0130 (2016).
271 Cline, A. N., Bess, J. W., Piatak, M., Jr. & Lifson, J. D. Highly sensitive SIV plasma viral load assay: practical considerations, realistic performance expectations, and application to reverse engineering of vaccines for AIDS. *J Med Primatol* **34**, 303-312, doi:10.1111/j.1600-0684.2005.00128.x (2005).
272 Salazar-Gonzalez, J. F. *et al.* Deciphering human immunodeficiency virus type 1 transmission and early envelope diversification by single-genome amplification and sequencing. *J Virol* **82**, 3952-3970, doi:JVI.02660-07 [pii] 10.1128/JVI.02660-07 (2008).
273 Malherbe, D. C. *et al.* Envelope variants circulating as initial neutralization breadth developed in two HIV-infected subjects stimulate multiclade neutralizing antibodies in rabbits. *J Virol* **88**, 12949-12967, doi:10.1128/JVI.01812-14 (2014).
274 Lynch, R. M. *et al.* The development of CD4 binding site antibodies during HIV-1 infection. *J Virol* **86**, 7588-7595, doi:10.1128/JVI.00734-12 (2012).
275 Zhou, T. *et al.* Transplanting supersites of HIV-1 vulnerability. *PLoS One* **9**, e99881, doi:10.1371/journal.pone.0099881 (2014).
276 Sanyal, A. *et al.* Novel assay reveals a large, inducible, replication-competent HIV-1 reservoir in resting CD4(+) T cells. *Nat Med* **23**, 885-889, doi:10.1038/nm.4347 (2017).
277 Srivastava, I. K. *et al.* Purification, characterization, and immunogenicity of a soluble trimeric envelope protein containing a partial deletion of the V2 loop

derived from SF162, an R5-tropic human immunodeficiency virus type 1 isolate. *J Virol* **77**, 11244-11259, doi:10.1128/jvi.77.20.11244-11259.2003 (2003).
278 Lockridge, K. M. *et al.* Pathogenesis of experimental rhesus cytomegalovirus infection. *J Virol* **73**, 9576-9583 (1999).
279 Bailey, C. *et al.* Systemic spironucleosis in 2 immunodeficient rhesus macaques (Macaca mulatta). *Vet Pathol* **47**, 488-494, doi:10.1177/0300985810363704 (2010).
280 Zalevsky, J. *et al.* Enhanced antibody half-life improves in vivo activity. *Nat Biotechnol* **28**, 157-159, doi:10.1038/nbt.1601 (2010).
281 Ho, Y. C. *et al.* Replication-competent noninduced proviruses in the latent reservoir increase barrier to HIV-1 cure. *Cell* **155**, 540-551, doi:10.1016/j.cell.2013.09.020 (2013).
282 Bruner, K. M. *et al.* Defective proviruses rapidly accumulate during acute HIV-1 infection. *Nat Med* **22**, 1043-1049, doi:10.1038/nm.4156 (2016).
283 Moir, S. *et al.* Evidence for HIV-associated B cell exhaustion in a dysfunctional memory B cell compartment in HIV-infected viremic individuals. *J Exp Med* **205**, 1797-1805, doi:10.1084/jem.20072683 (2008).
284 Jaworski, J. P. *et al.* Pre-existing neutralizing antibody mitigates B cell dysregulation and enhances the Env-specific antibody response in SHIV-infected rhesus macaques. *PLoS One* **12**, e0172524, doi:10.1371/journal.pone.0172524 (2017).
285 Neumann, B., Klippert, A., Raue, K., Sopper, S. & Stahl-Hennig, C. Characterization of B and plasma cells in blood, bone marrow, and secondary lymphoid organs of rhesus macaques by multicolor flow cytometry. *J Leukoc Biol* **97**, 19-30, doi:10.1189/jlb.1HI0514-243R (2015).
286 Salazar-Vizcaya, L. *et al.* Viral load versus CD4(+) monitoring and 5-year outcomes of antiretroviral therapy in HIV-positive children in Southern Africa: a cohort-based modelling study. *AIDS* **28**, 2451-2460 (2014).
287 Ndung'u, T., Dong, K. L., Kwon, D. S. & Walker, B. D. A FRESH approach: Combining basic science and social good. *Sci Immunol* **3**, doi:10.1126/sciimmunol.aau2798 (2018).
288 Dong, K. L. *et al.* Detection and treatment of Fiebig stage I HIV-1 infection in young at-risk women in South Africa: a prospective cohort study. *Lancet HIV* **5**, e35-e44, doi:10.1016/S2352-3018(17)30146-7 (2018).
289 WHO. Diagnosis of HIV infection in infants and children WHO recommendations. (2010).
290 Sengupta, S. & Siliciano, R. F. Targeting the Latent Reservoir for HIV-1. *Immunity* **48**, 872-895, doi:10.1016/j.immuni.2018.04.030 (2018).
291 Parsons, M. S. *et al.* Fc-dependent functions are redundant to efficacy of anti-HIV antibody PGT121 in macaques. *J Clin Invest* **129**, 182-191, doi:10.1172/JCI122466 (2019).
292 Greener, B. N. *et al.* Dolutegravir pharmacokinetics in the genital tract and colorectum of HIV-negative men after single and multiple dosing. *J Acquir Immune Defic Syndr* **64**, 39-44, doi:10.1097/QAI.0b013e31829ed7a4 (2013).
293 Ryman, J. T. & Meibohm, B. Pharmacokinetics of Monoclonal Antibodies. *CPT Pharmacometrics Syst Pharmacol* **6**, 576-588, doi:10.1002/psp4.12224 (2017).
294 Ferrantelli, F. *et al.* Time dependence of protective post-exposure prophylaxis with human monoclonal antibodies against pathogenic SHIV challenge in newborn macaques. *Virology* **358**, 69-78 (2007).

295 Bastidas, S. *et al.* CD8+ T cells are activated in an antigen-independent manner in HIV-infected individuals. *J Immunol* **192**, 1732-1744, doi:10.4049/jimmunol.1302027 (2014).
296 Sauter, R. *et al.* CD4/CD8 ratio and CD8 counts predict CD4 response in HIV-1-infected drug naive and in patients on cART. *Medicine (Baltimore)* **95**, e5094, doi:10.1097/MD.0000000000005094 (2016).
297 Sainz, T. *et al.* The CD4/CD8 ratio as a marker T-cell activation, senescence and activation/exhaustion in treated HIV-infected children and young adults. *AIDS* **27**, 1513-1516, doi:10.1097/QAD.0b013e32835faa72 (2013).
298 Margolick, J. B. *et al.* Impact of inversion of the CD4/CD8 ratio on the natural history of HIV-1 infection. *J Acquir Immune Defic Syndr* **42**, 620-626, doi:10.1097/01.qai.0000223028.55080.9d (2006).
299 Sugimoto, C. *et al.* Critical Role for Monocytes/Macrophages in Rapid Progression to AIDS in Pediatric Simian Immunodeficiency Virus-Infected Rhesus Macaques. *J Virol* **91**, doi:10.1128/JVI.00379-17 (2017).
300 Kim, W. K. *et al.* Monocyte heterogeneity underlying phenotypic changes in monocytes according to SIV disease stage. *J Leukoc Biol* **87**, 557-567, doi:10.1189/jlb.0209082 (2010).
301 Ziegler-Heitbrock, L. *et al.* Nomenclature of monocytes and dendritic cells in blood. *Blood* **116**, e74-80, doi:10.1182/blood-2010-02-258558 (2010).
302 Ziegler-Heitbrock, L. The CD14+ CD16+ blood monocytes: their role in infection and inflammation. *J Leukoc Biol* **81**, 584-592, doi:10.1189/jlb.0806510 (2007).
303 Chang, H. H. *et al.* Transcriptional network predicts viral set point during acute HIV-1 infection. *J Am Med Inform Assoc* **19**, 1103-1109, doi:10.1136/amiajnl-2012-000867 (2012).
304 Zhang, Z. N. *et al.* Transcriptomic analysis of peripheral blood mononuclear cells in rapid progressors in early HIV infection identifies a signature closely correlated with disease progression. *Clin Chem* **59**, 1175-1186, doi:10.1373/clinchem.2012.197335 (2013).
305 Ding, J. *et al.* An integrative genomic analysis of transcriptional profiles identifies characteristic genes and patterns in HIV-infected long-term non-progressors and elite controllers. *J Transl Med* **17**, 35, doi:10.1186/s12967-019-1777-7 (2019).
306 Zhang, W. *et al.* Transcriptomics and Targeted Proteomics Analysis to Gain Insights Into the Immune-control Mechanisms of HIV-1 Infected Elite Controllers. *EBioMedicine* **27**, 40-50, doi:10.1016/j.ebiom.2017.11.031 (2018).
307 Barouch, D. H. *et al.* Rapid Inflammasome Activation following Mucosal SIV Infection of Rhesus Monkeys. *Cell* **165**, 656-667, doi:10.1016/j.cell.2016.03.021 (2016).
308 Jacquelin, B. *et al.* Nonpathogenic SIV infection of African green monkeys induces a strong but rapidly controlled type I IFN response. *J Clin Invest* **119**, 3544-3555, doi:10.1172/JCI40093 (2009).
309 Leary, S., Underwood, W. & Anthony, R. AVMA Guidelines for the Euthanasia of Animals: 2013 Edition. *J Am Vet Med Assoc* (2013).
310 Team, R. C. in (ed R Foundation for Statistical Computing) https://www.R-project.org/ (2020).
311 Stuart, T. *et al.* Comprehensive Integration of Single-Cell Data. *Cell* **177**, 1888-1902 e1821, doi:10.1016/j.cell.2019.05.031 (2019).
312 Love, M. I., Huber, W. & Anders, S. Moderated estimation of fold change and dispersion for RNA-seq data with DESeq2. *Genome Biol* **15**, 550, doi:10.1186/s13059-014-0550-8 (2014).

313 Kolde, R. https://CRAN.R-project.org/package=pheatmap (2019).
314 Chen, H. https://CRAN.R-project.org/package=VennDiagram (2018).
315 Sui, Y. *et al.* Influence of gut microbiome on mucosal immune activation and SHIV viral transmission in naive macaques. *Mucosal Immunol* **11**, 1219-1229, doi:10.1038/s41385-018-0029-0 (2018).
316 Schillie, S. *et al.* Prevention of Hepatitis B Virus Infection in the United States: Recommendations of the Advisory Committee on Immunization Practices. *MMWR Recomm Rep* **67**, 1-31, doi:10.15585/mmwr.rr6701a1 (2018).
317 Zuin, G. *et al.* Impaired response to hepatitis B vaccine in HIV infected children. *Vaccine* **10**, 857-860, doi:10.1016/0264-410x(92)90050-t (1992).
318 Falconer, O., Newell, M. L. & Jones, C. E. The Effect of Human Immunodeficiency Virus and Cytomegalovirus Infection on Infant Responses to Vaccines: A Review. *Front Immunol* **9**, 328, doi:10.3389/fimmu.2018.00328 (2018).
319 Ndhlovu, Z. M. *et al.* Magnitude and Kinetics of CD8+ T Cell Activation during Hyperacute HIV Infection Impact Viral Set Point. *Immunity* **43**, 591-604, doi:10.1016/j.immuni.2015.08.012 (2015).
320 Piatosa, B. *et al.* B cell subsets in healthy children: reference values for evaluation of B cell maturation process in peripheral blood. *Cytometry B Clin Cytom* **78**, 372-381, doi:10.1002/cyto.b.20536 (2010).
321 Titanji, K. *et al.* Acute depletion of activated memory B cells involves the PD-1 pathway in rapidly progressing SIV-infected macaques. *J Clin Invest* **120**, 3878-3890, doi:10.1172/JCI43271 (2010).
322 Kuhrt, D. *et al.* Evidence of early B-cell dysregulation in simian immunodeficiency virus infection: rapid depletion of naive and memory B-cell subsets with delayed reconstitution of the naive B-cell population. *J Virol* **84**, 2466-2476, doi:10.1128/JVI.01966-09 (2010).
323 Pahwa, S. *et al.* CD4+/CD8+ T cell ratio for diagnosis of HIV-1 infection in infants: Women and Infants Transmission Study. *Pediatrics* **122**, 331-339, doi:10.1542/peds.2007-2308 (2008).
324 Pitcher, C. J. *et al.* Development and homeostasis of T cell memory in rhesus macaque. *J Immunol* **168**, 29-43, doi:10.4049/jimmunol.168.1.29 (2002).
325 Wang, X. *et al.* Profound loss of intestinal Tregs in acutely SIV-infected neonatal macaques. *J Leukoc Biol* **97**, 391-400, doi:10.1189/jlb.4A0514-266RR (2015).
326 Hoffmann, P. *et al.* Only the CD45RA+ subpopulation of CD4+CD25high T cells gives rise to homogeneous regulatory T-cell lines upon in vitro expansion. *Blood* **108**, 4260-4267, doi:10.1182/blood-2006-06-027409 (2006).
327 Mhandire, K. *et al.* Plasma IP-10 Concentrations Correlate Positively with Viraemia and Inversely with CD4 Counts in Untreated HIV Infection. *Open AIDS J* **11**, 24-31, doi:10.2174/1874613601711010024 (2017).
328 Jiao, Y. *et al.* Plasma IP-10 is associated with rapid disease progression in early HIV-1 infection. *Viral Immunol* **25**, 333-337, doi:10.1089/vim.2012.0011 (2012).
329 Liu, M. *et al.* CXCL10/IP-10 in infectious diseases pathogenesis and potential therapeutic implications. *Cytokine Growth Factor Rev* **22**, 121-130, doi:10.1016/j.cytogfr.2011.06.001 (2011).
330 Dzidic, M., Boix-Amoros, A., Selma-Royo, M., Mira, A. & Collado, M. C. Gut Microbiota and Mucosal Immunity in the Neonate. *Med Sci (Basel)* **6**, doi:10.3390/medsci6030056 (2018).
331 Koay, W. L. A., Siems, L. V. & Persaud, D. The microbiome and HIV persistence: implications for viral remission and cure. *Curr Opin HIV AIDS* **13**, 61-68, doi:10.1097/COH.0000000000000434 (2018).

332 Colby, D. J. *et al.* Rapid HIV RNA rebound after antiretroviral treatment interruption in persons durably suppressed in Fiebig I acute HIV infection. *Nat Med* **24**, 923-926, doi:10.1038/s41591-018-0026-6 (2018).
333 Maini, R. N. *et al.* Therapeutic efficacy of multiple intravenous infusions of anti-tumor necrosis factor alpha monoclonal antibody combined with low-dose weekly methotrexate in rheumatoid arthritis. *Arthritis Rheum* **41**, 1552-1563, doi:10.1002/1529-0131(199809)41:9<1552::AID-ART5>3.0.CO;2-W (1998).
334 Hausl, C. *et al.* High-dose factor VIII inhibits factor VIII-specific memory B cells in hemophilia A with factor VIII inhibitors. *Blood* **106**, 3415-3422, doi:10.1182/blood-2005-03-1182 (2005).
335 Saunders, K. O. *et al.* Sustained Delivery of a Broadly Neutralizing Antibody in Nonhuman Primates Confers Long-Term Protection against Simian/Human Immunodeficiency Virus Infection. *J Virol* **89**, 5895-5903, doi:10.1128/JVI.00210-15 (2015).
336 Atiqi, S., Hooijberg, F., Loeff, F. C., Rispens, T. & Wolbink, G. J. Immunogenicity of TNF-Inhibitors. *Front Immunol* **11**, 312, doi:10.3389/fimmu.2020.00312 (2020).
337 Mayer, K. H. *et al.* Safety, pharmacokinetics, and immunological activities of multiple intravenous or subcutaneous doses of an anti-HIV monoclonal antibody, VRC01, administered to HIV-uninfected adults: Results of a phase 1 randomized trial. *PLoS Med* **14**, e1002435, doi:10.1371/journal.pmed.1002435 (2017).
338 Cohen, Y. Z. *et al.* Safety, pharmacokinetics, and immunogenicity of the combination of the broadly neutralizing anti-HIV-1 antibodies 3BNC117 and 10-1074 in healthy adults: A randomized, phase 1 study. *PLoS One* **14**, e0219142, doi:10.1371/journal.pone.0219142 (2019).
339 Fuchs, S. P. *et al.* AAV-Delivered Antibody Mediates Significant Protective Effects against SIVmac239 Challenge in the Absence of Neutralizing Activity. *PLoS Pathog* **11**, e1005090, doi:10.1371/journal.ppat.1005090 (2015).
340 Martinez-Navio, J. M. *et al.* Host Anti-antibody Responses Following Adeno-associated Virus-mediated Delivery of Antibodies Against HIV and SIV in Rhesus Monkeys. *Mol Ther* **24**, 76-86, doi:10.1038/mt.2015.191 (2016).
341 Saunders, K. O. *et al.* Broadly Neutralizing Human Immunodeficiency Virus Type 1 Antibody Gene Transfer Protects Nonhuman Primates from Mucosal Simian-Human Immunodeficiency Virus Infection. *J Virol* **89**, 8334-8345, doi:10.1128/JVI.00908-15 (2015).
342 Gardner, M. R. *et al.* Anti-drug Antibody Responses Impair Prophylaxis Mediated by AAV-Delivered HIV-1 Broadly Neutralizing Antibodies. *Mol Ther* **27**, 650-660, doi:10.1016/j.ymthe.2019.01.004 (2019).
343 Pratt, K. P. Anti-Drug Antibodies: Emerging Approaches to Predict, Reduce or Reverse Biotherapeutic Immunogenicity. *Antibodies (Basel)* **7**, doi:10.3390/antib7020019 (2018).
344 Martinez, D. R., Fouda, G. G., Peng, X., Ackerman, M. E. & Permar, S. R. Noncanonical placental Fc receptors: What is their role in modulating transplacental transfer of maternal IgG? *PLoS Pathog* **14**, e1007161, doi:10.1371/journal.ppat.1007161 (2018).
345 Jennewein, M. F. *et al.* Fc Glycan-Mediated Regulation of Placental Antibody Transfer. *Cell*, doi:10.1016/j.cell.2019.05.044 (2019).
346 Alpert, M. D. *et al.* A novel assay for antibody-dependent cell-mediated cytotoxicity against HIV-1- or SIV-infected cells reveals incomplete overlap with antibodies measured by neutralization and binding assays. *J Virol* **86**, 12039-12052, doi:10.1128/JVI.01650-12 (2012).

347 Stelter, S. *et al.* Engineering the interactions between a plant-produced HIV antibody and human Fc receptors. *Plant Biotechnol J*, doi:10.1111/pbi.13207 (2019).
348 Sanyal, A. *et al.* Novel assay reveals a large, inducible, replication-competent HIV-1 reservoir in resting CD4+ T cells. *Nat Med* **23**, 885-889, doi:10.1038/nm.4347 (2017).
349 Huang, Y. *et al.* Engineered Bispecific Antibodies with Exquisite HIV-1-Neutralizing Activity. *Cell* **165**, 1621-1631, doi:10.1016/j.cell.2016.05.024 (2016).
350 Xu, L. *et al.* Trispecific broadly neutralizing HIV antibodies mediate potent SHIV protection in macaques. *Science* **358**, 85-90, doi:10.1126/science.aan8630 (2017).
351 Tabb, B. *et al.* Reduced inflammation and lymphoid tissue immunopathology in rhesus macaques receiving anti-tumor necrosis factor treatment during primary simian immunodeficiency virus infection. *J Infect Dis* **207**, 880-892, doi:10.1093/infdis/jis643 (2013).